Alma Mater Studiorum - Università di Bologna

DOTTORATO DI RICERCA IN

CHIMICA

CICLO XXIX
Settore Concorsuale di Afferenza: 03/B1
Settore Scientifico Disciplinare: CHIM/03

Design, Synthesis and Photophysical Characterization of Luminescent Metal Tetrazolate Complexes

Presentata da: Valentina Fiorini

Supervisore: Prof. Stefano Stagni

Coordinatore Dottorato: Prof. Aldo Roda

Esame Finale anno 2017

Abstract

Over the past few decades, the scenario of luminescent transition metal complexes has experienced a great blossom. In this context, the spotlight of the research program that I have carried out in my PhD studies has been dealing with the design, the preparation and the study of the photophysical properties of a new series of luminescent metal complexes containing anionic ligands such as 5-aryl tetrazolates [R-CN_4]$^-$. The choice of this specific class of nitrogen rich derivatives stemmed from the observation of how these ligands can effectively rule the luminescent output of the corresponding Ru (II) polypyridyls, Ir(III) bis-cyclometalates and tris carbonyl Re(I)-diimine complexes. In particular, the synthetic versatility of tetrazolate derivatives combined with the peculiar sensitivity to electrophilic additions – both permanent and reversible - that is displayed by the coordinated tetrazolate ring constitute the background for the further exploitment of their coordination chemistry and their applicative panorama. On these basis, we have recently prepared the first examples of anionic Ir(III) tetrazolate complexes and new Re(I)-based species containing ditopic tetrazolate ligands, with particular attention dedicated to their use as components for white light emitting Ir(III)-based ion pairs ("soft salts"), for covalently linked Ir(III)-Re(I) dyads, and for the investigation of Re(I) tetrazolate complexes as luminescent chemosensors. Moreover, studies which have dealt with Ru(II) tetrazolate complexes, pointed the way for the preparation of tetrazole –based Dye Sensitized Solar Cells.

Index

Chapter 1

Photophysics and photochemistry of organometallic compounds: a general overview

Abstract

The study of the photophysical and photochemical properties of coordination and organometallic compounds have attracted great interest since a long time. At a very early stage, the first work concerning the photosensitivity of metal complexes was that on the effect of light on AgCl, leading to the establishment of photography. At the beginning of the last century the importance of photochemistry has been clarified mainly due to the work of Giacomo Ciamician. Nowadays, the reasons at the basis of such an interest may be summarized in the use of coordination and organometallic compounds as photoactive components of processes aimed to perform artificial photosynthesis, the design of new DSSC (dye-sensitized solar cells), the development of luminescent sensors for biological systems, the development of new devices for illumination (OLED- light emitting devices, LED- light emitting diode, LEEC- light emitting electrochemical cells, and so on), the preparation of nanostructures capable of exhibiting new optical properties and luminescence imaging to be used in diagnostic and medicine. This chapter aims to recall and summarize some general information on the electronic structure of coordination and organometallic compounds, which is needed for understanding and discussing the photochemical and photophysical properties of metal complexes.

Electronic Structure

The molecular orbital theory (MOT) is the most complete approach to discuss about the electronic structure of metal complexes. However, because of MOT requires a great deal of computation, more handy approaches are used to describe the bonding in metal complexes. These theories are the crystal field theory (CFT) and the ligand-field theory (LFT).[1]

In the CFT, the ligands are assumed as negative point charges, which generate an electrostatic field. In the transition-metal ions all the partially occupied d orbitals are either filled or completely empty, producing interesting effects from the interaction of the electrostatic field of the ligands with the d electrons.

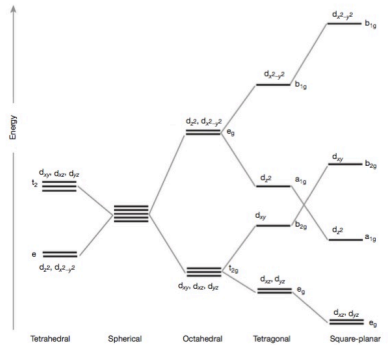

Figure 1.1: splitting of the five d orbitals in a central metal ion

For a gas state transition-metal ion, the five d orbitals are degenerate. In a complex where the ligand field is spherically symmetric, the five d orbitals would be higher in energy than in the free ion, because of the repulsion between the metal ion electron density and the spherical field of negative charge; however, a spherical field is never obtained; so the five d orbitals are no longer equivalent and they split according to the particular symmetry of the complex. For example, in a six-coordinated complex having the ligands located on the corners of an octahedron (Figure 1.1), the five d orbitals split into two sets: one set of three orbitals, d_{xy}, d_{xz}, and d_{yz}, equivalent to one another and labelled t_{2g}, and another set of two orbitals, d_{z^2} and $d_{x^2-y^2}$, equivalent to each other but different from the previous set, labelled e_g. Δ or 10 Dq, which width depends on the central ion and ligands involved, generally denotes the amount of splitting between e_g and t_{2g} orbitals.

Ligand-Field Theory

According to the experimental data, the crystal field theory, which is purely electrostatic, must be considered as a rough approximation of the electronic structure of complexes. A more realistic approach take into account the existence of a certain degree of overlap between the metal–ligand orbitals. The ligand field theory (LFT), preserves the advantages of the simple CFT and includes the effects of covalent bonding. According to this theory, the calculation of the energy-level diagrams proceeds in the same manner as in CFT, except that one takes into account that the interelectronic repulsion and spin–orbit coupling parameters are noticeably reduced when going from free to complexed metal ions, because of the delocalization of the 'metal' electrons.

Molecular Orbital Theory

The molecular orbitals (MOs) for metal complexes are composed as linear combinations of both metal and ligand orbitals.

Combinations of the ligand orbitals to obtain sets of composite ligand orbitals are first considered, then the symmetry orbitals of the ligands are combined with metal orbitals of the same symmetry to produce a set of MOs into which the electrons are added. The method is illustrated for an ML_6 octahedral complex, where M is a first-row transition metal and L is a ligand which possesses both σ and π orbitals.

Metal orbitals. There are the 3d, 4s, and 4p orbitals of the metal ion to be considered. In the Oh point group they may be classified as follows:

$$(3d_{z^2}, 3d_{x^2-y^2}),\ e_g$$

$$(3d_{xy}; 3d_{xz}; 3d_{yz}),\ t_{2g}$$

$$(4s),\ a_{1g}$$

$$(4p_x, 4p_y, 4p_z),\ t_{1u}$$

The e_g and a_{1g} orbitals are suitable only for σ bonding; the t_{2g} orbitals are suitable only for π bonding, and the t_{1u} orbitals may give both σ and π bonding.

Ligand orbitals. By choosing the linear combinations of ligand σ orbitals, which have the same symmetry properties as the various metal σ orbitals, six symmetry orbitals are constructed. They overlap effectively with a particular one of the six metal orbitals, which are suitable for σ bonding. Similarly, the 12 individual ligand π orbitals are combined into 12 symmetry orbitals; six of them will have appropriate symmetry to match the six metal π orbitals, and the other six will be nonbonding with respect to the metal complex.

Molecular orbitals. The bonding and anti bonding molecular orbitals for the complex are then obtained by combining metal and ligand orbitals which have the same symmetry properties. Each MO is indicated with the appropriate symmetry label, using the asterisk to signify the antibonding character. Once the relative MO energy order has been established, the valence electrons are assigned to the orbitals of lowest energy (Figure 2.1).

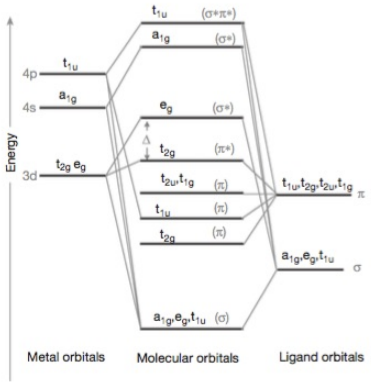

Figure 2.1: Molecular orbital-energy-level diagram for an octahedral complex containing ligands that possess σ and π orbitals

Some important features of energy-level diagrams are as follows:

1. The ligand σ orbitals are lower in energy than the metal σ orbitals. Therefore, the six bonding σ MOs have more the character of ligand orbitals than they do of metal orbitals. The opposite is true for the antibonding σ* MOs.
2. The e_g and t_{2g} orbitals at the center of the diagrams are mainly localized on the metal and correspond, respectively, to the higher- and lower- energy sets of d orbitals described by the CFT.
3. When the ligands do not possess π orbitals, the t_{2g} MOs are purely metal π nonbonding orbitals.
4. If the ligands possess only π orbitals of lower energy than the metal t_{2g} orbitals, the π interaction destabilizes the metal t_{2g} orbitals and the D value is lower than in the case of a σ interaction alone.
5. If the ligands have only π orbitals of higher energy than the metal t_{2g} orbitals, the π interaction stabilizes the metal t_{2g} orbitals and, thus, the D value is greater than in the case of a σ interaction alone.
6. If the ligands have both low-energy and high-energy π orbitals, the net effect depends on the competition between the interactions of the two types of ligand π orbitals with the metal t_{2g} orbitals.

Electronic Transitions and Excited States

By using the preponderant MO configuration of coordination compounds is possible to discuss about their photophysical and photochemical properties and, then, to make a classification of the electronic transitions according to the location of the MOs involved (Figure 3.1).

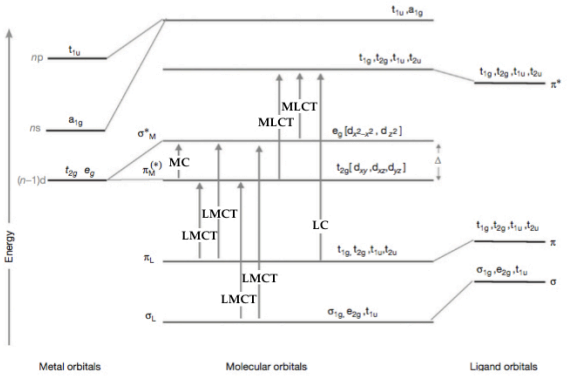

Figure 3: Electronic transitions in octahedral complexes. MC: metal centered transitions; LMCT: ligand to metal charge transfer transitions; MLCT: metal to ligand charge transfer transitions; LC: ligand centered transitions

Using this criterion, three types of electronic transitions may be distinguished:

1. Transitions between MOs mainly localized on the central metal. Electronic transitions occurring between MC orbitals, usually called d–d transitions or MC.
2. Transitions between MOs mainly localized on the ligands and MOs mainly localized on the central metal. These transitions are called charge transfer transitions (CT). Depending on whether the excited electron is originally located on the ligands or on the central metal, *ligand-to-metal* or *metal-to-ligand charge-transfer* (LMCT or MLCT, respectively) transitions can occur.
3. Transitions between MOs mainly localized on the ligands. These transitions, called '*ligand-centered*' (LC), only involve ligand orbitals which are almost unaffected by coordination to the metal.

Selection Rules

Selection rules specify the possible transitions among quantum levels due to absorption or emission of electromagnetic radiation.[2]

In electronic spectroscopy there are three:

- $\Delta l = \pm 1$, that is transitions which involve a change in the quantum number by one are formally allowed (s ⟶ p, p ⟶ d, d ⟶f), while the others are formally forbidden (d ⟶ d);
- Spin multiplicity of the states: transitions between states of the same multiplicity are allowed but not those between different multiplicity states (*spin forbidden*);
- *Laporte* or *Parity* selection rule: for high symmetric complexes which posses a centre of symmetry or inversion (*i.e.* Oh molecules), transitions between energy levels with the same symmetry are forbidden.

Fortunately, selection rules can be often bypassed with several mechanisms:

- *Spin-orbit coupling*: spin and orbital motions are coupled. Even if they are coupled very weakly, a little of each spin state mixes with the other in the ground and excited states by an amount dependent upon the energy difference in the orbital states and magnitude of the spin–orbit coupling

constant. Therefore electronic transitions occur between different states of spin multiplicity and also between states in which Δl is not equal to ± 1.

- *Laporte selection rule*: transitions between two *gerade* and two *ungerade* orbitals may be allowed either because the molecule is not totally symmetric, or because as the molecule vibrates, the centre of symmetry is temporarily removed (*vibronic coupling*). This means that d⟶d transitions are observed but they are not very intense, especially for Oh complexes. Since the magnitude of Δo, the d⟶d transitions in complexes will occur at high energy.

Absorption Bands

d-d transitions (MC)

The octahedral splitting of the metal d-orbitals results in a t_{2g} and an e_g set of orbitals.[1] Placing electrons in these levels for complexes containing more than one d electron results in further interactions, introducing several different spin states because the promoted $t_{2g} \longrightarrow e_g$ electron may either retain or change its spin orientation. As a consequence, each excited configuration gives rise to two distinct excited states, one having the same multiplicity as the ground state and the other of a different multiplicity.

Moreover, additional complications arise because degenerate sets of orbitals (e_g and t_{2g}) are involved in the transition. The interelectronic repulsions, in fact, depend also on the distribution of the electrons in the degenerate sets of orbitals.

If we consider the metal centre as a free ion (*i.e.* in the absence of any ligands), its ground state can be written as a spectroscopic term symbol according to the Russell-Saunders coupling scheme, which uses a letter to describe the electronic state and a number for the spin multiplicity.

In the ground state, a d^6 metal ion such as Ir(III), Re(I) or Ru(II) has 6 electrons in the d orbitals, which will occupy orbitals from the highest magnetic quantum number to the lowest according to the Hund's rules. L, the total angular momentum (given by $L = \Sigma m_l$) is therefore 2, a state labelled as D. The spin multiplicity is given by $(2S + 1)$ where S is the sum of the spin of electrons, and it's equal to 5. Thus, the spectroscopic term symbol, according to the Russell-Saunders notation for a d^6 metal ion is ^5D.

The electrons may be filled in orbitals by different arrangements since the orbitals have different m_l values and electrons may also occupy them singly or paired. Each different type of electronic arrangement gives rise to a microstate. Thus each electronic configuration will have a fixed number of microstates (d^6 = 210 microstates).

Under the influence of a crystal field, the d orbitals split into two sets - t_{2g} orbitals and e_g. These have T_{2g} and E_g symmetry respectively, giving the $^5T_{2g}$, ^5E_g crystal field substrates.

As mentioned above, these bands are weak since 'pure' d–d transitions are symmetry forbidden and they may occur only by mechanisms that permit the breakdown of the symmetry selection rule.

The large number of studies carried out on MC bands shows that ligands may be arranged in a series according to their capacity to cause d-orbital splitting, which is known as the "spectrochemical series" that for the more important ligands is:

CN > NO_2> phenantroline > bpyridine > SO_3^{2-}> NH_3> pyridine > NCS > H_2O > ONO > OH > F > SCN > Cl > Br > I.

For the same ligand, the splitting between the most stable and the most unstable d orbitals generally increases with increasing charge of the central metal and the principal quantum number of the metal d orbitals involved. So MC transitions move at higher energy on passing from Fe(II) to Ru(II) and to Os(II) compounds, belonging to the first, second, and third series of transition metals, respectively.

CT bands

The assignment of absorption bands as charge transfer (CT) transitions is based on the assumption that the central atom and the ligands interact weakly.[1, 3] Under this condition, the ground state can be described by a preponderant electron configuration consisting of 'localized' molecular orbitals. Thus, a defined oxidation state of the central metal can be determined and so CT transitions can be defined as those adding (or removing) one electron from the shell of the metal and hence changing its oxidation state by - 1 (or +1).

LMCT bands can be found in the UV region but they can extend to the visible spectral region, particularly for complexes containing highly reducing

ligands; MLCT transitions happens in complexes with central atoms having small ionization potentials and low oxidation state, with ligands which have available empty π* orbitals; LLCT (*ligand to ligand charge transfer*) can also take place when in the same complex are present an easily oxidizable ligand and a ligand with available empty π* orbitals. These transitions are common in cyclometalated compounds, especially where the cyclometalating ligands are negatively charged (*e.g.*, phenylpyridinato anion - ppy).

The above classification of electronic transitions, electronically excited states and energy ordering (Figure 3) loses its meaning whenever the involved states cannot be described by localized MO configurations. More generally, the excited-state energy levels are extremely sensitive to the type of the ligands and the nature and oxidation state of the metal centre.

Absorption spectral-bandwidth and excited states: Franck- Condon principle

The electron configuration of an excited state is usually different from that of the ground state, thus the geometry between these two states can be significantly different.[1,2,3]

The width of the absorption bands in transition-metal complexes provides useful information about the difference in the equilibrium nuclear configuration between ground and excited states. As a consequence of the Franck–Condon principle, the bandwidth is proportional to the slope of the potential curve of the excited state as a function of the internuclear distances, taken at the equilibrium point of the ground state.

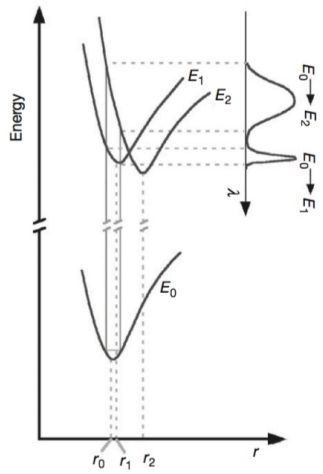

Figure 4.1: relation between bandwidth and equilibrium nuclear configuration in the ground and excited state

Even though this slope will also depend on the force constant of the

excited state, it can certainly be expected that the bandwidth will increase with the increasing difference between the ground and excited state equilibrium nuclear configurations (Figure 4.1).

The changes in shape and size of a complex in changing electronic state has an important role in determining not only the bandwidths of the radiative transitions, but also the rates of the radiation less conversions, and therefore the excited-state properties of the molecular species.

State energy diagrams: the Jablonski Diagram

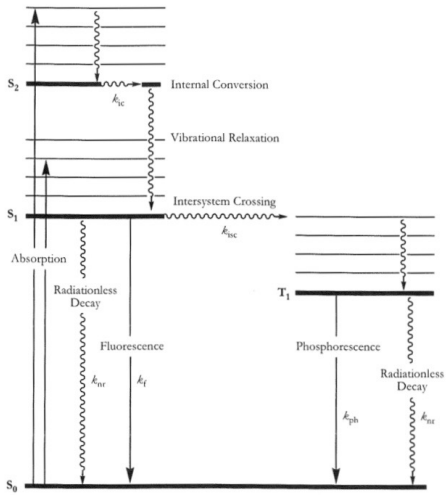

Figure 5.1: Jablonski diagram of photophysical processes

A state energy diagram displays electronic states, radiative and radiationless processes occurring between the ground state (S_0), the lowest energy excited state (S_1) and the lowest energy triplet state (T_1) of a molecule. Higher energy singlet and triplet states can also be included but as the Kasha's rule states, the excitation of these higher energy states generally results in deactivation of S_1 and T_1 faster than any other measurable process.[2]

In the Jablonski diagram (Figure 5.1), the *y*-axis represent the energy of the system, while the *x*-coordinate has no physical meaning because it is not a reaction coordinate. Transitions between any two electronic states in the diagram correspond to the possible connections between the states indicated and may be radiative or radiationless processes:

- Spin allowed singlet-singlet absorption of a photon ($S_0 + h\nu \longrightarrow S_1$); Absorption is a very fast transition, up to 10^{-15} seconds.
- Spin allowed singlet-singlet emission of a photon ($S_1 \longrightarrow S_0 + h\nu$) called

fluorescence, characterized by a rate constant K_f; Fluorescence is a slow process from 10^{-9} to 10^{-7} seconds;

- Spin forbidden singlet-triplet emission of a photon ($T_1 \longrightarrow S_0 + h\nu$) called *phosphorescence*, characterized by a rate constant K_p; Phosphorescence is a very slow process on the order of 10^{-4} to 10^{1} seconds;
- Spin allowed radiation less transitions between states of the same spin ($S_1 \longrightarrow S_0 +$ *heat*), called *internal conversion*, characterized by a rate constant K_{ic}; this process is very fast, between 10^{-14} and 10^{-11} seconds. Since this is a very fast transition, it is extremely likely to occur immediately following absorption.
- Spin forbidden radiationless transitions between excited states of different spin ($S_1 \longrightarrow T_1 +$ *heat*), called *intersystem crossing* characterized by a rate constant K_{isc}; ISC is a slow process, with a time scale from 10^{-8} to 10^{-3}seconds;
- Spin forbidden radiationless transitions between the triplet and the ground state ($T_1 \longrightarrow S_0 +$ *heat*), also called *intersystem crossing*.

The most relevant quantities employed to estimate the extent of competition among these processes are 1) the excited state lifetime (τ), expressed by the equation:

$$\tau = \frac{1}{K_f + K_{ic} + K_{isc} + K_{nr}}$$

that is generally defined by the time required for the emission intensity to fall to $1/e$ of its initial value and 2) the emission quantum yield (ϕ), which is the number of emitted photons relative to the number of absorbed photons

$$\phi = \frac{K_f}{K_f + K_{ic} + K_{isc} + K_{nr}}$$

Luminescent Metal Complexes of d^6 transition metal centres

Transition metal complexes displays interesting features and much more complicated photophysical properties as a consequence of the more complicated structure if compared to organic molecules. The presence of heavy metal ions induces a certain degree of spin orbit coupling that allows spin-forbidden electronic transitions.[3]

This effect becomes undeniable for second and third row transition metals, especially d^6 transition metals complexes such as ruthenium (II), iridium (III) and rhenium (I). In the ground state electronic configuration of these metal complexes there are no unpaired electrons, suggesting a singlet spin multiplicity (S_0). The spin orbit coupling allows an efficient ISC from the lowest singlet excited state to the lowest triplet manifold, inducing also an admixture between these states (^{3}MC, ^{3}MLCT ^{3}LC), eliminating the spin-forbidden nature of $T_1 \rightarrow S_0$ transition (*phosphorescence*).[2,3]

Both fluorescence and phosphorescence can be achieved through a right balance of electronic and geometrical requirements; as a general rule, luminescence can be observed even at room temperature if π-conjugated rigid ligands are employed, in order to avoid radiation less processes. Moreover, radiative processes are strictly correlated to the nuclear configuration of the ground and the excited states (Franck Condon Principle) and the degree of separation between these two electronic states (Energy Gap Law).[2,3]

The area of use of luminescent d^6 meal complexes can be determined by taking into account all the different characteristics and all the structural features of these systems.

Ruthenium (II) polypyridyl complexes

At a very early stage, transition metal photophysics was mainly dominated by studies concerning the class of ruthenium(II) polypyridyls, such as $[Ru(bpy)_3]^{2+}$ (bpy = 2,2′-bipyridine) and their ^{3}MLCT excited state, which makes the compound a relatively good luminophore.[3,4] (Figure 6.1)

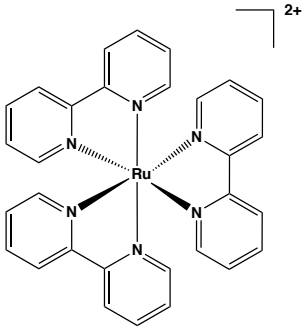

Figure 6.1: Structure of $[Ru(bpy)_3]^{2+}$

The emission maximum of $[Ru(bpy)_3]^{2+}$ occurs at λ = 620 nm, with a lifetime of about 1 ms and with an emission quantum yield Φ = 0.062. Its emission output is strongly dependent on temperature and on the rigidity of the media as a consequence of the presence of a low-lying ^{3}MC state, which contributes to the radiationless decay by a thermally activated surface crossing process.[5]

Within the wide selection of luminescent transition metal complexes known, this class is definitely the most extensively studied. Ruthenium polypyridyls in all their aspects have been employed both in bio-inorganics, as DNA intercalates (*i.e* $[Ru(bpy)_2(DPPZ)]$ Figure 7.1 left),[6] and as photosensitizers in the development of *Dye Sensitized Solar Cells* DSSCs ($[Ru(4,4'\text{-dicarboxy-}2,2'\text{-bipyridine})_2(NCS)_2]$ Figure 7.1, right).[7]

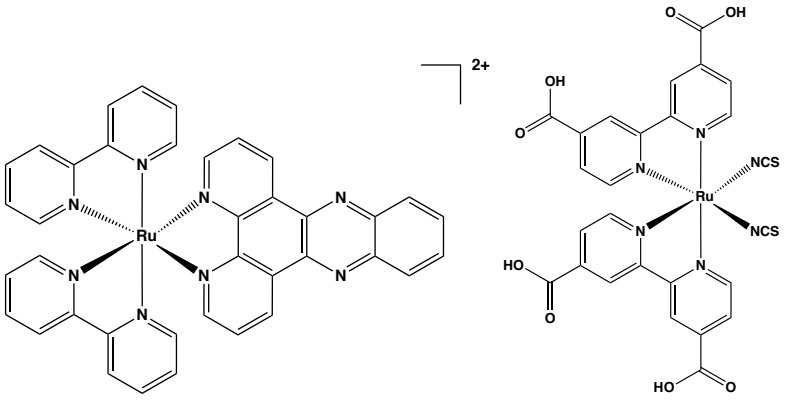

Figure 7.1 – Left: Structure of $[Ru(bpy)_2(DPPZ)]^{2+}$ – Right: Structure of $[Ru(dcbpy)_2(NCS)_2]$

Iridium (III) cyclometalated complexes

During the past decade, the scenario of luminescent metal complexes dominated by ruthenium(II) polypyridyl systems, has gradually been replaced by cyclometalated iridium(III) complexes with general formulae $[Ir(C\hat{}N)_2X_2]^+$ and $[Ir(C\hat{}N)_2(N\hat{}N)]^+$ (X = mono anionic ligands; C^N = cyclometalating ligands;

N^N = bidentate ligand), taking advantage of their less thermally accessible ^{3}MC state, high electrochemical reversibility that moves the MLCT states to higher energies, emission colour-tuning via ligand modifications and their photo and chemical stability.[3,4,8]

More than 90% of the known luminescent Ir(III) compounds, most of them cyclometalated species, have been reported in the last 10 years. Such a huge amount of studies is mainly associated with the application of luminescent Ir(III) systems as triplet emitters in the development of phosphorescent organic light emitting devices such as OLED (*Organic Light Emitting Devices*) and LEEC (*Light Emitting Electrochemical Cells*).

The first reported series of luminescent Ir(III) complexes is that of *fac*-tris-cyclometalated complexes, where the cyclometaling ligands (C^N) is represented by the phenylpyridinato anion (ppy).[9] The archetype $[Ir(ppy)_3]$ (Figure 8.1) is a neutral species with emission arising from an MLCT state, where the acceptor orbital is an empty π^* orbital mainly located at the pyridine ring.

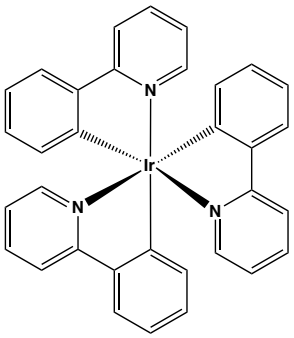

Figure 8.1: Structure of $[Ir(ppy)_3]$

This admixture between metal-centered and ligand-centered orbitals is common in cyclometalated iridium compounds, and, depending on the contribution to the HOMO composition, the emissive state can be termed as MLCT or LLCT. The photophysical properties of Ir(III) cyclometalates are extremely tunable, by the introduction of electron-withdrawing or electron-donating substituents on C^N ligands, as well as by choosing the appropriate set of ligands in preparing heteroleptic compounds.

Rhenium(I) triscarbonyl complexes

Besides ruthenium(II) and its heavier congener iridium(III), another d^6 MLCT class of compounds, that has attracted wide interest is the rhenium(I) triscarbonyl (N^N)-type complexes $[Re(CO)_3(N^N)X]^{0/+}$ (N^N = diimine; X =

anion or neutral ligand) (Figure 9.1).[2,3,4] These complexes were found to show intense luminescence and the origin has been attributed to the rhenium(I) to diimine MLCT excited state.[10]

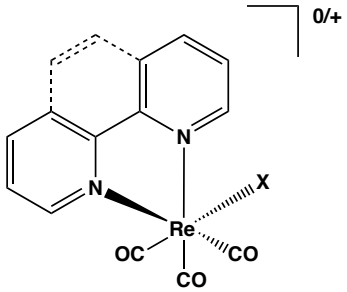

Figure 9.1: Structure of rhenium(I) triscarbonyl (N^N)-type complexes [Re(CO)$_3$(N^N)X]$^{0/+}$

The facile synthesis of *fac*–[Re(CO)$_3$(N^N)(L)]-type complexes and the modification of the diimine ligands themselves makes systematic tuning of the electronic properties easier for these complexes. Modification on the excited-state properties offers further insight about the role of the acceptor diimine ligand in the make up of both spectroscopic and photophysical features.

Many mononuclear diimine rhenium(I) triscarbonyl complexes are highly emissive and displays relatively long lifetimes (from 10 ns to 1 ms) in solution, due to the existence of lowest energy triplet-centered MLCT excited states.[11]

Clearly, there is an enormous interest around the photophysical and photochemical behavior of the excited states present in diimine rhenium(I) triscarbonyl complexes that has led to a wide range of applications, including their use as catalysts, [12] sensors, [13] light-emitting materials, [14] binding or photocleavage of DNA,[15] and radiopharmaceuticals.[16]

To summarize, the common thread of all the classes of luminescent metal complexes discussed above consist in the use of nitrogen-rich π-conjugated ligands.

In such a context, the spotlight of our research program is the preparation and the study of the physical and chemical properties of transition metal complexes containing 5-aryl tetrazolate [R-CN$_4$]$^-$ moiety. In particular we have demonstrated how these synthetically versatile nitrogen-rich ligands can actually rule the photophysical behavior of the corresponding Ru(II), Ir(III), and Re(I)– based species.

Chapter 2

Tetrazoles: synthetically versatile nitrogen-rich ligands for luminescent metal complexes

Abstract

This chapter focus on tetrazol(at)es and their numerous applications in organic chemistry, medicinal chemistry, explosives and, in particular, in coordination chemistry.

Introduction

Tetrazoles represent a class of heteocyclic compounds, which is characterized by the presence of at least one aromatic five-membered ring constituted by one carbon and four nitrogen atoms. In particular, 5-substituted 1*H*-tetrazoles [R-CN_4H] display Brønsted acidity values comparable to those of the corresponding carboxylic acids. This feature, in combination with their being metabolically more stable, less toxic and more lipophilic than the –COOH analogues, has primarily driven the application of tetrazole derivatives in pharmacology, with the introduction of the tetrazole group in place of carboxylic acids in the structure of antagonists of angiotensin, leading to a class of drugs (sartans) which has proven successful in the treatment of hypertension (Figure 1.2).[17, 18]

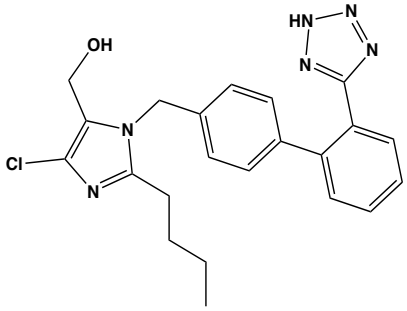

Figure 1.2: Losartan®, the first angiotensin receptor blocker

As nitrogen rich ligands, aromatic tetrazoles and tetrazolates can lead to the evolution of up to two molecule of dinitrogen. This is a key point for the development and application of tetrazoles as primary or secondary, propellants and pyrotechnics. Commonly referred as 'high energy-density materials' or 'energetic materials', their major drawback of insufficient thermal stability, has recently been solved.[19]

Syntheses of 5-aryl tetrazoles

Typically, the synthesis of tetrazoles relies upon the 1,3 dipolar cyclization of the azide anion onto the appropriate nitriles (Figure 2.2).

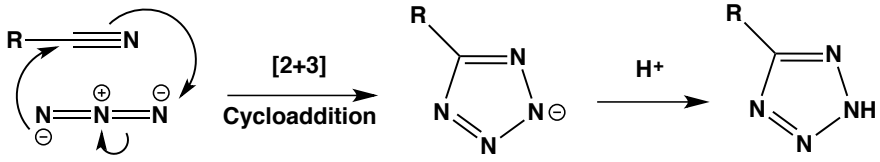

Figure 2.2: 1,3 dipolar cycloaddition mechanism

This Huisgen-type reaction has been modified and significantly improved from its first appearance in the late 50's. In 1958, indeed, Finnegan and coworkers described a procedure in which the 1,3 dipolar cyclization of the azide anion onto electron poor aromatic nitriles occurred in high boiling solvent such as DMF and in combination with various additives (NH_4Cl, LiCl, Figure 3.2).[20]

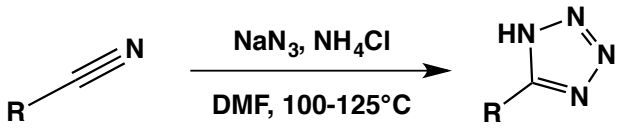

Figure 3.2: Finnegan's method for the preparation of tetrazoles

A method of general validity – thereby suitable for alkyl and aryl cyanides containing both electron donor and withdrawing groups, was reported only 40 years later when Koguro and coworkers established a synthetic protocol in which DMF was replaced by toluene and triethyl ammonium chloride was the only additive required (Figure 4.2).[21]

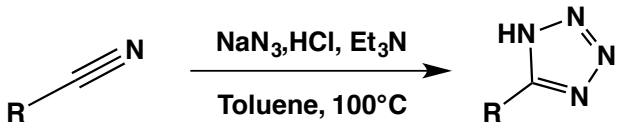

Figure 4.2: Koguro's method for the preparation of tetrazoles

A significant break-through in the synthesis of tetrazoles came in 2001 with a report from the group of Sharpless.[22] This method again involved the "usual" treatment of a nitrile with sodium azide but, different to the previous protocols, zinc bromide was employed as the additive for the reactions, which were performed in aqueous medium (Figure 5.2). Following the removal of $Zn(OH)_2$,

the desired tetrazoles could be obtained upon acidification of the aqueous solution. It is worth noting that the isolation of the intermediates represented by Zn-coordinated tetrazolates opened the way to the study of tetrazole and tetrazolate based MOFs, whose synthesis was successively optimized by the reaction the appropriate nitriles with a variety of metal salts in hydrothermal conditions.

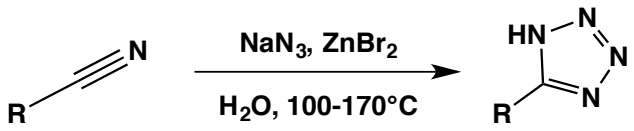

Figure 5.2: Sharpless' method for the preparation of tetrazoles

Luminescent Tetrazole-based Metal Complexes

Unlike the studies devoted to their application in pharmacology, the coordination chemistry of tetrazoles and tetrazolates has been developed only from the 2000's. This is quite surprising, especially in consideration of the fact that tetrazoles or tetrazolates contain three or four diimine-type nitrogens, all of which are capable of binding transition metal and lanthanide ions. As a consequence, this is a class of privileged ligands for coordination chemistry, and offer different coordination sites with the possibility to obtain mono and multinuclear transition metal arrays and lanthanide-based complexes (Figure 6.2).

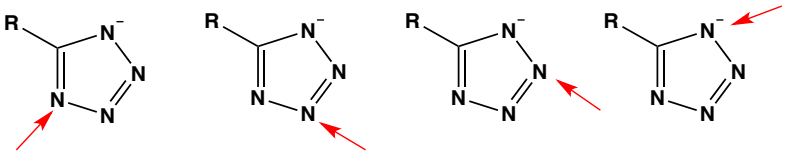

Figure 6.2: Coordination modes of 5-substitued tetrazolates

Over the past 15 years, the research group in which I have completed my PhD has actively pursued studies dealing with the coordination chemistry of 5-aryl tetrazolates and the reactivity toward electrophiles of metal tetrazolate complexes. In the earliest stage of such research, the first examples of "classical" organometallic Fe(II)-cyclopentadienyl complexes containing 5 aryl tetrazolates were reported,[23] enlightening also the possibility of inducing permanent (by the addition of CH_3^+) or reversible (by a protonation – deprotonation mechanism) modification of the structure of the tetrazolate ligands through electrophlic additions to the coordinated penatomic ring (Figure 7.2).

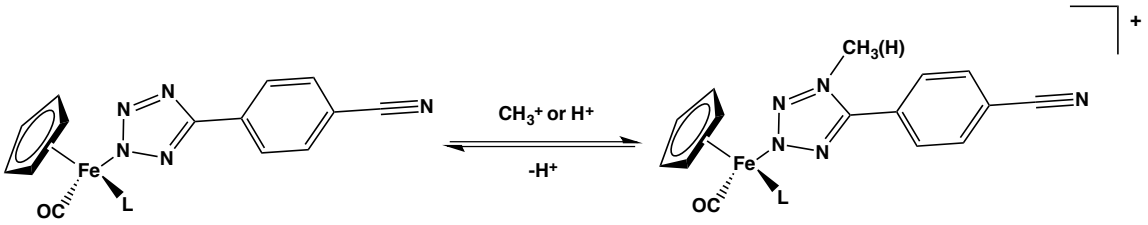

Figure 7.2: Electrophilic addition on Fe(II) tetrazolate complexes

Since the beginning, the research efforts have been devoted to the study of both structural and reactivity features of 5 aryl tetrazolate-organometallic compounds. In this context, the regioselective coordination of the $[R\text{-}CN_4]^-$ moiety to the Fe(II) metal centre together with the unique reactivity displayed through permanent or reversible electrophilic addition was observed.

The lessons learnt from the study of Fe(II)-tetrazolate complexes constituted the basis for the development of the coordination chemistry of 5-aryl tetrazolates toward Ru(II)-polypyridyl complexes. In the first instance, the Ru(bpy)(tpy)- moiety was chosen as the metal fragment, and the resulting Ru(II) 5-aryl tetrazolate complexes actually revealed the same structural feature and the same reactivity with electrophiles (Figure 8.2, top) that were displayed by the parent organometallic Fe(II) tetrazolate complexes.[24]

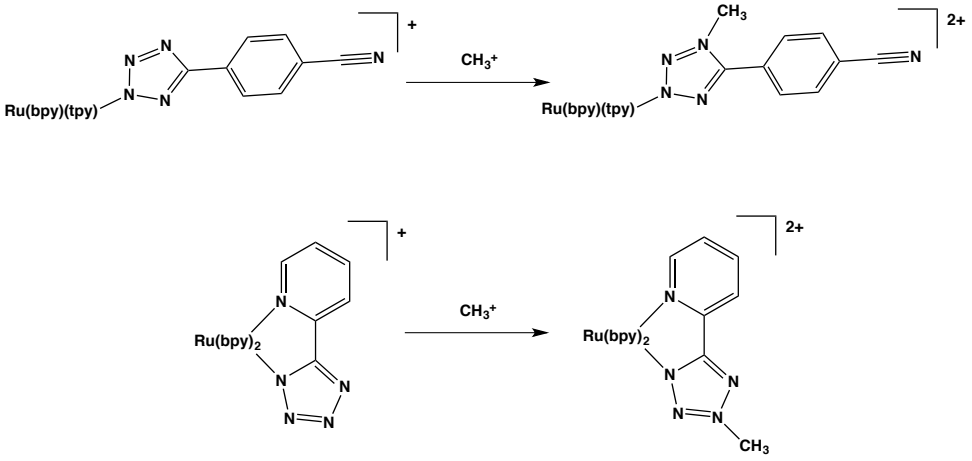

Figure 8.2: Electrophilic addition on Ru(II) tetrazolate complexes

In addition, the Ru(II) tetrazolate complexes revealed very interesting electrochemiluminescent performances, thereby paving the way for new research possibilities of Ru(II)- based metal tetrazolates. To gain more insights about the luminescence properties, the tetrazolates compounds were appended with 2-pyridyl or 2-pyrazinyl rings, leading to the formation of chelating ligands capable of coordination to $Ru(bpy)_2$- type fragments (bottom of Figure 8.2).[25,26] The

new Ru(II) chelates displayed peculiar reactivity toward electrophiles, whose addition again occurred to the coordinated tetrazolate ring in a regioselective manner. Importantly, a clear and distinguishable variation of the emission properties of the complexes was observed upon addition of electrophiles was observed, witnessing for the first time ever how the tetrazolate ligands could actually play a role in determining the energy and the composition of the HOMO and/or LUMO levels of the corresponding complexes.

This influence became extremely evident when our studies about the coordination chemistry of tetrazolate ligands were extended to the other classes of d^6 metal complexes such as Ir(III) cyclometalates and Re(I) triscarbonyl diimine derivatives. In particular, Ir(III)-tetrazolate cyclometalated complexes were found to be highly phosphorescent,[27] with emission colours that could be might be tuned either by changing the nature of the tetrazolate ligand or through electrophilic addition onto the $[R\text{-}CN_4]^-$ moiety, leading to the formation of the corresponding cationic species (Figure 9.2).[28] Such kind of reactivity was found to induce significant variations of the photophysical output of the starting neutral Ir(III) complexes,[29] whose emission maxima significantly red shift upon addition of electrophiles.

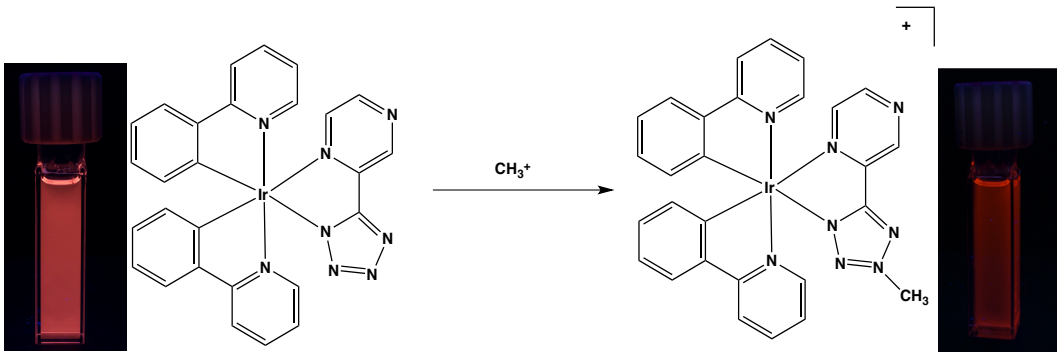

Figure 9.2: Electrophilic addition on Ir(III) tetrazolate complexes

These experimental evidences again witnessed the essential role played by the tetrazolate ligands in determining the photoluminescent output of the corresponding Ir(III) metal complexes and their relevant contribution in determining the composition of the LUMO energy level.

Relative to the studies dealing with Re(I) derivatives, the coordination of tetrazolate anions to *fac*-$[Re(CO)_3(N\text{^}N)(X)]$-type complexes, (where N^N =

diimine such as 1,10 phenantroline or 2,2′ bipyridine, X = Br), led to the formation of a new class of phosphorescent neutral compounds which displayed a photoluminescence properties in line with those "typical" of Re(I) triscarbonyl complexes (Figure 10.2).[30] Nevertheless, the emission properties of the Re-tetrazolate complexes appeared to be strongly influenced by the nature of the tetrazolate ligand, which was determined as major contributor to the HOMO level.[31]

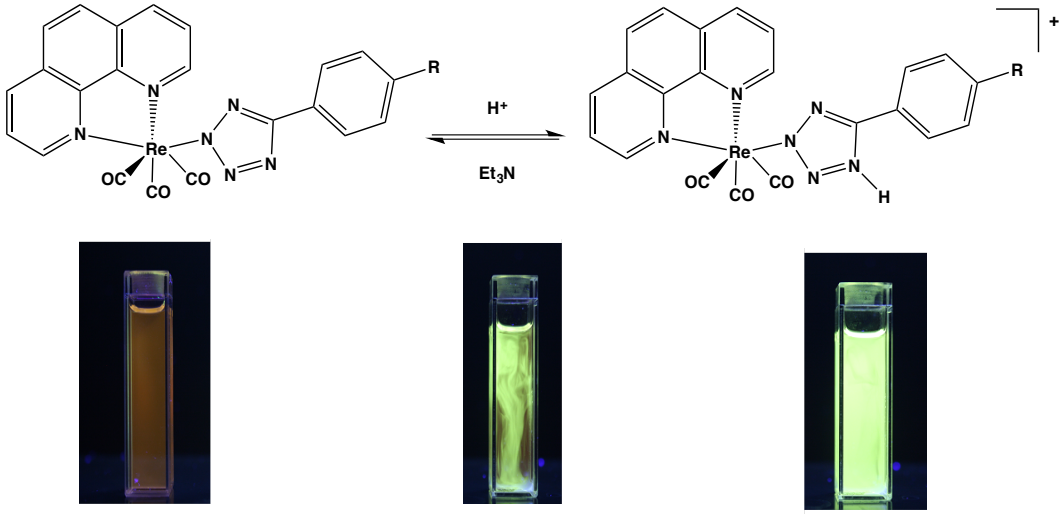

Figure 10.2: Electrophilic addition on Re(I) tetrazolate complexes

In a biological context, Re(I) tetrazolate derivatives have been studied since a specific class of neutral derivatives displayed a particular affinity for the so called "lipid droplets" (Figure 11.2). The "*in vivo*" selective localization of Re(I) tetrazolate complexes was recognized by the means of IR and Raman Spectroscopy as well as Confocal Microscopy.[32, 33]

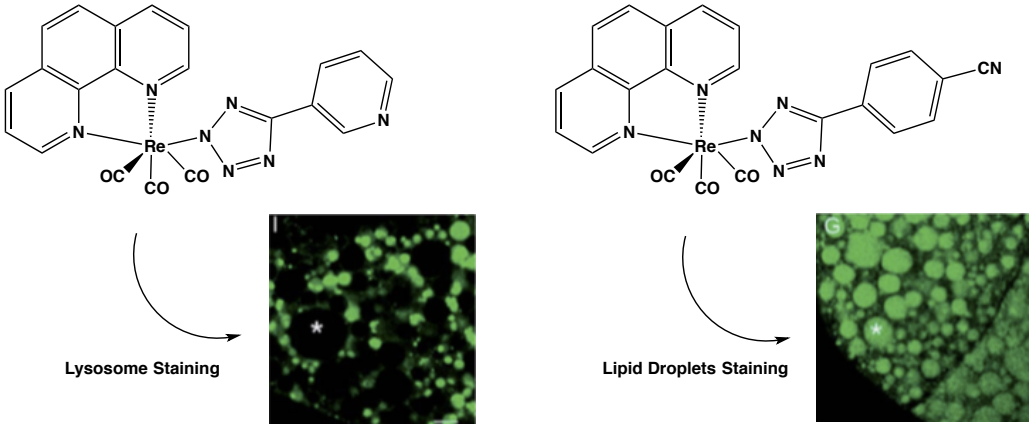

Figure 11.2: Selective intracellular localization of Re(I) tetrazolate complexes

It is very important to note that, analogously to Fe(II), Ru(II) ad Ir(III) tetrazolate systems, also neutral *fac*-[Re(N^N)$(CO)_3$(L)] tetrazolate complexes undergo electrophilic substitutions at the coordinated tetrazolate ring. Depending on the nature of the electrophile, these reactions can be considered either as reversible (*i.e.* protonation – deprotonation) or permanent, as in the case of the methylation reaction. In all cases, the addition of an electrophile corresponds to modification of the structure of the whole tetrazolate ligand and, importantly, involves an evident blue shift of the emission profile of the whole Re(I) complex. Also, the electrophilic attack determines an impressive "boosting" of the emission performances, as evidenced by the substantial increase of the PLQY values and the elongation of the phosphorescence lifetimes that take place upon the conversion of the starting neutral Re(I) tetrazolates into the corresponding cationic and protonated (or methylated) Re(I) tetrazole complexes.

On the basis of a similar scientific background, I focussed my PhD research activity on the design, the synthesis and reactivity studies of newer types or classes of Ir(III) and Re(I) tetrazolates as well as to endeavour the establishment of new strategies to combine different metal fragments within the same molecules through tetrazolate-based ligands. Also some examples of "oldies but goodies" Ru(II) tetrazolate complexes have been prepared and investigated.

In the first stage of my PhD, a new class of negatively charged Ir(III) complexes was prepared (Chapter 3 and 4). The combination of such anionic derivatives with cationic Ir(III)-tetrazole complexes gave rise to a series of ion pairs ("soft salts", Chapter 5) in which the emission white light can be achieved upon the choice of the appropriate ionic components. In all cases, the emission colour is sensitive to dissolved O_2, suggesting the use of these new ion pairs as O_2 luminescence sensors.

The potential as luminescent chemosensors of metal tetrazolate complexes has been explored starting from a new class of Re(I) triscarbonyl tetrazolato (Chapter 7). These Re(I) tetrazolate complexes displayed specific variations of their luminescent output upon interaction with metal divalent cations with a relevant biological role.

The sensing/antibacterial *in vitro* ability of metal tetrazolate complexes was further investigated with studies concerning the bactericidal abilities of

Ir(III) tetrazolate complexes against *E. coli* and *D. radiodurans*. The obtained results, *albeit* preliminary, appear extremely promising (Chapter 6).

This experimental work was also dedicated to the synthesis of heterobimetallic complexes in which different tetrazolates constitute the bridge between Ir(III) and Re(I) peripheral metal fragments (Chapter 8).

Moreover, studies which have dealt with Ru(II) tetrazolate complexes, pointed the way for the preparation of tetrazole –based Dye Sensitized Solar Cells (Chapter 9).

Chapter 3

Anionic Ir(III) Tetrazolate Complexes*

Abstract

Even through the scenario of Ir(III) cyclometalated complexes is largely dominated by neutral and cationic derivatives with general formula $[Ir(C^N)_2(N^N)]^{n+}$, negatively charged Ir(III) cyclometalated complexes have also attracted increasing attention in light of their favourable photophysical properties. At this regard, the coordination chemistry of tetrazolate derivatives has experienced a great development in the past years, leading to the preparation of both neutral and cationic Ir(III) complexes, luminescent compounds whose emission properties are strictly correlated to the nature of the tetrazolate moiety used. Further developments in the chemistry of Ir(III) tetrazolate complexes have been reached through the achievement of a new class of anionic derivatives, brightly phosphorescent compounds which complete the family of tetrazole-based Ir(III) complexes. The synthetic approach used, together with the unique photophysical properties displayed by these compounds will be discussed.

: This chapter is part of Dalton. Trans*, **2016, *45*, 3256.[34]

Introduction: A New Class of Anionic Ir(III) Cyclometalated Complexes

Expressions like "outstanding emission performances", "tuning of the emission colour" and "synthetic versatility" are all typically used to connote Ir(III) cyclometalated (C^N) compounds, a family of transition metal complexes that includes homoleptic neutral derivatives as well as heteroleptic neutral and ionic species. In its entirety, such a similar picture explains the reasons for which Ir(III) cyclometalated complexes have definitely become one of the most popular class of phosphorescent emitters for a variety of applications in important research fields such as sensing, luminescent targeting of biological molecules and, in particular, solid state lighting. Ir(III) cyclometalated complexes can be indeed customized for producing the emission of specific colours (*i.e.* the primary ones) or their net charge, providing therefore electrically neutral phosphors targeted for OLED (*Organic Light Emitting Diode*)-type technology, or ionic Ir(III) transition-metal complexes (*Ir-iTMC*) as emitters for Light Emitting Electrochemical Cells (LEECs), an alternative kind of electroluminescent devices.

Even though the scenario of luminescent Ir-iTMCs is largely dominated by cationic species with the general formula $[Ir(N^C)_2(N^N)]^+$, where the neutral ligand is most often represented by aromatic diimines (N^N),[35] negatively charged Ir(III) cyclometalated complexes have also attracted increasing attention in light of their favourable photophysical properties. More specifically, studies dealing with this family of brightly phosphorescent complexes, which is centred around the archetypal Ir(III)-cyanometallates $[Ir(ppy)_2(CN)_2]^-$ and its fluorinated

analogue $[Ir(F_2ppy)_2(CN)_2]^-$,[36] have demonstrated how the alkali salts of these anionic species can be considered as promising emissive materials both for LEECs and,[37] when paired to a cationic Ir(III) complexes to form the so called "Ir-based soft salts",[38] for OLED-type devices.[39]

Further to applications in the field of solid state lighting, the such anionic Ir(III) cyanometallates display the not less important and peculiar possibility of being incorporated into photophysically performing supramolecular assemblies, where $[Ir(ppy)(CN)_2]^-$ can act as the sensitizing unit for lanthanide (III) cations or as energy donor group for peripheral metal fragments.[40]

These results, in combination with our past and current research interests dealing with the study of luminescent metal complexes containing tetrazolate ligands, have prompted us to design and prepare a new family of negatively charged Ir(III) cyclometalated complexes based on the archetypes $[Ir(ppy)_2(CN)_2]^-$ and $[Ir(F_2ppy)_2(CN)_2]^-$ (Figure 1.3).

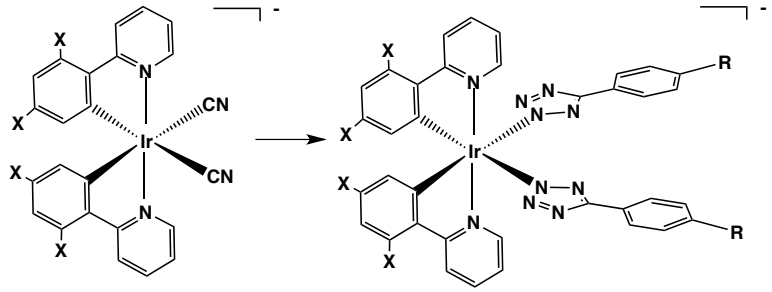

Figure 1.3: Left, general structure of $[Ir(C^N)_2(CN)_2]$; Right, general structure of Anionic Ir(III) Tetrazolate complexes

For doing this, we have modified the ligands set of such complexes by replacing the coordinated cyanides with two more bulkier anionic 5-aryl tetrazolates $[R\text{-}CN_4]^-$ such as the deprotonated form of [H-TphCN] (4-(1*H*-tetrazol-5-yl)benzonitrile), [H-Tph] (5-phenyl-1*H*-tetrazole) and [H-TphBr] (5-(4-bromophenyl)-1*H*-tetrazole), generally denoted as L, leading therefore to the series of derivatives with the general formula $[Ir(C^N)_2(L)_2]^-$ - from now on $[Ir(L)_2]^-$ (where (C^N) = ppy for the fluorine-free derivatives and for $[F_2Ir(L)_2]^-$ (C^N) = F_2ppy).

Importantly, the preparation of these unprecedented anionic Ir(III) complexes allowed us to complete the family of cyclometalated Ir(III)-tetrazolate complexes,[26, 27, 28] the examples of which were so far represented by the corresponding neutral and cationic species.

Synthesis and Characterization of Anionic $[Ir(L)_2]^-$ / $[F_2Ir(L)_2]^-$ Type Complexes

The preparation of the target anionic complexes has been accomplished through a slight modification of the literature first reported method.[36] In particular, (Figure 2.3) the chloride bridged Ir(III) dimer both fluorinated (F_2ppy) or not (ppy), was reacted with a molar excess of the appropriate 5-aryl tetrazole in the presence of an equimolar amount of a base such as triethylamine (Et_3N). In all cases, the expected saline compounds were simply precipitated with a small amount of Et_2O and filtered off after 24 hours at reflux, requiring no further purification.

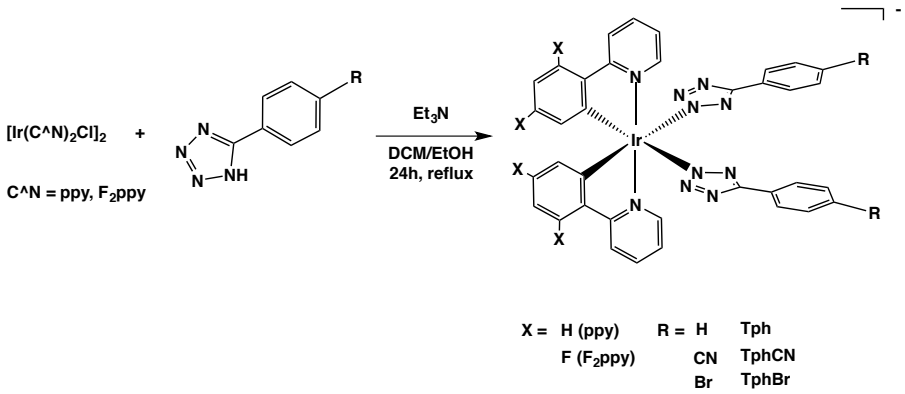

Figure 2.3: Synthetic procedure used for Anionic Ir(III) tetrazolate complexes and acronyms used

The formation of the desired anionic complexes was first deduced by Electron Spray Ionisation Mass Spectrometry (ESI-MS), which provided *m*/*z* signals congruent with the expected anions. The scans in the region of positive ions evidenced the presence of the pattern corresponding to triethylammonium $[Et_3NH]^+$ cations (Figure 3.3).

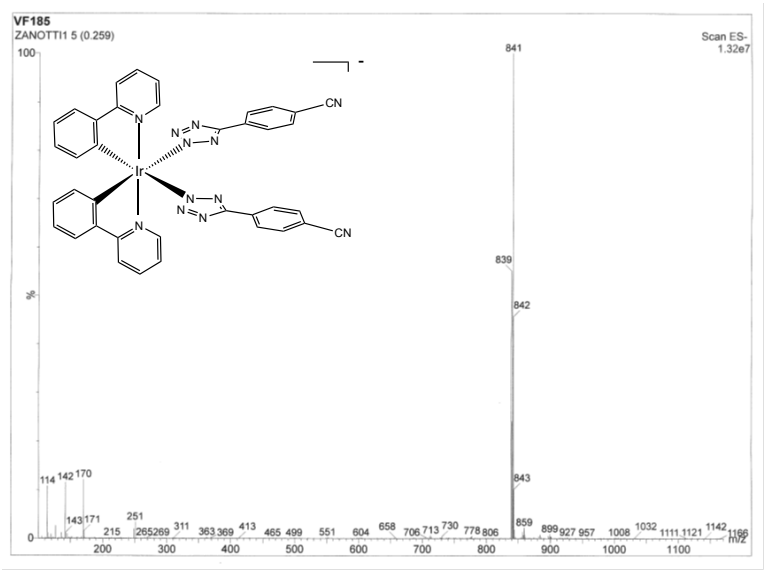

Figure 3.3: ESI-MS spectrum (negative ions region) of [Ir(TphCN)$_2$], [M]$^-$ = 841 (m/z)

The NMR characterization of the anionic complexes provided results consistent with the formation of species having the expected C_{2v} symmetry, as witnessed by the ^{1}H and ^{13}C NMR spectra displaying a number of resonances in the aromatic region equal to the half of the total number of the protons or carbons of the complexes.

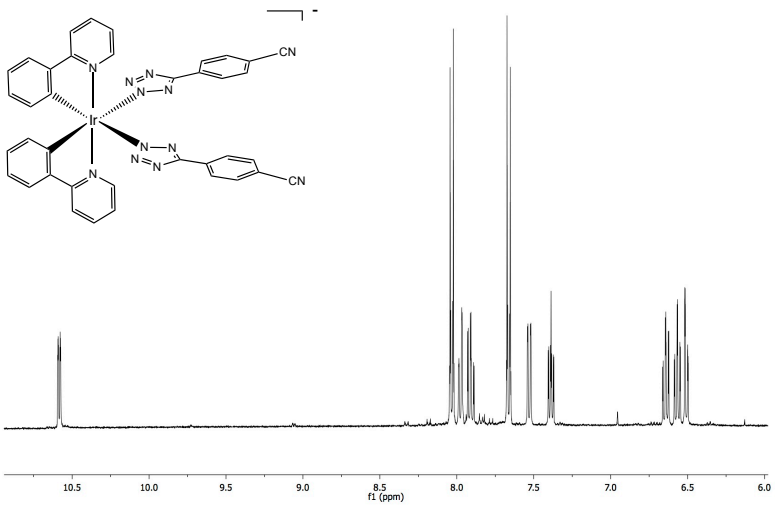

Figure 4.3: ^{1}H-NMR of [Ir(TphCN)$_2$]$^-$ Acetone-d$_6$, 400 MHz, r.t.

Also, from the deeper analysis of the ^{1}H (Figure 4.3) and, particularly, of the ^{13}C NMR spectra of the anionic complexes (Figure 5.3), it was possible to determine that each of the 5-aryl tetrazolates regioselectively coordinates the Ir(III) center through the N-2 position of the five-membered ring, as evidenced by the

presence of one single tetrazolate carbon (Ct) resonance falling at a chemical shifts value (Ct = *ca.*163 ppm) that is diagnostic for the occurrence of N-2 linkage isomers.

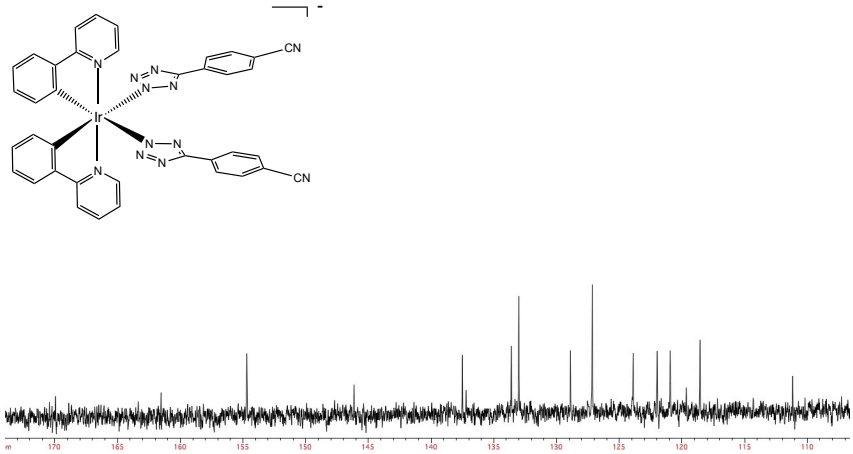

Figure 5.3: ^{13}C-NMR of [Ir(TphCN)$_2$]$^-$ Acetone-d$_6$, 100 MHz, r.t.

Photophysical Properties

In dichloromethane solutions maintained at room temperature, all the new Ir(III)-tetrazolate anionic complexes show quite typical and similar absorption profiles. Up to 300 nm, each spectrum is dominated by intense and spin allowed ligand centred (^{1}LC) π-π* transitions involving both the cyclometalating and the ancillary tetrazolate ligands. Weaker and broader spin allowed ^{1}MLCT and spin forbidden ^{3}MLCT bands are found at longer wavelength (300 to 380 nm) and tail off to the visible region (Figure 6.3).

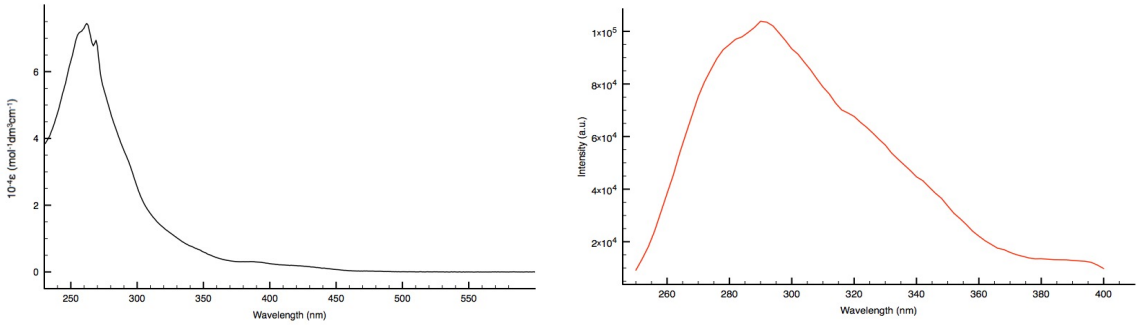

Figure 6.3: Left - Absorption profile [Ir(TphCN)$_2$], Right – Excitation profile [Ir(TphCN)$_2$]$^-$ λ_{em} = 490 nm; CH_2Cl_2, r.t.

Upon excitation of the ^{1}MLCT features (λ= 370 nm) of the corresponding diluted dichloromethane solution (*ca.* 10^{-5}M), each of the new Ir(III) complexes display brightly intense blue (in the cases of the [F$_2$Ir(L)$_2$]$^-$ derivatives, Figure 8.3) or blue-green (as for the fluorine-free [Ir(L)$_2$]-type complexes, Figure 7.3) luminescence

originating from excited states of triplet character, as witnessed by the increase of emission quantum yield (ϕ) and the concomitant elongation of the emission lifetimes (τ) that took place on passing from air-equilibrated to deoxygenated solutions (Table 1).

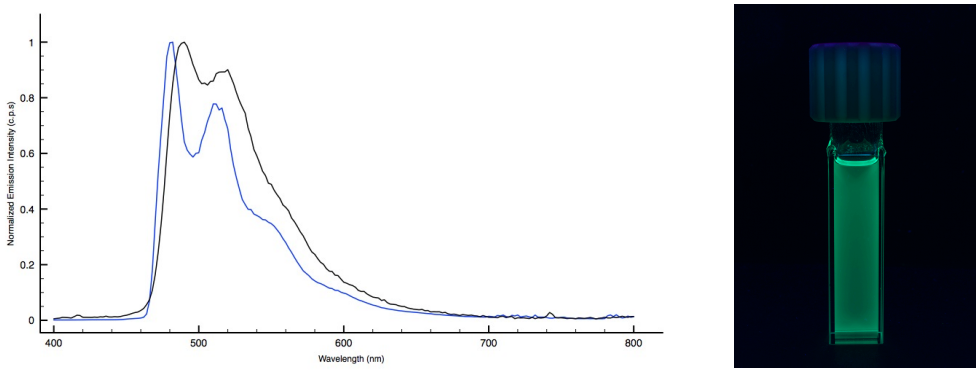

Figure 7.3: Left, Emission spectra [Ir(TphCN)$_2$], 298K (black line), 77K (blue line), CH_2Cl_2. Right, [Ir(TphCN)$_2$]10^{-5}M air equilibrated, CH_2Cl_2solution, r.t; λ_{exc}= 365 nm

In general, the photoluminescent output of the negatively charged Ir(III) tetrazolate complexes $[Ir(L)_2]^-$ and $[F_2Ir(L)_2]^-$ is almost completely governed by the nature of the cyclometalating ligands C^N (F_2ppy or ppy), with no detectable influence played by the various 5-aryl tetrazolates (denoted as L) that complete the coordination sphere of the Ir(III) center. This feature is evidenced by the analysis of the emission profiles of the new complexes, which are found coincident along the series of the $[Ir(L)_2]^-$ and $[F_2Ir(L)_2]^-$ based species and always consist of an intense band at higher energy followed by an almost equally intense vibronic progression (Table 1, Figures 7.3, 8.3).

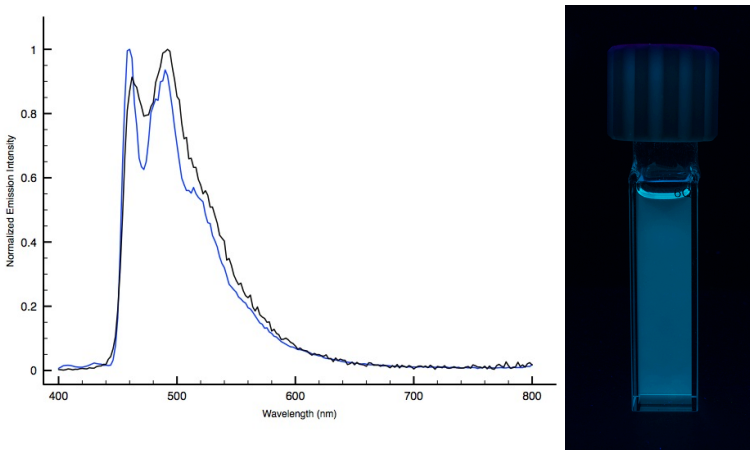

Figure 8.3: Left, Emission spectra [F$_2$Ir(TphCN)$_2$], 298K (black line), 77K (blue line), CH_2Cl_2. Right, [F$_2$Ir(TphCN)$_2$]$^-$ 10^{-5}M, air equilibrated CH_2Cl_2solution, r.t; λ_{exc}= 365 nm

The occurrence of such similarly structured emission spectra from Ir(III) cyclometalated complexes is representative for the interplay of ^{3}LC/^{3}MLCT type emissive excited states. In our cases, the likely prevalent contribution of the ^{3}LC states over the ^{3}MLCT ones is suggested by the rather small rigidochromic blue shift of the emission maxima that was encountered at 77K (Figures 7.3, 8.3).

Table 1: Photophysical Data of Anionic Ir(III) Tetrazolate Complexes

CH_2Cl_2 as solvent	***Absorption*** λ_{abs}(nm);($10^4\varepsilon$)($M^{-1}cm^{-1}$)	***Emission 298 K***					***Emission 77K***	
		λ_{em} (nm)	τ_{air} (μs)	τ_{Ar} (μs)	ϕ_{air}(%)	ϕ_{Ar}(%)	λ_{em}(nm)	τ (μs)
$[Ir(Tph)_2]^-$	255(4.8), 346(0.44), 387(0.20)	484, 514	0.12	1.27	5.5	60.6	480, 510	4.09
$[F_2(IrTph)_2]^-$	254(5.9), 308(1.2), 370(0.22)	462, 490	0.16	1.99	5.9	49	458, 490	3.23
$[Ir(TphCN)_2]^-$	260(7.3), 295(3.1) 393 (0.2)	490, 520	0.11	0.80	3.4	24.9	480, 516, 556$_{sh}$	4.03
$[F_2Ir(TphCN)_2]^-$	260(4.0), 377(0.24), 318(1.1)	462, 492	0.17	1.35	3.3	22	460, 490, 522$_{sh}$	3.25
$[Ir(TphBr)_2]^-$	260(4.2)	486, 518	0.11	1.18	3.6	55.2	476, 510	3.96
$[F_2Ir(TphBr)_2]^-$	256(4.1), 370(0.31)	462, 490	0.17	1.47	3.82	49.7	452, 484	3.47

The comparison of the photoluminescence properties of the Ir(III)-tetrazolate complexes described herein with those reported for the parent Ir(III)cyanometallates $[Ir(ppy)_2(CN)_2]^-$ and $[Ir(F_2ppy)_2(CN)_2]^-$, enlightens how the replacement of the cyanide groups with the bulkier 5-aryl tetrazolate ligands seems to not affect the emission performances of the resulting Ir(III) complexes, which again display remarkably high PLQY, ranging from 20% up to 60% in deoxygenated solutions, and radiative lifetimes in the microsecond scale (0.8 to 2 μs).

Conclusions

We have synthesized and fully characterized the very first examples of anionic Ir(III) tetrazolate complexes, bearing two cyclometalating ligands such as (ppy) or its fluorinated analogue (F_2ppy) and two variously decorated tetrazole ligands. Furthermore, this new class of anionic derivatives allowed us to complete the family of Ir(III) tetrazolate complexes, which is now composed by neutral, cationic and anionic components. The photophysical characterization of these new Ir(III) anionic derivatives has highlighted a sky blue or aqua phosphorescent emission arising from ^{3}LC/^{3}MLCT type emissive excited states, with no significant influence played by the different 5-aryl tetrazolate used. The likely prevalent contribution of the ^{3}LC states over the ^{3}MLCT states is suggested by the rather small rigidochromic blue shift that was encountered at 77 K. The high PLQY values, together with microsecond decay times suggest how these anionic tetrazolate derivatives can be used as dopants in the fabrication of LEEC-type devices, as well as their use as the anionic counterpart in making Ir(III) ion pairs (Chapter 5).

Experimental Section

General considerations. All the reagents and solvents were obtained commercially (e.g. Aldrich) and used as received without any further purification, unless otherwise specified. All the reactions were carried out under an argon atmosphere following Schlenk protocols. Where required, the purification of the Ir(III) complexes was performed via column chromatography with the use of neutral alumina as the stationary phase. ESI-mass spectra were recorded using a Waters ZQ-4000 instrument (ESI-MS, acetonitrile as the solvent). Nuclear magnetic resonance spectra (consisting of ^{1}H and ^{13}C) were always recorded using a Varian Mercury Plus 400 instrument (^{1}H, 400.1; ^{13}C, 101.0 MHz.) at room temperature. ^{1}H and ^{13}C chemical shifts were referenced to residual solvent resonances.

Photophysics. Absorption spectra were recorded at room temperature using a Perkin Elmer Lambda 35 UV/vis spectrometer. Uncorrected steady-state emission and excitation spectra were recorded on an Edinburgh FLSP920 spectrometer equipped with a 450 W xenon arc lamp, double excitation and single emission monochromators, and a Peltier-cooled Hamamatsu R928P photomultiplier tube (185–850 nm). Emission and excitation spectra were acquired with a cut-off filter (395 nm) and corrected for source intensity (lamp and grating) and emission spectral response (detector and grating) by a calibration curve supplied with the instrument. The wavelengths for the emission and excitation spectra were determined using the absorption maxima of the MLCT transition bands (emission spectra) and at the maxima of the emission bands (excitation spectra). Quantum yields (Φ) were determined using the optically dilute method by Crosby and Demas[41] at excitation wavelength obtained from absorption spectra on a wavelength scale [nm] and compared to the reference emitter by the following equation:[42]

$$\phi_s = \phi_r \left[\frac{A_r(\lambda_r)}{A_s(\lambda_s)}\right]\left[\frac{I_r(\lambda_r)}{I_s(\lambda_s)}\right]\left[\frac{n_s^2}{n_r^2}\right]\left[\frac{D_s}{D_r}\right]$$

where A is the absorbance at the excitation wavelength (λ), I is the intensity of the excitation light at the excitation wavelength (λ), n is the refractive index of the solvent, D is the integrated intensity of the luminescence, and Φ is the quantum yield. The subscripts r and s refer to the reference and the sample,

respectively. A stock solution with an absorbance > 0.1 was prepared, then two dilutions were obtained with dilution factors of 20 and 10, resulting in absorbances of about 0.02 and 0.08 respectively. The Lambert-Beer law was assumed to remain linear at the concentrations of the solutions. The degassed measurements were obtained after the solutions were bubbled for 10 minutes under Ar atmosphere, using a septa-sealed quartz cell. Air-equilibrated $[Ru(bpy)_3]Cl_2/H_2O$ solution (Φ = 0.028)[43] was used as reference. The quantum yield determinations were performed at identical excitation wavelengths for the sample and the reference, therefore deleting the $I(\lambda r)/I(\lambda s)$ term in the equation. Emission lifetimes (τ) were determined with the single photon counting technique (TCSPC) with the same Edinburgh FLSP920 spectrometer using pulsed picosecond LED (EPLED 360, fhwm < 800 ps) as the excitation source, with repetition rates between 1 kHz and 1 MHz, and the above-mentioned R928P PMT as detector. The goodness of fit was assessed by minimizing the reduced $\chi 2$ function and by visual inspection of the weighted residuals. To record the 77 K luminescence spectra, the samples were put in quartz tubes (2 mm diameter) and inserted in a special quartz dewar filled with liquid nitrogen. The solvent used in the preparation of the solutions for the photophysical investigations was of spectrometric grade. Experimental uncertainties are estimated to be ±8% for lifetime determinations, ±20% for quantum yields, and ±2 nm and ±5 nm for absorption and emission peaks, respectively.

Ligand synthesis

Following the general method reported by Koguro and coworkers,[21] tetrazole ligands [**Tph**-H] 5-phenyl-1*H*-tetrazole, [**TphCN**-H] 4-(1*H*-tetrazol-5-yl)benzonitrile and [**TphBr**-H] 5-(4-bromophenyl)-1*H*-tetrazole, were obtained in almost quatitative yield.

[**Tph-H**] ^{1}H-NMR (DMSO d^6, 400 MHz) δ (ppm) = 8.06 - 8.03 (m, 2H), 7.62 -7.60 (m, 3H). [**TphCN-H**] ^{1}H-NMR (DMSO d^6, 400 MHz) δ (ppm) = 8.06 (d, 2H, J_{H-H} = 3.99 Hz) 8.31 (d, 2H, J_{H-H} = 7.99 Hz). [**TphBr-H**] ^{1}H-NMR (DMSO d^6, 300 MHz) δ (ppm) = 7.99 (d, 2H, J_{H-H} = 8.39 Hz), 7.83 (d, 2H, J_{H-H} = 8.09 Hz).

General Procedure for the Preparation of the Anionic $[Ir(L)_2]^-$ / $[F_2Ir(L)_2]^-$ Type Complexes

In a 50 mL two neck round bottom flask equipped with a stirring bar, 0.100 g (1 equiv.) of dichlorobridged iridium dimer and 10 equiv. of the desired tetrazole ligand were added to a 3:1 solution of dichloromethane/ethanol. Then, 10 equiv. of Et_3N were added, and the resulting mixture was stirred at reflux for 24 h. A 1:1 EP/Et_2O solution was added to the mother liquor and the respective products, bright yellow solids, were precipitated from the solution, collected by filtration and washed with Et_2O (2x10 mL).

Yield: **$[Ir(Tph)_2][Et_3NH]$**$^+$ = 0.120 g; 72.1%. **$[F_2Ir(Tph)_2][Et_3NH]$**$^+$ = 0.133 g; 74.3%. **$[Ir(TphCN)_2][Et_3NH]$**$^+$ = 0.133 g; 0.152 mmol; 81.7%. **$[F_2Ir(TphCN)_2][Et_3NH]$**$^+$ = 0.104 g; 55.0%. **$[Ir(TphBr)_2][Et_3NH]$**$^+$ = 0.155 g; 79.45%. **$[F_2Ir(TphBr)_2][Et_3NH]$**$^+$ = 0.123 g; 69.41%.

$[Ir(Tph)_2]^-$ ^{1}**H-NMR** (CD_3CN, 400 MHz) δ (ppm) = 6.41 (m, 2H), 6.69 (m, 2H), 6.76 (m, 2H), 7.31 (m, 2H), 7.36 (m, 4H), 7.44 (m, 2H), 7.59 (m, 2H), 7.85 (d, 4H, $J_{H\text{-}H}$ = 5.6 Hz), 7.95 (m, 4H), 10.42 (d, 2H, $J_{H\text{-}H}$ = 5.6 Hz). ^{13}**C-NMR** (CD_3CN, 100 MHz) δ (ppm) = 168.52, 164.77, 153.34, 145.25, 137.06, 132.47, 131.07, 128.41, 128.38, 127.86, 126.00, 123.28, 121.81, 121.71, 120.55, 118.05. **ESI-MS** (*m*/*z*): [M$^-$] = 791; [M$^+$] = 102 (Et_3NH^+). Anal. Calcd. for $C_{42}H_{42}N_{11}Ir$ (893.07): C 56.48, H 4.74, N 17.25. Found: C 56.51, H 4.77, N 17.28%

$[F_2Ir(Tph)_2]^-$ ^{1}**H-NMR** (Acetone-d^6, 400 MHz) δ (ppm) = 5.97 (m, 2H), 6.35 (m, 2H), 7.25 (m, 2H), 7.30 (d, 4H, $J_{H\text{-}H}$ = 7.9 Hz), 7.50 (m, 2H), 7.89 (d, 4H, $J_{H\text{-}H}$ = 7.9 Hz), 8.04 (m, 2H), 8.26 (m, 2H), 10.51 (m, 2H).^{13}**C-NMR** (Acetone-d^6, 100 MHz) δ (ppm) = 165.03, 162.16, 153.81, 150.67, 137.88, 131.35, 128.22, 127.67, 125.99, 121.79, 121.62, 114.27, 114.10, 114.08, **ESI-MS** (*m*/*z*): [M$^-$] = 863; [M$^+$] = 102 (Et_3NH^+). Anal. Calcd. for $C_{42}H_{38}N_{11}F_4Ir$ (965.04): C 52.27, H 3.97, N 15.97. Found: C 52.25, H 3.99, N 16.00%

$[Ir(TphCN)_2]^-$ ^{1}**H-NMR** (Acetone-d^6, 400 MHz) δ (ppm) = 6.50 (m, 2H), 6.56 (m, 2H), 6.64 (m, 2H), 7.39 (m, 2H), 7.54 (m, 2H), 7.67 (d, 4H, $J_{H\text{-}H}$ = 7.9 Hz), 7.91 (m, 2H), 7.99 (m, 2H), 8.04 (d, 4H, $J_{H\text{-}H}$ = 7.6 Hz), 10.57 (m, 2H). ^{13}**C-NMR** (Acetone-d^6, 100 MHz) δ (ppm) = 169.98, 161.52, 154.71, 146.17, 137.52, 136.37, 133.63, 133.02,

128.91, 127.17, 123.91, 121.99, 120.96, 119.17, 118.58, 111.19. **ESI-MS** (*m*/*z*): [M^-] = 841; [M^+] = 102 (Et_3NH^+). Anal. Calcd. for $C_{44}H_{40}N_{13}Ir$ (943.09): C 56.04, H 4.28, N 19.31. Found: C 56.08, H 4.30, N 19.29%

[F_2Ir(TphCN)$_2$]$^-$ ^{1}**H-NMR** (Acetone-d^6, 400 MHz) δ (ppm) = 5.95 (m, 2H), 6.35 (m, 2H), 7.51 (m, 2H), 7.69 (d, 4H, J_{H-H} = 7.9 Hz), 7.76 (m, 2H), 8.04 (d, 4H, J_{H-H} = 7.6 Hz), 8.35 (m, 2H), 10.45 (m, 2H). ^{13}**C-NMR** (Acetone-d^6, 100 MHz) δ (ppm) = 166.03, 161.94, 154.66, 151.54, 138.87, 136.66, 133.97, 133.17, 133.14, 129.72, 127.55, 127.27, 127.24, 122.77, 119.57, 115.01, 111.57. **ESI-MS** (*m*/*z*): [M^-] = 913; [M^+] = 102 (Et_3NH^+). Anal. Calcd. for $C_{44}H_{36}N_{13}F_4Ir$ (1015.05): C 52.06, H 3.57, N 17.94. Found: C 52.04, H 3.59, N 17.97%

IrTphBr ^{1}**H-NMR** (CD_3CN, 400 MHz) δ (ppm) = 6.41 (d, 2H, J_{H-H} = 7.99 Hz), 6.67 (m, 2H), 6.78 (m, 2H), 7.43 (m, 2H), 7.50 (d, 4H, J_{H-H} = 11.99 Hz), 7.58 (d, 2H, J_{H-H} = 7.99 Hz), 7.79 (m, 4H), 7.98 – 7.90 (m, 4H), 10.35 (d, 2H, J_{H-H} = 7.99 Hz). ^{13}**C-NMR** (CD_3CN, 100 MHz) δ (ppm) = 168.80, 161.73 (Ct), 153.54, 153.43, 145.53, 137.39, 132.74, 131.76, 128.68, 128.10, 123.58, 122.01, 121.42, 120.89, 118.36 **ESI-MS** (*m*/*z*): [M^-] = 949; [M^+] = 102 (Et_3NH^+).

F_2IrTphBr ^{1}**H-NMR** (CD_3CN, 400 MHz) δ (ppm) = 10.25 (m, 2H), 8.28 (m, 2H), 8.01 (m, 2H), 7.80 (m, 4H), 7.53 (m, 4H), 7.48 (m, 2H), 6.44 (m, 2H), 5.89 (m, 2H). ^{19}**F-NMR** (CD_3CN 376 MHz) = -111.34, -112.63. ^{13}**C-NMR** (CD_3CN, 100 MHz) δ (ppm) = 164.85, 163.62 (Ct), 161.77, 161.11, 159.15, 158.13, 153.27, 138.22, 132.26, 131.54, 129.98, 128.92, 127.84, 122.26, 122.00, 121.39. **ESI-MS** (*m*/*z*): [M^-] = 1019; [M^+] = 102 (Et_3NH^+).

Chapter 4

Negatively charged Ir(III) cyclometalated complexes containing a chelating bis-tetrazolato ligand: synthesis, photophysics and the study of reactivity with electrophiles*

Abstract

The bis-tetrazolate dianion [1,2 BTB]$^{2-}$, which is the deprotonated form of 1,2 bis-(1H-tetrazol-5-yl)-benzene [1,2-H$_2$BTB], is for the first time exploited as an ancillary N^N ligand for negatively charged [Ir(C^N)$_2$(N^N)]-type complexes, where C^N is represented by cyclometalated 2-phenylpyridine (ppy) or 2-(2,4-difluorophenyl)pyridine (F$_2$ppy). The new Ir(III) complexes [Ir(ppy)$_2$(1,2 BTB)]$^-$ and [Ir(F$_2$ppy)$_2$(1,2 BTB)]$^-$ have been fully characterized and the analysis of the X-ray structure of [Ir(ppy)$_2$(1,2 BTB)]$^-$ confirmed the coordination of the [1,2 BTB]$^{2-}$ dianion in a bis chelated fashion through the N-atoms adjacent to each of the tetrazolic carbons. Both of the new anionic Ir(III) complexes displayed phosphorescence in the visible region, with intense sky-blue (λ max = 460–490 nm) or aqua (λ max = 490–520 nm) emissions originating from [Ir(F$_2$ppy)$_2$(1,2 BTB)]$^-$ and [Ir(ppy)$_2$(1,2 BTB)]$^-$, respectively. In comparison with our very recent examples of anionic Ir(III)tetrazolate cyclometalates, previously discussed in Chapter 3, the new Ir(III) tris chelate complexes [Ir(F$_2$ppy)$_2$(1,2 BTB)]$^-$ and [Ir(ppy)$_2$(1,2 BTB)]$^-$, display an improved robustness, allowing the study of their reactivity toward the addition of electrophiles such as H$^+$ and CH$_3^+$. In all cases, the electrophilic attacks occurred at the coordinated tetrazolate rings, involving the reversible – by a protonation deprotonation mechanism – or permanent – upon addition of a methyl moiety – switching of their global net charge from negative to positive and, in particular, the concomitant variation of their photoluminescence output.

: This chapter is part of Dalton. Trans,* **2016, *45, 12884.*[44]

Introduction: Expanding the Family of Anionic Ir(III) Tetrazolate derivatives

As discussed in Chapter 3, we have recently expanded the area of anionic Ir(III) complexes with a report of the sky-blue emitting [Ir(ppy)$_2$(N$_4$C-R)$_2$]$^-$ and aqua emitting [Ir(F$_2$ppy)$_2$(N$_4$C-R)$_2$]$^-$ species, where the two cyano ligands are substituted by the tetrazolate moieties [N$_4$C-R]$^-$ (Figure 1.4).[34] Moving beyond these promising results, we wanted to further investigate the chemistry of anionic Ir(III) tetrazolate complexes with respect to their reactivity toward electrophilic additions.

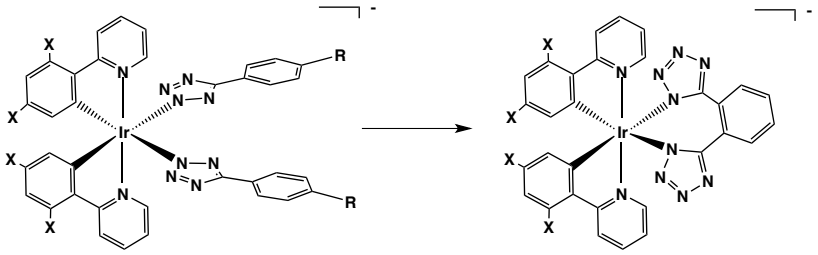

Figure 1.4: Left, Structure of anionic [Ir(C^N)$_2$(N$_4$C-R)$_2$]; Right, structure of Chelate Anionic Ir(III) Tetrazolate complexes [Ir(C^N)$_2$(N^N)]$^-$

In fact, we have previously shown how the photoluminescent properties of tetrazolato species of Re(I), Ir(III), and Pt(II) could be reversibly or irreversibly tuned by addition of electrophilic reagents to the metal-coordinated tetrazolato ring.[25,27,28] [45] Unfortunately, both $[Ir(ppy)_2(N_4C\text{-}R)_2]^-$ and $[Ir(F_2ppy)_2(N_4C\text{-}R)_2]^-$ complexes displayed pronounced lability of the tetrazolato ligands in the presence of electrophiles such as CH_3^+ or H^+. Therefore, to further continue our studies and determine the reactivity and luminescent switching of anionic Ir(III) tetrazolato species, we attempted to prepare a more inert complex by tethering the two tetrazolato rings into a phenyl moiety (Figure 1.4). To this extent, we herein report the synthesis, together with the spectroscopic, structural and photophysical characterization of two new $[Ir(ppy)_2(N^N)]^-$ and $[Ir(F_2ppy)_2(N^N)]^-$ -type complexes where N^N is a dianionic bis-tetrazolate, such as the fully deprotonated form of 1,2 bis-(1H-tetrazol-5-yl)benzene (1,2 BTB) (Figure 2.4). Furthermore, the new anionic Ir(III) complexes have been investigated with respect to their reactivity versus methyl triflate and triflic acid.

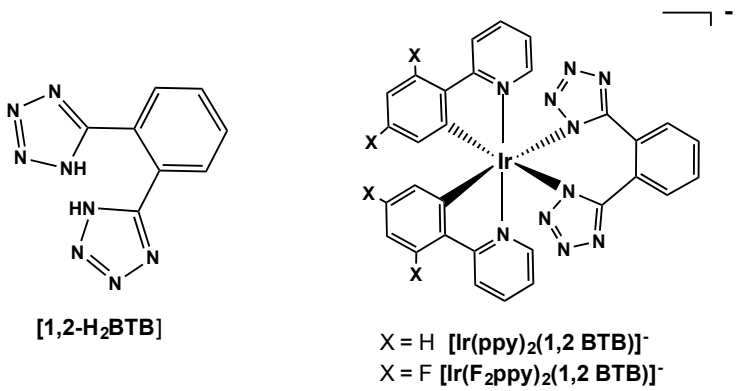

Figure 2.4: Left, Structure of 1,2 bis-(1H-tetrazol-5-yl)- benzene [1,2-H$_2$BTB]; Right, structure of Chelate Anionic Ir(III) Tetrazolate complexes [Ir(C^N)$_2$(N^N)] and acronyms used

Results and discussion

Synthesis of Anionic Tetrazolate [Ir(C^N)$_2$(N^N)]$^-$ type complexes

The 1,2-H$_2$BTB ligand was obtained in good yield by 1,3 dipolar cyclisation of the azide anion (N_3^-) onto 1,2-dicyano-benzene. Furthermore, the targeted Ir(III) anionic complexes were prepared according to our previously published procedure (Figure 3.4),[34] involving a reaction of the chloro-bridged Ir(III) dimer, $[Ir(ppy)_2Cl]_2$ or $[Ir(F_2ppy)_2Cl]_2$, with a 2.5 molar excess of 1,2-H$_2$BTB in the presence

of an equimolar amount of triethylamine (Et_3N). In all cases, after 24 hours at reflux temperature, the addition of diethyl ether to the crude mixtures caused the precipitation of the desired saline compounds. Conveniently, the products were simply filtered and did not require any further purification.

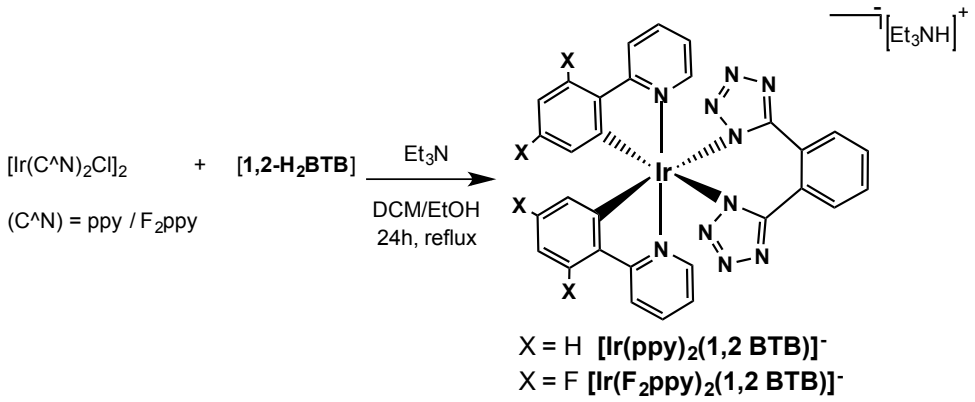

Figure 3.4: Synthetic procedure used for Anionic Ir(III) tetrazolate complexes and acronyms used

The formation of the desired anionic complexes, which were isolated as their triethylammonium [TEAH]$^+$ salts, was initially deduced by Electron Spray Ionisation Mass Spectrometry (ESI-MS), which provided *m*/*z* signals congruent with the expected anions (Figure 4.4).

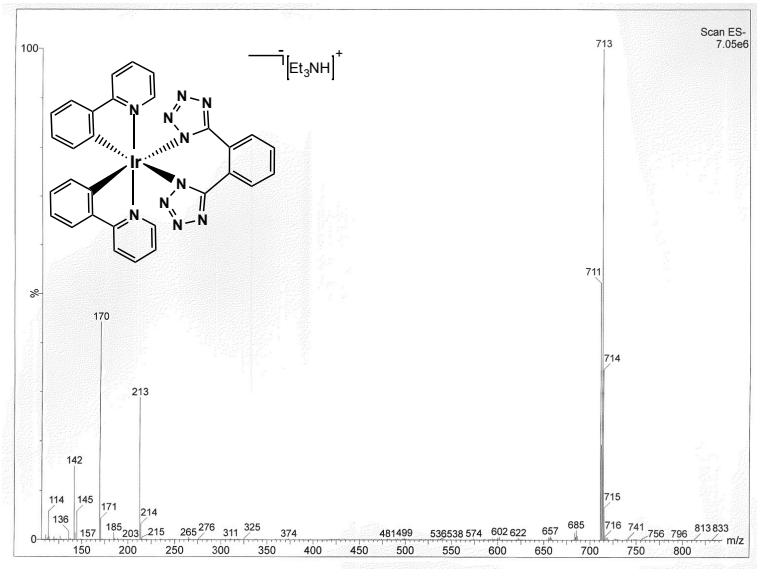

Figure 4.4: ESI-MS spectrum of [Ir(ppy)$_2$(1,2 BTB)] (negative ions region) [M] = 713 m/z, CH_3CN

Single crystals suitable for X-ray diffraction could be obtained for $[Ir(ppy)_2(1,2BTB)]^-$ (Figure 5.4, Table 2, Table C4), revealing how the coordination of the bis-tetrazolate anion $[1,2\ BTB]^{2-}$ to the Ir(III) metal centre effectively occurred in a chelating fashion through the N-1 nitrogen atoms (N(1) and N(5) according to crystallographic numbering in Figure 5.4) of each tetrazolate ring. Effectively, this binding mode describes a seven-membered $(–IrNC_4N–)$ coordination ring.

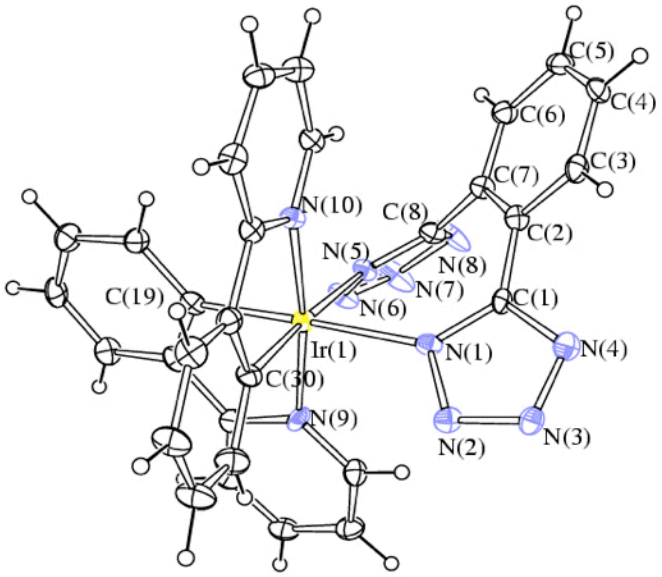

Figure 5.4: molecular stucture of $[Ir(ppy)_2(1,2BTB)]^-$ with key atoms labelled. Displacement ellipsoids are at the 30% probability level

Because of its chelating coordination, the $[1,2\ BTB]^{2-}$ ligand is not planar, with the two tetrazolate rings forming an angle of 71.8° between their least squares planes, whereas the angles formed between the least squares plane of each tetrazolate ring and the benzene ring are 37.8° and 51.1°, respectively. A similar coordination has been previously observed in the case of Tl(I), Cd(II) and Cu(II) derivatives of the same $[1,2\ BTB]^{2-}$ anion.[46]

Overall, the Ir(III) centre adopts a distorted octahedral coordination geometry with cis- metalated phenyl carbon donors and trans pyridine nitrogen donors, as was previously found in other complexes containing analogous cyclometalated ligands.[27,28] The Ir–N (tetrazolate) distances [2.157(6) and 2.176(6) Å] are longer than Ir–N (phenylpyridine) [2.067(7) and 2.058(6) Å] because of the

trans influence of the strongly σ-donating metalated carbon atoms. Intermolecular H-bonding is present involving the N(31)–H (31) group of the $[HNEt_3]^+$ cation as a donor and the N(8) atom of the $[Ir(ppy)_2(1,2\ BTB)]^-$ anion as an acceptor [N(31)–H(31) 0.93 Å, H(31)···N(8)#1 2.28 Å, N(31)···N(8)#1 3.187(15) Å, <N(31)H(31)N(8)#1 163.3°; symmetry transformations used to generate equivalent atoms #1 x, y − 1, z].

Table 2: Selected bond lengths (Å) and angles (deg) for [Ir(ppy)$_2$(1,2 BTB)]$^-$

Ir(1)-N(1)	2.157(6)	Ir(1)-N(5)	2.176(6)
Ir(1)-N(9)	2.067(7)	Ir(1)-N(10)	2.058(6)
Ir(1)-C(19)	2.016(8)	Ir(1)-C(30)	2.020(8)
N(1)-N(2)	1.361(9)	N(5)-N(6)	1.357(8)
N(2)-N(3)	1.318(9)	N(6)-N(7)	1.286(10)
N(3)-N(4)	1.340(10)	N(7)-N(8)	1.359(10)
C(1)-N(4)	1.338(10)	C(8)-N(8)	1.343(10)
C(1)-N(1)	1.352(10)	C(8)-N(5)	1.318(10)
C(1)-C(2)	1.467(11)	C(7)-C(8)	1.468(10)
C(2)-C(3)	1.398(10)	C(3)-C(4)	1.398(12)
C(4)-C(5)	1.389(12)	C(5)-C(6)	1.380(11)
C(6)-C(7)	1.389(11)	C(7)-C(2)	1.417(10)
N(1)-Ir(1)-C(19)	176.2(3)	N(5)-Ir(1)-C(30)	176.0(3)
N(9)-Ir(1)-N(10)	172.9(3)	N(1)-Ir(1)-N(5)	85.3(2)
N(9)-Ir(1)-C(19)	80.8(3)	N(10)-Ir(1)-C(30)	80.3(3)

The ^{1}H and ^{13}C NMR characterisation in CD_2Cl_2 of [Ir(ppy)$_2$(1,2BTB)]$^-$ and [Ir(F$_2$ppy)$_2$(1,2BTB)]$^-$ required variable temperature (VT) experiments. Well resolved ^{1}H and ^{13}C NMR spectra could only be obtained at 248 K (Figures 6.4, 7.4) and displayed a number of signals equal to the total number of hydrogen or carbon atoms in each complex, in agreement with the occurrence of C_s symmetry that can be reasonably explained in consideration of the not coplanar arrangement adopted by the coordinated (1,2 BTB) ligand.

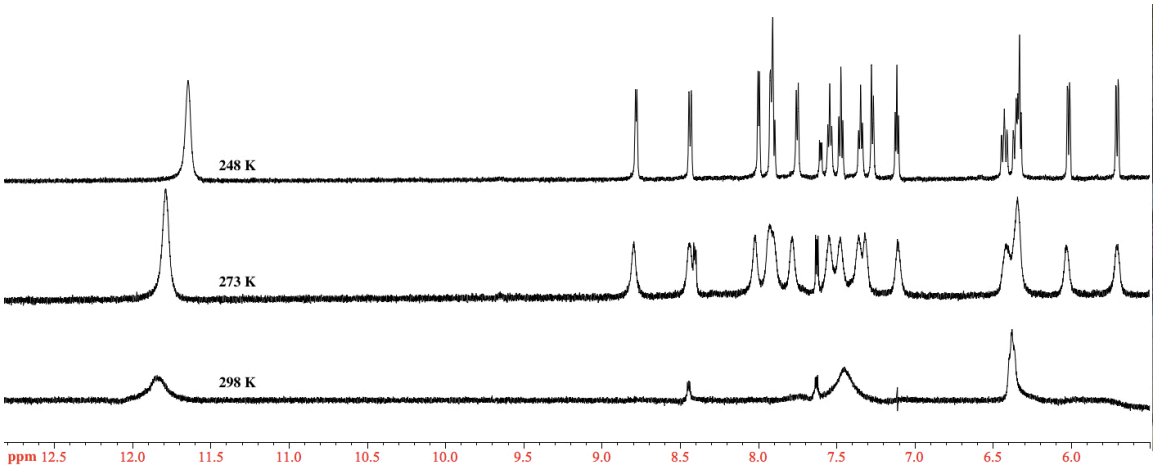

Figure 6.4: Stacking plot of ^{1}H NMR spectra (CD_2Cl_2 as the solvent, 600 MHz) of [Ir(F$_2$ppy)$_2$(1,2 BTB)]$^-$,recorded at 298 K (bottom), 273 K (middle), and 248 K (top)

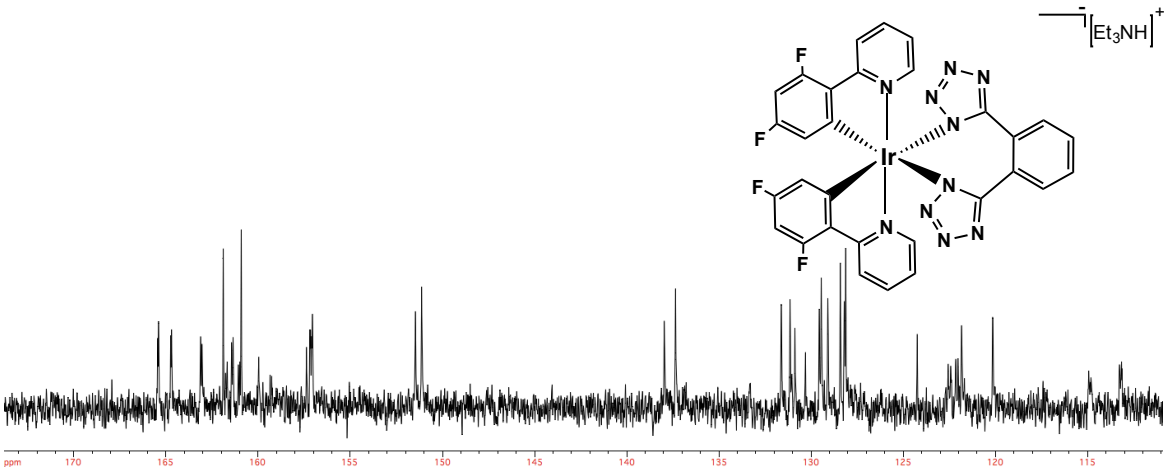

Figure 7.4: ^{13}C NMR of $[Ir(F_2ppy)_2(1,2\ BTB)]$ CD_2Cl_2, 600 MHz, 248K

The likely reason that might account for such a fluxional behavior might be attributed to the exchange through a ring inversion of the strained seven membered ring (-$IrNC_4N$-) that is described by the coordinated bis-tetrazolate ligand and the Ir(III) center. The occurrence of a similar mechanism has been described in previous reports dealing with heterocyclic analogues of benzocycloheptene.[47]

The reactivity of $[Ir(ppy)_2(1,2\ BTB)]^-$ and $[Ir(F_2ppy)_2(1,2\ BTB)]^-$ was screened with respect to the addition electrophiles such as H^+ and CH_3^+. In the former case, the protonation reactions were monitored upon performing emission titrations (*vide infra*), while the preparation of the bis-methylated complexes $[Ir(ppy)_2(1,2\ BTBMe_2)]^+$ and $[Ir(F_2ppy)_2(1,2\ BTBMe_2)]^+$ was accomplished through the reaction of the anionic precursors $[Ir(ppy)_2(1,2\ BTB)]^-$ and $[Ir(F_2ppy)_2(1,2\ BTB)]^-$ with a slight excess of methyl triflate (Figure 8.4). After a metathesis procedure, the cationic complexes were isolated as their hexafluorophosphate salts, as demonstrated by ESI-MS analysis.

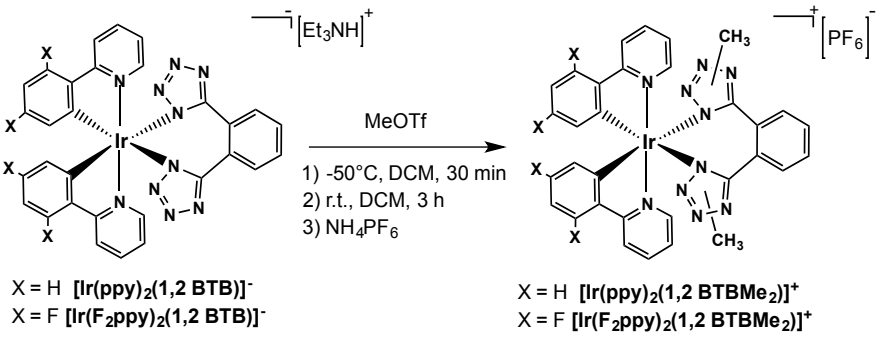

Figure 8.4: Synthetic procedure for the $[Ir(C\hat{}N)_2(1,2\ BTBMe_2)]^+$ type complexes

In contrast to what observed for the anionic derivatives, the NMR characterisation of the bis-methylated complexes $[Ir(ppy)_2(1,2\ BTBMe_2)]^+$ and $[Ir(F_2ppy)_2(1,2\ BTBMe_2)]^+$ could be accomplished at room temperature, without the need for VT experiments. In particular, each ^1H NMR spectrum displayed pattern of signals congruent with the occurrence of one bis-methylated compound in which the C_s symmetry of the starting anionic complexes is retained, as witnessed by the presence of a number of signals equal to the number of the aromatic hydrogens of the molecules and by the clear splitting of the CH_3 signals into two well spaced peaks having the same integral value (Figure 9.4). Analogous indications came from the analysis of the ^{13}C NMR spectra (Figure 10.4).

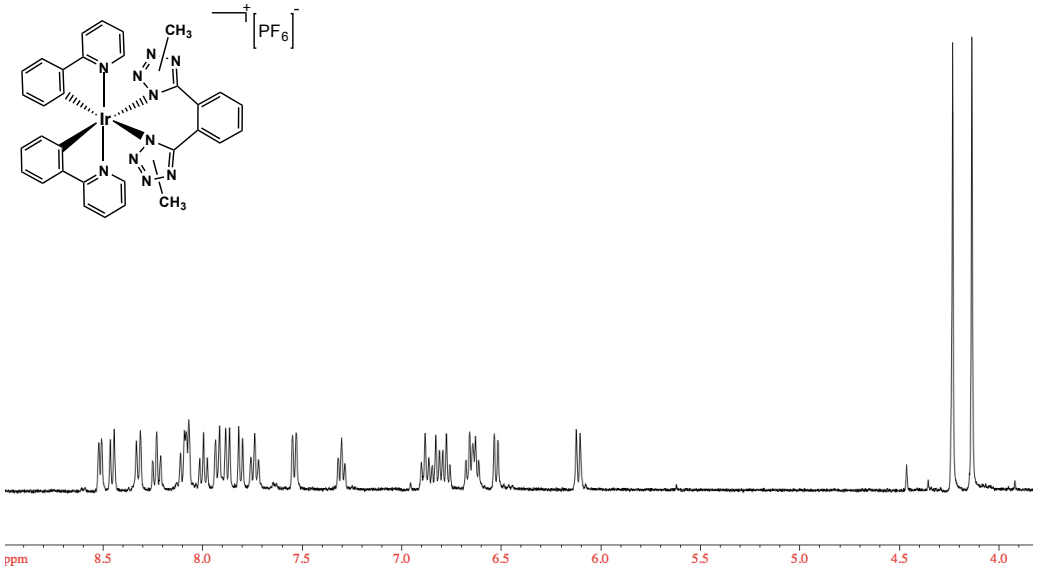

Figure 9.4: ^1H NMR spectrum of $[Ir(ppy)_2(1,2\ BTBMe_2)]^+$, Acetone d_6, 400 MHz, 298 K

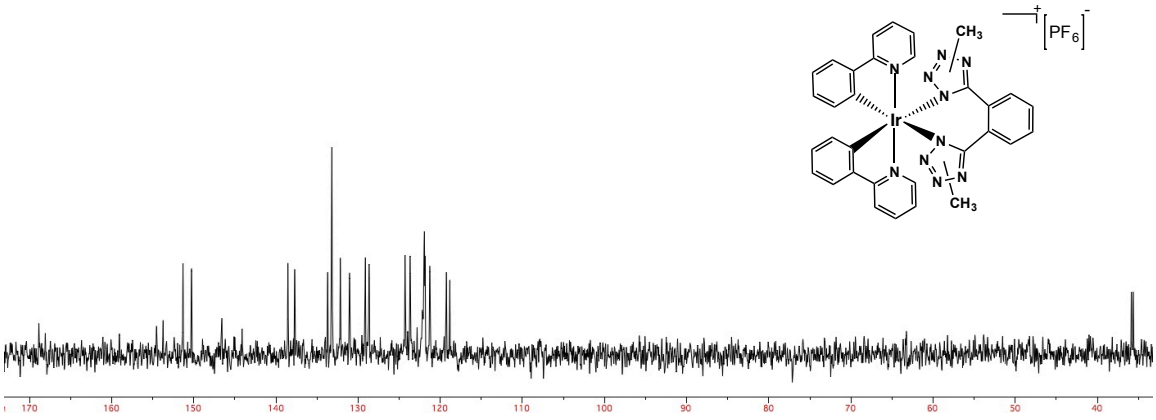

Figure 10.4: ^{13}C NMR of $[Ir(ppy)_2(1,2\ BTBMe_2)]^+$ Acetone-d_6, 298K

However, the isolation of one single dimethylated product points to the eventual regioselective character of the addition of the methyl group to the coordinated tetrazolato rings, each of which contains three diimine tipe nitrogens that are in principle prone to electrophilic attack. Even though all the attempts for obtaining crystals suitable for X-ray diffraction of both the cationic complexes were not successful, useful indications about the nature of the bis-methylated isomers could be deduced by means of nuclear Overhauser effect spectroscopy (NOESY). (Figure 11.4)

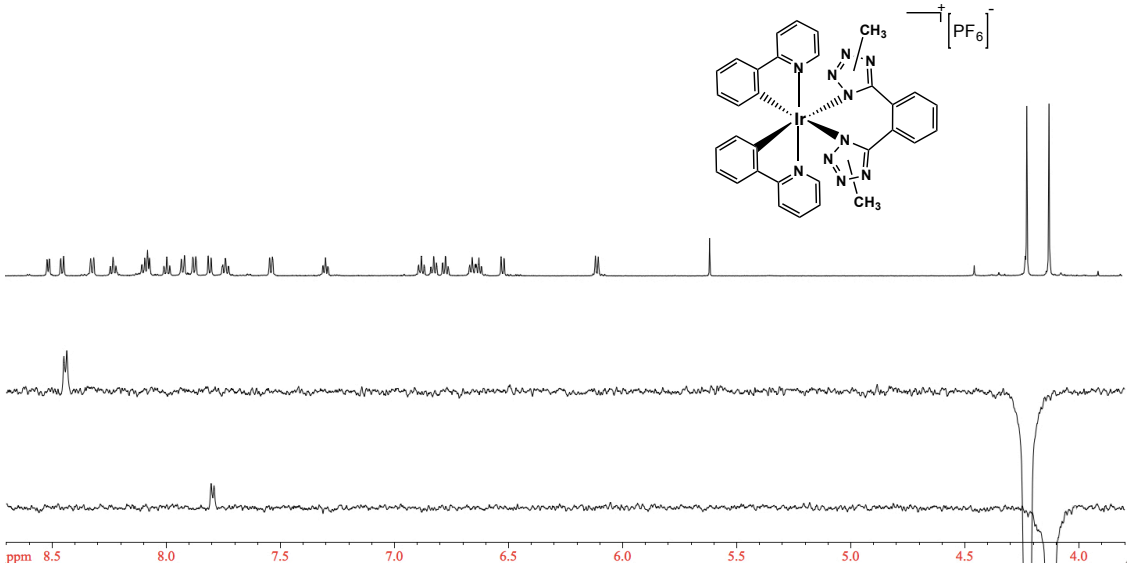

Figure 11.4: NOESY-NMR and ^{1}H-NMR spectrum (overlaid) of [Ir(ppy)$_2$(1,2 BTBMe$_2$)]$^+$ Acetone-d$_6$, 600 MHz, 298K

The analysis of the results of the NOESY experiments suggested how each methylation likely occurred at the position adjacent to the tetrazole carbon of each pentatomic ring. More specifically, in the case of the NOESY experiment performed onto the exemplar complex [Ir(ppy)$_2$(1,2 BTBMe$_2$)]$^+$ (Figure 11.4) the irradiation at the resonance frequency of the –CH$_3$ hydrogen signal centred at δ = 4.13 ppm, caused the enhancement of the resonance centred at δ = 7.80 ppm, which we assume as the 1,2 BTBMe$_2$ phenyl hydrogen labelled as H$_a$ in Figure 12.4.

Likewise, the irradiation of the signal centred at δ_H = 4.22 ppm, the one relative to the other CH$_3$ group of the molecule, resulted in the increase of the signal at δ_H = 8.44 ppm, which is in turn assigned to the 1,2 BTBMe$_2$ phenyl hydrogen labelled as H$_d$ in Figure 12.4.

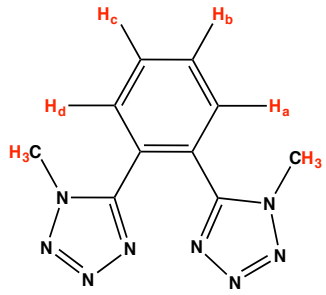

Figure 12.4: Hydrogen labelling of 1,2 BTBMe₂

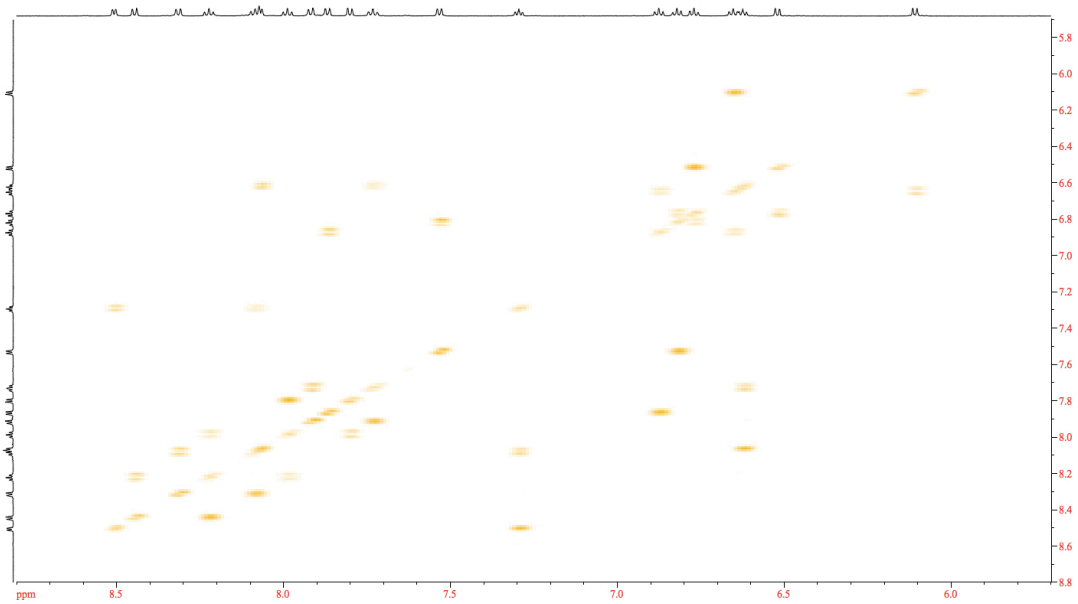

Figure 13.4: ^{1}H-^{1}H COSY-NMR of [Ir(ppy)₂(1,2 BTBMe₂)]⁺ Acetone-d₆, 600 MHz, 298K

Finally, by performing ^{1}H-^{1}H COSY correlation experiments, it was possible to assign the resonances relative to the remaining hydrogens H_b and H_c (Figure 13.4), which were found at $\delta_H = 7.97$ and $\delta_H = 8.25$, respectively. Analogous and congruent results were obtained by performing the same experiments (NOESY and ^{1}H-^{1}H COSY) onto the fluorinated complex [Ir(F₂ppy)₂(1,2 BTBMe₂)]⁺. Also in this case, the methyl moieties are likely bonded at the same positions as those of the not fluorinated complex [Ir(ppy)₂(1,2 BTBMe₂)]⁺, and the H_a, H_b, H_c and H_d hydrogens (see Figure 12.4 for labelling) were found to resonate at $\delta_H = 7.81$, 8.00, 8.23 and 8.44 ppm, respectively.

Photophysical properties

The photophysical data for [Ir(ppy)₂(1,2 BTB)]⁻ and [Ir(F₂ppy)₂(1,2 BTB)]⁻ are listed in table 3. In diluted dichloromethane solutions (≈ 10^{-5} M), the anionic Ir(III) complexes display similar absorption profiles (Figure 14.4), with intense ligand

centred (LC) transitions up to 300 nm and metal-to-ligand charge transfer (MLCT) bands tailing off above 350 nm.

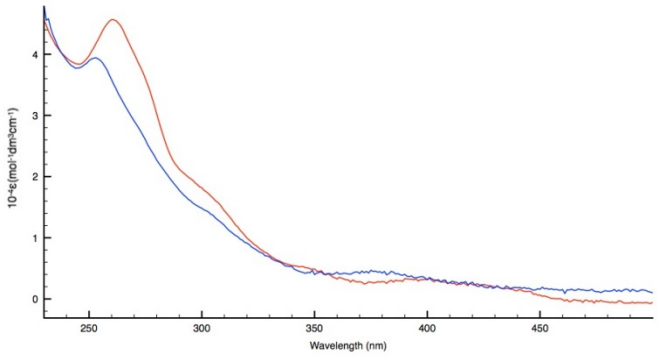

Figure 14.4: Absorption profiles of [Ir(ppy)$_2$(1,2 BTB)]$^-$ (red trace) and [Ir(F$_2$ppy)$_2$(1,2 BTB)]$^-$(blue trace)

Table 3: Photophysical properties for [Ir(C^N)$_2$(1,2 BTB)]$^-$, diprotonated [Ir(C^N)$_2$(1,2 BTBH$_2$)]$^+$ complexes and the dimethylated [Ir(C^N)$_2$(1,2 BTBMe$_2$)]$^+$ complexes

Complex	Absorption	Emission 298 K[a,b]					Emission 77K[c]	
Solvent: CH_2Cl_2	λ_{abs}(nm) (10^{-4} ε) (M^{-1} cm^{-1})	λ(nm)	τ_{Air}(μs)	τ_{Ar}(μs)	Φ_{Air}(%)	Φ_{Ar}(%)	λ(nm)	τ(μs)
[Ir(ppy)$_2$(1,2 BTB)]$^-$	261(4.56) 305(1.65) 350(0.49)	488 516	0.10	0.820	2.93	33.3	482 516 562	2.24
[Ir(ppy)$_2$(1,2 BTBMe$_2$)]$^+$	260 (7.26) 300 (2.81) 386 (0.55)	482 512	0.060	0.106	0.88	2.79	472 506	3.82
[Ir(F$_2$ppy)$_2$(1,2 BTB)]$^-$	254(2.72) 307(0.89) 370(0.29)	460 490 526	0.120	1.60	2.64	53.0	456 490 524	2.20
[Ir(F$_2$ppy)$_2$(1,2 BTBMe$_2$)]$^+$	248(11.63) 318 (3.13) 370 (1.00)	456 486	0.180	0.254	2.95	6.95	450 482	3.64

[a]: "Air" means air equilibrated solutions, "Ar" means deoxygenated solutions under argon atmosphere; [b]: [Ru(bpy)$_3$]Cl$_2$/H$_2$O was used as reference for quantum yield determinations (Φ_r = 0.028)[49]; [c]: frozen CH_2Cl_2 as the solvent

To confirm the identity of the charge transfer transitions, time-dependent density functional theory (TD-DFT) calculations were used for these complexes (Figure 21.4, Table 4). The structures of the complexes were minimised using the implicit solvent model (PCM).[48] The data indicate that the lower energy band in the spectrum belongs to the HOMO→LUMO+n (n=0-1) transition. The HOMO is mainly localised on the Ir(III) centre and phenyl rings of both the ppy ligands. On the other hand, the LUMO and LUMO+1 are localised on both the extended ppy ligands (Figure 41). The TD-DFT results confirm the MLCT nature of the

lowest excited state with admixture of LC character. Upon excitation of the MLCT features, the two anionic complexes gave rise to bright sky-blue (λ_{max} ca. 460 and 490 nm) or aqua (λ_{max} ca. 490 and 520 nm) emissions for $[Ir(F_2ppy)_2(1,2\ BTB)]^-$ and $[Ir(ppy)_2(1,2\ BTB)]^-$, respectively (Figure 15.4). The blue-shift occurring upon replacement of ppy with F_2ppy can be rationalised by a stabilisation of the HOMO localised on the phenyl rings due to the electron-withdrawing nature of the fluoride substituents.

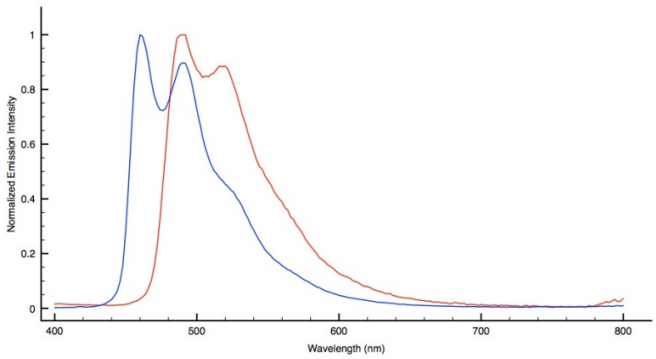

Figure 15.4: normalised emission profiles (right) of $[Ir(ppy)_2(1,2\ BTB)]^-$ (red trace) and $[Ir(F_2ppy)_2(1,2\ BTB)]^-$ (blue trace)

In both cases, the triplet character of the excited state was witnessed by the pronounced oxygen sensitivity that was displayed by the quantum yields (ϕ), which ranged from *ca.* 0.33 to *ca.* 0.53 for the deoxygenated solutions of $[Ir(F_2ppy)_2(1,2\ BTB)]^-$ and $[Ir(F_2ppy)_2(1,2\ BTB)]^-$, respectively, and the corresponding lifetimes (τ) values (Table 3). In addition, the occurrence of structured emission profiles further confirmed the interplay of ^{3}LC/^{3}MLCT emissive excited states, in agreement with the TD-DFT calculations for these complexes. The lack of rigidochromic effect observable for the small blue-shift on passing from room temperature to 77 K emission suggests a dominant LC character in the composition of the ^{3}LC/^{3}MLCT excited state (Figure 16.4).

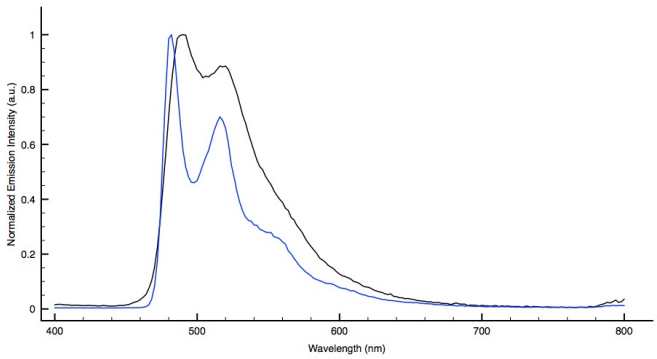

Figure 16.4: Normalized Emission profiles of $[Ir(ppy)_2(1,2\ BTB)]^-$ 10^{-5}M, CH_2Cl_2, 298K (black line) and 77 K (blue line)

Addition of electrophiles

The addition of electrophiles such as H^+ or CH_3^+ to the anionic complexes $[Ir(F_2ppy)_2(1,2\ BTB)]^-$ and $[Ir(ppy)_2(1,2\ BTB)]^-$ caused the switching to the corresponding cationic species and induced the concomitant variation of their photoluminescent features. The occurrence of these effects were first observed in the cases of the protonation reactions (Figure 17.4), which were carried out by performing emission titrations in which successive aliquots of triflic acid were added up to two molar equivalents.

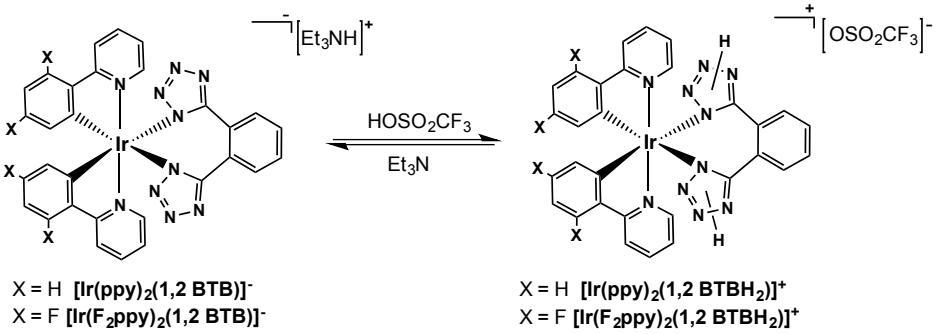

Figure 17.4: Reversible protonation reaction of $[Ir(C\hat{}N)_2(1,2\ BTB)]^-$ type complexes

From the analysis of each titration profile (Figure 18.4), followed by monitoring changes in the emission plots, it was observed that the sequential protonation of the tetrazolate rings caused significant reduction of the emission intensity. The emission spectra of the cationic products appeared in both cases only slightly blue shifted ($\Delta\lambda$ = 4-6 nm) with respect to those of the anionic precursors, whose vibronically structured shape of was maintained throughout the whole titrations.

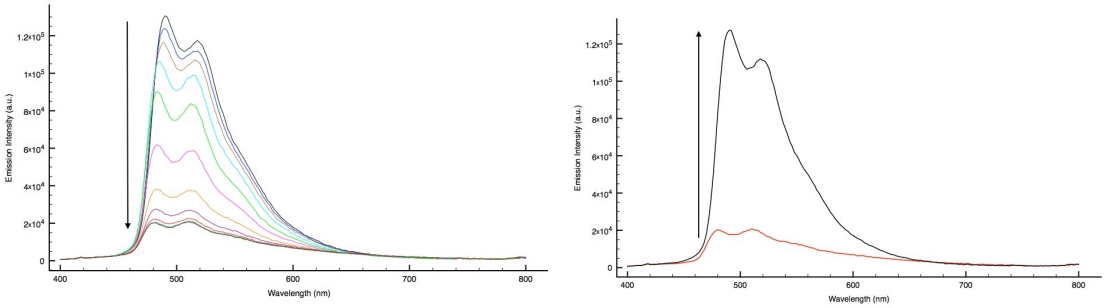

Figure 18.4: Left: Emission titration of $[Ir(ppy)_2(1,2\ BTB)]^-$ with 110µL of $HOSO_2CF_3$ 0,005 M in CH_2Cl_2. Right: Back Titration with Et_3N showing the reversible modulation of the emission intensity between the protonated $[Ir(ppy)_2(1,2\ BTBH_2)]^+$ and $[Ir(ppy)_2(1,2\ BTB)]^-$

It is worth noting that the protonation reactions described herein share the same reversible character that we have reported previously for Ir(III), Re(I) and Ru(II)-tetrazolato complexes, whose luminescence properties could be reversibly modulated by a protonation-deprotonation mechanism. Indeed, the addition of two molar equivalents of a relative weak base such as triethylamine (Et_3N) to the bis-protonated complexes $[Ir(ppy)_2(1,2\ BTBH_2)]^+$ and $[Ir(F_2ppy)_2(1,2\ BTBH_2)]^+$ restored the corresponding anionic precursors and their intense emission profiles (Table 3).

The photoluminescence behaviour that was observed when the anionic complexes $[Ir(ppy)_2(1,2\ BTB)]^-$ and $[Ir(F_2ppy)_2(1,2\ BTB)]^-$ were irreversibly transformed into the dimethylated complexes $[Ir(ppy)_2(1,2\ BTBMe_2)]^+$ and $[Ir(F_2ppy)_2(1,2\ BTBMe_2)]^+$, respectively, followed a trend analogous to that observed upon performing the protonation reactions (Figure 19.4).

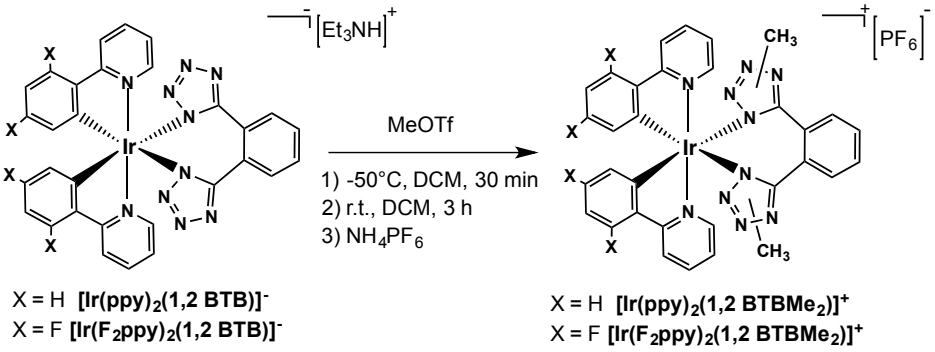

Figure 19.4: Irreversible methylation reaction of $[Ir(C^N)_2(1,2\ BTB)]$ type complexes

In particular, as the emission profiles of the dimethylated species were found almost exactly superimposable to those of the diprotonated analogues (Figure 20.4).

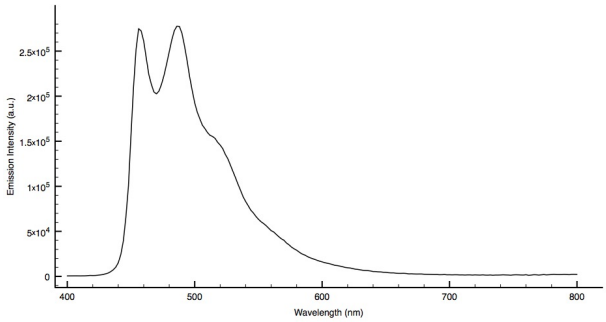

Figure 20.4: Emission profile of $[Ir(F_2ppy)_2(1,2\ BTBMe_2)]^+$ 10^{-5} M, CH_2Cl_2, 298K

It was possible to determine that the addition of electrophiles such as H^+ or CH_3^+ to the starting anionic complexes did not involve appreciable change in the colour of their sky-blue or aqua emissions, but concomitantly caused the reduction of the emission quantum yields to *ca.* one tenth of the initial values (Table 3). Congruently with the analysis of TDDFT calculations, the occurrence of such particular behaviour, suggests that the protonated [1,2 $BTBH_2$] or methylated [1,2 $BTBMe_2$] ligands might play a not negligible role in determining the composition of the emissive excited states. In particular, such a pronounced intervention of not-radiative processes might be explained by considering the reduction of the sigma donor character of the dianionic bis-tetrazolate ligand $[(1,2\ BTB)]^{2-}$ that takes place upon its transformation into its neutral and protonated [1,2 $BTBH_2$] or methylated [1,2 $BTBMe_2$] derivative, likely resulting in the weakening of the Ir(III)-N(tetrazole) bond strength.

TD-DFT Calculations

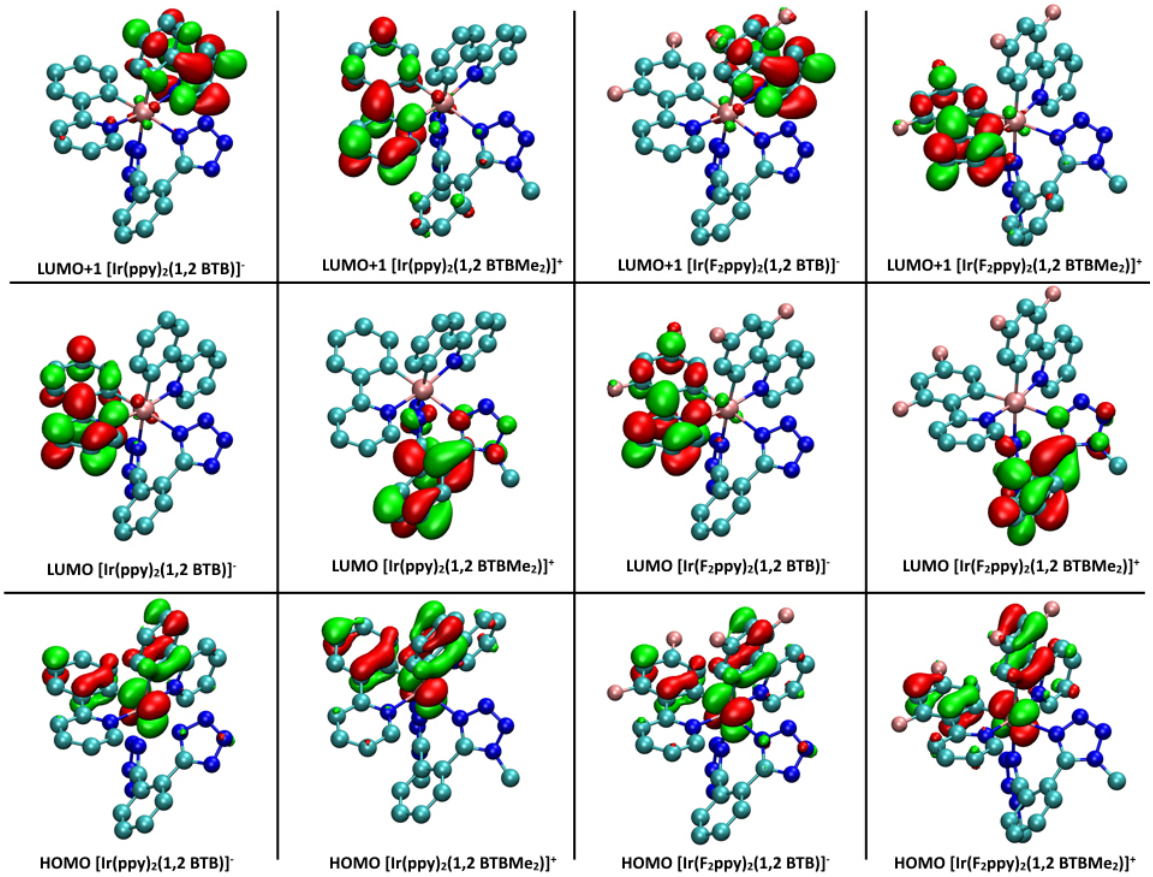

Figure 21.4: Localisation of the HOMO, LUMO, and LUMO+1 orbitals for the anionic and cationic Ir(III) complexes

In line with what emerged from NOESY experiments, the TD-DFT analysis relative to the cationic complexes $[Ir(ppy)_2(1,2\ BTBMe_2)]^+$ and $[Ir(F_2ppy)_2(1,2\ BTBMe_2)]^+$ was carried out by assuming that methylation occurred at the N-4 and N-8 positions of both tetrazole rings (Figure 21.4). Similarly to their anionic precursors $[Ir(ppy)_2(1,2\ BTB)]^-$ and $[Ir(F_2ppy)_2(1,2\ BTB)]^-$, the low energy band of the bis methylated cationic complexes is again ascribed to the HOMO→LUMO+n (n=0-1) transition, with the HOMO localised on the Ir(III) centre and phenyl rings of the ppy or F_2ppy cyclometalating ligands.

Contrastingly, the LUMO and LUMO+1 of $[Ir(ppy)_2(1,2\ BTBMe_2)]^+$ and $[Ir(F_2ppy)_2(1,2\ BTBMe_2)]^+$ were no longer localised only on the the ppy or F_2ppy ligands, but a significant contribution of the phenyl ring of the bis-tetrazole ligand [1,2 $BTBMe_2$] was observed in in the composition of the LUMO of each of the bis-methylated complexes $[Ir(ppy)_2(1,2\ BTBMe_2)]^+$ and $[Ir(F_2ppy)_2(1,2$

$BTBMe_2)]^+$ (Figure 21.4, Table 4). This computational evidence might provide an explanation of how the addition of electrophiles to the anionic precursors can determine the modification of the emission performances of the product cationic complexes.

Table 4: Low energy absorption transitions obtained from the TD-DFT calculations for anionic and cationic Ir(III) complexes. For brevity we report here only the transitions with character greater than 10%

Complex	Wavelength (nm)	Intensity (a.u.)	Transition	Character (%)
$[Ir(ppy)_2(1,2\ BTB)]^-$	341.45	0.184	HOMO -> LUMO	84.9
	331.95	0.062	HOMO -> LUMO+1	84.8
	286.38	0.096	HOMO-4 -> LUMO	17.0
			HOMO-2 -> LUMO	45.0
			HOMO -> LUMO+2	15.7
	281.09	0.193	HOMO -> LUMO+2	62.7
$[Ir(ppy)_2(1,2\ BTBMe_2)]^+$	329.58	0.207	HOMO -> LUMO+1	66.4
			HOMO -> LUMO+2	13.7
	320.67	0.076	HOMO -> LUMO+2	61.7
	276.16	0.285	HOMO-2 -> LUMO+1	30.0
			HOMO-1 -> LUMO+1	31.4
	273.50	0.070	HOMO --> LUMO+4	56.4
$[Ir(F_2ppy)_2(1,2\ BTB)]^+$	322.42	0.177	HOMO -> LUMO	80.1
	314.42	0.066	HOMO -> LUMO+1	81.1
	278.89	0.161	HOMO-2 -> LUMO	11.9
			HOMO-1 -> LUMO	55.6
	269.14	0.072	HOMO-4 -> LUMO	47.1
			HOMO-3 -> LUMO	10.3
			HOMO-2 -> LUMO	14.3
$[Ir(F_2ppy)_2(1,2\ BTBMe_2)]^+$	312.50	0.218	HOMO-1 -> LUMO+1	14.3
			HOMO -> LUMO+1	62.7
			HOMO -> LUMO+2	11.8
	305.21	0.103	HOMO-1 -> LUMO+2	12.5
			HOMO -> LUMO+2	64.7
	284.84	0.003	HOMO -> LUMO	89.3
	272.90	0.323	HOMO-2 -> LUMO+1	42.4
			HOMO-1 -> LUMO+1	25.4

Conclusions

In conclusion, we successfully synthesised two new negatively charged Ir(III) tris-chelate complexes with general formulae $[Ir(ppy)_2(N^N)]^-$ and $[Ir(F_2ppy)_2(N^N)]^-$, where a bis-tetrazolate dianion such as the deprotonated form of 1,2 bis - (*1H* tetrazol-5-yl)benzene [1,2-H_2BTB] is used for the first time as the ancillary N^N ligand. These complexes have been designed in order to provide an upgraded and more robust version of the first examples of brightly luminescent tetrazolate based anionic Ir(III) cyclometalates $[Ir(F_2ppy)_2(N_4C\text{-}R)_2]^-$ and $[Ir(ppy)_2(N_4C\text{-}R)_2]^-$, in which the negative charge was brought by the coordination of two 5-aryl tetrazolato ligands $[N_4C\text{-}R]^-$. The tethering of two tetrazolate moieties into the bis chelating ligand $[1,2\ BTB]^{2-}$ did not affect the luminescent performances of the resulting anionic complexes $[Ir(F_2ppy)_2(1,2\ BTB)]^-$ and $[Ir(ppy)_2(1,2\ BTB)]^-$, which also displayed sky-blue or aqua phosphorescent emissions, respectively, with quantum yield values up to 53%, as for deoxygenated solutions of $[Ir(F_2ppy)_2(1,2\ BTB)]^-$. Further studies about the use of the new anionic complexes as emissive dopants for LEECs (Light Emitting Electrochemical Cells) are currently underway. The improved robustness of the new Ir(III) tris chelate complexes $[Ir(F_2ppy)_2(1,2\ BTB)]^-$ and $[Ir(ppy)_2(1,2\ BTB)]^-$, allowed the systematic study of their reactivity toward the addition of electrophiles such as H^+ and CH_3^+. In particular, we could determine that the addition of such electrophiles to the negatively charged $[Ir(F_2ppy)_2(1,2\ BTB)]^-$ and $[Ir(ppy)_2(1,2\ BTB)]^-$ caused the reversible - by a protonation-deprotonation mechanism – or permanent, as in the case of methylation reaction, switching to their cationic analogues, which displayed the same emission colours of the starting anionic derivatives even if with emission quantum yields significantly reduced.

Experimental Section

General considerations. All the reagents and solvents were obtained commercially (e.g. Aldrich) and used as received without any further purification, unless otherwise specified. All the reactions were carried out under an argon atmosphere following Schlenk protocols. Where required, the purification of the Ir(III) complexes was performed via column chromatography with the use of neutral alumina as the stationary phase. ESI-mass spectra were recorded using a Waters ZQ-4000 instrument (ESI-MS, acetonitrile as the solvent). Nuclear magnetic resonance spectra (consisting of ^{1}H and ^{13}C) were always recorded using a Varian Mercury Plus 600 (^{1}H, 599.7; ^{13}C, 150.8 MHz.) for variable temperature experiments (from -50°C to +25°C) and a Varian Mercury Plus 400 (^{1}H, 399.9; ^{13}C, 101.0 MHz.) for room temperature experiments. ^{1}H and ^{13}C chemical shifts were referenced to residual solvent resonances.

Photophysics. Absorption spectra were recorded at room temperature using a Perkin Elmer Lambda 35 UV/vis spectrometer. Uncorrected steady-state emission and excitation spectra were recorded on an Edinburgh FLSP920 spectrometer equipped with a 450 W xenon arc lamp, double excitation and single emission monochromators, and a Peltier-cooled Hamamatsu R928P photomultiplier tube (185–850 nm). Emission and excitation spectra were acquired with a cut-off filter (395 nm) and corrected for source intensity (lamp and grating) and emission spectral response (detector and grating) by a calibration curve supplied with the instrument. The wavelengths for the emission and excitation spectra were determined using the absorption maxima of the MLCT transition bands (emission spectra) and at the maxima of the emission bands (excitation spectra). Quantum yields (Φ) were determined using the optically dilute method by Crosby and Demas[41] at excitation wavelength obtained from absorption spectra on a wavelength scale [nm] and compared to the reference emitter by the following equation:[42]

$$\phi_s = \phi_r \left[\frac{A_r(\lambda_r)}{A_s(\lambda_s)}\right]\left[\frac{I_r(\lambda_r)}{I_s(\lambda_s)}\right]\left[\frac{n_s^2}{n_r^2}\right]\left[\frac{D_s}{D_r}\right]$$

where A is the absorbance at the excitation wavelength (λ), I is the intensity of the excitation light at the excitation wavelength (λ), n is the refractive index of

the solvent, D is the integrated intensity of the luminescence, and Φ is the quantum yield. The subscripts r and s refer to the reference and the sample, respectively. A stock solution with an absorbance > 0.1 was prepared, then two dilutions were obtained with dilution factors of 20 and 10, resulting in absorbances of about 0.02 and 0.08 respectively. The Lambert-Beer law was assumed to remain linear at the concentrations of the solutions. The degassed measurements were obtained after the solutions were bubbled for 10 minutes under Ar atmosphere, using a septa-sealed quartz cell. Air-equilibrated $[Ru(bpy)_3]Cl_2/H_2O$ solution ($\Phi = 0.028$)[43] was used as reference. The quantum yield determinations were performed at identical excitation wavelengths for the sample and the reference, therefore deleting the $I(\lambda r)/I(\lambda s)$ term in the equation. Emission lifetimes (τ) were determined with the single photon counting technique (TCSPC) with the same Edinburgh FLSP920 spectrometer using pulsed picosecond LED (EPLED 360, fhwm < 800 ps) as the excitation source, with repetition rates between 1 kHz and 1 MHz, and the above-mentioned R928P PMT as detector. The goodness of fit was assessed by minimizing the reduced $\chi 2$ function and by visual inspection of the weighted residuals. To record the 77 K luminescence spectra, the samples were put in quartz tubes (2 mm diameter) and inserted in a special quartz dewar filled with liquid nitrogen. The solvent used in the preparation of the solutions for the photophysical investigations was of spectrometric grade. Experimental uncertainties are estimated to be ±8% for lifetime determinations, ±20% for quantum yields, and ±2 nm and ±5 nm for absorption and emission peaks, respectively.

TD-DFT calculations Time-dependent density functional theory calculations were performed with GAUSSIAN 09.[49] Prior to these calculations, the structures were relaxed at the CAM-B3LYP level of theory.[50] The Ir atoms were treated with the Stuttgart-Dresden effective core potential,[51] the Pople 6-311G** basis set was used for C, H, F and N atoms, and the effect of the solvent was mimicked with the PCM solvation model,[9] with parameters adequate for dichloromethane.

Ligand synthesis

Following the general method reported by Finnegan and coworkers,[20] the ligand [1,2 H_2-BTB] was obtained in almost quantitative yield.

[1,2 H_2-BTB] ^{1}H-NMR (400 MHz, DMSO d^6) δ (ppm) = 7.91 – 7.89 (m, 2H), 7.81 – 7.78 (m, 2H).

General Procedure for the Preparation of the Anionic [Ir(C^N)$_2$(N^N)]$^-$ Type Complexes
In a 50 mL two neck round bottom flask equipped with a stirring bar, 1 equiv of dichlorobridged iridium dimer and 2.5 equiv of [1,2 H_2-BTB] were added to a 3:1 solution of CH_2Cl_2/EtOH. Then, 2.5 equiv of Et_3N were added, and the resulting mixture was stirred at reflux for 24 h. The solution was restored to r.t. and a small amount of Et_2O (5mL) was added to the mother liquor and the respective products, bright yellow solids, precipitated from the solution, collected by filtration and washed with Et_2O (2x10 mL).

[Ir(ppy)$_2$(1,2 BTB)]$^-$ Y = 76.5%, 0.058 g ^{1}**H-NMR** (600 MHz), CD_2Cl_2, 248K, δ (ppm) = 11.45 (s, br, 1H), 8.73 (s, br, 1H, H_d), 8.02 (d, 1H, J_{H-H} = 8.39 Hz, H_c), 7.84 (m, 2H, H_b and ppy), 7.71 (d, 1H, J_{H-H} = 7.79 Hz, H_a), 7.54 (m, 2H), 7.38 – 7.34 (m, 2H), 7.21 – 7.05 (m, 3H), 6.84 – 6.82 (m, 1H), 6.79 – 6.77 (m, 1H), 6.74 – 6.72 (m, 1H), 6.62 – 6.60 (m, 1H), 6.49 (d, 1H, J_{H-H} = 7.79 Hz), 6.23 (m, 1H), 6.12 (d, 1H, J_{H-H} = 7.79 Hz). ^{13}**C-NMR** (150.8 MHz), CD_2Cl_2, 248K, δ (ppm) = 168.60, 168.06, 151.33, 150.70, 145.10, 144.08, 137.30, 136.53, 132.53, 131.63, 131.20, 131.15, 129.95, 128.90, 128.63. **ESI-MS** (*m*/*z*) CH_3CN, $[M]^-$ = 712; $[M]^+$= 102 (Et_3NH). Crystals suitable for X-ray analysis (identified as [Ir(ppy)$_2$(1,2 BTB)][Et_3NH]) were obtained by slow diffusion of diethyl ether into a solution of the complex in dichloromethane. Anal. Calcd. for $C_{36}H_{36}N_{11}Ir$ (814.96): C 53.06, H 4.45, N 18.91. Found: C 53.07, H 4.47, N 18.90 %

[Ir(F_2ppy)$_2$(1,2 BTB)]$^-$ Y = 59%, 0.043 g ^{1}**H-NMR** (600 MHz), CD_2Cl_2, 248K, δ (ppm) = 11.64 (s, br, 1H), 8.78 (d, 1H, J_{H-H} = 5.99 Hz, H_d), 8.44 (d, 1H, J_{H-H} = 8.99 Hz, H_c), 8.00 (d, 1H, J_{H-H} = 4.79 Hz, H_b), 7.92 – 7.89 (m, 2H, H_a and F_2ppy), 7.75 (m, 1H), 7.55 – 7.53 (m, 1H), 7.48 – 7.46 (m, 1H), 7.36 – 7.33 (m, 1H), 7.27 (m, 1H), 7.12 – 7.10 (m, 1H), 6.44 – 6.37 (m, 1H), 6.35 – 6.32 (m, 1H), 6.02 – 6.00 (m,1H), 5.71 – 5.69 (m, 1H). ^{13}**C-NMR** (150.8 MHz), CD_2Cl_2, 248K, δ (ppm) = 165.42, 164.76, 163.13, 161.91, 161.46, 160.93, 157.74, 157.21, 151.48, 151.14, 137.98, 137.37, 131.63, 131.15, 130.74, 129.57, 129.54, 129.46, 129.20, 128.64, 128.43, 128.21, 128.14, 123.92, 122.51, 122.08, 121.85, 120.16, 114.63, 113.18. **ESI-MS** (*m*/*z*) $[M]^-$ = 784; $[M]^+$= 102 (Et_3NH) Anal. Calcd. for $C_{36}H_{32}N_{11}F_4Ir$ (886.92): C 48.75, H 3.64, N 17.37. Found: C 48.70, H 3.66 ,N 17.40 %

Emission titration of Anionic Ir(III) tetrazolate complexes with $HOSO_2CF_3$

In the $HOSO_2CF_3$ emission titration a 10 mL stock solution of **$[Ir(ppy)_2(1,2\ BTB)]^-$** ($1{,}23*10^{-4}$M) in CH_2Cl_2 was prepared. 2 mL of the stock solution were then transferred to a quartz cuvette and the emission spectrum of the solution was measured after successive additions (10 μL aliquots for 12 additions) with $HOSO_2CF_3$ in CH_2Cl_2, 0,005 M. For the $HOSO_2CF_3$ emission titration of **$[Ir(F_2ppy)_2(1,2\ BTB)]^-$**, a 10 mL stock solution ($1{,}13*10^{-4}$M) in CH_2Cl_2 was prepared. 2 mL of the stock solution were then transferred to a quartz cuvette and the emission spectrum of the solution was measured after successive additions (10 μL aliquots for 12 additions) with $HOSO_2CF_3$ in CH_2Cl_2, 0,01 M.

General Procedure for the preparation of $[Ir(C^N)_2(N^NMe_2)]^+$ - type complexes

Methylation of $[Ir(ppy)_2(1,2\ BTB)]^-$ and $[Ir(F_2ppy)_2(1,2\ BTB)]^-$ was carried out according to a previously reported procedure.[5] The complex $[Ir(C^N)_2(1,2\ BTB)]^-$ (1 eq.) was added to dichloromethane and the mixture was allowed to cool down by immersion into an ethanol/liquid nitrogen cold bath. Then, methyl trifluoromethanesulfonate (2.1 eq., solution in dichloromethane 0.179 M) was added. The reaction was stirred under nitrogen for 30 minutes while being kept in the cold bath, and then allowed to warm up to room temperature and stirred for 3 hours. Anion exchange was carried out by adding an excess of NH_4PF_6 in water to the solution and stirring for 20 minutes. The product was then extracted using dichloromethane (3 × 10 mL) and the organic components were combined and dried over anhydrous $MgSO_4$.

$[Ir(ppy)_2(1,2\ BTBMe_2)]^+$ Y = 31.7%, 0.021 g. **^{1}H-NMR** (400 MHz), Acetone-d^6, 298K, δ (ppm) = 8.51 (d, 1H, $J_{H\text{-}H}$ = 5.59 Hz), 8.44 (m, 1H, H_d), 8.32 (m, 1H), 8.25-8.19 (m, 1H, H_c), 8.09-8.05 (m, 2H), 8.00-7.96 (m, 1H, H_b), 7.92-7.85 (m, 2H), 7.80-7.78 (m, 1H, H_a), 7.74-7.70 (m, 1H), 7.53-7.51 (m, 1H), 7.30-7.29 (m, 1H), 6.87-6.76 (m, 3H), 6.66-6.61 (m, 2H), 6.52 (d, 1H, $J_{H\text{-}H}$ =7.59 Hz), 6.11 (d, 1H, $J_{H\text{-}H}$ = 7.59 Hz), 4.22 (s, 3H, CH_3), 4.12 (s, 3H, CH_3). **^{13}C-NMR** (100 MHz), Acetone-d^6, 298K, δ (ppm) = 168.86, 168.09, 154.54 (Ct), 153.74 (Ct), 151.32, 150.28, 146.58, 144.12, 138.54, 137.72, 133.71, 13.19, 132.16, 131.04, 129.12, 128.65, 124.28, 123.66, 122.82, 121.97, 121.92, 121.83, 121.27, 119.25, 118.84, 35.86, 35.63. **ESI-MS** (*m*/*z*) $[M]^+$ = 743; $[M]^-$= 145 (PF_6). Anal. Calcd. for $C_{32}H_{26}N_{10}F_6P_1Ir_1$ (887.80): C 43.29, H 2.95, N 15.78. Found: C 43.31, H 2.94,N 15.77 %

[Ir(F_2ppy)$_2$(1,2 BTBMe$_2$)] Y = 28.7%, 0.019 g ^{1}**H-NMR** (400 MHz), Acetone-d^6, 298K, δ (ppm) = 8.52 (d, 1H, J_{H-H} = 8.39 Hz), 8.43-8.41 (m, 2H, H_a and F_2ppy), 8.24-8.17 (m, 3H, H_c and F_2ppy), 8.07 (d, 1H, J_{H-H} = 8.39 Hz), 8.00-7.96 (m, 1H, H_b), 7.85-7.80 (m, 2H, H_a and F_2ppy), 7.37-7.34 (m, 1H), 6.73-6.70 (m, 1H), 6.64-6.51 (m, 2H), 5.97-5.94 (m, 1H), 5.64-5.62 (m, 1H), 4.24 (s, 3H, CH_3), 4.14 (s, 3H, CH_3). ^{13}**C-NMR** (100 MHz), Acetone-d^6, 298K, δ (ppm) = 165.72, 165.10, 164.59, 161.93, 160.51, 159.94, 155.56 (Ct), 154.86 (Ct), 152.41, 152.03, 151.97, 151.86, 151.78, 140.61, 139.89, 134.76, 134.32, 133.25, 129.84, 129.11, 123.99, 123.78, 123.36, 122.82, 116.14, 114.23, 99.20, 99.12, 98.85, 98.66, 36.91, 36.72. **ESI-MS** (*m*/*z*) $[M]^+$ = 815; $[M]^-$= 145 (PF_6). Anal. Calcd. for $C_{32}H_{22}N_{10}F_{10}P_1Ir_1$ (959.76): C 40.05, H 2.31, N 14.59. Found: C 40.00, H 2.30, N 14.61 %

X-ray crystallography

Crystal data and collection details for [$HNEt_3$][Ir(ppy)$_2$(1,2-BTB)] are reported in Table S1, ESI. The diffraction experiments were carried out on a Bruker APEX II diffractometer equipped with a CCD detector and using Mo-Ka radiation. Data were corrected for Lorentz polarization and absorption effects (empirical absorption correction SADABS.[52] Structures were solved by direct methods and refined by full-matrix least-squares based on all data using F^2.[53] H-atoms were placed in calculated positions, and refined isotropically using a riding model. All non-hydrogen atoms were refined with anisotropic displacement parameters, a part from disordered atoms. One Et groups of the $[HNEt_3]^+$ cation is disordered: this has been split into two positions and refined isotropically using one occupancy factor per disordered group. Similar *U* restraints (SIMU line in SHELXL; s.u. 0.01) were applied to the $[HNEt_3]^+$ cation.

CCDC 1486766 for [$HNEt_3$][Ir(ppy)$_2$(1,2-BTB)]$^-$ contain the supplementary crystallographic data for this chapter.

Table C4: Crystal data and collection details $[HNEt_3][Ir(ppy)_2(1,2\ BTB)]$.

Formula	$C_{36}H_{36}IrN_{11}$
Fw	814.96
***T*, K**	100(2)
***λ*, Å**	0.71073
Crystal system	Triclinic
Space Group	$P\bar{1}$
***a*, Å**	12.0892(5)
***b*, Å**	12.2178(5)
***c*, Å**	12.8423(6)
***a*, °**	72.808(3)
***β*, °**	73.021(2)
***g*, °**	63.995(2)
Cell Volume, Å^3	1599.23(12)
Z	2
D_{calc}, g cm^{-3}	1.692
μ, mm^{-1}	4.221
F(000)	812
Crystal size, mm	0.13×0.11×0.09
θ limits, °	1.91–25.03
Index ranges	-14≤ h ≤ 14 -14≤ k ≤ 10 -15≤ l ≤15
Reflections collected	22006
Independent reflections	5648 [R_{int} = 0.0638]
Completeness to θ max	99.8%
Data / restraints / parameters	5648 / 51 / 433
Goodness on fit on F^2	1.066
R_1 (I> 2σ(I))	0.0444
wR_2 (all data)	0.1140
Largest diff. peak and hole, e Å^{-3}	3.463 / –1.933

Chapter 5

Fully Ir(III) tetrazolate soft salts: the road to white light emitting ion pairs*

Abstract

Ir(III)-based ionic transition-metal complexes (Ir-iTMC) occupy a prominent position in the scenery of phosphorescent molecules to be used in solid state lighting, luminescent chemosensing and for bioimaging applications. This is a direct consequence of their belonging to the family of Ir(III) cyclometalated complexes, a class of compounds that displays a combination of outstanding photo- and electroluminescent performance, together with the ease of emission colour tunability via modification of the ligand environment. In this context, even though the family of Ir-iTMC is largely dominated by cationic species with the general formula $[Ir(N^C)_2(L^L)]^+$, where the neutral ligand (L^L) is often represented by aromatic diimines (N^N), negatively charged Ir(III) cyclometalated complexes have also attracted increasing attention in light of their favourable properties. More specifically, the studies dealing with this class of brightly phosphorescent complexes, have led to interesting results on the use of their alkali metal salts as emissive materials for light-emitting electrochemical cells (LEECs), the construction of Ir(III)-Ln(III) arrays,and, in combination with other cationic Ir(III) complexes, the formation of the so called "Ir-based soft salts" where further colour tuning of the emission can be achieved with the combination or modulation of energy transfer processes between the ionic components.

*: *This chapter is part of Dalton. Trans*, **2016**, *45*, 3256;[a] *Dalton. Trans*, **2016**, *45, 12884*.[a]

Introduction: Ir(III) fully tetrazolate soft salts

Since the first report of organic light-emitting devices (OLED), an extensive amount of research has been dedicated to this field. One of the most successful phosphorescent emitters are cyclometalated Ir(III) complexes due to their strong spin-orbit coupling, phosphorescent lifetimes in the microsecond scale, high PL quantum yields even at room temperature and good emission color tunability in all the visible spectrum. Both neutral and ionic Ir(III) complexes have these photophysical properties. Neutral Ir based complexes have been used in OLED structures, while Cationic Ir complexes have been used in light-emitting electrochemical cells (LEC), an alternative kind of electroluminescent devices, while the studies of anionic Ir(III) complexes have been mainly focused on their photophysics. "Soft salt" is a term introduced to describe ionic materials that are composed of only organometallic compounds, lacking other ions commonly present as counterions for these materials. These salts are named "soft", because their ions have larger radii than simple halide or alkali ions.[38a, b, c] Various cluster ions and soft salts with different transition metals have been studied. Mononuclear Ir-based soft salts have not been extensively examined and are interesting alternatives in OLEDs to the neutral materials that have been

explored extensively in this application. These ion pairs can be easily synthesized through metathesis reactions and presents clearly distinct emission arising from the anionic and the cationic complexes, due to the independent nature of oppositely charged ions.

Herein, we present the synthesis, characterization and photophysical properties for ten different soft salts. The results presented highlight the formation of soft salts whose emission is highly dependent on the oxygen content, suggesting a potential for the luminescence-sensing response to the presence of dissolved O_2, and a unique example of white-emitting Ir(III) based soft salts.

Results and discussion

Synthesis and Characterization

As previously described in chapter 3 and 4, the preparation of the anionic complexes has been accomplished through a slightly modified procedure by Nazeeruddin and coworkers, where the chloride bridged Ir(III) dimer was reacted with an excess of 5-aryl tetrazole and base.[36] The targeted anionic complexes were confirmed by NMR spectroscopy and ESI-Mass spectrometry (see Chapter 3, 4). In particular, the NMR characterisation provided results consistent with the formation of species having the expected C_{2v} symmetry. Resonances at *ca*. 163 ppm in the ^{13}C-NMR spectra suggest that the tetrazolate ligands are exclusively coordinated via the N-2 atoms.

The cationic complexes $[Ir(ppy)_2TPYZ\text{-}Me]^+$ and $[Ir(bzq)_2TPYZ\text{-}Me]^+$ (where bzq = benzo[*h*]quinolinato) were obtained by the reaction of the neutral Ir(III) tetrazolate precursors with one equivalent of methyl triflate (Figure 1.5).

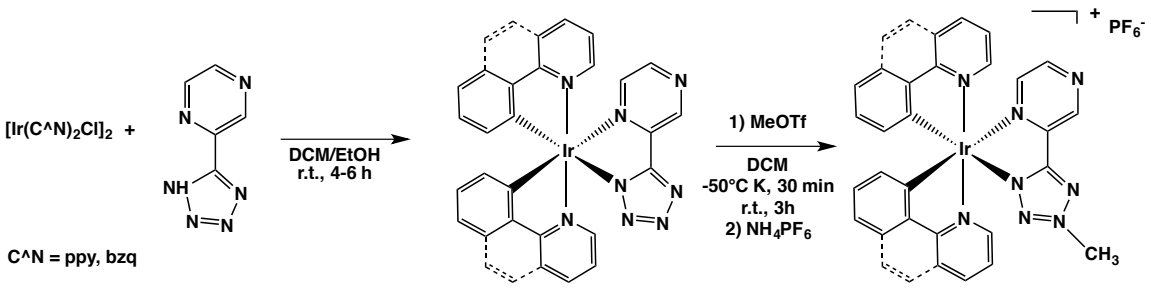

Figure 1.5: Synthetic procedure used for the preparation of Cationic Ir(III) tetrazolate complexes

The formation of the cationic products was first deduced by the means of ESI-MS, which confirmed the presence of the desired cationic complexes producing the expected isotopic pattern at $[M]^+ = 663$ *m/z* for $[Ir(ppy)_2TPYZ\text{-}Me]^+$ and $[M]^+ = 711$ *m/z* for $[Ir(bzq)_2TPYZ\text{-}Me]^+$ in the positive ions region. The saline nature of both cationic Ir(III) derivative was confirmed by the presence of the signal attributable to $[PF_6]^-$ counter ion in the negative regions at $[M]^- = 145$ *m/z*. (Figure 2.5).

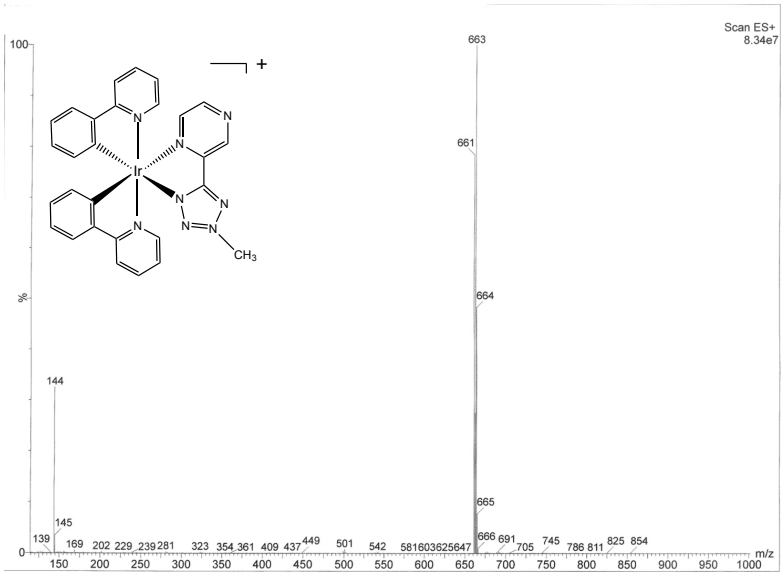

Figure 2.5: ESI-MS spectrum of $[Ir(ppy)_2(TPYZ\text{-}Me)]^+$ (positive ions region) [M] = 663 m/z, CH_3CN

The ^{1}H-NMR spectra of the cationic complexes revealed the presence of a number of resonances equal to the total number of protons in the molecules, as expected for C_s symmetry-type complexes (Figure 3.5).

The methylation reaction performed onto neutral Ir(III) derivatives according to the conditions reported in Figure 1.5, regioselectively occurred at the N-3 position of the coordinated tetrazolate ring, as suggested by the presence of one single tetrazole carbon (Ct) resonance at ca. 166 ppm for $[Ir(ppy)_2TPYZ\text{-}Me]^+$ (Figure 4.5).[34, 44]

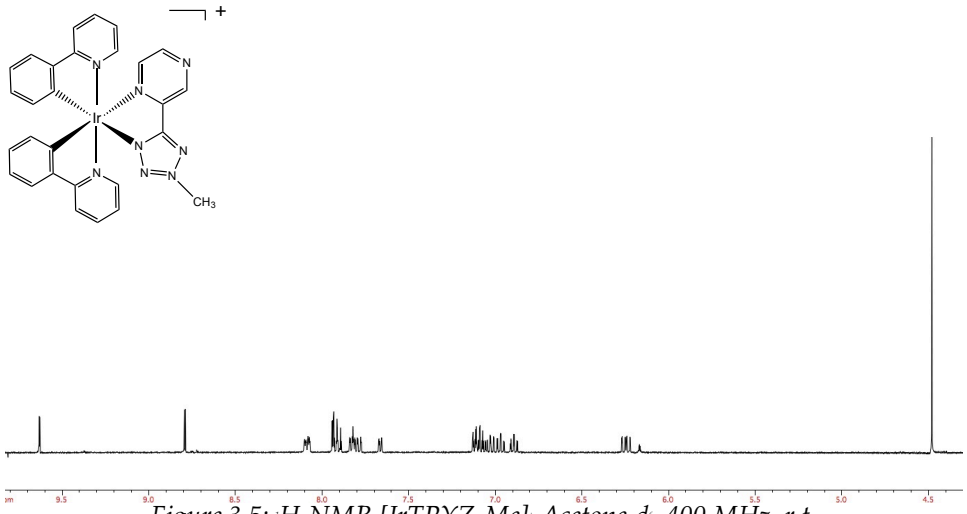

Figure 3.5: ^{1}H-NMR [IrTPYZ-Me]$^{+}$ Acetone-d$_6$, 400 MHz, r.t.

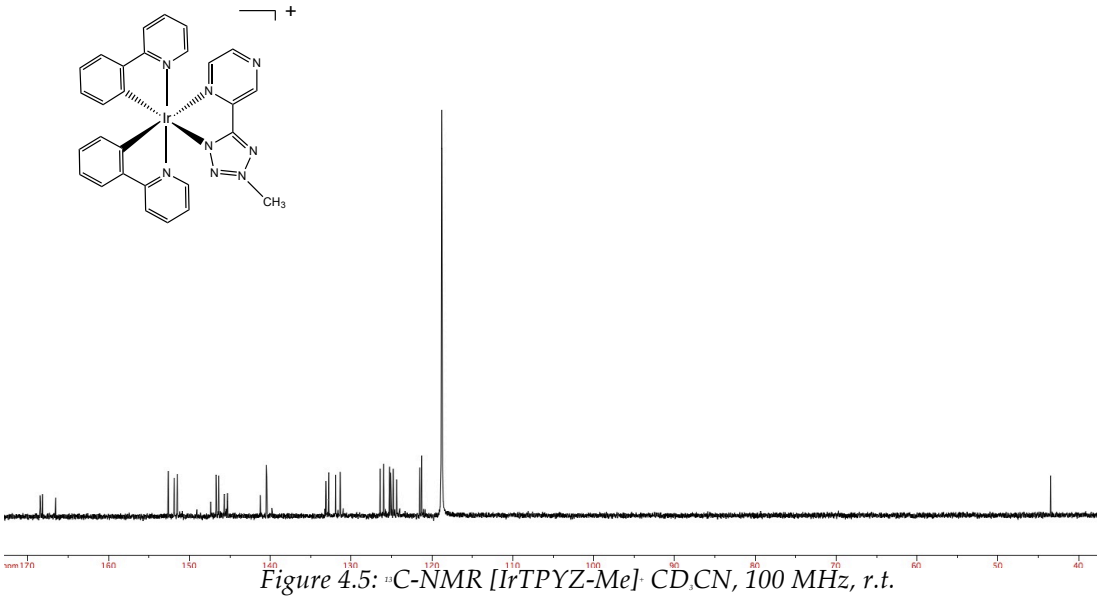

Figure 4.5: ^{13}C-NMR [IrTPYZ-Me]$^{+}$ CD$_3$CN, 100 MHz, r.t.

According to the method reported by Thompson and co-workers,[38a] the new Ir(III)-based soft salts SS1-10 were prepared by dissolving equimolar amounts of the anionic (both $[Ir(C^N)_2(L)_2]^-$ and $[Ir(C^N)_2(N^N)]^-$type complexes) and cationic Ir(III) complexes in H_2O at room temperature (Figure 5.5, 6.5).

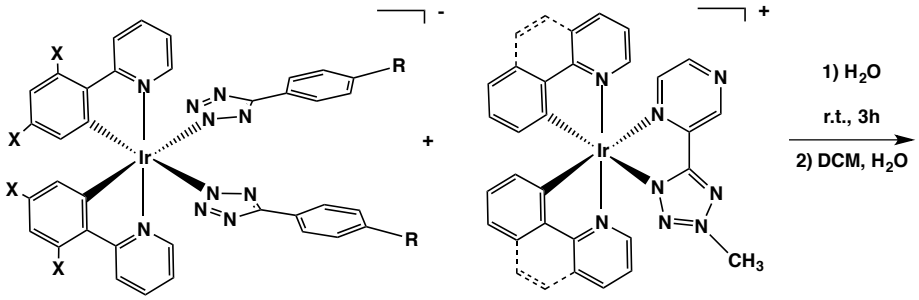

Figure 5.5: Synthetic procedure used for the preparation on Ir(III) soft salts

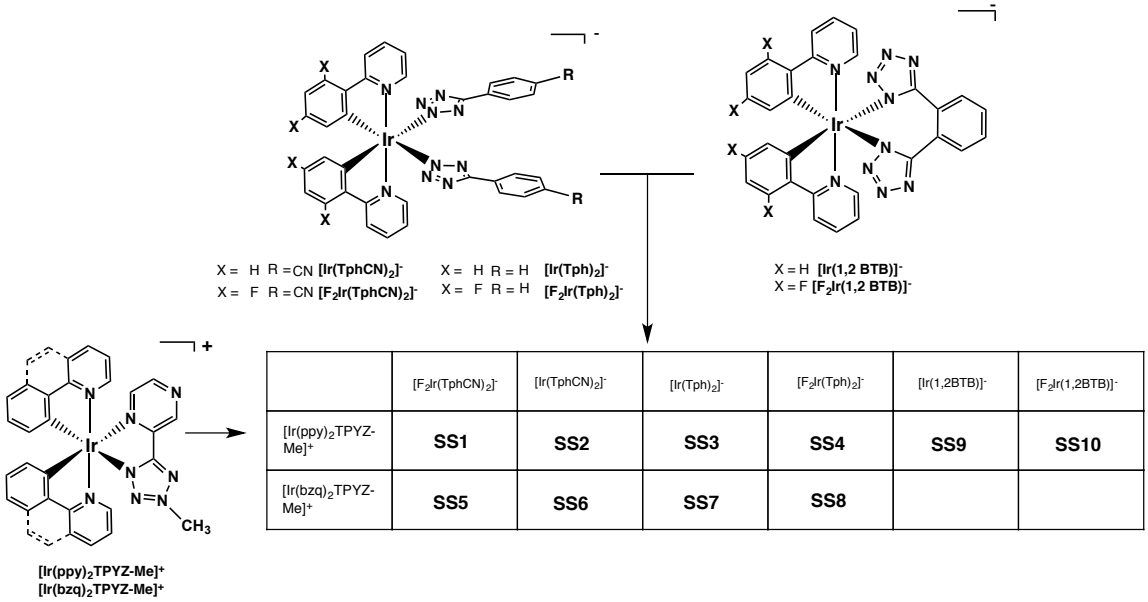

	$[F_2Ir(TphCN)_2]^-$	$[Ir(TphCN)_2]^-$	$[Ir(Tph)_2]^-$	$[F_2Ir(Tph)_2]^-$	$[Ir(1,2BTB)]^-$	$[F_2Ir(1,2BTB)]^-$
$[Ir(ppy)_2TPYZ\text{-}Me]^+$	**SS1**	**SS2**	**SS3**	**SS4**	**SS9**	**SS10**
$[Ir(bzq)_2TPYZ\text{-}Me]^+$	**SS5**	**SS6**	**SS7**	**SS8**		

Figure 6.5: Acronyms used for Ir(III) soft salts

The subsequent extraction with dichloromethane gave rise to crude products whose ^{1}H-NMR analysis confirmed the presence of two distinct patterns of signals in 1/1 ratio. The isolation of the soft salt was further confirmed by the lack of triethylammonium peaks in the ^{1}H-NMR spectra (Figure 7.5).

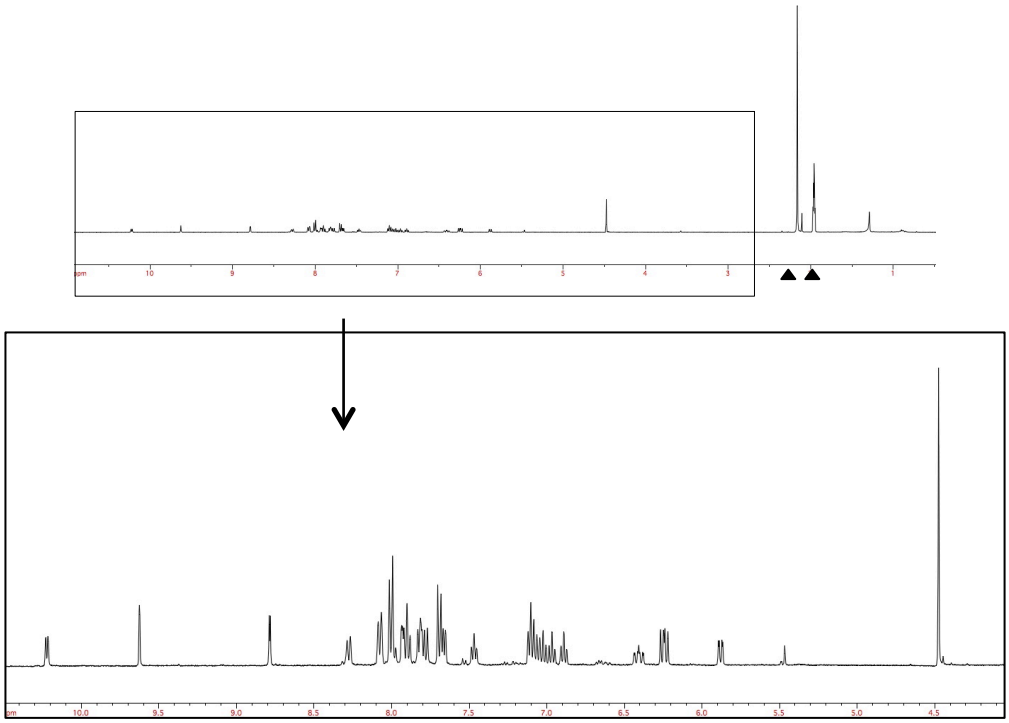

Figure 7.5: ^{1}H-NMR SS1 CD_3CN, 400 MHz, r.t. ▲ = ^{1}H signals of residual of non deuterated CD_3CN and water

Photophysical properties

Anionic Ir(III) tetrazolate complexes

As previously described in Chapter 3 and 4, in dichloromethane solutions at room temperature, all the anionic Ir(III) complexes show quite typical absorption profiles, with the spectral region up to 300 nm dominated by intense ligand centred (^{1}LC) π-π* transitions involving both the cyclometalating and the ancillary tetrazolate ligands.[34, 44] Weaker and broader spin allowed (^{1}MLCT) and spin forbidden (^{3}MLCT) bands are found at longer wavelength (300 to 380 nm, Figure 8.5, Left).

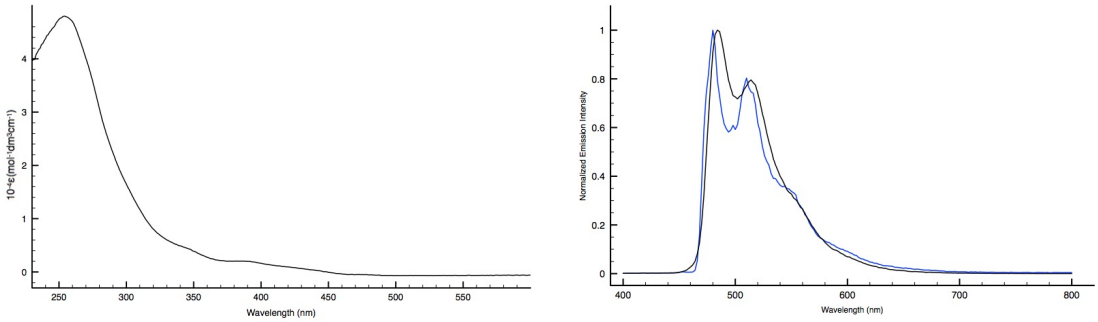

Figure 8.5: Left - Absorption profile of [Ir(Tph)$_2$], Right Emission spectra of [Ir(Tph)$_2$], 298K (black line), 77K (blue line), CH_2Cl_2, 10^{-5}M

All the anionic Ir(III) complexes display wavelength-independent and intense sky-blue or aqua emission originating from excited states of triplet character, an assignment supported by the oxygen sensitivity of the quantum yield (ϕ) lifetimes (τ) values (Table 5). The emission profiles appear strongly structured, which is representative for the interplay of ^{3}LC/^{3}MLCT type emissive excited states. The likely prevalent contribution of the ^{3}LC states over the ^{3}MLCT ones is suggested by the rather small rigidochromic blue shift that was encountered at 77K (Figure 8.5, right).

Table 5: Selected Photophysical data of Anionic Ir(III) tetrazolate complexes

CH_2Cl_2 as solvent	***Absorption***	***Emission 298 K***					***Emission 77K***	
	λ_{abs}(nm);($10^{-3}\varepsilon$)($M^{-1}cm^{-1}$)	λ_{em}(nm)	τ_{em} (μs)	τ_{Av}(μs)	ϕ_{em}(%)	ϕ_{Av}(%)	λ_{em}(nm)	τ (μs)
[Ir(Tph)$_2$]$^-$	255(4.8), 346(0.44), 387(0.20)	484, 514	0.12	1.27	5.5	60.6	480, 510	4.09
[F$_2$(IrTph)$_2$]$^-$	254(5.9), 308(1.2), 370(0.22)	462, 490	0.16	1.99	5.9	49	458, 490	3.23
[Ir(TphCN)$_2$]$^-$	260(7.3), 295(3.1) 393 (0.2)	490, 520	0.11	0.80	3.4	24.9	480, 516, 556$_{sh}$	4.03
[F$_2$Ir(TphCN)$_2$]$^-$	260(4.0), 377(0.24), 318(1.1)	462, 492	0.17	1.35	3.3	22	460, 490, 522$_{sh}$	3.25
[Ir(ppy)$_2$(1,2 BTB)]$^-$	261(4.56) 305(1.65)	488 516	0.10	0.820	2.93	33.3	482 516	2.24
[Ir(F$_2$ppy)$_2$(1,2 BTB)]$^-$	254(2.72) 307(0.89)	460 490	0.120	1.60	2.64	53.0	456 490	2.20

Cationic Ir(III) tetrazolate complexes

The absorption spectra of the cationic complexes $[Ir(ppy)_2TPYZ\text{-}Me]^+$ and $[Ir(bzq)_2TPYZ\text{-}Me]^+$ (Figure 9.5, left) are in agreement with the peculiarities of octahedral d^6 transition metal complexes, displaying a slight hypsochromic shift displayed by the MLCT bands in respect of those observed from anionic Ir(III) derivatives.

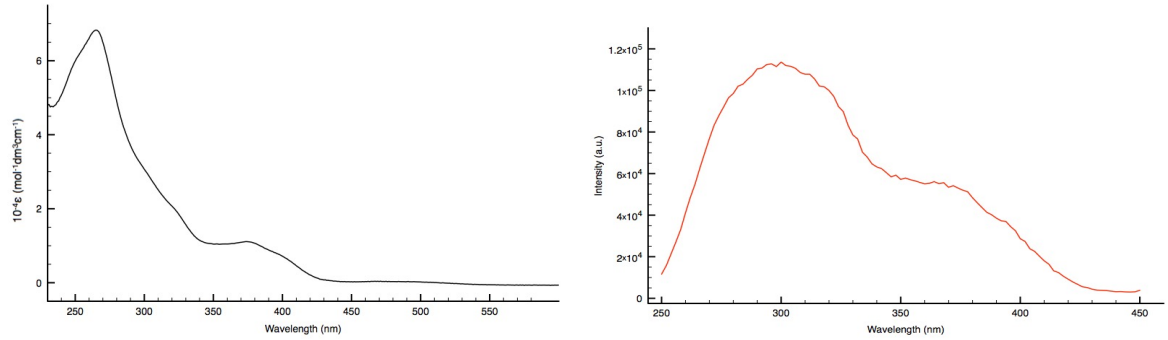

Figure 9.5: Left - Absorption profile $[Ir(ppy)_2TPYZ\text{-}Me]^+$, Right – Excitation profile $[Ir(ppy)_2TPYZ\text{-}Me]^+$, λ_{emi} = 686 nm; CH_2Cl_2, r.t.

The addition of a methyl group to the coordinated tetrazolate ring of the neutral precursors $[Ir(ppy)_2TPYZ]$ and $[Ir(bzq)_2TPYZ]$ resulted in the formation of the corresponding deep-red emitting cationic derivatives $[Ir(ppy)_2TPYZ\text{-}Me]^+$ and $[Ir(bzq)_2TPYZ\text{-}Me]^+$ (λ = 686 nm and 671 nm respectively, Table 6). The cationic Ir(III) complexes displayed broad and structureless emission profiles, again originating from excited states of triplet multiplicity. The MLCT character of emissive excited states was made evident in consideration of the pronounced rigidochromic blue shift at 77K (Figure 10.5).

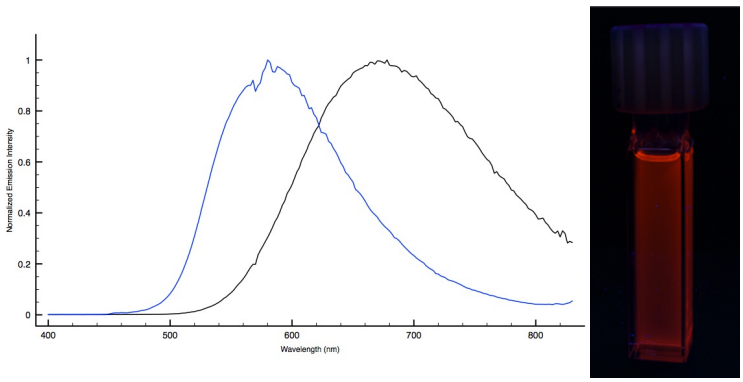

Figure 10.5: Emission spectra $[Ir(ppy)_2TPYZ\text{-}Me]^+$, 298K (black line), 77K (blue line), CH_2Cl_2

Table 5: Selected Photophysical data of Cationic Ir(III) tetrazolate complexes

CH_2Cl_2as solvent	***Absorption*** λ_{abs}(nm);($10^{-4}\varepsilon$)($M^{-1}cm^{-1}$)	***Emission 298 K***					***Emission 77K***	
		λ_{em}(nm)	τ_{av} (μs)	τ_{nr}(μs)	ϕ_{em}(%)	ϕ_{nr}(%)	λ_{em}(nm)	τ (μs)
[Ir(ppy)$_2$TPYZ-Me]$^+$	265(6.8), 327(1.7), 377(1.1)	686	0.09	0.095	2.71	3.61	582	4.50
[Ir(bzq)$_2$TPYZ-Me]$^+$	257(5.9), 312(2.2), 411(0.67)	671	0.09	0.11	2.27	2.40	580	2.50

Fully Ir(III) tetrazolate Soft Salts

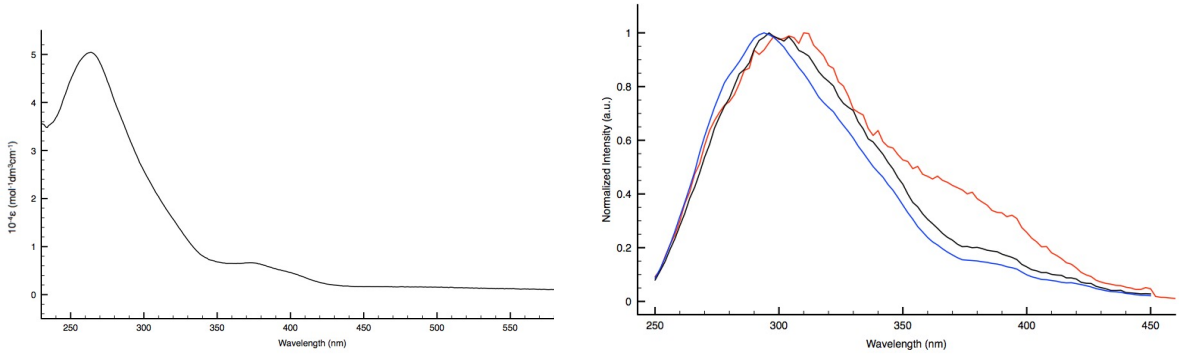

Figure 11.5: Left - Absorption profile SS1; Right – Normalized Excitation profiles SS1 λ_{exc} = 460 nm (black trace), 490 nm (blue trace) 680 nm (red trace), CH_2Cl_2, r.t.

In dichloromethane solutions at room temperature, all the Ir(III) soft salts displayed absorption profiles ranging from 300 nm to 400 nm, which displayed both the contribution stemming from the anion and the cation, making for instance the selective excitation of one component of the ion pair impossible (Figure 11.5).

Table 7: Photophysical data of Ir(III) tetrazolate soft salts

CH_2Cl_2 as solvent	***Absorption*** λ_{abs}(nm);($10^{-4}\varepsilon$)($M^{-1}cm^{-1}$)	***Emission 298 K***					***Emission 77K***	
		λ_{em} (nm)	τ_{air} (μs)	τ_{Ar}(μs)	ϕ_{air}(%)	ϕ_{Ar}(%)	λ_{em}(nm)	τ (μs)
SS1 $[F_2Ir(TphCN)_2]$ $[Ir(ppy)_2TPYZ\text{-}Me]$	261(4.93), 314(1.50), 377(0.39)	460, 490, 680	0.16, 0.15, 0.09	1.19, 1.11, 0.11	2.82	7.02	454, 484, 574	3.8, 3.9, 4.6
SS2 $[Ir(TphCN)_3]$ $[Ir(ppy)_2TPYZ\text{-}Me]$	263(7.09), 343(1.18), 385(0.69)	486, 518, 664	0.10, 0.10, 0.11	0.66, 0.65, 0.14	3.14	14.83	480, 574	1.07, 2.45
SS3 $[Ir(Tph)_3]$ $[Ir(ppy)_2TPYZ\text{-}Me]$	262(5.19), 320(1.49), 381(0.63)	486, 518, 680	0.12, 0.12, 0.09	1.46, 1.44, 0.11	3.56	12.3	480, 574, 510	3.13, 3.16, 3.27
SS4 $[F_2(IrTph)_2]$ $[Ir(ppy)_2TPYZ\text{-}Me]$	255(3.60), 317(0.95), 377(0.43)	462, 490, 680	0.19, 0.20, 0.09	1.28, 1.22, 0.10	3.02	16.9	454, 488, 578	2.28, 2.80, 3.07
SS5 $[F_2Ir(TphCN)_2]$ $[Ir(bzq)_2TPYZ\text{-}Me]$	257(6.1), 314(2.3), 413(0.43)	462, 490, 666	0.14, 0.13, 0.10	1.14, 1.19, 0.11	1.89	9.71	452, 484, 546	3.25, 3.40,3.75
SS6 $[Ir(TphCN)_3]$ $[Ir(bzq)_2TPYZ\text{-}Me]$	257(5.7), 310(2.1), 413(0.26)	488, 520, 664	0.08, 0.10, 0.09	1.00, 1.02, 0.10	2.05	6.33	480, 510, 552	3.83, 4.05,3.50
SS7 $[F_2Ir(Tph)_2]$ $[Ir(bzq)_2TPYZ\text{-}Me]$	257(5.1), 314(1.8), 415(0.45)	486, 518 654	0.13, 0.13, 0.11	1.59, 1.56, 0.17	2.11	10.0	474, 510 548	3.27, 5.65 5.86
SS8 $[Ir(Tph)_3]$ $[Ir(bzq)_2TPYZ\text{-}Me]$	253(5.1), 310(1.8), 417(0.46)	460, 490 656	0.24, 0.23, 0.12	2.05, 1.96, 0.16	1.90	5.70	454, 486 544	3.16, 3.22 6.40
SS9 $[Ir(1,2\ BTB)]$ $[Ir(ppy)_2TPYZ\text{-}Me]$	262(7.0), 307(2.9) 379(1.0)	490, 522, 670	0.08, 0.07, 0.10	1.30, 1.20, 0.10	3.1	22.4	568	3.9
SS10 $[F_2Ir(1,2\ BTB)]$ $[Ir(ppy)_2TPYZ\text{-}Me]$	259(5.6), 312(2.0) 380(0.8)	464, 490, 674	0.12, 0.12, 0.07	0.65, 0.68, 0.08	2.9	16.6	574	3.7

Ion pairs with $[Ir(bzq)_2(TPYZ\text{-}Me)]^+$ as cationic counterpart: SS5-8

At first, the photophysical behaviour of the ion pairs SS5-8 will be discussed. In these soft salts, the anionic counterparts are constituted by $[Ir(C^N)_2(L)_2]^-$type complexes (discussed in chapter 3) and the cationic Ir(III) tetrazolate complex is the $[Ir(bzq)_2(TPYZ\text{-}Me)]^+$, with λ max = 671 nm (Figure 12.5).

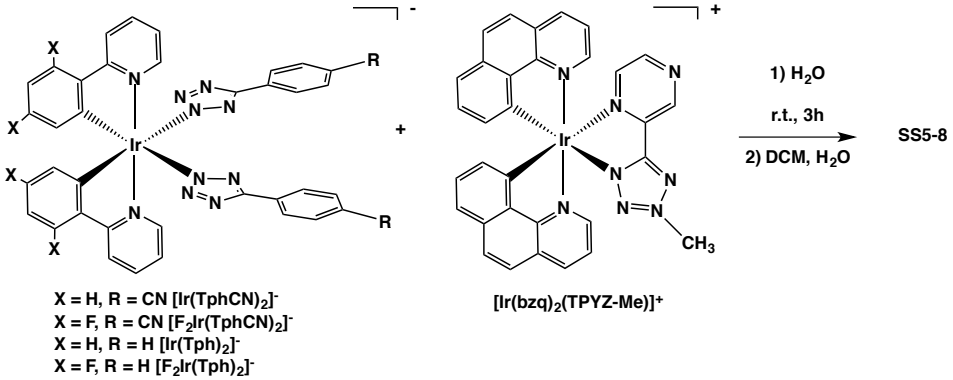

Figure 12.5: Synthetic procedure used for SS5-8

Table 8: Photophysical data of SS5-8

CH_2Cl_2 as solvent	***Emission 298 K***					***Emission 77K***		***CIE***	
	λ_{em} (nm)	τ_{av} (μs)	τ_{av}(μs)	ϕ_{em}(%)	ϕ_{tot}(%)	λ_{em}(nm)	τ (μs)	*ox*	*deox*
SS5 $[F_2Ir(TphCN)_2]^-$ $[Ir(bzq)_2TPYZ\text{-}Me]^+$	462, 490, 666	0.14, 0.13, 0.10	1.14, 1.19, 0.11	1.89	9.71	452, 484, 546	3.25, 3.40,3.75	X = 0.365 Y= 0.356	X = 0.258 Y = 0.404
SS6 $[Ir(TphCN)_2]^-$ $[Ir(bzq)_2TPYZ\text{-}Me]^+$	488, 520, 664	0.08, 0.10, 0.09	1.00, 1.02, 0.10	2.05	6.33	480, 510, 552	3.83, 4.05,3.50	X=0.420 Y=0.4659	X=0.2987 Y=0.5421
SS7 $[F_2Ir(Tph)_2]^-$ $[Ir(bzq)_2TPYZ\text{-}Me]^+$	486, 518 654	0.13, 0.13, 0.11	1.59, 1.56, 0.17	2.11	10.0	474, 510 548	3.27, 5.65 5.86	X=0.4713 Y=0.4402	X=0.2999 Y=0.5153
SS8 $[Ir(Tph)_2]^-$ $[Ir(bzq)_2TPYZ\text{-}Me]^+$	460, 490 656	0.24, 0.23, 0.12	2.05, 1.96, 0.16	1.90	5.70	454, 486 544	3.16, 3.22 6.40	X=0.3910 Y=0.3655	X=0.2776 Y=0.3779
$[Ir(bzq)_2TPYZ\text{-}Me]^+$	671	0.09	0.11	2.27	2.40	580	2.50	n.d	n.d
$[Ir(Tph)_2]^-$	484, 514	0.12	1.27	5.5	60.6	480, 510	4.09	n.d	n.d
$[F_2(IrTph)_2]^-$	462, 490	0.16	1.99	5.9	49	458, 490	3.23	n.d	n.d
$[Ir(TphCN)_2]^-$	490, 520	0.11	0.80	3.4	24.9	480,516, 556_{sh}	4.03	n.d	n.d
$[F_2Ir(TphCN)_2]^-$	462, 492	0.17	1.35	3.3	22	460,490, 522_{sh}	3.25	n.d	n.d

Upon excitation (λ_{exc} = 370 nm) of the corresponding air-equilibrated and diluted (10^{-5} M) dichloromethane solutions, the photoluminescence spectra of the newly obtained soft salts display the emission of both the anionic and cationic

counterparts (Figure 13.5), with lifetimes parameters that do not differ appreciably with respect to those of the individual mononuclear complexes (Tables 5, 7 and 8).

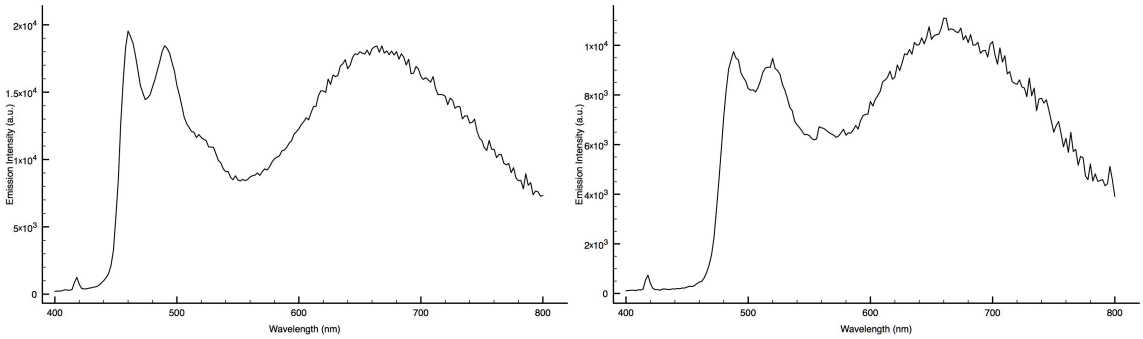

Figure 13.5: Emission Profiles of SS5 (Left) and SS6 (Right), air equilibrated 10^{-5} M CH_2Cl_2 solutions, r.t.

This feature led to the emission of an orange colour from the SS6 and SS8 ion pairs (due to the presence of the aqua-emission contribution of the anionic counterpart) while, relative to the ion pair SS5 and SS7 a magenta emission (as a consequence of the blue shifted emission maxima of the fluorine-anionic derivative, Table 8 for CIE) was observed.

This picture changed dramatically upon passing to deoxygenated solutions, which all displayed the predominant emission of the anionic complexes (Figure 14.5 for SS6, Figure 15.5 for SS5).

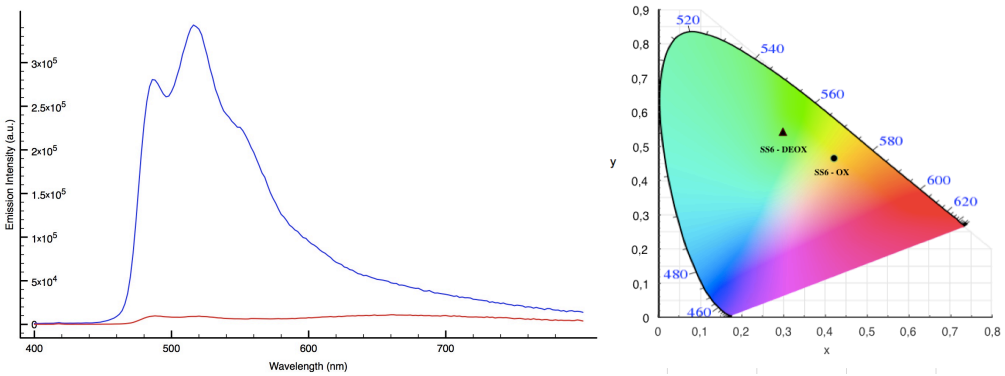

Figure 14.5: Left, Emission Profile of SS6, air equilibrated solution (red line) and deoxygenated solution (blue line), 10^{-5}M, CH_2Cl_2, r.t; Right, CIE coordinates for SS6, air equilibrated and deoxygenated solutions

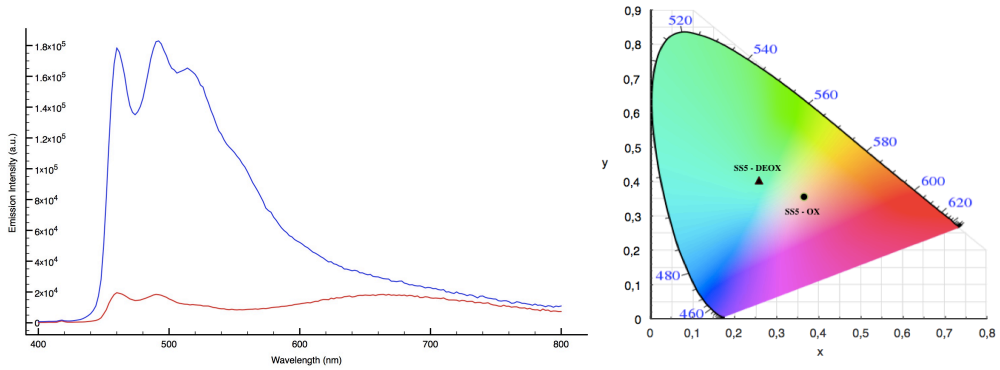

Figure 15.5: Left, Emission Profile of SS5, air equilibrated solution (red line) and deoxygenated solution (blue line), 10^{-5}M, CH_2Cl_2, r.t; Right, CIE coordinates for SS5, air equilibrated and deoxygenated solutions

Ion pairs with non fluorinated $[Ir(ppy)_2(L)_2]$/$[Ir(ppy)_2(L)]$-type anions and $[Ir(ppy)_2(TPYZ\text{-}Me)]^+$ as cationic counterpart: SS2, 3, 9

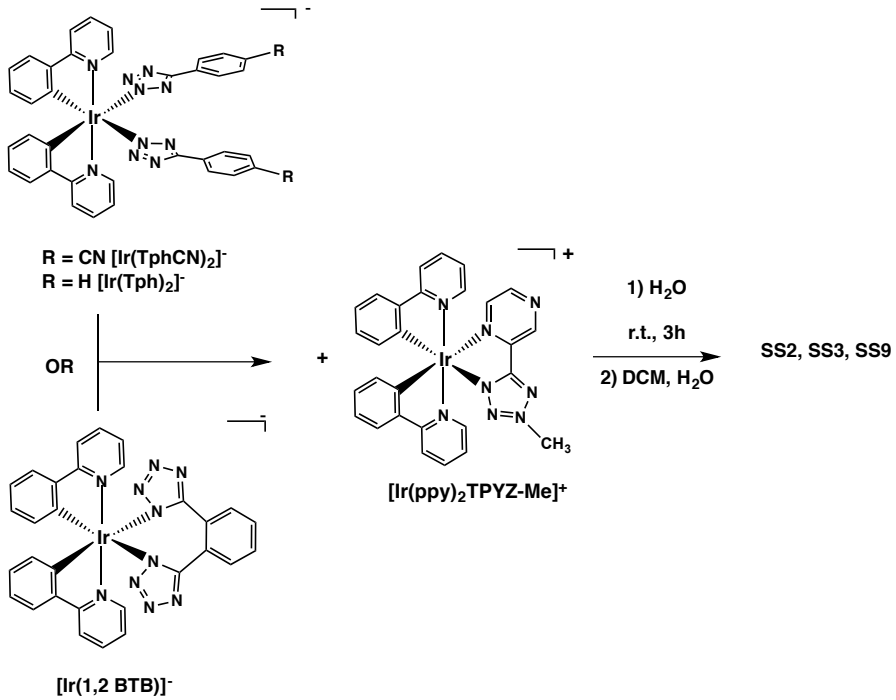

Figure 16.5: Synthetic procedure used for SS2, 3, 9

Taking advantage of the photophysical additive behaviour observed from SS5-8, the aim was to further extend the magnitude of the emission profiles resulting from Ir(III) soft salts as a further tool for tuning the emission colour of the ion pairs. The effects produced by the introduction of $[Ir(ppy)_2(TPYZ\text{-}Me)]^+$ as cationic counterpart (λ max = 686 nm) of non fluorinated anionic Ir(III) tetrazolate complexes are discussed (Figure 16.5).

Table 9: Photophysical data of SS2, 3, 9

CH_2Cl_2 as solvent	*Emission 298 K*					*Emission 77K*		*CIE*	
	λ_{em} (nm)	τ_{air} (μs)	τ_{Ar} (μs)	ϕ_{air}(%)	ϕ_{Ar}(%)	λ_{em}(nm)	τ (μs)	*ox*	*deox*
SS2 [Ir(TphCN)$_2$]$^+$ [Ir(ppy)$_2$TPYZ-Me]$^+$	486, 518, 664	0.10, 0.10, 0.11	0.66, 0.65, 0.14	3.14	14.83	480, 574	1.07, 2.45	X = 0.448 Y= 0.446	X = 0.283 Y = 0.517
SS3 [Ir(Tph)$_2$]$^+$ [Ir(ppy)$_2$TPYZ-Me]$^+$	486, 518, 680	0.12, 0.12,0.09	1.46, 1.44, 0.11	3.56	12.3	480, 574, 510	3.13, 3.16, 3.27	X=0.463 Y=0.431	X=0.273 Y=0.510
SS9 [Ir(1,2 BTB)]$^+$ [Ir(ppy)$_2$TPYZ-Me]$^+$	490, 522, 670	0.08, 0.07, 0.10	1.30, 1.20, 0.10	3.1	22.4	568	3.9	X = 0.430 Y = 0.463	X = 0.267 Y = 0.539
[Ir(ppy)$_2$TPYZ-Me]$^+$	686	0.09	0.095	2.71	3.61	582	4.50	n.d	n.d
[Ir(Tph)$_2$]$^+$	484, 514	0.12	1.27	5.5	60.6	480, 510	4.09	n.d	n.d
[Ir(TphCN)$_2$]$^+$	490, 520	0.11	0.80	3.4	24.9	480,516, 556$_m$	4.03	n.d	n.d
[Ir(ppy)$_2$(1,2 BTB)]$^+$	488 516	0.10	0.820	2.93	33.3	482, 516 562	2.24	n.d	n.d

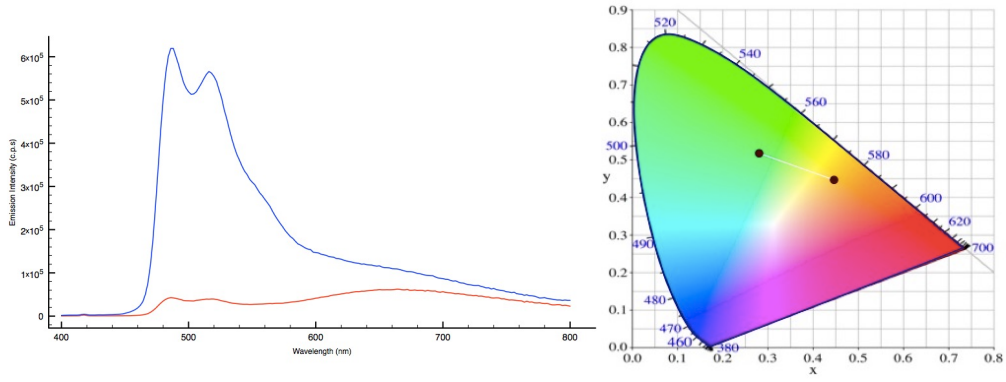

Figure 17.5: Emission spectra of SS2 oxygenated solution (red line), deoxygenated solution (blue line), 298K, CH_2Cl_2, r.t.; Right, CIE coordinates for SS2, air equilibrated and deoxygenated solutions

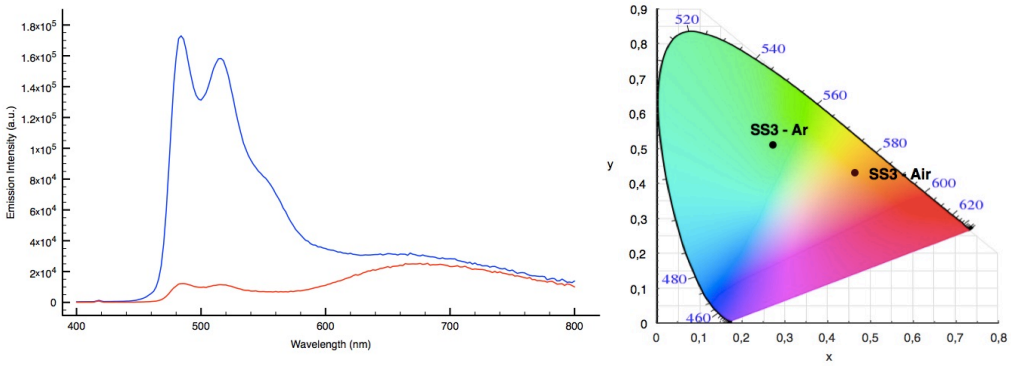

Figure 18.5: Emission spectra of SS3 oxygenated solution (red line), deoxygenated solution (blue line), 298K, CH_2Cl_2, r.t.; Right, CIE coordinates for SS3, air equilibrated and deoxygenated solutions

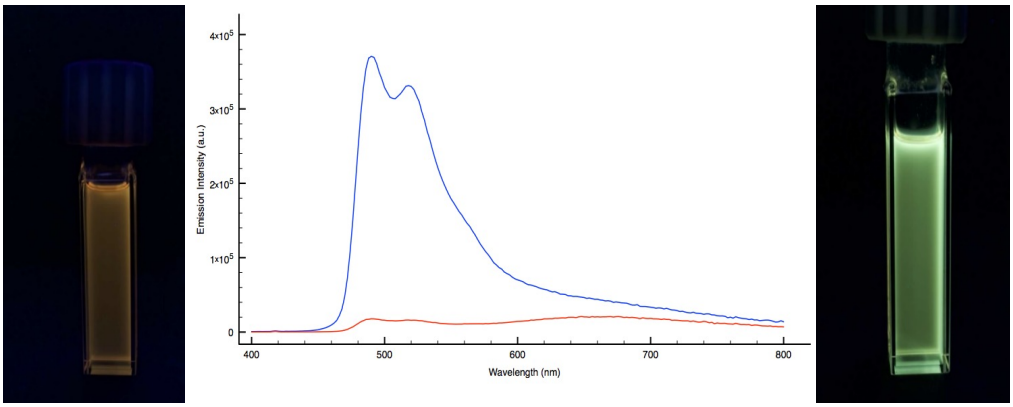

Figure 19.5: Left, Emission profile of SS9 10⁻⁵M, CH_2Cl_2, 298K: Air equilibrated (red line, orange cuvette) deoxygenated solution (blue line, green cuvette)

At first, the broadening of the emission profile of the soft salts has been accomplished by the introduction of $[Ir(ppy)_2(TPYZ\text{-}Me)]^+$ cation, a deep red emitter (λmax = 686 nm). As the photophysical behavior of the anionic Ir(III) tetrazolate complexes is almost not affected by the nature of the tetrazolate ligand used, the resulting emission profile is mainly regulated by the nature of the cyclometalated phenyl pyridine (ppy). For these reason, the emission maxima of the anionic complexes involved in the formation of SS2, SS3 and SS9 are found at λ = 480 and λ = 520 nm.

Once coupled with $[Ir(ppy)_2(TPYZ\text{-}Me)]^+$ the emission color observed for the ion pairs SS2, SS3 and SS9, as long as their photophysical properties (τ, Φ) can be considered as the rough sum of both anionic and cationic contributions, resulting in a orange emission (Figures 17.5, 18.5 and 19.5).

Upon passing to deoxygenated solutions, also in this case, the ion pairs displayed the predominant emission of the anionic complexes resulting in a green emission.

Ion pairs with fluorinated $[F_2Ir(ppy)_2(L)_2]$-/$[F_2Ir(ppy)_2(L)]$-type anions and $[Ir(ppy)_2(TPYZ\text{-}Me)]^+$ as cationic counterpart: SS1, 4, 10

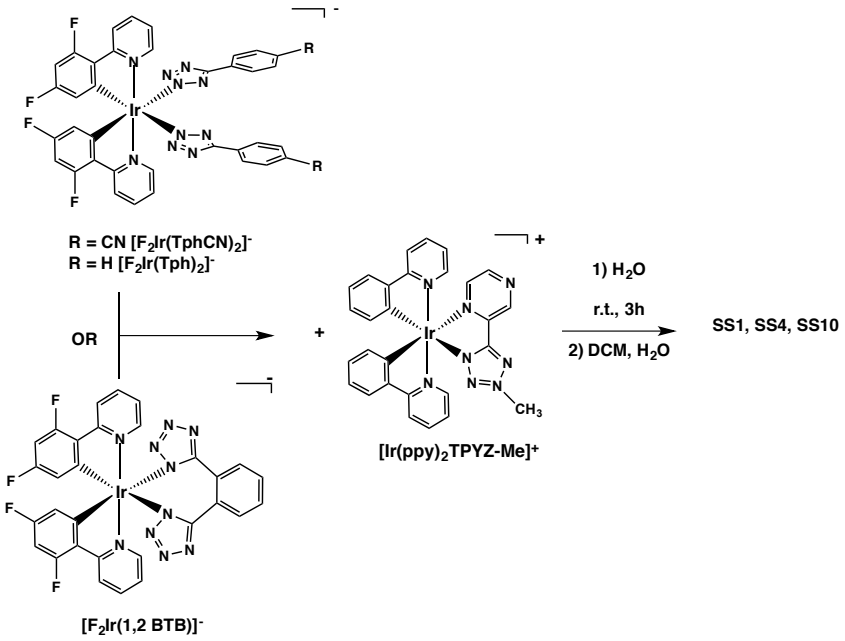

Figure 20.5: Synthetic procedure used for SS1, 4, 10

The design of ion pair denoted as SS1, SS4 and SS10 is based on the use of the fluorinated anionic Ir(III) tetrazolate complexes $[F_2Ir(TphCN)_2]^-$, $[F_2Ir(Tph)_2]^-$ and $[F_2Ir(1,2BTB)]^-$, respectively (Figure 20.5). The main feature of these anionic complexes is their intense sky blue phosphorescent emission centred between 460 and 480 nm (Table 10).

Table 10: Photophysical data of SS1, 4, 10

CH_2Cl_2 as solvent	***Emission 298 K***					***Emission 77K***		***CIE***	
	λ_{em} (nm)	τ_{av} (μs)	τ_{av}(μs)	ϕ_{av}(%)	ϕ_{av}(%)	λ_{em}(nm)	τ (μs)	*ox*	*deox*
SS1 $[F_2Ir(TphCN)_2]^-$ $[Ir(ppy)_2TPYZ\text{-}Me]^+$	460, 490, 680	0.16, 0.15, 0.09	1.19, 1.11, 0.11	2.82	7.02	454, 484, 574	3.8, 3.9, 4.6	X=0.3288 Y=0.3284	X=0.2033 Y=0.3202
SS4 $[F_2Ir(Tph)_2]^-$ $[Ir(ppy)_2TPYZ\text{-}Me]^+$	462, 490, 680	0.19, 0.20, 0.09	1.28, 1.22, 0.10	3.02	16.9	454, 488, 578	2.28, 2.80, 3.07	X=0.3080 Y=0.3298	X=0.1972 Y=0.3277
SS10 $[F_2Ir(1,2\ BTB)]^-$ $[Ir(ppy)_2TPYZ\text{-}Me]^+$	464, 490, 674	0.12, 0.12, 0.07	0.65, 0.68, 0.08	2.9	16.6	574	3.7	X = 0.339 Y = 0.363	X = 0.243 Y = 0.385
$[Ir(ppy)_2TPYZ\text{-}Me]^+$	686	0.09	0.095	2.71	3.61	582	4.50	n.d	n.d
$[F_2Ir(Tph)_2]^-$	462, 490	0.16	1.99	5.9	49	458, 490	3.23	n.d	n.d
$[F_2Ir(TphCN)_2]^-$	462, 492	0.17	1.35	3.3	22	460,490, 522$_{sh}$	3.25	n.d	n.d
$[F_2Ir(1,2\ BTB)]^-$	460, 490 526	0.120	1.60	2.64	53.0	456, 490 524	2.20	n.d	n.d

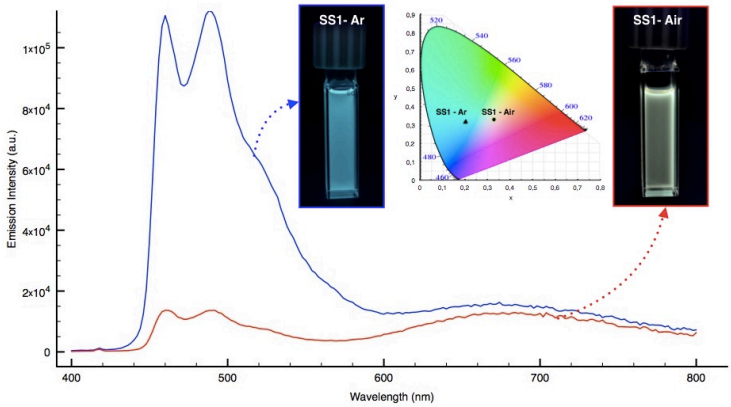

Figure 21.5: Emission profiles of SS1, air equilibrated (red trace) and deoxygenated solution (blue trace), CH_2Cl_2, r.t.

The blue contribution stemming from $[F_2Ir(TphCN)_2]$, $[F_2Ir(Tph)_2]^-$ or $[F_2Ir(1,2BTB)]^-$, and the red one originating from the $[Ir(ppy)_2TPYZ\text{-}Me]^+$ component did coexist in the appropriate balance to give an almost pure white light (1931 CIE coordinates X = 0.3288; Y = 0.3284 for SS1, Table 9 for SS4 and SS10). As well as the previously discussed soft salts, upon passing to deoxygenated solutions, all the ion pairs displayed the predominant emission of the anionic complexes (Figure 21.5). This behaviour has also been investigated through Stern Volmer experiments for the exemplar soft salts denoted as SS3 (Figures 22.5 and 23.5) and SS4 (Figures 24.5 and 25.5).

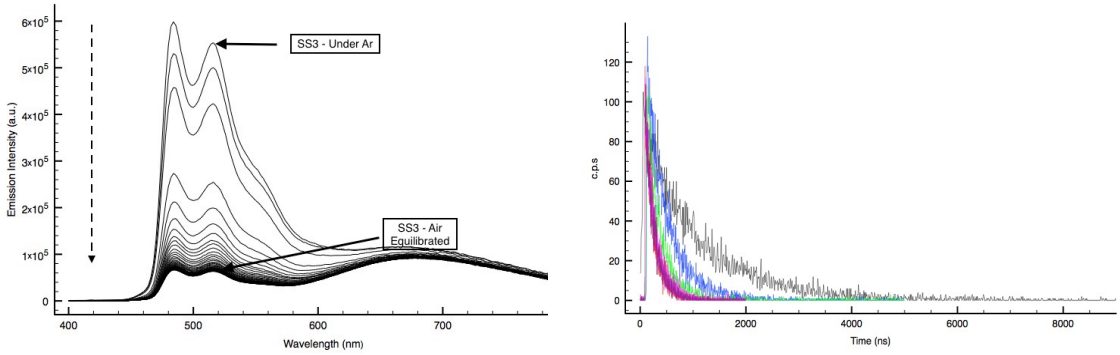

Figure 22.5: Left, Multiple Emission Scans of SS3 from deoxygenated to air equilibrated solution, 37 scans recorded at 2 minutes intervals, CH_2Cl_2, r.t. Right: Decay times of SS3 (at λ_{max} = 486 nm) recorded during the Stern Volmer analysis at 10 minutes intervals, CH_2Cl_2, r.t.

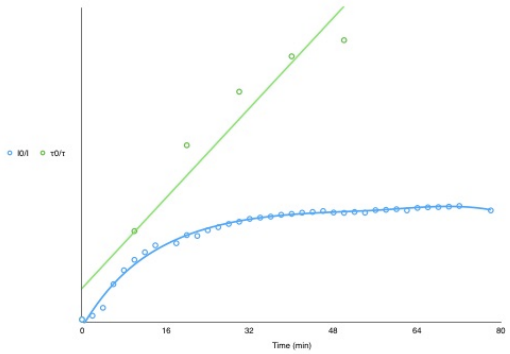

Figure 23.5: Stern Volmer Plot of SS3

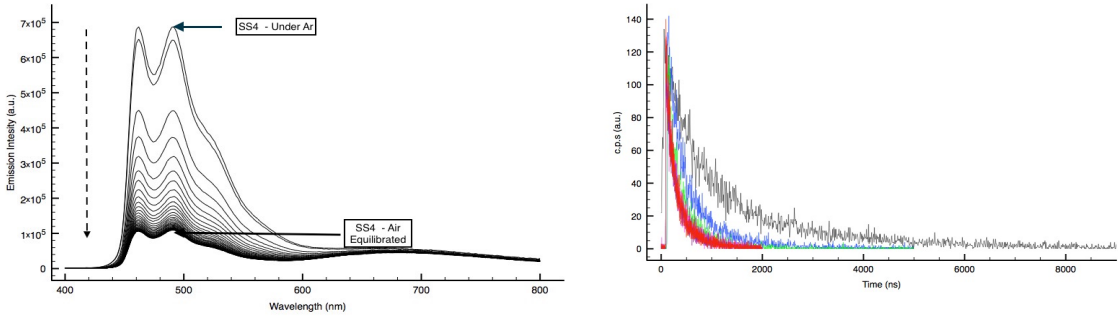

Figure 24.5: Left, Multiple Emission Scans of SS4 from deoxygenated to air equilibrated solution, 37 scans recorded at 2 minutes intervals, CH_2Cl_2, r.t. Right: Decay times of SS4 (at λ_{max} = 460 nm) recorded during the Stern Volmer analysis at 10 minutes intervals, CH_2Cl_2, r.t.

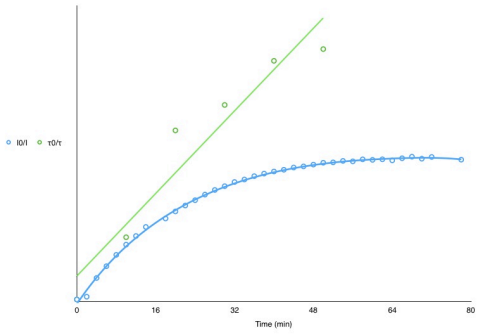

Figure 25.5: Stern Volmer Plot of SS4

The Stern-Volmer plot for SS3 and SS4 are observed to curve downwards towards the *x*- axis (I0/I vs Time, blue trace), which is characteristic of two populations of fluorophore(anion and cation contribution to the ion pair), one of which is less sensitive to the quencher (O_2).

The occurrence of such similar trend can be traced back to the different rates of enhancement of the emission intensities that are displayed by the single

mononuclear complexes and points again to how the anion and cation that constitute the soft salts basically behave as photophysically independent entities, with a likely minor role played by energy and/or electron transfer processes, the intervention of which is probably limited by the presence of the bulky 5-aryl tetrazolates in the structures of the anionic complexes.

Conclusions

In conclusion, it appears how the new anionic Ir(III) tetrazolate complexes can be coupled to new Ir(III) cationic tetrazole derivatives to form "fully tetrazolate" soft salts in which it is possible to achieve a properly additive synthesis of the emission colours. Based on this behaviour, an almost pure white light emission can be obtained upon the appropriate choice of the ionic components. In all cases, the emission colour is sensitive to the presence of dissolved dioxygen, a peculiarity that might entail the use of these new ion pairs as ratiometric O_2 luminescence sensors. Studies are in progress in our laboratories in order to achieve the emission of white light also from O_2 free solutions, a feature that might favour the use of these systems in the fabrication of light emitting devices.

Experimental Section

General considerations. All the reagents and solvents were obtained commercially (e.g. Aldrich) and used as received without any further purification, unless otherwise specified. All the reactions were carried out under an argon atmosphere following Schlenk protocols. Where required, the purification of the Ir(III) complexes was performed via column chromatography with the use of neutral alumina as the stationary phase. ESI-mass spectra were recorded using a Waters ZQ-4000 instrument (ESI-MS, acetonitrile as the solvent). Nuclear magnetic resonance spectra (consisting of ^{1}H and ^{13}C) were always recorded using a Varian Mercury Plus 400 instrument (^{1}H, 400.1; ^{13}C, 101.0 MHz.) at room temperature. ^{1}H and ^{13}C chemical shifts were referenced to residual solvent resonances.

Photophysics. Absorption spectra were recorded at room temperature using a Perkin Elmer Lambda 35 UV/vis spectrometer. Uncorrected steady-state emission and excitation spectra were recorded on an Edinburgh FLSP920 spectrometer equipped with a 450 W xenon arc lamp, double excitation and single emission monochromators, and a Peltier-cooled Hamamatsu R928P photomultiplier tube (185–850 nm). Emission and excitation spectra were acquired with a cut-off filter (395 nm) and corrected for source intensity (lamp and grating) and emission spectral response (detector and grating) by a calibration curve supplied with the instrument. The wavelengths for the emission and excitation spectra were determined using the absorption maxima of the MLCT transition bands (emission spectra) and at the maxima of the emission bands (excitation spectra). Quantum yields (Φ) were determined using the optically dilute method by Crosby and Demas[41] at excitation wavelength obtained from absorption spectra on a wavelength scale [nm] and compared to the reference emitter by the following equation:[42]

$$\phi_s = \phi_r \left[\frac{A_r(\lambda_r)}{A_s(\lambda_s)}\right]\left[\frac{I_r(\lambda_r)}{I_s(\lambda_s)}\right]\left[\frac{n_s^2}{n_r^2}\right]\left[\frac{D_s}{D_r}\right]$$

where A is the absorbance at the excitation wavelength (λ), I is the intensity of the excitation light at the excitation wavelength (λ), n is the refractive index of the solvent, D is the integrated intensity of the luminescence, and Φ is the quantum yield. The subscripts r and s refer to the reference and the sample,

respectively. A stock solution with an absorbance > 0.1 was prepared, then two dilutions were obtained with dilution factors of 20 and 10, resulting in absorbances of about 0.02 and 0.08 respectively. The Lambert-Beer law was assumed to remain linear at the concentrations of the solutions. The degassed measurements were obtained after the solutions were bubbled for 10 minutes under Ar atmosphere, using a septa-sealed quartz cell. Air-equilibrated $[Ru(bpy)_3]Cl_2/H_2O$ solution (Φ = 0.028)[43] was used as reference. The quantum yield determinations were performed at identical excitation wavelengths for the sample and the reference, therefore deleting the $I(\lambda r)/I(\lambda s)$ term in the equation. Emission lifetimes (τ) were determined with the single photon counting technique (TCSPC) with the same Edinburgh FLSP920 spectrometer using pulsed picosecond LED (EPLED 360, fhwm < 800 ps) as the excitation source, with repetition rates between 1 kHz and 1 MHz, and the above-mentioned R928P PMT as detector. The goodness of fit was assessed by minimizing the reduced $\chi 2$ function and by visual inspection of the weighted residuals. To record the 77 K luminescence spectra, the samples were put in quartz tubes (2 mm diameter) and inserted in a special quartz dewar filled with liquid nitrogen. The solvent used in the preparation of the solutions for the photophysical investigations was of spectrometric grade. Experimental uncertainties are estimated to be ±8% for lifetime determinations, ±20% for quantum yields, and ±2 nm and ±5 nm for absorption and emission peaks, respectively.

Ligand synthesis

Following the general method reported by Koguro and coworkers,[21] tetrazole ligand [H-**TPYZ**] 2-(1*H*-tetrazol-5-yl)pyrazine, was obtained in quantitative yield. [H-**TPYZ**] ^{1}H-NMR, 400 MHz, DMSO-d^6 δ (ppm) = 9.39 (m, 1H); 8.87 (m, 2H).

General Procedure for the Preparation of the Cationic Ir(III) complex

The cationic complexes $[Ir(ppy)_2TPYZ\text{-}Me]^+[PF_6]^-$ and $[Ir(bzq)_2TPYZ\text{-}Me]^+$ were obtained according to a previously reported procedure.[27] Yield: $[Ir(ppy)_2TPYZ\text{-}Me]^+[PF_6]^-$ 0.038 g, 61.5%; $[Ir(bzq)_2TPYZ\text{-}Me]^+$ = 51.6 %

$[Ir(ppy)_2TPYZ\text{-}Me]^+$ ^{1}H-NMR (Acetone-d^6, 400 MHz) δ (ppm) = 9.76 (s, 1H), 8.99 (m, 1H), 8.26 (d, 2H, $J_{H\text{-}H}$ = 8.8 Hz), 8.11 (s, 1H), 8.02 – 7.95 (m, 3H), 7.91 – 7.85 (m,

3H), 7.15 – 6.85 (m, 6H), 6.32 – 6.27 (m, 2H), 4.61 (s, 3H). ^{13}**C-NMR** (CD_3CN, 100 MHz) δ (ppm) = 168.48, 168.18, 166.55 (Ct), 152.62, 151.90, 151.52, 147.39, 146.72, 146.38, 145.74, 145.69, 145.30, 141.25, 140.51, 133.14, 132.77, 131.93, 131.36, 126.41, 125.98, 125.26, 125.11, 124.80, 124.38, 121.51, 121.28, 118.81, 43.47. **ESI-MS** (*m*/*z*): [M^+] = 663 [M^-] = 145 (PF_6). Anal. Calcd. for $C_{28}H_{22}N_8F_6PIr$ (807.71): C 41.63, H 2.75, N 13.87. Found: C 41.62, H 2.77, N 13.89%

[Ir(bzq)$_2$TPYZ-Me]$^+$ ^{1}**H-NMR** (Acetone-d_6, 400 MHz) δ (ppm) = 9.41 (d, 1H, J_{H-H}= 1.2 Hz), 8.43 (d, 1H, J_{H-H}= 3.2 Hz), 8.39-8.33 (m, 2H), 8.21 (d, 1H, J_{H-H}= 5.6 Hz), 7.84-7.66 (m, 6H), 7.51-7.48 (m, 1H), 7.40-7.37 (m, 2H), 7.30 (d, 1H, J_{H-H}= 8 Hz), 7.06-7.02 (m, 1H), 6.96-6.92 (m, 1H), 6.30 (d, 1H, J_{H-H}= 7.2 Hz), 6.18 (d, 1H, J_{H-H}= 7.4 Hz). ^{13}**C-NMR** (CD_3CN, 100 MHz) δ (ppm) = 168.11 (Ct), 157.05, 156.95, 149.32, 148.85, 147.53, 146.82, 145.01, 144.43, 144.37, 143.98, 143.90, 137.17, 137.09, 129.52, 129.49, 129.45, 129.14, 129.04, 128.81, 126.95, 126.91, 124.05, 123.81, 122.53, 122.10, 120.45, 119.78. **ESI-MS** (*m*/*z*): [M^+] = 711 [M^-] = 145 (PF_6).

General Procedure for the Preparation of Ir(III) Soft Salts

The desired anionic tetrazolate complex (0.020 g, 1 equiv.) and the proper cationic tetrazolate complex (1 equiv.) were added to water (15 mL). The reaction mixture was stirred for 3 h at room temperature and then extracted with dichloromethane. The organic phase was washed repeatedly with water until the signal of the counterion Et_3NH^+ was absent in the ^{1}H-NMR spectrum, leading to the formation of the Ir(III) soft salt in almost quantitative yield.

SS1 ^{1}**H-NMR** (CD_3CN, 400 MHz), δ (ppm): 4.47 (s, 3H cation), 5.86-5.89 (m, 2H, anion); 6.22-6.28 (m, 2H, cation), 6.37-6.43 (m, 2H, anion), 6.87-7.12 (m, 8H anion and cation overlapped), 7.45-7.48 (m, 2H, anion), 7.65-8.08 (m, 17H, anion and cation overlapped), 8.26-8.28 (m, 2H, anion), 8.78 (s, 1H, cation), 9.62 (s, 1H, cation), 10.21 (m, 2H, anion). Anal. Calcd. for $C_{66}H_{42}N_{20}F_4Ir_2$•$2H_2O$ (1611.63): C 49.18, H 2.88, N 17.38. Found: C 49.25, H 2.85, N 17.42%

SS2 ^{1}**H-NMR** (CD_3CN, 400 MHz), δ (ppm): 4.47 (s, 3H cation), 6.22-6.26 (m, 2H, cation); 6.40-6.43 (m, 2H, anion), 6.65-6.69 (m, 2H, anion), 6.74-6.78 (m, 2H, anion), 6.89-7.12 (m, 8H anion and cation overlapped), 7.41-7.44 (m, 2H, anion), 7.57-8.01 (m, 17H, anion and cation overlapped), 8.07-8.10 (m, 2H, anion), 8.78 (s, 1H, cation), 9.63 (s, 1H, cation), 10.34 (m, 2H, anion). Anal. Calcd. for $C_{66}H_{46}N_{20}Ir_2$•$2H_2O$ (1539.67): C 51.48, H 3.27, N 18.19. Found: C 51.51, H 3.25, N

18.21%

SS3 ^{1}**H-NMR** (CD_3CN, 400 MHz), δ (ppm): 4.47 (s, 3H, cation), 6.22-6.27 (m, 2H, cation), 6.41-6.44 (2H, anion), 6.64-6.68 (m, 2H, anion), 6.73-6.78 (m, 2H, anion), 6.87-7.12 (m, 6H, cation), 7.27-7.45 (m, 8H anion), 7.56-7.58 (m, 2H, anion), 7.64-7.67 (m, 2H cation), 7.72-7.98 (m, 13H, anion and cation overlapped), 8.07-8.09 (m, 2H, anion), 8.78 (s, 1H, cation), 9.63 (s, 1H, cation), 10.45 (m, 2H, anion). Anal. Calcd. for $C_{64}H_{48}N_{18}Ir_2$•$2H_2O$ (1489.65): C 51.60, H 3.52, N 16.92. Found: C 51.63, H 3.54, N 16.95%

SS4 ^{1}**H-NMR** (CD_3CN, 400 MHz), δ (ppm): 4.47 (s, 3H, cation), 5.87-5.90 (m, 2H anion), 6.22-6.27 (m, 2H, cation), 6.36-6.42 (m, 2H anion), 6.87-7.12 (m, 6H, cation), 7.29-7.49 (m, 8H anion), 7.65-7.67 (m, 2H, cation), 7.77-8.09 (m, 13H, anion and cation overlapped), 8.26-8.28 (m, 2H anion), 8.78 (s, 1H, cation), 9.62 (s, 1H, cation), 10.32 (m, 2H, anion). (Anal. Calcd. for $C_{64}H_{44}N_{18}F_4Ir_2$•$2H_2O$ (1561.61): C 49.22 H 3.10, N 16.14. Found: C 49.26, H 3.05, N 16.18%

Table C5: Stern Volmer data summary for SS3

time (min)[a]	I0/I[b]	τ0/τ[c]
0[d]	1	1
2	1.073	
4	1.225	
6	1.679	
8	1.947	
10	2.148	2.70
12	2.293	
14	2.426	
18	2.466	
20	2.622	4.35
22	2.607	
24	2.716	
26	2.774	
28	2.837	
30	2.880	5.38
32	2.935	
34	2.959	
36	2.978	
38	3.014	
40	3.031	6.06
42	3.054	
44	3.068	
46	3.086	
48	3.057	
50	3.051	6.37
52	3.068	
54	3.054	
56	3.103	
58	3.109	
60	3.121	
62	3.097	
64	3.145	
66	3.157	
68	3.161	
70	3.170	
72	3.183	
78	3.097	

[a] = Sum of the acquisition time for the emission spectrum (dwell time = 0.250. 1 minute for each spectrum from 400 to 800 nm. λ_{exc} = 370 nm) and waiting time between each scan (1 minute) for 37 total scans.

[b] = integral of the emission profile of the degassed sample after the solution was bubbled for 10 minutes under Ar atmosphere using a septa-sealed quartz cell (**I0**) over the integral of the emission profile after (minutes) of air re-equilibration of the sample by the removal of the septum (**I**).

[c] = lifetime value of the degassed sample after the solution was bubbled for 10 minutes under Ar atmosphere using a septa-sealed quartz cell (**τ0**) over lifetime value after (minutes) of air re-equilibration of the sample by the removal of the septum (**τ**). During the acquisition of each decay time (periods of 2 minutes) the quartz cuvette was sealed in order to prevent uncontrolled air contamination of

the sample. Emission lifetimes were determined using pulsed picosecond LED as the excitation source (369 nm) at λ_{max} = 460 nm.

[d] = sample under Ar atmosphere, closed vessel.

Table C5.1: Stern Volmer data summary for SS4

time (min)[a]	**I0/I**[b]	**τ0/τ**[c]
0[d]	1	1
2	1.06	
4	1.44	
6	1.68	
8	1.91	
10	2.12	2.27
12	2.30	
14	2.48	
18	2.65	
20	2.80	4.45
22	2.92	
24	3.03	
26	3.14	
28	3.24	
30	3.31	4.97
32	3.40	
34	3.45	
36	3.56	
38	3.57	
40	3.61	5.87
42	3.65	
44	3.69	
46	3.72	
48	3.75	
50	3.79	6.11
52	3.80	
54	3.83	
56	3.82	
58	3.86	
60	3.85	
62	3.86	
64	3.84	
66	3.88	
68	3.91	
70	3.87	
72	3.91	
78	3.85	

[a] = Sum of the acquisition time for the emission spectrum (dwell time = 0.250. 1 minute for each spectrum from 400 to 800 nm. λ_{exc} = 370 nm) and waiting time between each scan (1 minute) for 37 total scans.

[b] = integral of the emission profile of the degassed sample after the solution was bubbled for 10 minutes under Ar atmosphere using a septa-sealed quartz cell (**I0**) over the integral of the emission profile after (minutes) of air re-equilibration of the sample by the removal of the septum (**I**).

[c] = lifetime value of the degassed sample after the solution was bubbled for 10 minutes under Ar atmosphere using a septa-sealed quartz cell (**τ0**) over lifetime value after (minutes) of air re-equilibration of the sample by the removal of the septum (**τ**). During the acquisition of each decay time (periods of 2 minutes) the quartz cuvette was sealed in order to prevent uncontrolled air contamination of the sample. Emission lifetimes were determined using pulsed picosecond LED as the excitation source (369 nm) at λ_{max} = 460 nm.

[d] = sample under Ar atmosphere, closed vessel.

Chapter 6

Evaluation of the antibacterial activity of Ir(III) tetrazolate complexes

Abstract

Transition metal complexes have been extensively studied as imaging or therapeutic agents over the past decade. Due to their unique electronic and structural properties, these complexes provide sundry modes of action in living organism. Especially those complexes with phosphorescent properties are particularly advantageous as they not only possess the aforesaid properties but also enable the detection and estimation of the targets by luminescence methods. In these preliminary studies we are investigating on the antibacterial strength of a series of Ir(III) cyclometalated tetrazolate complexes, both in neutral ([Ir(C^N)(N^N)]) and cationic design ([Ir(C^N)(N^N)]$^+$), taking into consideration different bacteria-cells lines such as E.coli (Gram negative) and D. radiodurans (Gram positive). Moreover, the cationic [F$_2$IrPTZ-Me]$^+$ was choosen to be supported on SiO$_2$NPs and applied over woven fabrics of cotton by the means of dip-pad-dry-cure method. The phosphorescent-texitiles were then screened as anti -E. Coli agents through the production of $^1O_2$ (singlet oxygen).

Introduction: antimicrobial and anti-proliferative ability of transition metal complexes

Only specific classes of metals are devoted to essential cellular functions, hence indispensable for life in all organisms. Cell membranes, DNA, cellular processes such as electron transfer and catalysis are strictly correlated to the presence of Na, Mg, K, Ca, V, Cr, Mn, Fe, Co, Ni, Cu, Zn and Se.[54] However, these essential metals are poisonous to all cells when present in excess. Additionally, Ag, Hg and Te metals that has been ranked as non-essential, are extremely toxic to most bacteria even at low concentrations, hence employed as antimicrobial agents since ages.[55] Nowadays, antibiotic resistance and the lack of new antimicrobial agents made crucial the introduction of new drugs with different mechanism of action. In this context, an impressive amount of research has been devoted to the development of new antimicrobial metal compounds – metal surfaces and coatings, chelates and nanomaterials capable to exercise synergistic bactericidal activity with other biocides, inhibit metabolic pathways in a discerning manner and kill multidrug-resistant bacteria.[56]

Several metal-induced antimicrobial mechanisms have been studied; these include the production of ROS – reactive oxygen species, and the investigation of metal-induced oxidative stress.

Using various chemical and biological techniques, many studies have shown certain metal ions are capable of increase intracellular ROS by catalyzing the production of superoxides (O_2^-) which inhibit enzyme activities that are crucial

for cell growth.[57] In *E. coli*, the disinvolvement of Fe metabolism leads to DNA damage, and exposure to Cu(II) and Te(IV) nullify enzymatic activities similar to those lost during H_2O_2 and O_{2^-} corruption. Therefore, toxicities associated with these metals might be due to ROS-mediated cellular damage and different metal-catalyzed oxidation reactions could manage protein, membrane or DNA damage.[58]

At least three mechanisms have been proposed for the explanation of increased ROS production. Firstly, certain metals in addition to iron can catalyze Fenton-type reactions (Cu, Cr, Co, V and Ni) and the formation of hydroxyl radical.[59] Second, some transition metals are capable of damage cellular donor ligands that coordinate Fe, resulting in the release of ROS-producing species into the cytoplasm.[60] Also an extensive number metal species undergo to thiol-mediated reduction, leading to the formation of ROS via intermediate S radical chemistry. A final but important facet of oxidative stress in the course of bacterial metal poisoning is the oxidation of cellular thiols by soft and borderline metal atoms.[61]

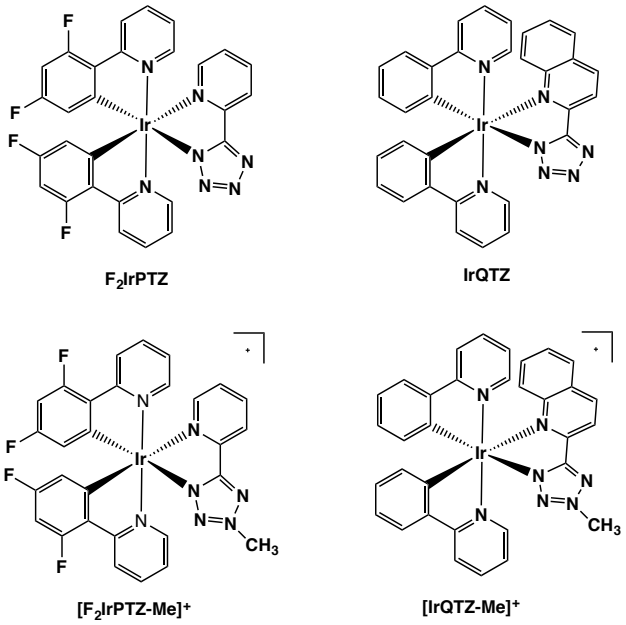

Figure 1.6: Structure and acronyms used for neutral and cationic Ir(III) tetrazolate complexes discussed in this chapter

Against this background, only few studies have been focused on third row transition metal complexes such as Ir(III)-cyclometalates as antibacterial agents.[62] The aim of this chapter is to describe the synthesis and the photophysical characterization of a series of phosphorescent neutral and cationic Ir(III) tetrazolate complexes with general formula $[Ir(C^N)_2(N^N)]$ or

$[Ir(C^N)_2(N^N)^+][PF_6^-]$, where (C^N) can be either 2-phenylpyridine (ppy) or 2-(2,4-difluorophenylpyridine) (F_2ppy) and (N^N) are the deprotonated form of H-PTZ (2-(1*H*-tetrazol-5-yl)pyridine) or H-QTZ (2-(1*H*-tetrazol-5-yl)quinoline). The cationic derivatives were obtained by the means of methylation reaction (Figure 1.6).[27,28] The biological evaluation of these new cationic complexes against *E. Coli* and *D. radiodurans* are presented. Moreover, the promising results gathered by the disk diffusion assays prompted us to support one of these complexes on SiO_2NPs. Phosphorescent colloidal SiO_2 solutions have been fixed on woven fabrics of cotton by the means of *dip-pad-dry-cure* technique and tested as *E.coli* growth-inhibition materials in view of the production of singlet oxygen ($^1O_2$), a poisonous ROS species.

Results and discussion

Synthesis of neutral and cationic Ir(III) tetrazolate complexes

The preparation of the neutral complexes has been accomplished through the reaction of a 2.5 molar excess of [H-PTZ] or [H-QTZ] tetrazoles with the chloride bridged Ir(III) dimer both fluorinated (F_2ppy) or not (ppy) (Figure 2.6). In all cases, the compounds were obtained after 6 hours at room temperature and subsequent purification of the crude by silica gel column chromatography.

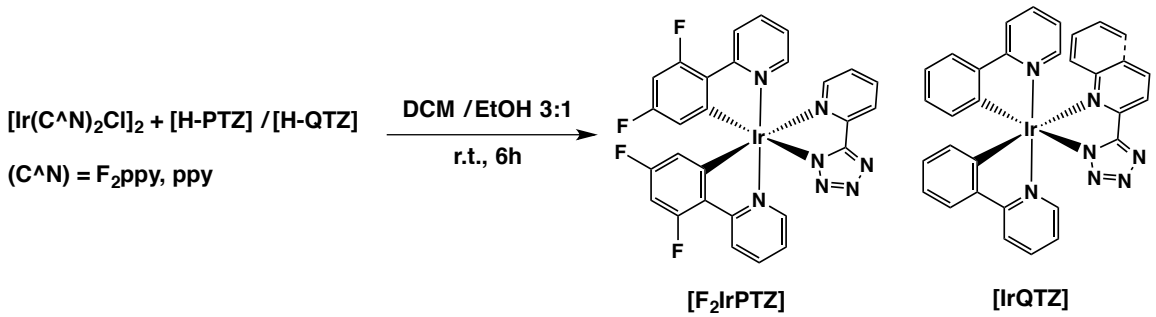

Figure 2.6: synthetic procedure used for neutral Ir(III) tetrazolate complexes

The formation of the expected neutral Ir(III)-cyclometalates was at first confirmed by ESI-MS spectrometry, which revealed the presence of the characteristic isotopic patterns in the positive region ions (F_2IrPTZ, [M+Na] (*m*/*z*) = 742; [M+K] = 758 (Figure 3.6); IrQTZ, [M+H] (*m*/*z*) = 713).

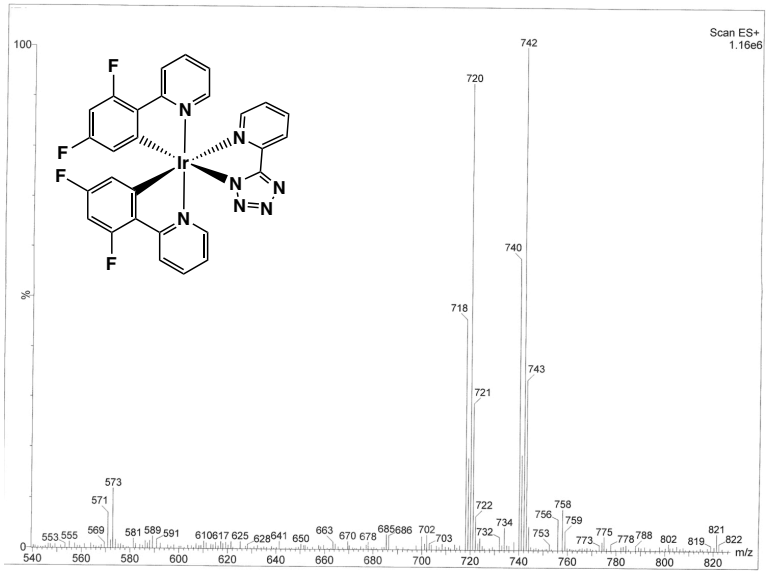

Figure 3.6: F_2IrPTZ – positive region ions – CH_3CN as the solvent. $[M]^+$ = 720 m/z; $[M+Na]^+$ = 742 m/z; $[M+K]^+$ = 758 m/z

The ^{1}H-NMR characterization provided the expected protonic resonances in the aromatic region (8.5-5.5 ppm), which further confirmed the formation of the neutral F_2IrPTZ (Figure 3.7) and IrQTZ complexes.

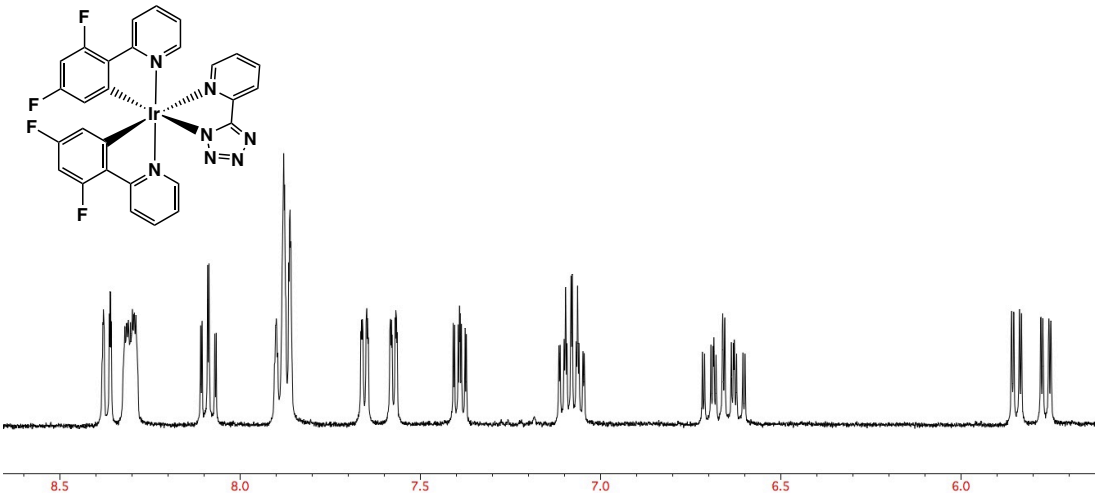

Figure 4.6: ^{1}H NMR of [F_2IrPTZ], CD_3CN, 400 MHz

Following a previously reported synthetic method (Figure 5.6),[34, 44] the addition of methyl triflate to the neutral Ir(III) tetrazolate complexes produced the corresponding cationic derivatives.

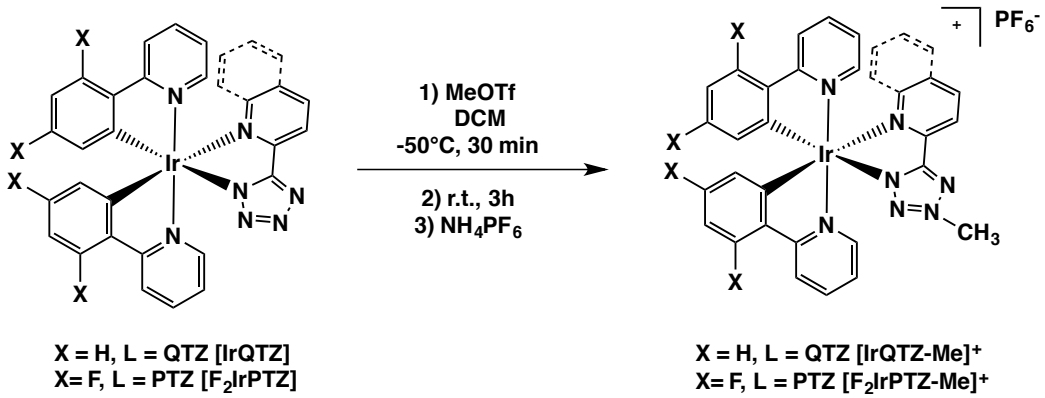

Figure 5.6: Synthetic procedure used for cationic Ir(III) tetrazolate complexes

The addition of a methyl-group on the [R-CN_4] moiety regioselectively occurs at the N2 position of the tetrazolate ring, as witnessed by ^{13}C-NMR resonance of Ct (tetrazolic carbon) which has been found at 166.54 ppm for $[F_2IrPTZ\text{-}Me]^+$ and 167.93 ppm for $[IrQTZ\text{-}Me]^+$ (Figure 6.6).[27, 28, 34, 44]

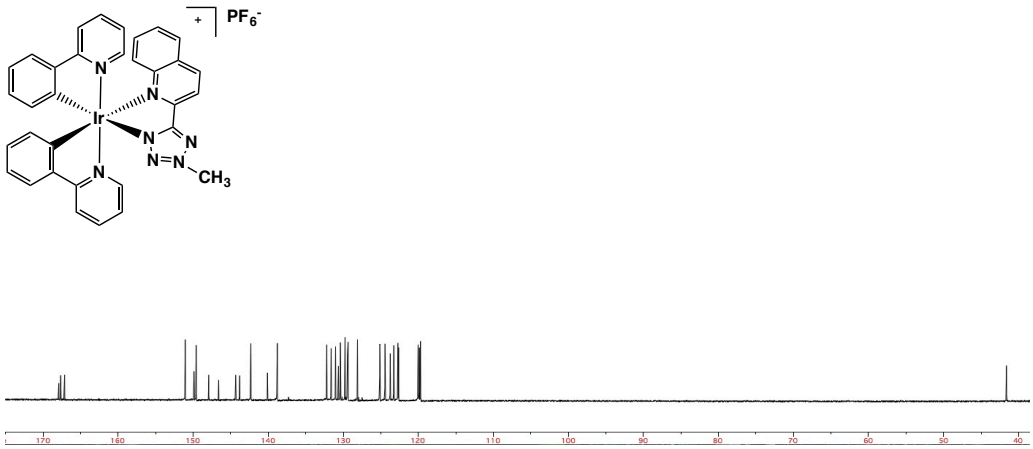

Figure 6.6: ^{13}C-NMR of $[IrQTZ\text{-}Me]^+$, Acetone-d_6, 100 MHz

Single crystals suitable for X-ray diffraction were obtained for $[IrQTZ\text{-}Me]^+$ and $[F_2IrPTZ\text{-}Me]^+$ (Figure 7.6). In all the cases, the Ir(III) center adopts a distorted octahedral coordination geometry with *cis*- metalated carbons and *trans*-phenylpyridine nitrogen atoms, as was previously found in other complexes containing analogous cyclometalated C^N ligands,[63] as well as the Ir-N (N^N) distances, which are found to be longer than Ir-N (C^N).[64] The methylation reaction effectively occurred at the N3-nitrogen atom of $[QTZ]^-$ and $[PTZ]^-$ ligands, confirming also the Ct chemical shift value found in ^{13}C-NMR experiments (Figure 7.6, structure and labeling).

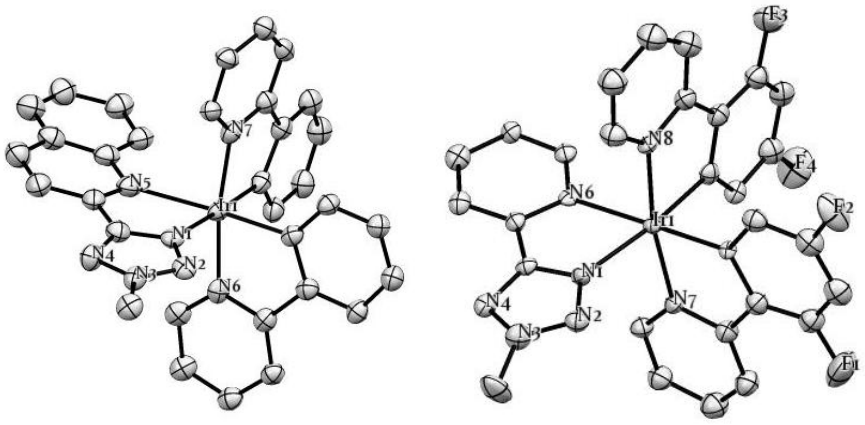

Figure 7.6: (Left) X-ray structure of [IrQTZ-Me]·[PF$_6$]; (Right) X-ray structure of [F$_2$IrPTZ-Me]·[PF$_6$]

Photophysical properties

Table 11: Photophysical data of neutral and cationic Ir(III) tetrazolate complexes

CH_2Cl_2 as solvent	***Absorption*** λ_{abs}(nm);($10^{-5}\varepsilon$)($M^{-1}cm^{-1}$)	***Emission 298 K***					***Emission 77K***	
		λ_{em}(nm)	τ_{em} (μs)	τ_{Av}(μs)	ϕ_{em}(%)	ϕ_{Av}(%)	λ_{em}(nm)	τ (μs)
[IrQTZ]	260 (6.48), 342 (1.60), 386 (0.72), 423 (0.45)	580	0.21	0.84	2.65	16.31	516, 550	4.2
[IrQTZ-Me]$^+$	253 (4.25), 310 (1.41), 374 (0.78)	638	0.22	0.44	5.80	13.05	568	1.56
[F$_2$IrPTZ]	252 (7.84), 304 (3.30), 369 (1.04)	456, 486	0.096	0.16	2.8	6.9	456, 486	2.69
[F$_2$IrPTZ-Me]$^+$	257 (6.24), 318 (2.70), 351 (1.20)	454, 486, 526	0.03 (56%) 0.9 (44%);	0.03 (40%) 0.14 (60%)	1.75	4.67	448 480	6.62

In 10^{-5}M CH_2Cl_2 solutions, all the neutral and cationic Ir(III) complexes display similar absorption profiles, with intense ligand centred (LC) transitions up to 260 nm and metal-to-ligand charge transfer (MLCT) bands tailing off above 380 nm.

Upon excitation of the MLCT features (λ = 370 nm), [F$_2$IrPTZ] display a sky-blue emission colour through a structured emission profile with λmax = 456 and 486 nm (Table 11), suggesting an interplay of ^{3}LC/^{3}MLCT-type emissive excited states. The lack of rigidochromic effect on passing from room temperature to 77 K emission suggests a dominant LC character in the composition of the excited state (Figure 8.6).

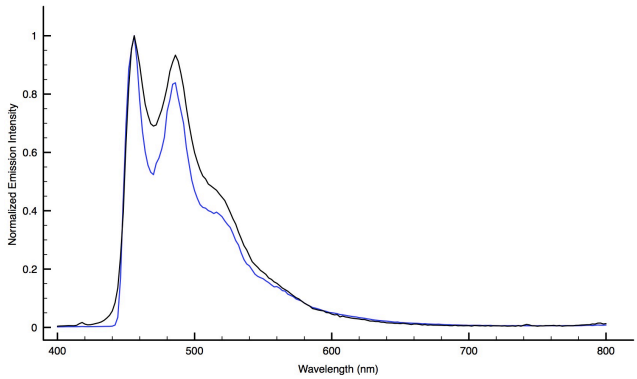

Figure 8.6: Normalized emission profiles of [F$_2$IrPTZ]: 298K (black line), 77K (blue line), CH$_2$Cl$_2$

Upon methylation reaction, the neutral [F$_2$IrPTZ] was converted in its cationic analogue [F$_2$IrPTZ-Me]$^+$ (λmax = 454, 486 and 526 nm, Table 11). It was possible to determine that the addition of CH$_3^+$ to the neutral [F$_2$IrPTZ] complex did not involve appreciable change in the colour of the sky-blue emission of [F$_2$IrPTZ-Me]$^+$. The occurrence of such behaviour suggests that the anionic [PTZ]$^-$ or methylated [PTZ-Me] ligands might play a minor role in determining the composition of the emissive excited states, which are mainly regulated by the –Ir(C^N)$_2$- fragment (Figure 9.6).

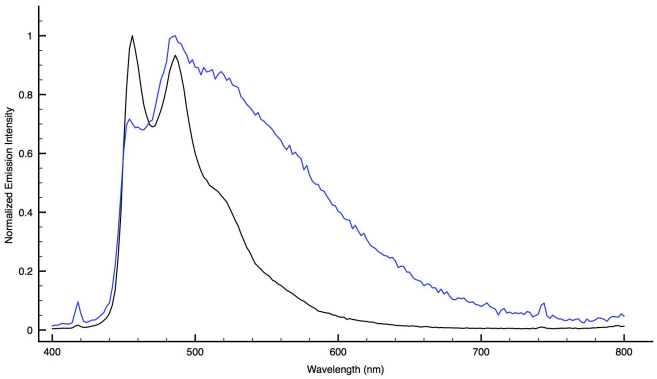

Figure 9.6: Normalized emission profiles of [F$_2$IrPTZ] (black line) and [F$_2$IrPTZ-Me]$^+$ (blue line), CH$_2$Cl$_2$

In both cases, the phosphorescent character of the excited state was confirmed by the noticeable oxygen sensitivity that was displayed by the quantum yields (ϕ) and the corresponding lifetimes (τ) values (Table 11).

On the contrary, the excitation of the MLCT features of [IrQTZ] produced a broad and unstructured emission profile with λmax = 580 nm, typical of ^{3}MLCT-type emissive excited states (Figure 10.6, black line). This feature was further confirmed by the noticeable rigidochromic shift observed in frozen solvent

matrix at 77K (*c.a* 40 nm, Figure 10.6, blue line).

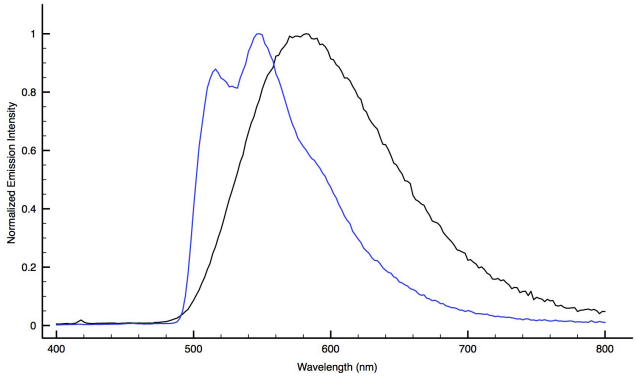

Figure 10.6: Normalized emission profiles of [IrQTZ], 298K (black line) and 77K (blue line), CH_2Cl_2

By the means of electrophilic addition, the neutral [IrQTZ] has been converted into its cationic analogue $[IrQTZ\text{-}Me]^+$. The overall change in the net charge of the complex produced a red shift of the emission maxima from 580 to 628 nm ($\Delta\lambda$ = 48 nm, Figure 11.6), as a consequence of the involvement of $[QTZ\text{-}Me]^+$ in the composition of the LUMO energy level. This behavior is in agreement with previously reported methylated Ir(III) tetrazolate complexes.[28]

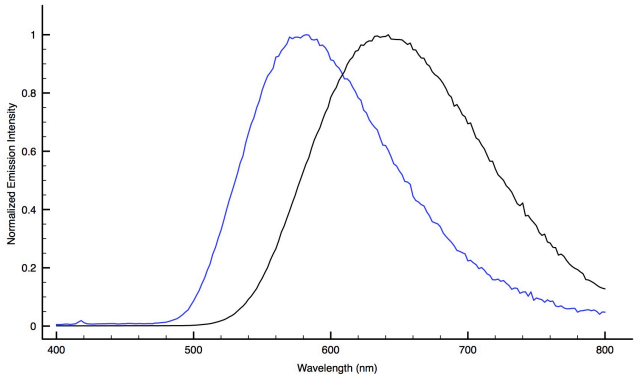

Figure 11.6: Normalized emission profiles of $[IrQTZ\text{-}Me]^+$ (black line) and $[IrQTZ]^+$ (blue line), CH_2Cl_2

For both [IrQTZ] and its cationic congener $[IrQTZ\text{-}Me]^+$, the phosphorescent emission arising from the excited state was confirmed by the increased emission intensities, higher quantum yields values (ϕ) and the elongation of decays time on passing from air equilibrated to deoxygenated solutions (Table 11).

Evaluation of the antibacterial activity

The evaluation of the antibacterial activity of both neutral and cationic Ir(III) tetrazolate complexes was tested against Gram-negative *E. coli* and Gram-positive *D. radiodurans* using a disk diffusion assay and liquid bacterial cultures. To firstly evaluate the bactericidal effect of Ir(III) complexes, pre-cultures of *E. coli* and *D. radiodurans* were grown on LB and TGY agar plates, respectively, in order to obtain a bacterial lawn. DMSO solution of the Ir(III) metal complexes (20 μM, final) has been soaked on sterile paper disks and finally placed onto the plates together with ampicillin (100 μg/mL) and a control disk with DMSO 1.5%.

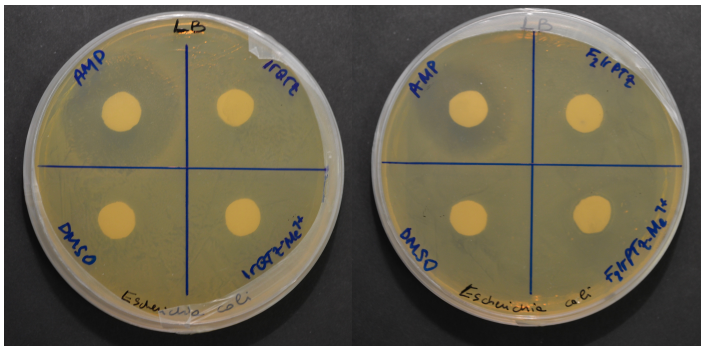

Figure 12.6: Anti- E. coli 24 h disk diffusion assay of (left) [IrQTZ-Me]⁺and[IrQTZ]; (right) [F₂IrPTZ-Me]⁺ and [F₂IrPTZ]. LB broth medium agar plates

The antimicrobial activity of neutral complexes [F₂IrPTZ] and [IrQTZ], together with the cations [F₂IrPTZ-Me]⁺ and [IrQTZ-Me]⁺ has been evaluated at first against *E. coli* bacterial cultures grown on LB agar plates. After 24 h, the growth inhibition zone was found only in the ampicillin surroundings, revealing how both neutral and cationic Ir(III) complexes did not hinder *E. coli* activity (Figure 12.6). On the contrary, *D. radiodurans* has been grown on TGY agar plates. Also in this case, both neutral and cationic Ir(III) complexes was screened in respect of their growth inhibition abilities. After 24 h, the absence of bacterial growth around the disks soaked with the cationic [F₂IrPTZ-Me]⁺ and [IrQTZ-Me]⁺ and less clear growth inhibition in the enclosing of neutral complexes soaked disks was observed (Figure 13.6). Prompted by these encouraging results, the bacterial growth rate was screened also in liquid medium cultures of *E. coli* and *D. radiodurans*, in the presence of Ir(III) neutral and cationic complexes.

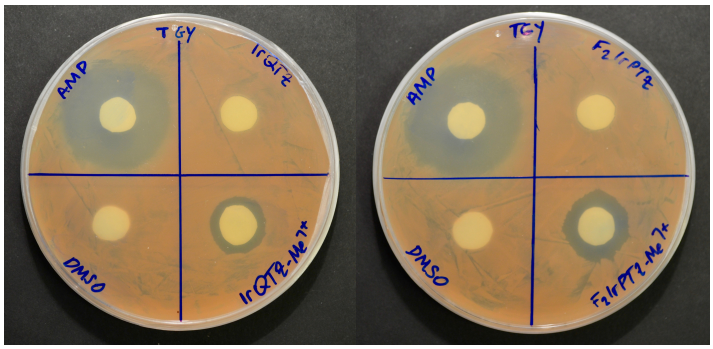

Figure 13.6: Anti- D. radiodurans 24 h disk diffusion assay of (left) [IrQTZ-Me]·and[IrQTZ]; (right) [F2IrPTZ-Me]·and [F2IrPTZ]. TGY broth medium agar plates

To investigate the bacteria growth rate and to plot the respective kinetic growth curves in absence or presence of neutral or cationic Ir(III) tetrazolate complexes, bacterial pre-cultures were prepared from single colonies in 2 mL of LB broth maintained at 37°C for 18 hours under shaking (for *E. coli*), while *D. radiodurans* was cultivated in TGY broth kept at 30°C for 30 hours. The bacteria pre-cultures were then diluted to OD = 0.05 (at λ = 600 nm) and suddenly inoculated in 5mL of the respective liquid broth medium inside 50 mL falcon tubes, supplemented with 5µM and 20µM solutions of the complexes. A blank falcon tube without the Ir(III) complex, together with two DMSO containing samples (0.4 and 1.5%, respectively) were prepared as reference for every trial.

The absorbance value at λ = 600 nm was measured after appropriate time intervals for each sample in order to plot the various kinetics growth curves.

D. radiodurans kinetics of growth

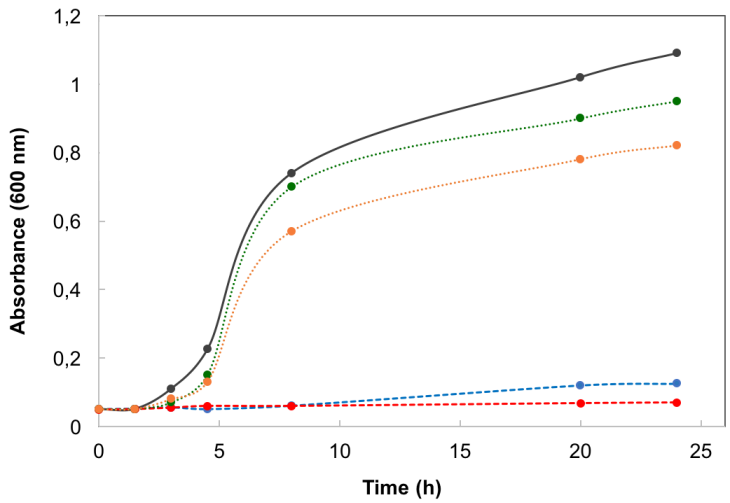

Figure 14.6: Kinetics of growth at 30 °C of Deinococcus radiodurans cultures in the presence of 5 mM [F2IrPTZ-Me]· (blue dots), 20 mM [F2IrPTZ-Me]· (red dots), 0.4% DMSO (green dots), 1.5% DMSO (orange dots). A control culture without any complex was performed (black curve)

The liquid bacterial growth curves suggested how the cationic $[F_2IrPTZ\text{-}Me]^+$ 5 µM (Figure 14.6, blue line) oversights *D. radiodurans* growth in 0-24 h time laps (0.05 to 0.12 OD, Table 12), while blank sample and DMSO falcon tubes did not arrest the bacteria evolvement. Up to 20 µM concentration of $[F_2IrPTZ\text{-}Me]^+$ (Figure 14.6, red line), no significant variations in the initial 0.05 OD value were detected all along the experiment, suggesting a complete growth-inhibition ability of $[F_2IrPTZ\text{-}Me]^+$ towards Gram-positive *D. radiodurans*.

Table 12: growth inhibition data collected for $[F_2IrPTZ\text{-}Me]^+$ against D. radiodurans

Time	Absorbance at 600 nm				
	Control	5µM $[F_2IrPTZ\text{-}Me]^+$	20 µM $[F_2IrPTZ\text{-}Me]^+$	0.4% DMSO	1.5% DMSO
0	0.05	0.05	0.05	0.05	0.05
1.5	0.051	0.051	0.051	0.051	0.051
3	0.11	0.055	0.055	0.07	0.08
4.5	0.225	0.05	0.06	0.15	0.13
8	0.74	0.06	0.06	0.7	0.57
20	1.02	0.12	0.068	0.9	0.78
24	1.09	0.125	0.07	0.95	0.82

The growth inhibition ability of $[IrQTZ\text{-}Me]^+$ was screened in the same manner as described above (Figure 15.6).

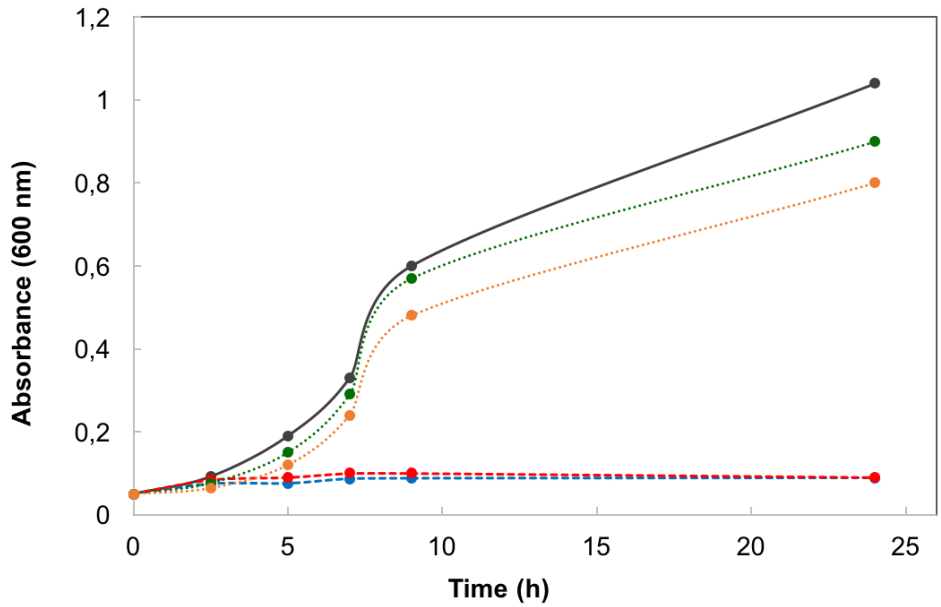

Figure 15.6: netics of growth at 30 °C of Deinococcus radiodurans cultures in the presence of 5 mM $[IrQTZ\text{-}Me]^+$ (blue dots), 20 mM $[IrQTZ\text{-}Me]^+$ (red dots), 0.4% DMSO (green dots), 1.5% DMSO (orange dots). A control culture without any complex was performed (black curve)

As previously deduced by the disk diffusion susceptibility assay, the cationic $[IrQTZ\text{-}Me]^+$ has been able to prevent *D. radiodurans* rising in both 5μM and 20μM concentrations throughout the duration of the experiment (0-24 h, Figure 15.6, blue and red lines respectively, Table 13) with OD values ranging from 0.05 to 0.1. On the contrary, blank and DMSO samples OD values are set at around 0.1 – 1 (Table 12), suggesting a strong bacteria growth.

Table 13: growth inhibition data collected for $[IrQTZ\text{-}Me]^+$ against D. radiodurans

Time	Absorbance at 600 nm				
	Control	5μM $[IrQTZ\text{-}Me]^+$	20 μM $[IrQTZ\text{-}Me]^+$	0.4% DMSO	1.5% DMSO
0	0.05	0.05	0.05	0.05	0.05
2.5	0.092	0.074	0.084	0.076	0.064
5	0.19	0.075	0.09	0.15	0.12
7	0.33	0.086	0.1	0.29	0.24
9	0.60	0.087	0.1	0.57	0.48
24	1.04	0.088	0.09	0.9	0.8

The neutral $[F_2IrPTZ]$ and [IrQTZ] tetrazolate complexes were subjected to the same treatment to assess whether the information collected from the disk diffusion susceptibility test are met (Figure 16.6).

Even if in the initial stage of the experiment (0-8 h) the OD values were found to be lower than those observed from both blank and DMSO samples (0.175 OD at 8h from 20μM $[F_2IrPTZ]$ against 0.44 OD at 8h of blank sample, Table 14), the variance between doped and control samples significantly decreased in the 10-27 h time laps, revealing how the antibacterial abilities of neutral Ir(III) tetrazolate complexes is less pronounced if compared to the results obtained from cationic $[IrQTZ\text{-}Me]^+$ and $[F_2IrPTZ\text{-}Me]^+$.

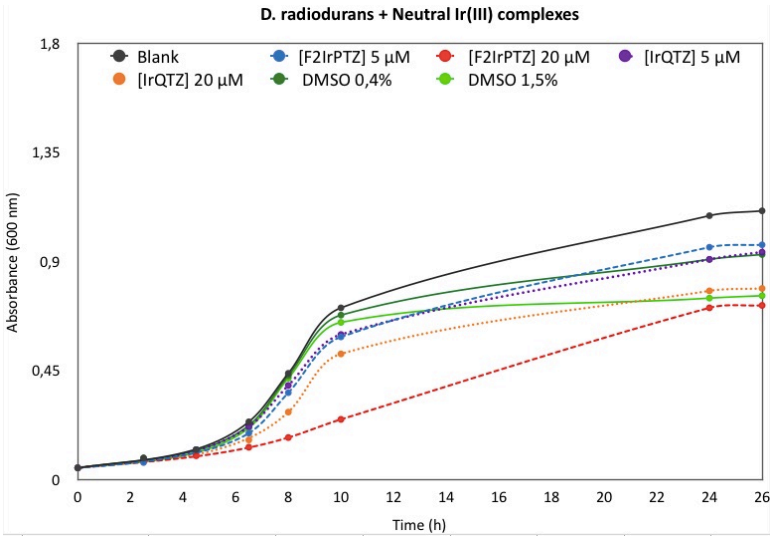

Figure 16.6: growth inhibition curves from $[F_2IrPTZ]$ and [IrQTZ] and D. radiodurans

Table 14: growth inhibition data collected for[F₂IrPTZ] and [IrQTZ]against D. radiodurans

Time (h)	Blank Abs (λ = 600 nm)	[F₂IrPTZ]⁺ 5 μM Abs (λ = 600 nm)	[F₂IrPTZ]⁺ 20 μM Abs (λ = 600 nm)	[IrQTZ] 5 μM Abs (λ = 600 nm)	[IrQTZ]⁺ 20 μM Abs (λ = 600 nm)	DMSO 0,4% Abs (λ = 600 nm)	DMSO 1,5% Abs (λ = 600 nm)
0	0.05	0.05	0.05	0.05	0.05	0.05	0.05
2.5	0.09	0.072	0.076	0.08	0.081	0.091	0.08
4.5	0.125	0.125	0.1	0.125	0.115	0.125	0.12
6.5	0.24	0.193	0.135	0.22	0.165	0.225	0.215
8	0.44	0.36	0.175	0.39	0.28	0.43	0.42
10	0.71	0.59	0.25	0.6	0.52	0.68	0.65
24	1.09	0.96	0.71	0.91	0.78	0.91	0.75
26	1.11	0.97	0.72	0.94	0.79	0.93	0.76

E. coli growth inhibition through $^1O_2$ photoinduced production

Although no significant growth inhibition of Gram-negative *E. coli* has been observed from the disk diffusion assay test (Figure 12.6), the cationic $[F_2IrPTZ\text{-}Me]^+$ complex has been chosen to be supported on SiO_2NPs and subsequently affixed on woven fabrics of cotton. This choice has been made taking into account the remarkable stability in the process conditions displayed by $[F_2IrPTZ\text{-}Me]^+$ over the other Ir(III) complexes discussed in this chapter. The evaluation of anti- *E. coli* activity of these textiles has been evaluated taking advantage of the $^1O_2$ (singlet oxygen) photo induced production from $[F_2IrPTZ\text{-}Me]^+$.

Photosensitized generation of $^1O_2$

Despite being discovered in 1924, singlet molecular oxygen received a considerable amount of interest only after 1963, when Khan and Kasha interpreted the chemiluminescence of the hypochlorite-peroxide reaction as caused by singlet oxygen release.[65]

Since then, the whole entirety of physical, chemical and biological properties of this energetically rich form of molecular oxygen have attracted considerable attention. In particular, the photosensitized production of singlet oxygen received increasing attention in a wide range of areas from photooxidation, DNA damage, photodynamic therapy (PDT) of cancer, to polymer science.

Molecular oxygen has two low-lying singlet excited states, $^1\Delta_g$ and $^1\Sigma_g^+$above the triplet state $^3\Sigma_g^-$, respectively. Once O_2 is in its singlet-excited state, it can be deactivated by other species to return to its ground state by following two different deactivation (or quenching) mechanisms:

1) Physical quenching: $^1O_2 + A \longrightarrow {}^3O_2 + A$, in which interaction with A deactivate $^1O_2$ with no O_2 consumption or product formation;
2) Chemical quenching: $^1O_2 + A \longrightarrow {}^3O_2 + P$, where the quencher reacts with singlet oxygen to give a new product.

Photosensitized generation is a straightforward method for the production of $^1O_2$, requiring only oxygen, light of an appropriate wavelength, and a photosensitizer capable of absorbing and using that energy to excite oxygen to its singlet state. Sensitizer excitation is generally achieved via a one-photon transition (hν) between the ground state, S_0, and a singlet excited state S_n. Relaxation of the S_n state yields the lowest excited singlet state of the sensitizer S_1. Intersystem crossing generates the sensitizer triplet state, T_1, which can react by following two different pathways, defined as Types I and II mechanisms (Figure 17.6).

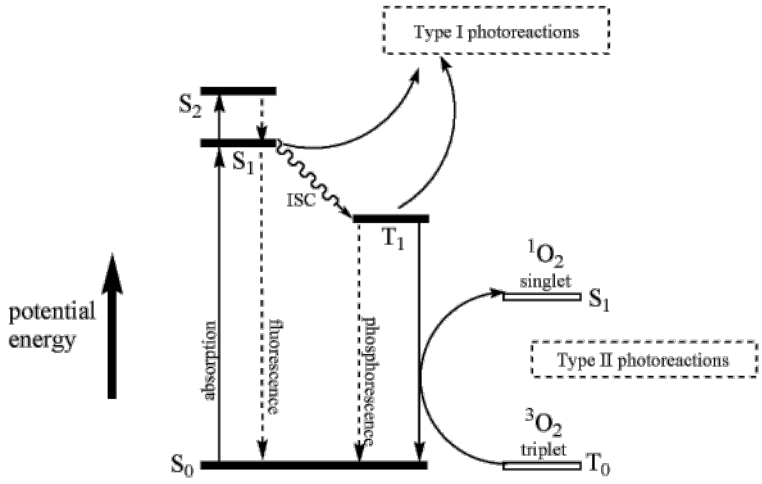

Figure 17.6: extended Jabonski diagram with $^1O_2$ deactivation mechanisms

In Type I mechanism, the formation of free radicals by energy transfer from T_1 photosensitizer to biological substrates; in Type II mechanism, singlet oxygen is generated through energy transfer from T_1 phosensitizer to $^3O_2$.

There are several groups of UV-vis absorbing molecules that are capable of producing singlet oxygen. The majority of the studies dealing with singlet oxygen photosensitization involve organic molecules. However, some metal complexes have also been shown to be efficient photosensitizers. Transition metal complexes of ruthenium(II) and iridium(III), for example, possess strong absorption in the UV-vis region of the spectrum and their long-lived phosphorescent emission from the ^{3}MLCT states allows the concomitant formation of $^1O_2$.

[F_2IrPTZ-Me]$^+$@SiO_2NPs -coated cotton textiles

On the basis of the foregoing, the phosphorescent sky-blue emitter [F_2IrPTZ-Me]$^+$ has been incorporated in SiO_2 colloidal suspension and then applied over cotton textiles as photosensitizer for *in-situ* production of antimicrobial $^1O_2$ – singlet oxygen. For doing this, the cationic [F_2IrPTZ-Me]$^+$ has been blended with negatively charged colloidal SiO_2 (LUDOX®HS-40 colloidal silica 20%*w/t*, pretreated with Dowex Ion exchange resin 50x8 until pH = 4). Woven fabrics of cotton have been padded three times with the newly obtained phosphorescent colloidal [F_2IrPTZ-Me]$^+$- SiO_2NPs solution and tested at first with FEG-SEM to ensure the fiber integrity (Figure 18.6, right).

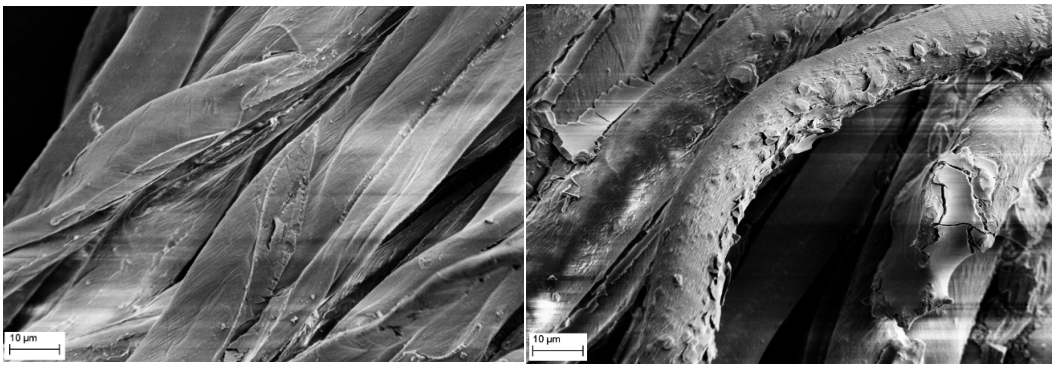

Figure 18.6: FEG-SEM images of cotton fibers before (left) and after (right) dip-pad-dry-cure process

Coated cotton textiles were then water flushed both in static and dynamic mode, to ensure the layers cohesion. The washing waters has been analyzed with inductively coupled plasma (ICP), revealing a minimum SiO_2-loss percentage (14.83 ppm, 1.64 % weight loss after 10 days) and no sign of Ir(III) in solution (Table 15).

Table 15: ICP value after static water flushing of 3 layers-coated cotton textiles in 1h-10d time laps

Time	ppm Si (251 nm)	ppm Ir (212 nm)	Loss SiO_2(%)	Loss Ir(III) (%)
1h	1,31	0,00	0,14	-*
2h	1,87	0,00	0,21	-*
3h	3,13	0,00	0,35	-*
4h	2,48	0,00	0,27	-*
1d	7,01	0,00	0,77	-*
3d	10,76	0,00	1,19	-*
4d	13,37	0,00	1,48	-*
7d	13,63	0,00	1,50	-*
10d	14,83	0,00	1,64	-*

* = under the instrument detection limit.

The emission profile of [F_2IrPTZ-Me]$^+$@SiO_2NPs -coated cotton textiles confirmed the presence of the phosphorescent cationic Ir(III) tetrazolate complex (Figure 19.6) together with a minor interference played by the fluorescent emission of the optical brightener applied on the textile (λ_{max} = 420 nm).

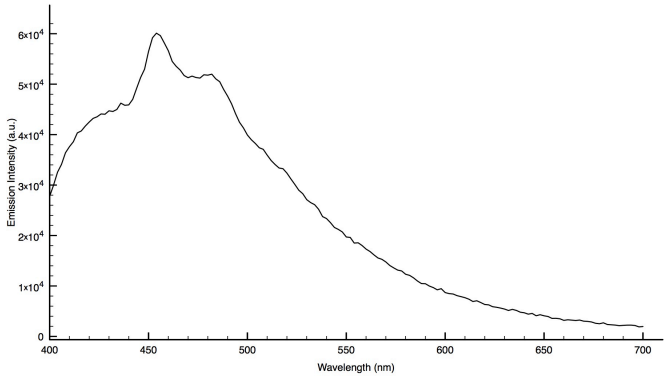

Figure 86: Emission profile of [F_2IrPTZ-Me]$^+$@SiO_2NPs -coated cotton textiles, r.t.

The evaluation of the antibacterial activity of [F_2IrPTZ-Me]$^+$@SiO_2NPs -coated cotton textiles has been made by following the modified AATCC-147 procedure (Antibacterial Activity of Fabrics, Assessment of Textile Materials: Parallel Streak Method)[66]. Prior to initiating the test, sterilized molten growth agar has been poured into three different petri dishes and allowed to solidify completely before inoculating. *E. coli* pre-cultures were prepared from single colonies in 2 mL of LB broth maintained at 37°C for 18 hours under shaking. *E. coli* suspension were then diluted in sterile distilled water. The diluted inoculum suspension was then used to streak five consecutive spaced streaks onto the solidified growth agar. [F_2IrPTZ-Me]$^+$@SiO_2NPs -coated cotton samples, have been cut to 25 x 50 mm, and finally placed across the five parallel streaks. The above described Petri plates were subsequently incubated for 24 h at 30°C with different illumination conditions: I) dark II) sunlight III) Sunlight and UV (Figure 20.6).

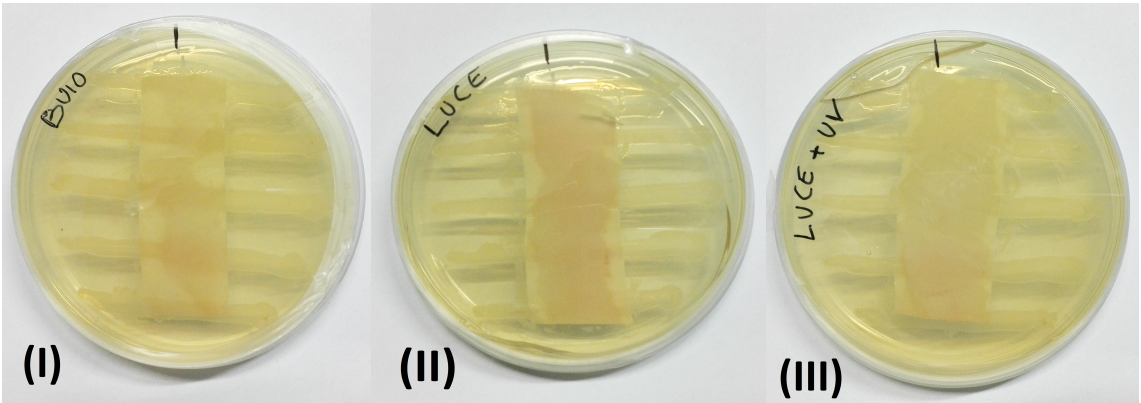

Figure 20.6: left (I) dark-exposed Petri plate; center (II) sunlight- exposed Petri plate; right (III) sunlight + UV- exposed Petri plate, Streaking test method with E. coli

The preliminary results obtained by the streaking test method applied to [F_2IrPTZ-Me]@SiO_2NPs -coated cotton samples suggest how the phosphorescent Ir(III) complex [F_2IrPTZ-Me] is capable of photo-induce the production of $^1O_2$, as suggested by the reduced *E. coli* growth in sample (II) and (III). On the contrary, a clear lawn of *E. coli* bacteria was found in the surroundings of the dark-exposed sample (I) (Figure 20.6).

[F_2IrPTZ-Me]@SiO_2NPs -coated cotton samples growth inhibition abilities has been screened also in liquid culture medium (Figure 21.6). Small textile portions were placed into three falcon tubes together with 40µL *E. coli* inoculum and 1960 µL of LB broth medium (Table 16).

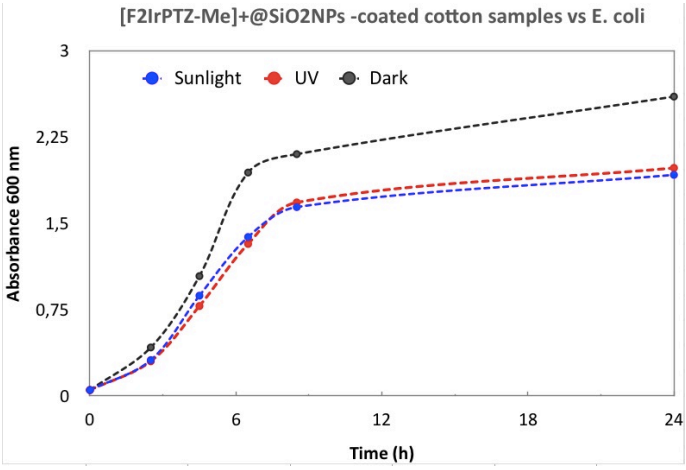

Figure 21.6: growth curves of [F_2IrPTZ-Me]@SiO_2NPs -coated cotton samples against E. coli

In the 0-6h time laps, *E. coli* was capable of grown in all the different samples tested, while after that time, the sunlight and UV-exposed falcon tubes reduced *E. coli* population significantly in respect of the dark-exposed falcon tube.

Table 16: growth inhibition data collected for[F_2IrPTZ-Me]@SiO_2NPs -coated cotton samples]against E. coli

Time (h)	Sunlight Abs (λ = 600 nm)	UV Abs (λ = 600 nm)	Dark Abs (λ = 600 nm)
0	0.05	0.05	0.05
2.5	0.31	0.3	0.42
4.5	0.87	0.78	1.04
6.5	1.38	1.32	1.94
8.5	1.64	1.68	2.1
24	1.92	1.98	2.60

Conclusions

A series of four different Ir(III) tetrazolate complexes were fully synthesized and characterized. Both the neutral [F_2IrPTZ] and [IrQTZ] and the cationic [F_2IrPTZ-Me]$^+$ and [IrQTZ-Me]$^+$ has been screened against Gram negative *E. coli* and Gram positive *D. radiodurans* by the means of disk diffusion susceptibility assay and liquid culture medium, revealing promising growth inhibition abilities of the cationic [F_2IrPTZ-Me]$^+$ and [IrQTZ-Me]$^+$vs *D. radiodurans*.

Moreover, the cationic [F_2IrPTZ-Me]$^+$ was successfully blended with SiO_2NPs and then layered over woven fabrics of cotton. This phosphorescent textile has been screened against *E. coli*, revealing how the in-situ production of $^1O_2$ accomplished by [F_2IrPTZ-Me]$^+$ can fairly inhibit the bacteria grown.

Experimental section

General considerations. All the reagents and solvents were obtained commercially (e.g. Aldrich) and used as received without any further purification, unless otherwise specified. All the reactions were carried out under an argon atmosphere following Schlenk protocols. Where required, the purification of the Ir(III) complexes was performed via column chromatography with the use of SiO_2 as the stationary phase. ESI-mass spectra were recorded using a Waters ZQ-4000 instrument (ESI-MS, acetonitrile as the solvent). Nuclear magnetic resonance spectra (consisting of ^{1}H and ^{13}C) were always recorded using a Varian Mercury Plus 400 (^{1}H, 399.9; ^{13}C, 101.0 MHz.). ^{1}H and ^{13}C chemical shifts were referenced to residual solvent resonances.

Photophysics. Absorption spectra were recorded at room temperature using a Perkin Elmer Lambda 35 UV/vis spectrometer. Uncorrected steady-state emission and excitation spectra were recorded on an Edinburgh FLSP920 spectrometer equipped with a 450 W xenon arc lamp, double excitation and single emission monochromators, and a Peltier-cooled Hamamatsu R928P photomultiplier tube (185–850 nm). Emission and excitation spectra were acquired with a cut-off filter (395 nm) and corrected for source intensity (lamp and grating) and emission spectral response (detector and grating) by a calibration curve supplied with the instrument. The wavelengths for the emission and excitation spectra were determined using the absorption maxima of the MLCT transition bands (emission spectra) and at the maxima of the emission bands (excitation spectra). Quantum yields (Φ) were determined using the optically dilute method by Crosby and Demas[41] at excitation wavelength obtained from absorption spectra on a wavelength scale [nm] and compared to the reference emitter by the following equation:[42]

$$\phi_s = \phi_r \left[\frac{A_r(\lambda_r)}{A_s(\lambda_s)}\right]\left[\frac{I_r(\lambda_r)}{I_s(\lambda_s)}\right]\left[\frac{n_s^2}{n_r^2}\right]\left[\frac{D_s}{D_r}\right]$$

where A is the absorbance at the excitation wavelength (λ), I is the intensity of the excitation light at the excitation wavelength (λ), n is the refractive index of the solvent, D is the integrated intensity of the luminescence, and Φ is the quantum yield. The subscripts r and s refer to the reference and the sample, respectively. A stock solution with an absorbance > 0.1 was prepared, then two

dilutions were obtained with dilution factors of 20 and 10, resulting in absorbances of about 0.02 and 0.08 respectively. The Lambert-Beer law was assumed to remain linear at the concentrations of the solutions. The degassed measurements were obtained after the solutions were bubbled for 10 minutes under Ar atmosphere, using a septa-sealed quartz cell. Air-equilibrated $[Ru(bpy)_3]Cl_2/H_2O$ solution (Φ = 0.028)[43] was used as reference. The quantum yield determinations were performed at identical excitation wavelengths for the sample and the reference, therefore deleting the $I(\lambda r)/I(\lambda s)$ term in the equation. Emission lifetimes (τ) were determined with the single photon counting technique (TCSPC) with the same Edinburgh FLSP920 spectrometer using pulsed picosecond LED (EPLED 360, fhwm < 800 ps) as the excitation source, with repetition rates between 1 kHz and 1 MHz, and the above-mentioned R928P PMT as detector. The goodness of fit was assessed by minimizing the reduced $\chi 2$ function and by visual inspection of the weighted residuals. To record the 77 K luminescence spectra, the samples were put in quartz tubes (2 mm diameter) and inserted in a special quartz dewar filled with liquid nitrogen. The solvent used in the preparation of the solutions for the photophysical investigations was of spectrometric grade. Experimental uncertainties are estimated to be ±8% for lifetime determinations, ±20% for quantum yields, and ±2 nm and ±5 nm for absorption and emission peaks, respectively.

Ligand synthesis

Warning! Tetrazole derivatives are used as components for explosive mixtures.[18a, b] In this lab, the reactions described here were only run on a few grams scale and no problems were encountered. However, great caution should be exercised when handling or heating compounds of this type.

Following the general method reported by Koguro and coworkers,[21] tetrazole ligand [H-**PTZ**] and [H-**QTZ**] were obtained in quantitative yield.

[H-**PTZ**] ^{1}**H-NMR** (DMSO d^6, 400 MHz) δ (ppm) = 8.77 (d, 1H, J_{H-H} = 5.6 Hz), 8.20 (d, 1H, J_{H-H} = 8 Hz) 8.07–8.03 (m, 1H), 7.62–7.59 (m, 1H). ^{13}**C-NMR**, 100 MHz, DMSO-d^6 δ (ppm) = 155.3 (Ct), 150.5, 144.1, 138.7, 126.6, 123.1. [H-**QTZ**] ^{1}**H-NMR**, (DMSO-d^6, 400 MHz) δ (ppm) = 8,65 (d, 1H, J_{H-H} = 8.79 Hz), 8,31 (d, 1H, J_{H-H} = 8.40 Hz), 8,17 (d, 1H, J_{H-H} = 8.40 Hz), 8,12 (d, 1H, J_{H-H} = 7.99 Hz), 7,90 (t, 1H), 7.74 (t, 1H);

General Procedure for the Preparation of the Neutral Ir(III) complexes

To a 3:1 solution of DCM/EtOH (15 mL) were added the dichlorobridged Ir(III) dimer $[Ir(C^N)_2Cl]_2$ (1 eq) and 2.5 eq of [H-PTZ] or [H-QTZ]. The solution was stirred at r.t. for 6h. The solvent was removed by rotary-evaporation and the crude was subsequently purified with Al_2O_3 column chromatography eluted with a 8:2 DCM/acetone mixture, yielding the desired neutral Ir(III) complex (second fraction).

F_2IrPTZ ^{1}H-NMR (CD_3CN, 400 MHz) δ (ppm): 8.38-8.36 (m, 1H); 8.32-8.29 (m, 2H); 8.11-8.07 (m, 1H); 7.90-7.86 (m, 3H); 7.67-7.65 (m, 1H); 7.59-7.56 (m, 1H); 7.41-7.37 (m, 1H); 7.12-7.05 (m, 2H); 6.72-6.60 (m, 2H); 5.86-5.83 (m, 1H); 5.78-5.75 (m, 1H). ^{13}**C-NMR** (CD_3CN, 100 MHz) δ (ppm) = **ESI-MS** (*m*/*z*): $[M]^+$ = 720 m/z; $[M+Na]^+$ = 742 m/z; $[M+K]^+$ = 758 m/z. ^{13}**C-NMR** (CD_3CN, 100 MHz) δ (ppm) = 164.86, 164.17, 164.00, 163.93, 163.86, 162.59, 162.22, 162.08, 161.64, 161.51, 160.13, 160.01, 159.64, 159.51, 156.42, 156.35, 152.17, 157.11, 150.50, 149.75, 149.44, 148.71, 139.98, 139.07, 138.93. Anal. Calcd. For $C_{28}H_{16}N_7F_4Ir_1$ (718.68): C 46.8, H 2.24, N 13.64. Found: C 46.60, H 2.29, N 13.69 %.

IrQTZ ^{1}H-NMR (CD_3CN, 400 MHz) δ (ppm): 8.61 – 8.53 (m, 2H), 8.06 – 8.00 (m, 2H), 7.97 – 7.92 (m, 2H), 7.89 – 7.87 (m, 1H), 7.81 – 7.68 (m, 4H), 7.53 – 7.49 (m, 1H), 7.33 – 7.32 (m, 1H), 7.19 – 7.15 (m, 1H), 7.06 – 7.02 (m, 1H), 6.99 – 6.93 (m, 3H), 6.90 – 6.87 (m, 1H), 6.83 – 6.79 (m, 1H), 6.49 – 6.48 (m, 1H), 6.15 – 6.13 (m, 1H). ^{13}**C-NMR** (CD_3CN, 100 MHz) δ (ppm) = 169.45, 168.55, 166.76 (Ct), 157.09, 155.48, 152.50, 151.96, 150.26, 149.05, 146.01, 145.18, 145.07, 142.16, 139.34, 139.27, 133.48, 132.33, 131.45, 130.82, 130.75, 130.26, 129.12, 129.11, 126.29, 126.17, 125.51, 124.59, 124.34, 123.25, 123.23, 121.20, 120.76. **ESI-MS** (*m*/*z*): $[M+Na]^+$ = 720. Anal. Calcd. For $C_{32}H_{22}N_7Ir_1$ (696.78): C 55.16, H 3.18, N 14.07. Found: C 55.20, H 3.22, N 14.10 %.

General Procedure for the Preparation of the Cationic Ir(III) complexes

1 eq of the desired neutral Ir(III) tetrazoalate complex was added to dichloromethane and the mixture was allowed to cool down by immersion into an ethanol/liquid nitrogen cold bath. Then, methyl trifluoromethanesulfonate (1.2 eq., solution in dichloromethane 0.179 M) was added. The reaction was stirred under nitrogen for 30 minutes while being kept in the cold bath, then

allowed to warm up to room temperature and stirred for 3 hours. Anion exchange was carried out by adding an excess of NH_4PF_6 in water to the solution and stirring for 20 minutes. The product was then extracted using dichloromethane (3 × 10 mL) and the organic components were combined and dried over anhydrous $MgSO_4$. Subsequent purification by column chromatography on alumina (gradient: CH_2Cl_2/Acetone 8:2, second fraction) yielded 0.059 g of **[F_2IrPTZ-Me]$^+$[PF_6]$^-$** and 0.067 g of **[IrQTZ-Me]$^+$[PF_6]$^-$**

IrQTZ-Me ^{1}**H-NMR** (Acetone-d^6, 400 MHz) δ (ppm): 8.98 (d, 1H, J_{H-H} = 8.39 Hz), 8.67 (d, 1H, J_{H-H} = 8.39 Hz), 8.27 (d, 1H, J_{H-H} = 7.99 Hz), 8.19 – 8.07 (m, 4H), 8.01 – 7.83 (m, 5H), 7.73 (m, 1H), 7.37 (m, 1H), 7.10 – 6.98 (m, 5H), 6.86 (m, 1H), 6.44 (d, 1H, J_{H-H} = 7.59 Hz), 6.18 (d, 1H, J_{H-H} = 7.59 Hz), 4.59 (s, 3H). ^{13}**C-NMR** (Acetone-d^6, 100 MHz) δ (ppm) = 167.93 (Ct), 167.69, 167.15, 151.08, 149.91, 149.61, 147.95, 146.63, 144.35, 143.83, 142.34, 140.12, 138.84, 138.80, 132.22, 131.63, 131.04, 130.66, 130.40, 129.78, 129.46, 129.37, 128.12, 125.15, 124.46, 123.76, 123.28, 122.73, 122.63, 120.04, 119.87, 119.72, 41.62. **ESI-MS** (*m*/*z*): [M^+] = 712 [M^-] = 145 (PF_6). Anal. Calcd. For $C_{33}H_{25}N_7F_6P_1Ir_1$ (856.78): C 46.26, H 2.94, N 11.44. Found: C 46.31, H 3.02, N 11.50 %.

F_2IrPTZ–Me ^{1}**H-NMR** (CD_3CN, 400 MHz) δ (ppm): 8.46-8.44 (d, 1H, J_{H-H}= 8.00 Hz); 8.36-8.33 (d, 2H, J_{H-H}= 8.80 Hz); 8.26-8.23 (m, 1H); 8.02-7.95 (m, 3H); 7.87-7.86 (d, 1H, J_{H-H}= 5.20 Hz); 7.66-7.63 (m, 2H); 7.17-7.12 (m, 2H); 6.79-6.69 (m, 2H); 5.75-5.73 (m, 2H); 4.47 (s, 3H). ^{13}**C-NMR** (CD_3CN, 100 MHz) δ (ppm): 166.54, 164.69, 164.57, 164.13, 164.00, 163.60, 163.53, 163.27, 163.20, 162.59, 162.08, 162.02, 161.95, 161.47, 159.88, 159.50, 151.76, 151.71, 151.47, 151.30, 151.23, 150.43, 150.37, 150.05, 149.97, 149.61, 148.40, 148.32, 144.02, 140.94, 140.80, 140.77, 139.80, 139.62, 139.36, 139.32, 129.93, 129.83, 128.20, 124.84, 124.77, 124.74, 42.08. **ESI-MS** (*m*/*z*): [M]$^+$ = 735 [M]$^-$ = 145 (PF_6). Anal. Calcd. For $C_{29}H_{19}N_7F_{10}P_1Ir_1$ (878.68): C 39.64, H 2.18, N 11.6. Found: C 39.58, H 2.25, N 11.9 %

Chapter 7

Targeting divalent metal cations with Re(I) tetrazolato complexes*

Abstract

In order to exploit their potential as versatile luminescent sensors, four new Re(I)-tetrazolato complexes with the general formula fac-[Re(CO)$_3$(diim)(L)], where diim is 2,2′-bipyridine (bipy) or 1,10-phenanthroline (phen) and L− is either the anion 5-(2′-pyridyl)tetrazolato (2-PTZ$^-$) or 5-(2′-quinolyl)tetrazolato (2-QTZ$^-$), were prepared and fully characterized. In all cases, the regioselective coordination of the Re(I) center through the N2 atom of the tetrazolato ring was observed. This particular feature ensures the availability of the diiminic (N^N) site that was systematically incorporated into the structure of the 2-PTZ$^-$ and 2-QTZ$^-$ ligands for further coordination with metal cations. Such a diimine-type coordination mode was preliminarily tested by using the mononuclear Re(I) complexes as N^N ligands for the preparation of two [(N^N)Cu(POP)] cationic species, where POP is the chelating diphosphine bis[2-(diphenylphosphino)-phenyl]ether. The X-ray structures of the resulting Re(I)–Cu(I) dyads revealed that the Re(I) mononuclear complexes effectively behaved as chelating N^N ligands with respect to the [Cu(POP)]$^+$ fragment, the coordination of which also resulted in significant modification of the Re(I)-centered luminescence. With these data in hand, the luminescent sensing abilities of the four new Re(I) tetrazolato complexes were screened with respect to divalent metal ions of toxicological and biological importance such as Zn(II), Cd(II) and Cu(II). The interaction of the Re(I) complexes with Zn(II) and Cd(II) was witnessed by the evident blue shift (Δλmax = 22–36 nm) of the emission maxima, which was also accompanied by a significant elongation of the emission lifetimes. On the contrary, the addition of the cupric ion caused substantial quenching of the radiative processes originating from the Re(I) luminophores. Prompted by these encouraging results, the design of fac-[Re(CO)$_3$(diim)(L)] has been further extended with the employment of (L) = (1,3 BTB)$^{2-}$ and (2,6 BTP)$^{2-}$ tetrazolate dianions (1,3-di(1H-tetrazol-5-yl)benzene and 2,6-di(1H-tetrazol-5-yl)pyridine, respectively) in the development of a series of dinuclear Re(I) complexes with general formula fac-[Re(CO)$_3$(diim)]$_2$(L). The choice of using such bis tetrazolate-terpyrdine-like ligands is explained in consideration of the use of the corresponding Re(I) complexes as enlarged luminescent sensors for the above mentioned metal divalent cations.

: This chapter is part of Dalton. Trans*, **2015, *44*, 20597.[45a]

Introduction

The prevalent charge transfer character that connotes the nature of the emissive excited states of facial tricarbonyl Re(I) diimine species (*e.g.* metal-to-ligand charge transfer of triplet spin multiplicity, ^{3}MLCT) is one of the key factors that have favored the development of this class of compound as precursors for emissive materials and as luminescent probes for sensing.[67] Various classes of analytes have been investigated in relation to how they modulate the specific photophysical properties upon interaction with rhenium complexes. These species range from the simplest electrophile H$^+$, alkali and transition metal cations, to biologically relevant macromolecules such as proteins and DNA. In all cases, the detection of such analytes is related to the variation of the luminescent output of the Re(I) chemosensors that occurs upon the perturbation

of the chemical or physical parameters of their surrounding environment.[68] On the basis of this, considerable research effort has been devoted to the design of numerous Re(I)-based luminescent complexes in which the development of their sensing abilities toward specific targets has been combined with the improvement of their affinity to cellular substrates in terms of, for example, cellular uptake and specific organelle localization.[69] We have recently contributed to this research framework by describing the synthesis, photophysical properties,[31,70] reactivity toward electrophiles,[28, 45b] and biological behaviour[71] of a family of neutral fac-[Re(diim)(CO)$_3$(L)], where diim represents a conventional diimine ligand such as 1,10-phenanthroline (phen) or 2,2′-bipyridine (bipy) and L is a monodentate 5-aryl tetrazolato ancillary ligand (Figure 1.7).

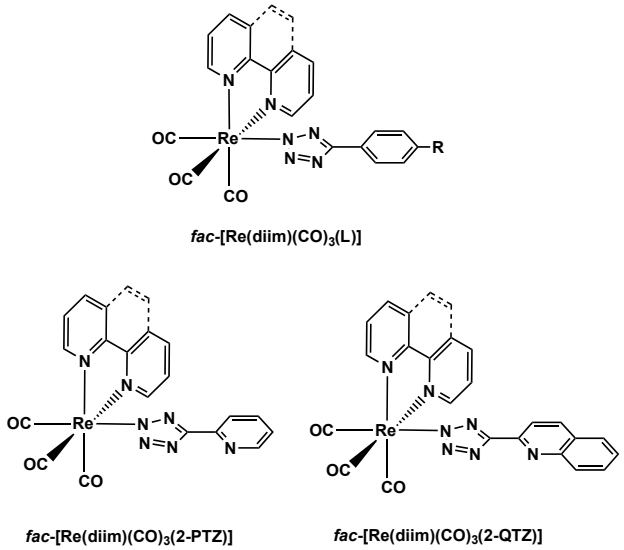

Figure 1.7: general formulation of the fac-[Re(diim)(CO)$_3$(L)] complexes described in this chapter, where diim represents 1,10-phenantroline (phen) or 2,2′-bipyrdine (bipy) and (L) is the 2-pyrdidyl tetrazolato (2-PTZ) or 2.quinolyl tetrazolato (2-QTZ) anion

With this class of complexes, we have in fact demonstrated the first example of direct staining of neutral lipid droplets in live Drosophila and human adipose 3T3-L1 cell lines, highlighting how facile chemical modifications of the ancillary ligands can be exploited to confer the complexes with defined cellular specificity without the need for bioconjugation.[71]

From the point of view of the luminescence properties, these neutral Re(I)-tetrazolato complexes display bright phosphorescent emission that originates from admixtures of ^{3}MLCT and ^{3}LLCT (ligand-to-ligand charge transfer) excited states, with a significant contribution from the tetrazolato heterocycle in determining the composition of HOMO-type orbitals.[33, 45b] As a consequence, the

luminescent output of these complexes could be efficiently modulated by lowering the electron-rich nature of the tetrazolato via reaction with electrophilic reagents such as H^+ and CH_3^+. In fact, the reversible protonation or irreversible methylation caused a marked blue shift of emission maxima ($\Delta\lambda$max *ca.* 50 nm) with a concomitant 6–10 fold increase of quantum yield and the extension of the emissive lifetime from a few hundreds of nanoseconds to microseconds.[68] Prompted by these results, we have decided to investigate the possibility of improving the sensitivity of this class of rhenium complexes to divalent transition metal ions of biological and/or toxicological importance. To this end, we have prepared a series of four Re(I) tetrazolato complexes, where the tetrazolato heterocycle is conjugated to either 2′-pyridine (2-PTZ$^-$) or 2′-quinoline (2-QTZ$^-$) in order to introduce a diimine-type coordination vacancy (Figure 89). A detailed description of the synthesis, structural features and optical properties of these Re(I) species is reported herein, including an investigation into their sensing capacity towards Zn^{2+}, Cd^{2+} and Cu^{2+} which are used as exemplar biological species.[72] Moreover, the bistetrazolate dianions (1,3 BTB)$^{2-}$ and (2,6 BTP)$^{2-}$ have been used in the synthesis of a family of dinuclear Re(I) species on the side of offering a terpyridine-like coordination position for the above mentioned metal divalent cations (Figure 2.7).

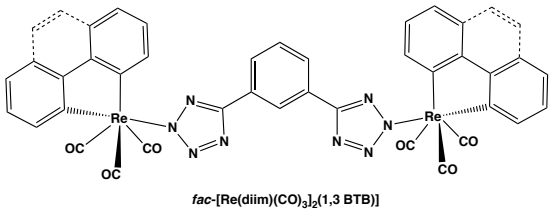

fac-[Re(diim)(CO)$_3$]$_2$(1,3 BTB)]

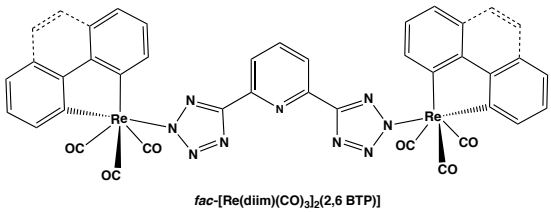

fac-[Re(diim)(CO)$_3$]$_2$(2,6 BTP)]

Figure 2.7: general formulation of the dinulear fac-[Re(diim)(CO)$_3$]$_2$ (L) complexes described in this chapter, where diim represents 1,10-phenantroline (phen) or 2,2′-bipyrdine (bipy) and (L) is the (1,3 BTB)$^{2-}$ or (2, BTP)$^{2-}$ tetrazolato dianion

Results and discussion

Synthesis and spectroscopic characterization of the complexes

All the tetrazole ligands (2-PTZH, 2-QTZH, 1,3 BTB-H_2 and 2,6 BTP H_2) have been obtained by following two well established methods reported in the literature, both of which involved the 1,3 dipolar cyclization reaction of the azide anion (N_3^-) with the corresponding nitrile precursors 2-cyanopyridine, 2-cyanoquinoline, 1, 3 dicyanobenzene and 2, 6 dicyanopirydine respectively. The neutral Re(I) complexes have been prepared by a simple metathesis between *fac*-[Re(*diim*)$(CO)_3$Br], where diim is bipy or phen, and the deprotonated tetrazole ligand in a refluxing 3 : 1 ethanol/water mixture (Figure 3.7)*. This methodology is very convenient, as the targeted complexes precipitate out of the solution and require a simple filtration to isolate them.

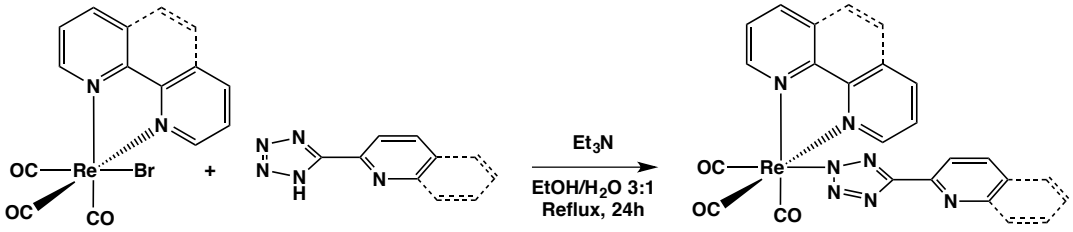

*Figure 3.7: Synthetic procedure used for the fac-[Re(diim)$(CO)_3$(L)]-type complexes. *For dinuclear fac-[Re(diim)$(CO)_3$]$_2$ (L) the same protocol has been applied except of fac -[Re(diim)$(CO)_3$Br] molar equivalents and ligands used*

Infrared (IR) spectroscopy from dichloromethane solutions provided results congruent with neutral Re(I) complexes with facial configuration of the three CO ligands. The carbonyl stretching region shows one sharp band centred at ca. 2030 cm^{-1}, assigned to the totally symmetric in-phase stretching A′(1), and a broader band at ca. 1922 cm^{-1}, which results from the superimposition of the totally symmetric out-of-phase stretching A′(2) and the asymmetric stretching A″.

Table 17: CO stretching values for Re(I) complexes, CH_3CN as the solvent

Complex	CO A′(1)	CO A′(2)/A″
fac-[Re(phen)$(CO)_3$(2-PTZ)]	2030	1923
fac-[Re(bipy)$(CO)_3$(2-PTZ)]	2028	1923
[Re-(2-PTZ)-Cu]$^+$	2031	1925
fac-[Re(phen)$(CO)_3$(2-QTZ)]	2033	1922
fac-[Re(bipy)$(CO)_3$(2-QTZ)]	2032	1922
[Re-(2-QTZ)-Cu]$^+$	2032	1927

Whereas the ^{1}H NMR spectra of the neutral Re(I) complexes all displayed patterns of signals that were expected from the presence of one symmetrical diimine ligand and one axially coordinated tetrazolato anion, the analysis of the ^{13}C NMR spectra provided indications of the coordination binding mode of the tetrazolato ligand.[26, 27, 28, 31, 45b, 73] For each complex, a single tetrazolato carbon resonance (Ct = ca. 163 ppm) was observed within the chemical shift range of 160–165 ppm. This value suggests the regioselective coordination of the Re(I) fragment through the N2 atom of the tetrazolato ring (Figure 4.7 and 5.7) as further confirmed by X-ray diffraction data.

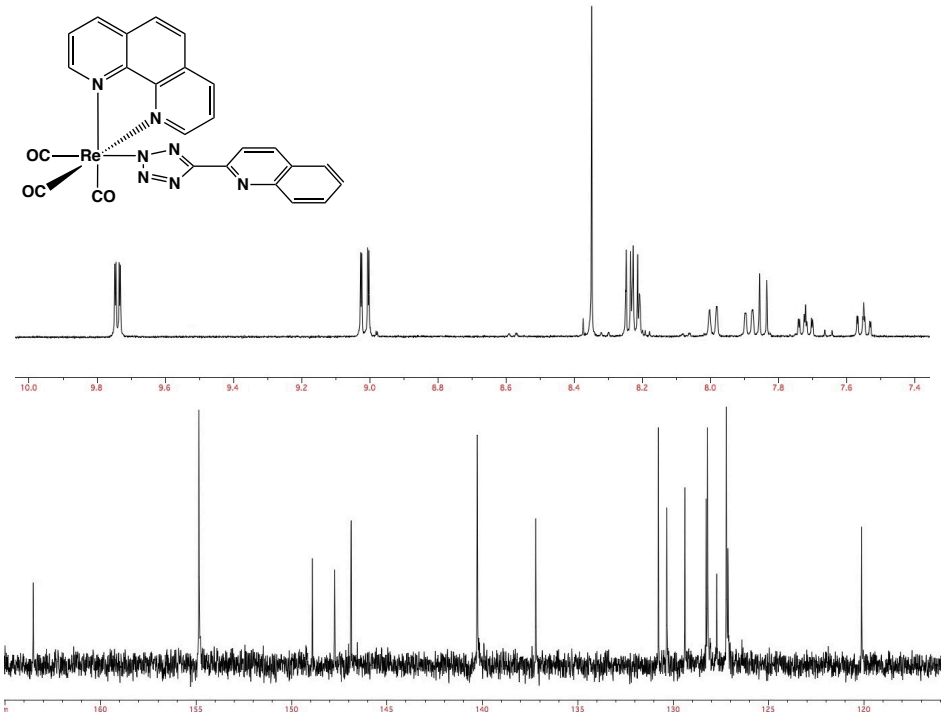

Figure 4.7: top fac-[Re(phen)(CO)$_3$(2-QTZ)] ^{1}H-NMR (Acetone-d$_6$,400 MHz, r.t.); bottom: fac-[Re(phen)(CO)$_3$(2-QTZ)] ^{13}C-NMR (DMSO-d$_6$,100 MHz, r.t.)

On the contrary, ^{1}H-NMR spectra of the dinuclear Re(I) complexes presented a number of resonances equal to the half of total protons of the molecule as expected for C_{2v} symmetry-type molecules (Figure 93). As their mononuclear Re(I) analogue, the Ct was found to resonate at *ca.* 163 ppm.

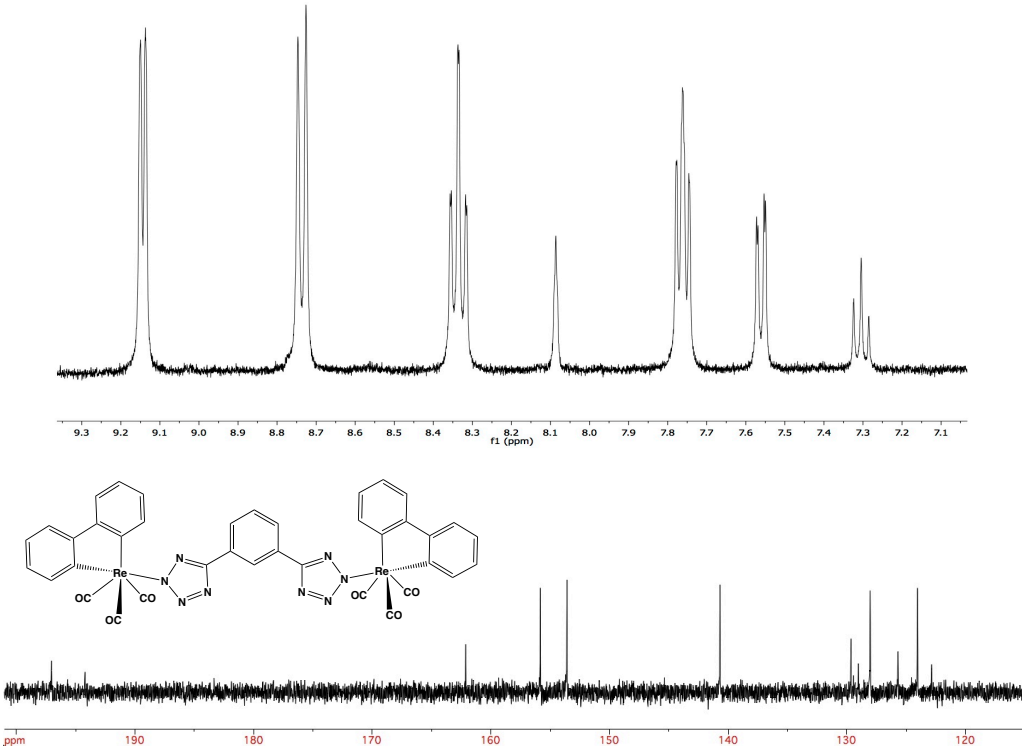

Figure 5.7: top fac-[Re(bipy)(CO)$_3$]$_2$(1,3 BTB) ^{1}H-NMR (DMSO-d$_6$,400 MHz, r.t.); bottom: fac-[Re(bipy)(CO)$_3$]$_2$(1,3 BTB)^{13}C-NMR (DMSO-d$_6$,100 MHz, r.t.)

In order to assess the binding capacity of the tetrazolato diiminic site, we have employed the complexes fac-[Re(bipy)-(CO)$_3$2-PTZ)] and fac-[Re(bipy)(CO)$_3$2-QTZ)] as the neutral N^N ligands for Cu(I). In particular, we have targeted the cationic species [(N^N)Cu(POP)]$^+$, herein referred to as [Re-(2-PTZ)-Cu]$^+$ and [Re-(2-QTZ)-Cu]$^+$, where POP is the chelating diphosphine bis[2-(diphenylphosphino)phenyl]ether (Figure 6.7).

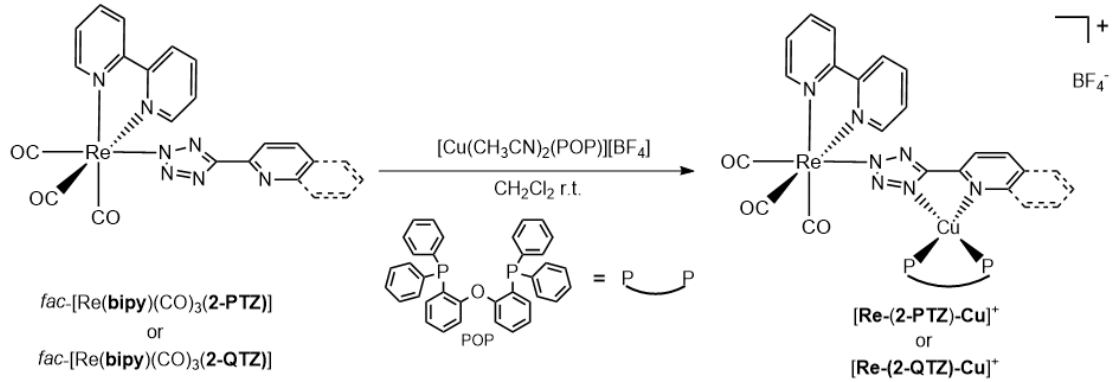

Figure 6.7: Synthetic procedure for the preparation of the dinuclear species [Re-(2-PTZ)-Cu]$^+$ and [Re-(2-QTZ)-Cu]$^+$

Using the same procedure that we have reported for the preparation of analogous tetrazole-based Cu(I) cationic derivatives,[74] the targeted Re(I)–Cu(I) dyads were isolated and their structures were confirmed by X-ray diffraction.

Crystal structures

The structures of *fac*-[Re(bipy)(CO)$_3$(2-PTZ)], *fac*-[Re(phen)(CO)$_3$(2-PTZ)] and *fac*-[Re(phen)(CO)$_3$(2-QTZ)]·0.5CH_2Cl_2 have been determined by single crystal X-ray diffraction studies (Figure 7.7, 8.7). Their structures and bonding parameters closely resemble those previously reported for analogous *fac*-[Re(diim)(CO)$_3$(L)] complexes (diim = bipy, phen; L = tetrazolate ligands).

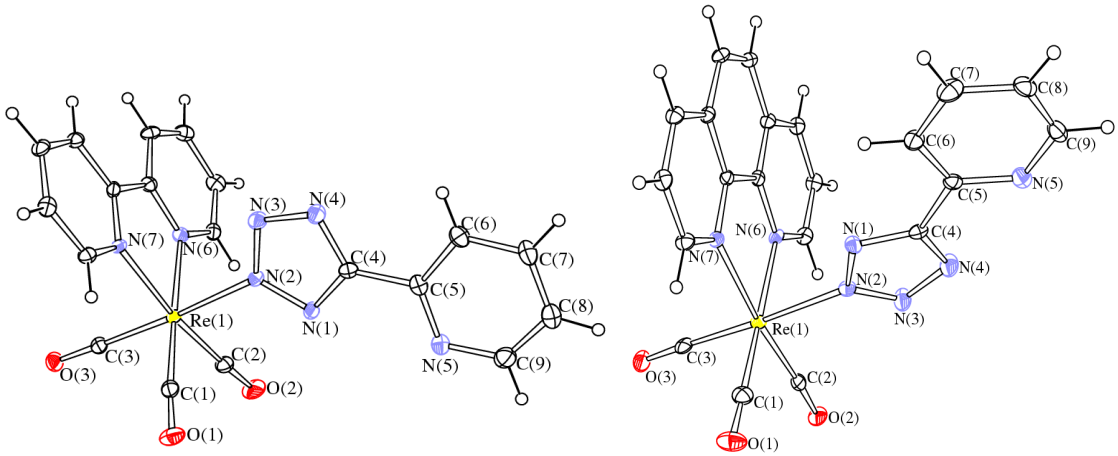

Figure 7.7: Molecular structure of fac-[Re(bipy)(CO)$_3$(2-PTZ)] with key atoms labelled. Displacement ellipsoids are at the 30% probability level. Molecular structure of fac-[Re(phen)(CO)$_3$(2-PTZ)] with key atoms labelled. Displacement ellipsoids are at the 30% probability level

Thus, the Re centers display an octahedral geometry being coordinated to three CO ligands (in a *facial* arrangement), a *cis*-chelating diimine ligand (bipy or phen) and a substituted tetrazolate ring bonded to the metal through its N2 atom.

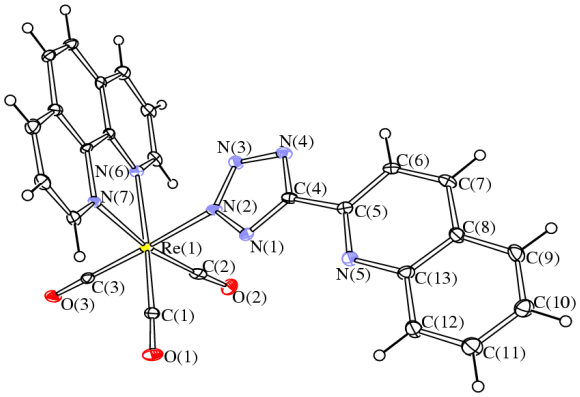

Figure 8.7: Molecular structure of fac-[Re(phen)(CO)$_3$(2-QTZ)] with key atoms labelled. Displacement ellipsoids are at the 30% probability level

The structures of [Re-2-PTZ-Cu][BF_4]·2 Et_2O and [Re-2-QTZ-Cu][BF_4]·1.67 CH_2Cl_2 (Figures 9.7 and 10.7) reveal the expected coordination of the Cu(I) center to the diiminic site of the tetrazolato ligands via the tetrazolic N4 and heterocyclic 2-pyridyl or 2 quinolyl N atoms. The Cu(I) center displays a distorted tetrahedral geometry as previously found in analogous complexes.[75,76] The N(4)–Cu(1)–N(5) bite angle [79.6(3) and 80.2(4)° for *fac*-[Re-2-PTZ-Cu]$^+$ and *fac*-[Re-2-QTZ-Cu]$^+$, respectively] is very close to the one found in [Cu(N^N)(POP)]$^+$ [78.6(2)°]. The P(1)–Cu(1)–P(2) angle [109.61(9) and 111.26(12)°] is in the usual range for a chelating POP ligand, which normally displays a rather large natural bite angle.[75,77]

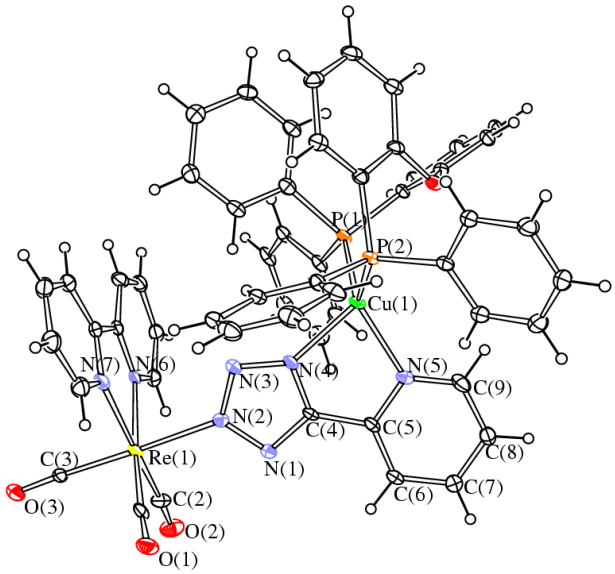

Figure 9.7: Molecular structure of [Re-2-PTZ-Cu]$^+$ with key atoms labelled. Displacement ellipsoids are at the 30% probability level

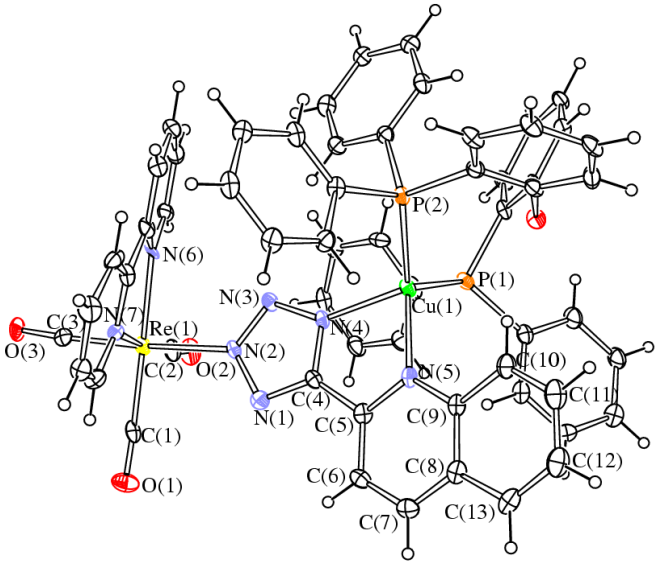

Figure 10.7: Molecular structure of [Re-2-QTZ-Cu]$^+$ with key atoms labelled. Displacement ellipsoids are at the 30% probability level

Photophysical properties

Table 18: summary of photophysical data for the complexes from diluted dichloromethane solutions

	Absorption	***Emission 298K***[a,b,c]							***Emission 77K***[c,d]	
Complex	λ_{abs}(nm) (10^{-4} ε) (M^{-1} cm^{-1})	λ_{em} (nm)	τ_{air} (ns)	$\tau_{under\ Ar}$ (ns)	ϕ_{air} (%)	ϕ_{Ar} (%)	K_r ($10^5 s^{-1}$)	K_{nr} ($10^5 s^{-1}$)	λ_{em} (nm)	τ (μs)
***fac*-[Re(phen)(CO)$_3$(2-PTZ)]**	268 (8.23) 360 (0.96)	584	308	838	6.24	20.27	2.41	9.51	522	7.19
***fac*-[Re(bipy)(CO)$_3$(2-PTZ)]**	280 (9.62) 338 (0.78) 422 (0.21)	596	103	115	1.2	7.9	6.87	80.10	528	2.7 (48) 5.6 (52)
***fac*-[Re(phen)(CO)$_3$(2-QTZ)]**	255 (9.54) 319 (2.30) 370 (0.76)	580	342	938	6.15	18.8	2.00	8.66	520	6.81
***fac*-[Re(bipy)(CO)$_3$(2QTZ)]**	244 (14.2), 318 (4.79) 370 (0.90)	598	104	128	3.53	5.81	4.53	73.6	536	6.03 (57) 1.66 (43)
***fac*-[Re(phen)(CO)$_3$]$_2$(1,3 BTB)**	260 (5.97) 295 (2.86) 361 (0.73)	594	0.27	0.67	5.86	15.6	n.d	n.d	532	7.56
***fac*-[Re(phen)(CO)$_3$]$_2$(2,6 BTP)**	261 (4.89) 297 (2.86) 357 (0.77)	586	0.39	0.76	9.23	26.4	n.d	n.d	534	7.20
fac*-[Re(bipy)(CO)$_3$]$_2$(1,3 BTB)	249 (3.05) 291 (1.45) 318 (1.08) 353 (0.44)	614	0.04	0.08	0.85	0.71	n.d	n.d	529	2.86
***fac*-[Re(bipy)(CO)$_3$]$_2$(2,6 BTP)**	291 (1.69) 248 (1.97) 368 (0.50)	600	0.09	0.14	0.71	0.83	n.d	n.d	536	3.04

[a]*Measured from an air-equilibrated solution.* [b]*Measured from a degassed matrix. (O_2-free) solution.* [c]$K_r = (\Phi/\tau)$, $k_{nr} = (1 - \Phi/\tau)$. [d]*In a frozen CH_2Cl_2 * measured in CH_3CN; n.d = not determined*

The relevant absorption and emission data from diluted (10^{-4} M) dichloromethane solutions of all the complexes are listed in Table 18. In general, the absorption and emission features are analogous to previously reported rhenium tetrazolato complexes. In detail, the UV-vis absorption profiles display a UV region dominated by intense ligand centered spin allowed (^{1}LC) absorptions followed, at lower energy, by weaker charge transfer (CT) bands consisting of spin allowed metal to ligand charge transfer (^{1}MLCT) type transitions (Figure 11.7).

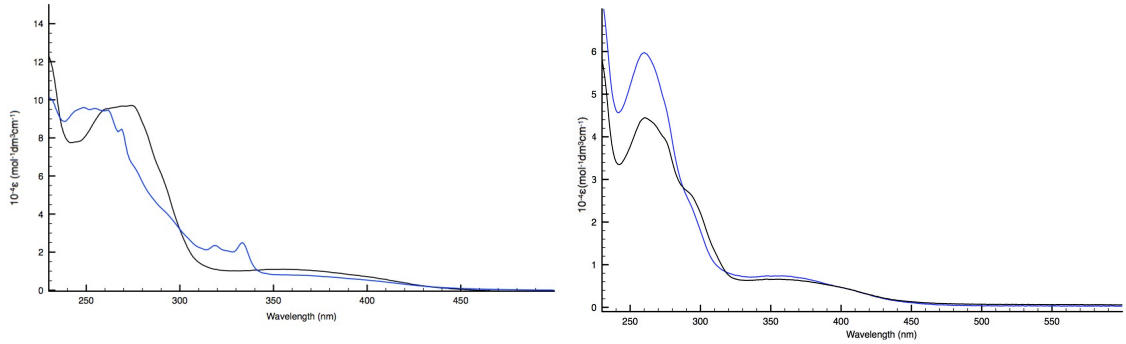

Figure 11.7: (Left) Absorption Spectra of complexes fac-[Re(phen)(CO)$_3$(2-QTZ)] (blue line) and fac-[Re(phen)(CO)$_3$(2-PTZ)] (black line), Solvent: CH_2Cl_2; (Right) Absorption Spectra of complexes fac-[Re(phen)(CO)$_3$]$_2$(1,3 BTB) (blue line) and fac-[Re(phen)(CO)$_3$]$_2$(2,6 BTP) (black line), Solvent: CH_2Cl_2

The complexes display typically broad and structureless emission profiles centered in the 580–600 nm region at room temperature, with maxima blue-shifted by about 15–20 nm for the phen-bound complexes (Figure 12.7). In all cases, the excited state lifetime (τ) and quantum yield (Φ) are both sensitive to the presence of dissolved O_2. Also, at 77 K, the emission profiles appear blue-shifted as a consequence of rigidochromism. Taken together, these data suggest that emission can be here ascribed mainly to phosphorescence from charge transfer states of triplet multiplicity, ^{3}CT (Table 18).

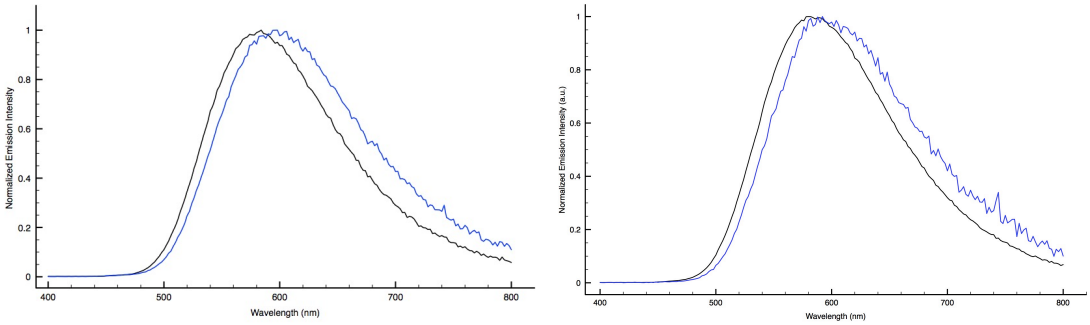

Figure 12.7: (Left) Normalized emission spectra of air equilibrated CH_2Cl_2 solutions, of the fac-[Re(bipy)(CO)$_3$(2-PTZ)] (blue trace) and fac-[Re(phen)(CO)$_3$(2-QTZ)] complexes, (black trace); (Right) Normalized emission spectra of air equilibrated CH_2Cl_2 solutions, of the -[Re(phen)(CO)$_3$]$_2$(1,3 BTB) (blue trace) and fac-[Re(bipy)(CO)$_3$]$_2$(2,6 BTP) complexes

In further support of this assignment, a bathochromic shift of the emission bands ($\Delta\lambda$max = 10–16 nm) is observed on passing from dichloromethane to more polar acetonitrile solutions (see Table 20 for data on CH_3CN), enlightening a trend that is commonly encountered when dealing with similar Re(I) complexes.[78,79]

The luminescence features of the Re(I)–Cu(I) bimetallic species [Re-(2-PTZ)-Cu]$^+$ and [Re-(2-QTZ)-Cu]$^+$ appear to be strongly influenced by the presence of the Cu(I) fragment. At room temperature, the assemblies displayed Re(I)-centered emissions with a much lower intensity than that observed under identical experimental conditions for the corresponding mononuclear Re(I) species (Table 19). In addition, following the behavior we have reported previously in the case of the Cu(I) tetrazole-based complex [(N^N)Cu(POP)]$^+$,[75] both the heterodinuclear complexes displayed bright luminescence in the solid state at room temperature, with broad and unstructured emission profiles (Figure 13.7).

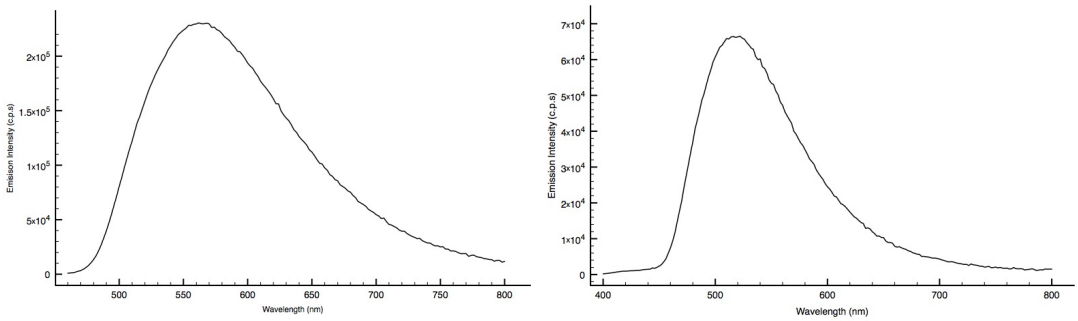

Figure 13.7: (Left) Emission spectrum of [Re-(2-QTZ)-Cu]⁺, solid state, room temperature; (Right) Emission spectrum of [Re-(2-PTZ)-Cu]⁺, solid state, room temperature

Table 19: Photophysical data for [Re-(2-QTZ)-Cu]⁺ and [Re-(2-PTZ)-Cu]⁺ (CH_2Cl_2 as the solvent)

Complex	Absorption	Emission 298K		Emission solid		Emission 77K	
	λ(10⁴ε)	λ (nm)	τ(ms)	λ(nm)	τ(ms)	λ(nm)	τ(ms)
[Re-(2-QTZ)-Cu]⁺	250(12.08), 282(6.07), 317(3.57), 338(2.13), 382(0.99)	597	n.d	562	11.99	548	/
[Re-(2-PTZ)-Cu]⁺	249(7.03), 282(5.34), 319(2.44), 352(0.85)	590	n.d	518	17.89	522	/

Effects on binding metal cations

The neutral tetrazolato complexes were screened with respect to the addition of the divalent metal ions Zn(II), Cd(II) and Cu(II). In all cases, steady state emission titrations and time-resolved analyses were performed on air equilibrated acetonitrile solutions, to which successive aliquots of the perchlorate salts of the metal ions were added.

fac-[Re(N^N)(CO)$_3$(2-PTZ)] and fac-[Re(N^N)(CO)$_3$(2-QTZ)]

Table 20: Summary of the photophysical data of the Re(I) complexes in CH_3CN before and after the addition of the CH_3CN solutions of the divalent metal ions

Complex (CH_3CN)	***Absorption***	***Emission 298K***[a,b]			
	λ_{abs} (nm) (10^4 ε) (M^{-1} cm^{-1})	λ_{em} (nm)	τ_{air} (ns)	$\Delta\lambda$ (nm)	I/I_0
***fac*-[Re(phen)(CO)$_3$(2-QTZ)]**	243 (18.38), 274 (12.85), 318 (5.22), 332 (5.52)	594	107	0	1
***fac*-[Re(phen)(CO)$_3$(2-QTZ)]+*Zn*$^{2+}$**	249 (16.49), 275 (9.03), 323 (4.14), 335 (3.81)	564	324	30	1.55
***fac*-[Re(phen)(CO)$_3$(2-QTZ)]+*Cd*$^{2+}$**	249 (19.89), 274 (11.64), 323 (5.28), 336 (4.70)	570	219	24	1.41
***fac*-[Re(phen)(CO)$_3$(2-QTZ)]+*Cu*$^{2+}$**	253 (22.66), 275 (12.62), 330 (5.73), 341 (5.36)	594	n.d	0	$4.0 * 10^{-3}$
***fac*-[Re(bipy)(CO)$_3$(2-QTZ)]**	243 (7.13), 317 (2.92), 332 (2.13)	608	104	0	1
***fac*-[Re(bipy)(CO)$_3$(2-QTZ)]+*Zn*$^{2+}$**	250 (11.17), 319 (3.88), 336 (2.53)	572	270	36	2.38
***fac*-[Re(bipy)(CO)$_3$(2-QTZ)]+*Cd*$^{2+}$**	248 (7.50), 319 (2.78), 337 (1.76)	578	135	30	2.63
***fac*-[Re(bipy)(CO)$_3$(2-QTZ)]+*Cu*$^{2+}$**	246(15.49), 276 (14.24), 330 (3.07)	608	n.d.	n.d.	0.017
***fac*-[Re(phen)(CO)$_3$(2-PTZ)]**	262 (9.21), 269 (9.39), 276 (8.81), 349 (1.11)	598	108	0	1
***fac*-[Re(phen)(CO)$_3$(2-PTZ)]+*Zn*$^{2+}$**	262 (7.38), 269 (7.93), 276 (7.99), 350 (0.90)	570	175	28	1.96
***fac*-[Re(phen)(CO)$_3$(2-PTZ)]+*Cd*$^{2+}$**	262 (8.03), 269 (8.64), 276 (8.81), 353 (0.96)	576	135	22	1.42
***fac*-[Re(phen)(CO)$_3$(2-PTZ)]+*Cu*$^{2+}$**	272 (6.68), 297 (3.75), 360 (0.68)	584	n.d	14	0.04
***fac*-[Re(bipy)(CO)$_3$(2-PTZ)]**	280 (4.22), 308 (2.95), 318 (2.79), 356 (0.56)	612	44	0	1
***fac*-[Re(bipy)(CO)$_3$(2-PTZ)]+*Zn*$^{2+}$**	280 (7.18), 308 (4.01), 318 (3.89), 356 (0.81)	582	99	30	2.38
***fac*-[Re(bipy)(CO)$_3$(2-PTZ)]+*Cd*$^{2+}$**	280 (6.58), 308 (6.37), 318 (6.61), 356 (1.89)	582	97	30	2.23
***fac*-[Re(bipy)(CO)$_3$(2-PTZ)]+*Cu*$^{2+}$**	241 (10.58), 285 (7.30), 318 (5.10), 342 (1.43)	592	n.d	0	0.033

[a]: *$\Delta\lambda$ (nm) = $|\lambda_{max}$ complex - λ_{max} complex + $M^{2+}|$;* [b]: *I/I_0 = Emission intensity at λ_{max} of the complex + M^{2+} (I) over emission intensity at λ_{max} of the free complex (I_0). Data obtained from air equilibrated CH_3CN solutions*

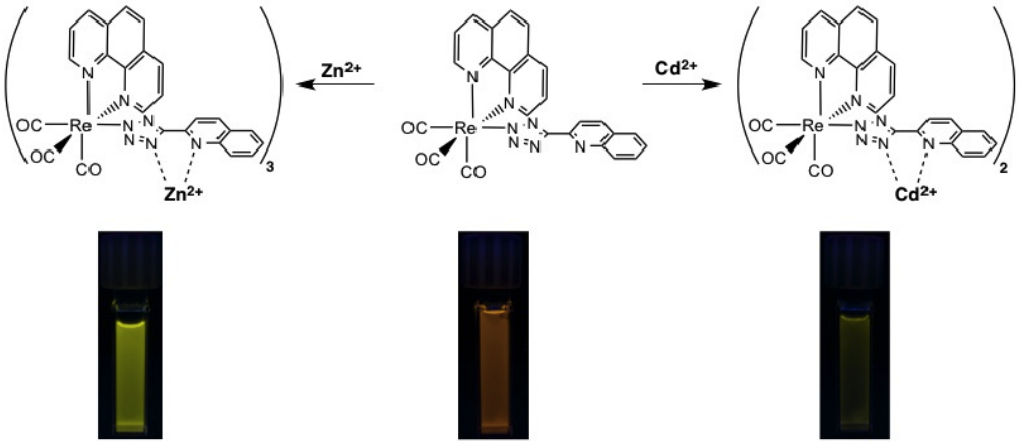

Figure 14.7: Top: complexation of fac-[Re(phen)(CO)₃(2-QTZ)] with Zn(II) (left), and Cd(II) (right). Bottom: images of the cuvettes containing the CH_2Cl_2 solutions of fac-[Re(phen)(CO)₃(2-QTZ)] (middle) and the corresponding adducts with Zn(II) (left), and Cd(II) (right). λexc = 365 nm

Upon interaction with Zn(II) and Cd(II), a significant increase of the emission intensity and a concomitant blue shift of the emission maxima of the Re(I) complexes are seen (Figures 14.7-16.7). These variations occurred to their maximum extent – *i.e.* the "equivalence point" of the titrations – in correspondence to molar ratios Re/Zn = 3/1 and Re/Cd = 2/1, respectively.

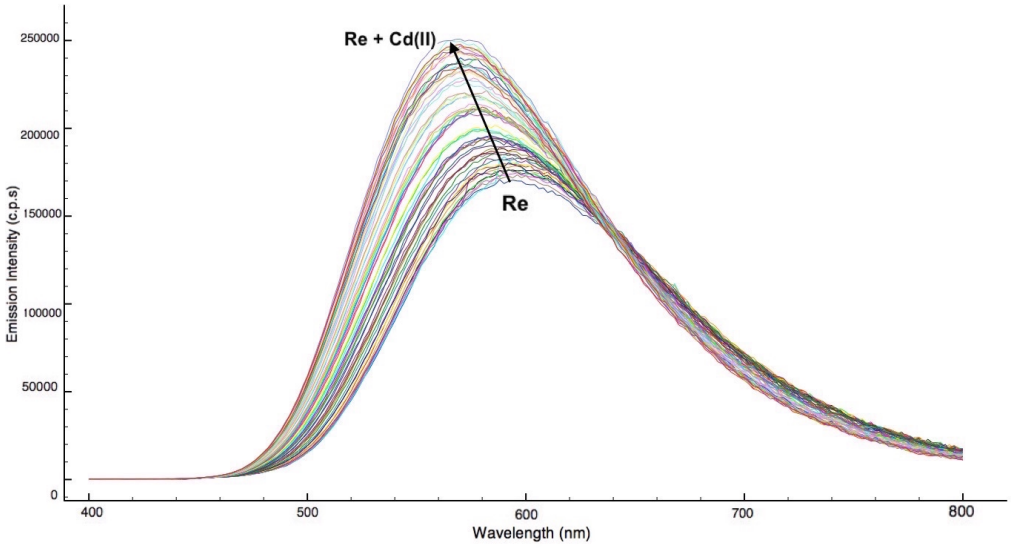

*Figure 15.7: Steady-state emission spectra showing the blue shift and the increase of emission intensity of fac-[Re(phen)(CO)₃(2-QTZ)] (1,55*10⁻⁵M in CH_3CN), denoted as "Re", upon successive additions of 10 μL aliquots of [Cd(ClO₄)₂] (2,38*10⁻³M in CH_3CN)*

From a deeper analysis of the data of steady-state spectra, it could be noticed (see Table 20) that the addition of the Zn(II) ion to the neutral Re(I) complexes

generally induced a blue shift of the emission maximum ($\Delta\lambda_{max}$ = 28–36 nm) that is very similar to the one detected following their interaction with Cd(II) ($\Delta\lambda_{max}$ = 22–30 nm). For both the divalent ions, the amplification factors of the Re(I)-based emission intensities (I/I_0, see Table 20) were found to span between 1.4 and 2.6, enlightening a trend that appears to be essentially governed by the presence of phen or bipy ancillary ligands in the structure of the Re(I) complexes, respectively.

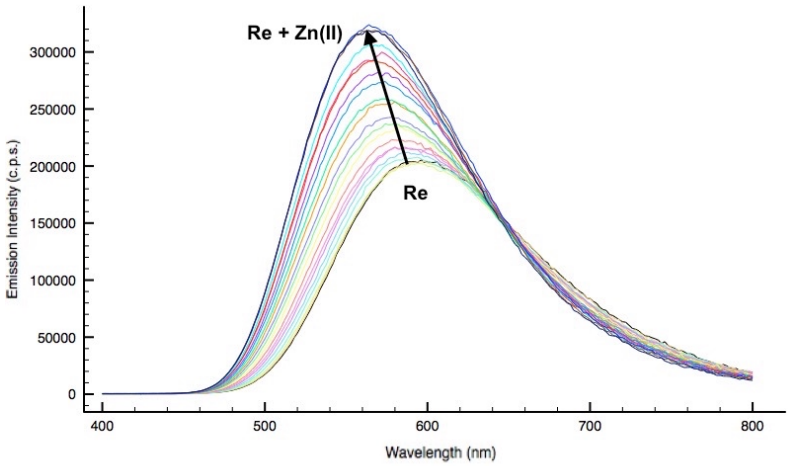

*Figure 15.7: Steady-state emission spectra showing the blue shift and the increase of emission intensity of fac-[Re(phen)(CO)$_3$(2-QTZ)] (1,55*10^{-4}M in CH$_3$CN), denoted as "Re", upon successive additions of 10 μL aliquots of [Zn(ClO$_4$)$_2$] (5,37*10^{-4}in CH$_3$CN)*

With regard to the time-resolved measurements, it is worth noting that further complexation of all the neutral Re(I) species with Zn(II) or Cd(II) resulted in ca. 1.5 to 2.5-fold elongation of the emission lifetimes (τ) (Figure 16.7).

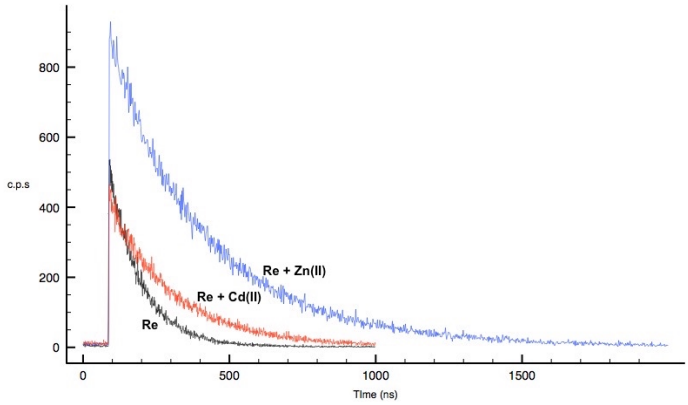

*Figure 16.7: Lifetime decays fac-[Re(phen)(CO)$_3$(2-QTZ)] (1,55*10^{-4}M in CH$_3$CN), denoted as "Re"(black line), fac-[Re(phen)(CO)$_3$(2-QTZ)]+Zn^{2+} (blue line) and fac-[Re(phen)(CO)$_3$(2-QTZ)]+ Cd^{2+}(red line)*

Overall, such an improved performance is in agreement with the energy gap law and,[80] even if occurring to an extent slightly lower than what was observed for the protonation and for the methylation of similar Re(I) tetrazolato substrates ($\Delta\lambda_{max}$ = 48 nm), it provides further evidence of the effective reduction of the contribution coming from the tetrazolato ligand in the composition of the emissive excited states, which therefore become mostly ^{3}MLCT (Re → diim) in nature.

However, the nature of the targeted metal ion played a fundamental role in determining the luminescence response of the complexes. Indeed, in contrast to what was observed for the interaction of Zn(II) or Cd(II) with the Re(I) tetrazolato complexes, the addition of the Cu(II) ion caused progressive suppression of the Re(I) based phosphorescence (Table 20, Figure 17.7).

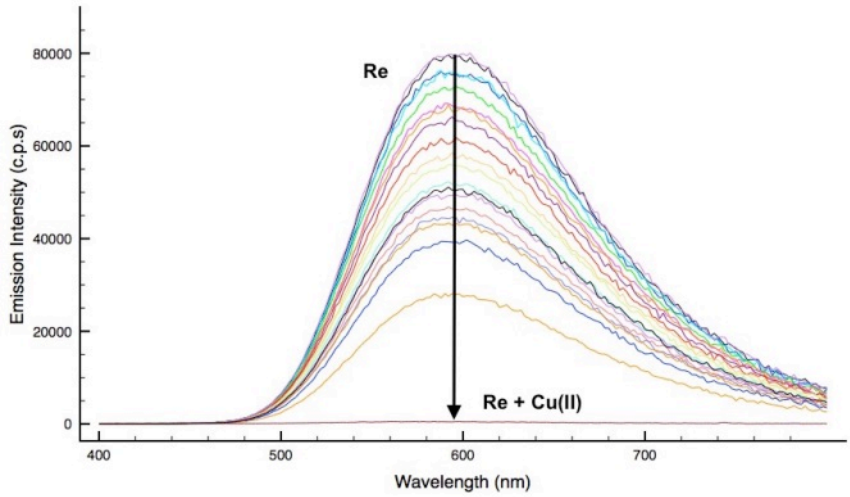

*Figure 17.7: Steady-state emission spectra showing the suppression of radiative processes of fac-[Re(phen)(CO)$_3$(2-QTZ)] (1,55*10^{-5}M in CH$_3$CN), denoted as "Re", upon successive additions of 5 μL aliquots of [Cu(ClO$_4$)$_2$] (2,69*10^{-3}M in CH$_3$CN)*

The occurrence of such a "turn- off" effect might be confidently explained taking into consideration the well-known ability of Cu(II) ions to quench emissive excited states,[81] including the intervention of Re(I)–Cu(II) energy transfer which is likely to be among the factors that govern the quenching mechanisms. The quenching of emission has been investigated by a Stern–Volmer analysis and the obtained trend (Figure 18.7) suggests that this process may be eventually described as a combination of both static and dynamic quenching.

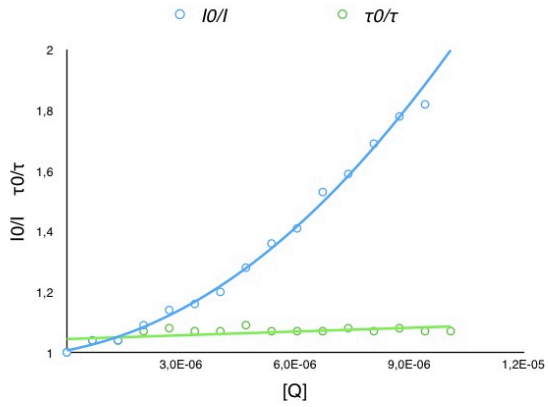

Figure 18.7: Stern Volmer Plot of fac-[Re(phen)(CO)$_3$(2-QTZ)]

fac-[Re(N^N)(CO)$_3$]$_2$(1,3 BTB) and fac-[Re(N^N)(CO)$_3$]$_2$(2,6 BTP)

The introduction of a *terpyridine-like* interaction site has been accomplished by the insertion of [1,3 BTB]$^{2-}$ and [2,6 BTP]$^{2-}$ tetrazolate anions in the design of dinuclear Re(I) complexes. As previously discussed for mononuclear Re(I) diimine complexes, the *fac*-[Re(N^N)(CO)$_3$]$_2$(L)-type complexes (L = 1,3 BTB or 2,6 BTP) have undergone emission titrations with Zn (II) and Cd (II) ions in diluted dichloromethane solutions (10^{-5} M). Upon interaction with Zn(II) and Cd(II), the dinuclear *fac*-[Re(N^N)(CO)$_3$]$_2$(2,6 BTP) complexes displayed a significant increase of the emission intensity (1.3 to 2.2-fold for (N^N) = phen and bipy, respectively) and a concomitant blue shift of the emission maxima of *c.a* 20 nm (Figure 19.7 for Zn(II) emission titration, Table 21).

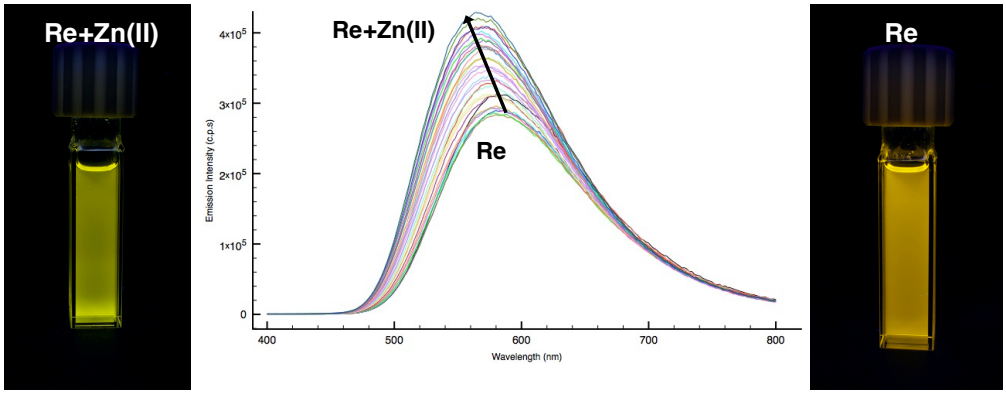

*Figure 19.7: Steady-state emission spectra showing the blue shift and the increase of emission intensity of fac-[Re(phen)(CO)$_3$]$_2$(2,6 BTP), denoted as "Re" (8,97*10^{-5}M in CH_2Cl_2), upon 30 additions of 5 µL aliquots of [Zn(ClO$_4$)$_2$] (5,37*10^{-4}in CH_3CN) – Re+Zn(II)*

Table 21: Summary of the photophysical data of the dinuclear Re(I) complexes in CH_2Cl_2 before and after the addition of the CH_3CN solutions of the divalent metal ions

Complex (CH_2Cl_2)	***Emission 298K***[a,b]			
	λ_{em} (nm)	τ_{air} (ns)	$\Delta\lambda$ (nm)	I/I_0
***fac*-[Re(phen)(CO)$_3$]$_2$(2,6 BTP)**	582	344	0	1
***fac*-[Re(phen)(CO)$_3$]$_2$(2,6 BTP) +*Zn*$^{2+}$**	566	521	16	1.32
***fac*-[Re(phen)(CO)$_3$]$_2$(2,6 BTP) +*Cd*$^{2+}$**	564	508	18	1.28
***fac*-[Re(bipy)(CO)$_3$]$_2$(2,6 BTP)**	592	98	0	1
***fac*-[Re(bipy)(CO)$_3$]$_2$(2,6 BTP)+*Zn*$^{2+}$**	572	237	20	2.18
***fac*-[Re(bipy)(CO)$_3$]$_2$(2,6 BTP)+*Cd*$^{2+}$**	570	227	22	2.27
***fac*-[Re(phen)(CO)$_3$]$_2$(1,3 BTB)**	594	270	0	1
***fac*-[Re(phen)(CO)$_3$]$_2$(1,3 BTB)+*Zn*$^{2+}$**	564	533	30	2.14
***fac*-[Re(phen)(CO)$_3$]$_2$(1,3 BTB)+*Cd*$^{2+}$**	580	346	14	1.27
fac*-[Re(bipy)(CO)$_3$]$_2$(1,3 BTB)	614	46	0	1
fac*-[Re(bipy)(CO)$_3$]$_2$(1,3 BTB) +*Zn*$^{2+}$	586	75	28	2.31
fac*-[Re(bipy)(CO)$_3$]$_2$(1,3 BTB) +*Cd*$^{2+}$	600	58	14	1.46

[a] *$\Delta\lambda$ (nm) = $|\lambda_{max}$ complex - λ_{max} complex + $M^{2+}|$;* [b] *: I/I_0 = Emission intensity at λ_{max} of the complex + M^{2+} (I) over emission intensity at λ_{max} of the free complex (I_0). *Data obtained from air equilibrated CH_3CN solutions*

The addition of Zn(II) and Cd(II) to the dinuclear *fac*-[Re(N^N)(CO)$_3$]$_2$(1,3 BTB)-type complexes produced a blue shift of the emission maximum which is more pronounced in the case of Zn(II) ions (28-30 nm, Figure 20.7 and Table 21) if compared to the variations observed upon addition of Cd(II), which caused a blue shift of 14 nm (Figure 21.7, Table 21).

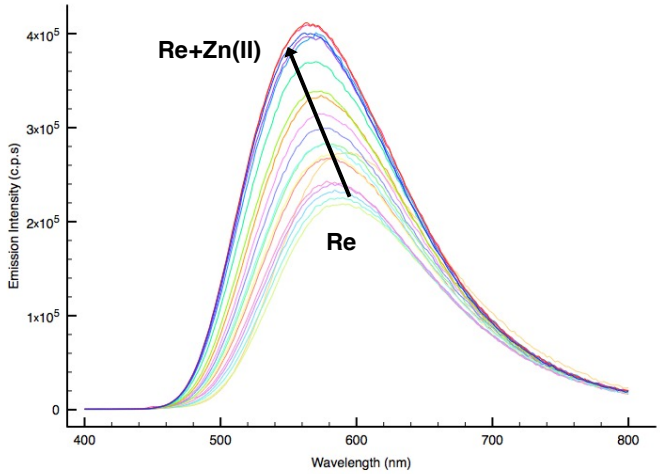

*Figure 20.7: Steady-state emission spectra showing the blue shift and the increase of emission intensity of fac-[Re(phen)(CO)$_3$]$_2$(1,3 BTB), denoted as "Re" (8,97*10^{-5}M in CH_2Cl_2), upon 19 additions of 20 μL aliquots of [Zn(ClO$_4$)$_2$] (5,37*10^{-4}in CH_3CN) – Re+Zn(II)*

In all cases, the amplification factors of the Re(I)-based emission intensities (I/I_0, see Table 21) were found to span between 1.4 and 2.3. The time-resolved measurements have revealed also for this class of dinuclear Re(I) complexes that the Zn(II) or Cd(II) complexation resulted in *ca.* 1.5 to 3-fold elongation of the emission lifetimes (Table 21).

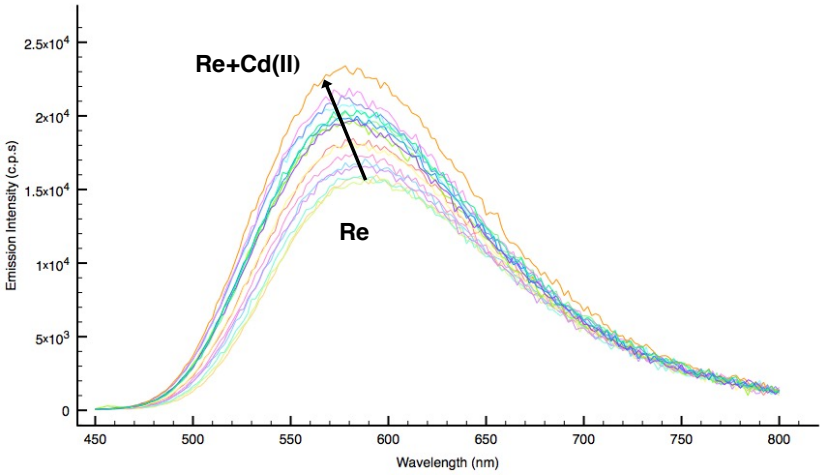

*Figure 21.7: Steady-state emission spectra showing the blue shift and the increase of emission intensity of fac-[Re(phen)(CO)$_3$]$_2$(1,3 BTB), denoted as "Re" (8,97*10^{-6}M in CH_2Cl_2), upon 20 additions of 10 µL aliquots of [Cd(ClO$_4$)$_2$] (4,77*10^{-4}in CH_3CN) – Re+Cd(II)*

Conclusions

Taking advantage of the possibility of varying the emission features of luminescent metal tetrazolato complexes upon the addition of electrophiles to the coordinated tetrazolato ring, we endeavoured to design Re(I) tetrazolato complexes capable of providing further and specific *diimine*-type or *terpy*-like coordinative interactions with some selected divalent metal cations. We pursued this goal by introducing either 2-pyridyl tetrazolato, 2-quinolyl tetrazolato or 1,3 bistetrazolylbenzene and 2,6 bisetrazolylpyridine as anionic ancillary ligands to the Re(I) complexes. These new compounds displayed orange to red colored emission originating from ^{3}CT excited states. At first, the chelating ability of the ancillary ligands toward further metal ions was verified with the preparation of discrete Re(I)– Cu(I) dyads. Equally important information was deduced from the investigation examining how the coordination of the Cu(I) moiety through the Re(I)-appended 2-PTZ$^-$ or 2-QTZ$^-$ ligand did involve a substantial variation of the luminescent features of the "free" Re(I) mononuclear derivatives. The sensing abilities of the new Re(I) complexes were investigated with respect to

their interaction with divalent metal cations of biological and toxicological importance, such as Zn(II), Cd(II) and Cu(II). By performing emission titrations, we investigated how the local perturbation of the tetrazolato ligands that was caused by their complexation with the Zn(II) or Cd(II) ions determined a blue shift of the emission profiles of the Re(I) complexes, which also caused an appreciable increase of the phosphorescence intensities and elongated emission lifetimes. It is important to note that the intrinsic nature of the added divalent ions also played a key role in determining the variation of the emission properties of the Re(I)-tetrazolato complexes described herein. Indeed, an exactly opposite trend – *i.e.* the "turn off" of the luminescence of the Re(I) complexes – was detected upon the addition of a common quencher of emissive excited states such the Cu(II) ion. The occurrence of such antithetic effects might suggest the potential of these new Re(I) tetrazolato complexes to serve as prototypal discriminatory probes. To this end and to widen the applicative scenario of these new Re(I) species, the investigation of their biological behaviour with respect to live substrates such as *Yarrowia lipolytica* yeast cells is currently underway.

Experimental Section

General considerations All the reagents and solvents were obtained commercially (e.g. Aldrich) and used as received without any further purification, unless otherwise specified. $[Cu(CH_3CN)_4][BF_4]$ was prepared according to a published procedure.[82] All the reactions were carried out under an argon atmosphere following Schlenk protocols. Where required, the purification of the Re complexes was performed via column chromatography with the use of neutral alumina as the stationary phase. ESI-mass spectra were recorded using a Waters ZQ-4000 instrument (ESI-MS, acetonitrile as the solvent). IR spectra were recorded as dichloromethane (DCM) solutions, using a NaCl (5mm) disc on a Perkin-Elmer Spectrum 2000 FT-IR spectrometer. Nuclear magnetic resonance spectra (consisting of ^{1}H, and ^{13}C experiments) were always recorded using a Varian Mercury Plus 400 instrument (^{1}H, 400.1; ^{13}C, 101.0 MHz) at room temperature. ^{1}H and ^{13}C chemical shifts were referenced to residual solvent resonances.

Photophysics. Absorption spectra were recorded at room temperature using a Perkin Elmer Lambda 35 UV/vis spectrometer. Uncorrected steady-state emission and excitation spectra were recorded on an Edinburgh FLSP920 spectrometer equipped with a 450 W xenon arc lamp, double excitation and single emission monochromators, and a Peltier-cooled Hamamatsu R928P photomultiplier tube (185–850 nm). Emission and excitation spectra were corrected for source intensity (lamp and grating) and emission spectral response (detector and grating) by a calibration curve supplied with the instrument. The wavelengths for the emission and excitation spectra were determined using the absorption maxima of the MLCT transition bands (emission spectra) and at the maxima of the emission bands (excitation spectra). Quantum yields (Φ) were determined using the optically dilute method by Crosby and Demas[41] at excitation wavelength obtained from absorption spectra on a wavelength scale [nm] and compared to the reference emitter by the following equation:[42]

$$\phi_s = \phi_r \left[\frac{A_r(\lambda_r)}{A_s(\lambda_s)}\right]\left[\frac{I_r(\lambda_r)}{I_s(\lambda_s)}\right]\left[\frac{n_s^2}{n_r^2}\right]\left[\frac{D_s}{D_r}\right]$$

where A is the absorbance at the excitation wavelength (λ), I is the intensity of the excitation light at the excitation wavelength (λ), n is the refractive index of the solvent, D is the integrated intensity of the luminescence, and Φ is the quantum yield. The subscripts r and s refer to the reference and the sample, respectively. A stock solution with an absorbance > 0.1 was prepared, then two dilutions were obtained with dilution factors of 20 and 10, resulting in absorbance's of about 0.02 and 0.08 respectively. The Lambert-Beer law was assumed to remain linear at the concentrations of the solutions. The degassed measurements were obtained after the solutions were bubbled for 10 minutes under Ar atmosphere, using a septa-sealed quartz cell. Air-equilibrated $[Ru(bpy)_3]Cl_2/H_2O$ solution (Φ = 0.028)[43] was used as reference. The quantum yield determinations were performed at identical excitation wavelengths for the sample and the reference, therefore deleting the $I(\lambda r)/I(\lambda s)$ term in the equation. Emission lifetimes (τ) were determined with the single photon counting technique (TCSPC) with the same Edinburgh FLSP920 spectrometer using pulsed picosecond LED (EPLED 360, fhwm < 800 ps) as the excitation source, with repetition rates between 1 kHz and 1 MHz, and the above-mentioned R928P PMT as detector. The goodness of fit was assessed by minimizing the reduced $\chi 2$ function and by visual inspection of the weighted residuals. To record the 77 K luminescence spectra, the samples were put in quartz tubes (2 mm diameter) and inserted in a special quartz dewar filled with liquid nitrogen. The solvent used in the preparation of the solutions for the photophysical investigations was of spectrometric grade. Experimental uncertainties are estimated to be ±8% for lifetime determinations, ±20% for quantum yields, and ±2 nm and ±5 nm for absorption and emission peaks, respectively.

Ligand synthesis

Following the general method reported by Koguro and coworkers,[21] 2-(*1H*-tetrazol-5-yl) quinoline **(2-QTZH)** was obtained in almost quantitative yield (0.769 g, 99%),[1]**H-NMR**, 400 MHz, DMSO-d^6 δ (ppm): 8.65 (d, 1H, $J_{H\text{-}H}$ = 8.79 Hz), 8.31 (d, 1H, $J_{H\text{-}H}$ = 8.40 Hz), 8.17 (d, 1H, $J_{H\text{-}H}$ = 8.40 Hz), 8.12 (d, 1H, $J_{H\text{-}H}$ = 7.99 Hz), 7.90 (t, 1H), 7.74 (t, 1H).

In a slightly different approach,[20] 2-(1H-tetrazol-5yl) pyridine **(2-PTZH), (1,3 BTB-H_2), (2,6 BTP-H_2)** were obtained in good yield (72%, 84% and 73%, respectively) by reaction of the corresponding nitrile precursor with NaN_3, in the

presence of NH_4Cl and LiCl, in DMF as solvent. **(2-PTZH)** ^{1}**H-NMR**, 400 MHz, DMSO-d^6 δ (ppm): 8.77 (d, 1H, J_{H-H} = 5.6 Hz), 8.20 (d, 1H, J_{H-H} = 8 Hz), 8.07-8.03 (m, 1H), 7.62-7.59 (m, 1H). ^{13}**C-NMR**, 100 MHz, DMSO-d^6 δ (ppm): 155.3 (Ct), 150.5, 144.1, 138.7, 126.6, 123.1; **(1,3 BTB-H$_2$)** ^{1}**H-NMR**, 400 MHz, DMSO-d^6 δ (ppm): 8.78 (m, 1H, J_{H-H} = 2.8 Hz), 8.21 (m, 1H, J_{H-H} = 9.60 Hz), 7.84 (m, 2H, J_{H-H} =15.6 Hz). **(2,6 BTP-H$_2$)** ^{1}H-NMR, 400 MHz, DMSO-d^6 δ (ppm): 8.24 – 8.22 (m, 2H), 8.16 – 8.13 (m, 1H).

General Procedure for the Preparation of the Neutral fac-[Re(N^N)(CO)$_3$L]-Type Complexes

A 0.100 g amount of *fac*-[Re(N^N)(CO)$_3$Br] (0.22 mmol for N^N = bipy; 0.13 mmol if N^N = phen) was dissolved in 20 mL of an ethanol/water mixture (3:1 v/v) under an argon atmosphere. A 5.0 mL portion of an ethanol/water (3:1 v/v) solution containing 1.5 molar equivalents of the appropriate tetrazolate salt was added drop wise. Once the addition was completed, the resulting suspension was stirred at the reflux temperature for 24 h. After this time, the mixture was cooled to r.t. and filtered through a glass frit, affording the desired complexes as a yellow microcrystalline powder. The product complexes did not require any further purification process.

***fac*-[Re(phen)(CO)$_3$(2-QTZ)]**: 0.102 g, 84%. **ESI-MS** (*m*/*z*) = 647 $[M+H]^+$. ^{1}**H-NMR** 400 MHz, Acetone-d^6 δ (ppm): 9.74 (d, 2H, J_{H-H} = 6.40 Hz), 9.01 (d, 2H, J_{H-H} = 9.60 Hz), 8.34 (s, 2H), 8.23 (m, 3H), 7.99 (d, 1H, J_{H-H} = 8.79 Hz), 7.87 (m, 2H), 7.72 (m, 1H), 7.55 (m, 1H). ^{13}**C-NMR** 100 MHz, Acetone-d^6 δ (ppm): 197.31 (CO), 195.40 (CO), 189.9 (CO), 163.55 (Ct), 154.87 (C_{ipso}), 148.93, 147.76, 146.90, 140,29, 137.22, 130.79, 130.35, 129.41, 128.29, 128.23, 127.74, 127.24, 127.15, 120.15. Crystals suitable for X-ray analysis (identified as *fac*-[Re(phen)(CO)$_3$(2-QTZ)]·0.5CH_2Cl_2, $C_{25.5}H_{15}N_7ClO_3Re$) were obtained by slow diffusion of diethyl ether into a solution of the complex in dichloromethane. Anal. Calcd. for $C_{25.5}H_{15}N_7ClO_3Re$ (689.10): C 44.44, H 2.19, N 14.23. Found: C 44.48, H 2.25, N 14.28%.

***fac*-[Re(bipy)(CO)$_3$(2-QTZ)]**: 0.076 g, 62%. **ESI-MS** (*m*/*z*) = 624 $[M+H]^+$. ^{1}**H-NMR** 400 MHz, Acetone-d^6 δ (ppm): 9.29 (m, 2H), 8.70 (d, 2H, J_{H-H} = 7.99 Hz), 8.37 (m, 2H), 8.24 (d, 1H, J_{H-H} = 8.79 Hz), 7.98 (m, 2H), 7.88 (d, 1H, J_{H-H} = 8.39 Hz), 7.85 (m, 2H), 7.13 (m, 1H), 7.53 (m, 1H). ^{13}**C-NMR** 100 MHz, DMSO-d^6 δ (ppm): 164.18 (Ct), 156.77, 154.59, 149.54, 148.32, 141.69, 137.74, 130.85, 129.95, 129.07, 128.80,

128.27, 127.64, 125.08, 120.76. Anal. Calcd. for $C_{23}H_{14}N_7O_3Re$ (622.61) C 44.37, H 2.27, N 15.75. Found: C 44.45, H 2.31, N 15.82%.

***fac*-[Re(phen)(CO)$_3$(2-PTZ)]**: 0.072 g, 91%. **ESI-MS** (*m*/*z*) = 580 $[M+H]^+$. **^{1}H-NMR** 400 MHz, DMSO-d^6 δ (ppm): 9.57 (m, 2H), 8.97 (m, 2H), 8.48 (m, 1H), 8.30 (s, 2H), 8.12 (m, 2H), 7.69 (m, 1H), 7.53 (m, 1H), 7.24 (m, 1H). **^{13}C-NMR** 100 MHz, DMSO-d^6 δ (ppm): 163.85 (Ct), 155.31, 150.34, 149.38, 147.29, 137.69, 131.24, 128.69, 127.70, 124.32, 122.35. Crystals suitable for X-ray analysis (identified as *fac*-[Re(phen)(CO)$_3$(2-PTZ)]·CH_2Cl_2, $C_{22}H_{14}N_7Cl_2O_3Re$) were obtained by slow diffusion of diethyl ether into a solution of the complex in dichloromethane. Anal. Calcd. for $C_{22}H_{14}N_7Cl_2O_3Re$ (681.50) C 38.77, H 2.07, N 14.39. Found: C 38.85, H 2.12, N 14.31%.

***fac*-[Re(bipy)(CO)$_3$(2-PTZ)]**: 0.058 g, 58%. **ESI-MS** (*m*/*z*) = 573 $[M+H]^+$. **^{1}H-NMR** 400 MHz, DMSO-d^6 δ (ppm): 9.14 (d, 2H, J_{H-H} = 4.8 Hz), 8.37 (d, 2H, J_{H-H} = 8.4 Hz), 8.33 (t, 2H), 7.76 (d, 1H, J_{H-H} = 8 Hz), 7.29 (s, 1H). **^{13}C-NMR** 100 MHz, DMSO-d^6 δ (ppm): 163.50 (Ct), 156.18, 154.05, 149.94, 148.85, 141.19, 137.38, 128.55, 124.52, 124.01, 122.04. Crystals suitable for X-ray analysis (identified as fac-[Re(CO)$_3$(bipy)(2-PTZ)], $C_{19}H_{12}N_7O_3Re$) were obtained by slow diffusion of diethyl ether into a solution of the complex in dichloromethane. Anal. Calcd. for $C_{19}H_{12}N_7O_3Re$ (572.56) C 39.86, H 2.11, N 17.12. Found: C 39.79, H 2.09, N 17.09%.

General Procedure for the Preparation of the Cu-POP fac-[Re(bipy)(CO)$_3$L]-Type Complexes

In a 100 mL Schlenk tube protected from light and under an argon atmosphere, 0.041 g of $[Cu(CH_3CN)_4][BF_4]$ (1.0 mmol, 1 equiv) were dissolved in 10 mL of dichloromethane. Once the Cu(I) salt was completely dissolved, 0.070 g (0.130 mmol, 1 equiv) of the POP diphosphine was added to the solution. The mixture was left to stir at r.t. for 2 h, after which time 5.0 mL of a dichloromethane solution containing 1 equiv. of the appropriate Re(I) complex, *fac*-[Re(**bipy**)(CO)$_3$(**2-PTZ**)] or *fac*-[Re(**bipy**)(CO)$_3$(**2-QTZ**)] was added drop wise over a period of 30 min. After two hours of stirring at r.t., the solvent was removed in vacuum until the total volume was reduced to ca. 5.0 mL.

[Re-(2-PTZ)-Cu]$^+$: 0.201 g, 76%. **ESI-MS** (*m*/*z*) = 1174 $[M]^+$. **^{1}H-NMR** 400 MHz, $CDCl_3$ δ (ppm): 8.91 (d, 2H, J_{H-H}= 5.2 Hz), 8.73 (d, 2H, J_{H-H}= 8.3 Hz), 8.13 (m, 2H), 7.78 (m, 3H), 7.40 (m, 2H), 7.28-7.12 (m, 20H), 6.96 (m, 5H), 6.58 (m, 2H), 6.49 (m,

4H). ^{13}**C-NMR** 100 MHz, $CDCl_3$ δ (ppm): 157.27 (Ct), 155.75, 151.47, 147.96, 144.85, 139.76, 137.51, 133.36, 133.10, 131.00, 130.46, 130.20, 129.39, 129.05, 128.61, 127.60, 125.77, 124.02, 123.79, 123.47, 123.14, 121.16, 119.13, 118.70. Crystals suitable for X-ray analysis (identified as *fac*-[Re(bipy)$(CO)_3$(2-PTZ)Cu(POP)][BF_4]·2Et_2O, $C_{63}H_{60}N_7O_6P_2BF_4CuRe$) were obtained by slow diffusion of diethyl ether into a solution of the complex in dichloromethane. Anal. Calcd. for $C_{63}H_{60}N_7O_6P_2BF_4CuRe$ (1409.67) C 53.68, H 4.29, N 6.95.Found: C 53.72, H 4.34, N 6.91%.

[**Re-(2-QTZ)-Cu**]$^+$:0.187 g, 85%. **ESI-MS** (*m*/*z*) = 1224 $[M]^+$. ^{1}**H-NMR** 400 MHz, $CDCl_3$ δ (ppm): 8.96 (d, 2H, $J_{H\text{-}H}$= 4.8 Hz), 8.71 (d, 2H, $J_{H\text{-}H}$= 6.8 Hz), 8.35 (d, 1H, $J_{H\text{-}H}$= 7.9 Hz), 7.88 (d, 1H, $J_{H\text{-}H}$= 8.8 Hz), 7.80 (m, 2H), 7.43-7.20 (m, 19H), 7.11 (m, 3H), 7.00 (m, 2H), 6.90 (m, 4H), 6.83 (m, 4H), 6.59 (m, 2H), 6.41 (m, 4H). ^{13}**C-NMR** 100 MHz, $CDCl_3$ δ (ppm): 158.57 (Ct), 156.54, 152.56, 145.77, 140.81, 138.80, 134.52, 134.32, 134.24, 134.15, 131.93, 131.85, 131.77, 131.52, 131.05, 130.52, 130.39, 129.76, 129.37, 128.66, 128.61, 128.20, 128.15, 128.10, 127.66, 127.51, 126.97, 124.99, 124.88, 120.07, 119.15. Crystals suitable for X-ray analysis (identified as *fac*-[Re(bipy)$(CO)_3$(2-QTZ)Cu(POP)][BF_4]·1.67CH_2Cl_2 $C_{60.67}H_{45.33}N_7O_4Cl_{3.33}P_2BF_4CuRe$ were obtained by slow diffusion of diethyl ether into a solution of the complex in dichloromethane. Anal. Calcd. for $C_{60.67}H_{45.33}N_7O_4Cl_{3.33}P_2BF_4CuRe$ (1453.03) C 50.15, H 3.14, N 6.75. Found: C 50.19, H 3.19, N 6.71%.

General Procedure for the Preparation of the Neutral fac-[Re(N^N)$(CO)_3$]$_2$(L)-Type Complexes

A 0.100 g amount of *fac*-[Re(N^N)$(CO)_3$Br] (0.22 mmol for N^N = bipy; 0.13 mmol if N^N = phen) was dissolved in 20 mL of an ethanol/water mixture (3:1 v/v) under an argon atmosphere. A 5.0 mL portion of an ethanol/water (3:1 v/v) solution containing 0.5 molar equivalents of the appropriate tetrazolate salt was added drop wise. Once the addition was completed, the resulting suspension was stirred at the reflux temperature for 24 h. After this time, the mixture was cooled to r.t. and filtered through a glass frit, affording the desired complexes as a yellow microcrystalline powder. The product complexes did not require any further purification process.

***fac*-[Re(phen)$(CO)_3$]$_2$(1,3 BTB)** 0.057 g, 55%. **ESI-MS** $[M+Na]^+$ = 1135 *m*/*z;* $[M+K]^+$ = 1153 *m*/*z*. ^{1}**H-NMR** (400 MHz, dmso-d^6) (δ) ppm: 9.56 (d, 4H, $J_{H\text{-}H}$ = 6.7 Hz), 8.96 (d, 4H, $J_{H\text{-}H}$= 9.6 Hz), 8.29 (s, 4H), 8.11 (m, 4H), 7.85 (s, 1H), 7.35 (d, 1H, $J_{H\text{-}H}$= 9.6

Hz), 7.18 (m, 1H). ^{13}C-NMR, (100 MHz, dmso d^6) (δ) ppm = 162.40 (C_{tet}), 154.77, 146.88 (C_{ipso}), 140.21, 130.73, 129.90, 128.19, 127.16, 126.02, 123.09. IR-ATR (cm^{-1}): 2022 (CO), 1889 (CO).

***fac*-[Re(phen)(CO)$_3$]$_2$(2,6 BTP)** 0.094 g, 94%. **ESI-MS** [M]+Na^+= 1136 *m/z;* [M]+K^+ = 1152 *m/z*.^{1}**H-NMR**, (400 MHz, dmso-d^6) (δ) ppm: 9.56 (d, 4H, J_{H-H}= 3.6 Hz), 8.95 (d, 4H, J_{H-H}= 9.6 Hz), 8.28 (s, 4H), 8.10 (m, 4H), 7.63 (m, 1H), 7.39 (d, 2H, J_{H-H}= 7.6 Hz). ^{13}**C-NMR**, (100 MHz, dmso d^6) (δ) ppm: 163.24 (C_{tet}), 154.84, 148.94, 146.80, 140.25, 130.75, 128.21, 127.22, 121.76. **IR-ATR** (cm^{-1}): 2023 (CO), 1897 (CO).

***fac*-[Re(bipy)(CO)$_3$]$_2$(1,3 BTB)** 0.100 g, 94%. **ESI-MS** [M]+Na^+= 1087 *m/z;* [M]+K^+ = 1105 *m/z*.^{1}**H-NMR**, (400 MHz, dmso-d^6) (δ) ppm: 9.14 (d, 4H, J_{H-H}= 5.2 Hz), 8.73 (d, 4H, J_{H-H}= 8.4 Hz), 8.32 (m, 4H), 8.08 (s, 1H), 7.75 (m, 4H), 7.55 (d, 2H, J_{H-H}= 5.9 Hz), 7.29 (t, 1H, J_{H-H}= 7.6 Hz). ^{13}**C-NMR**, (100 MHz, dmso d^6) (δ) ppm: 162.05 (C_{tet}), 155.85, 153.60, 140.71, 129.66, 128.06, 125.71, 124.06, 122.88. **IR-ATR** (cm^{-1}): 2020 (CO), 1895 (CO).

***fac*-[Re(bipy)(CO)$_3$]$_2$(2,6 BTP)** 0.103 g, 97%. **ESI-MS** [M]+Na^+= 1090 *m/z;* [M]+K^+ = 1106. ^{1}**H-NMR**, (400 MHz, dmso-d^6) (δ) ppm: 9.15 (d, 4H, J_{H-H}= 6.39 Hz), 8.72 (d, 4H, J_{H-H}= 7.99 Hz), 8.32 (m, 4H), 7.75 (m, 5H), 7.58 (d, 2H, J_{H-H}= 7.99 Hz). **IR-ATR** (cm^{-1}): 2021 (CO), 1893 (CO).

Ion-Dependent Emission Studies

In the ion-dependent emission studies, a 10 mL stock solution of ***fac*-[Re (phen)(CO)$_3$(2-QTZ)]** complex (1,55*10^{-4}M) in CH_3CN was prepared. 2 mL of the stock solution were then transferred to a quartz cuvette and the emission spectrum of the solution was measured after successive additions (10 μL aliquots for 20 additions with $Zn(ClO_4)_2$ in CH_3CN, 5,37*10^{-4}M; 10 μL aliquots for 60 additions with $Cd(ClO_4)_2$ in CH_3CN, 2,38*10^{-4}M; 5 μL aliquots for 20 additions with $Cu(ClO_4)_2$ in CH_3CN, 2,69*10^{-4}M) of the ion solution at 2 min intervals;

A 10 mL stock solution ***fac*-[Re (bipy)(CO)$_3$(2-QTZ)]** complex, a 10 mL stock solution (1,61*10^{-4}M) in CH_3CN was prepared. 2 mL of the stock solution was transferred to a quartz cuvette and the emission spectrum of the solution was

measured after successive additions (10 μL aliquots for 20 additions with $Zn(ClO_4)_2$ in CH_3CN, 5,37*10^{-4}M; 10 μL aliquots for 60 additions with $Cd(ClO_4)_2$ in CH_3CN, 2,38*10^{-4}M; 100 μL aliquots for 3 additions with $Cu(ClO_4)_2$ in CH_3CN, 2,69*10^{-4}M) of the ion solution at 2 min intervals;

A 10 mL stock solution ***fac*-[Re (phen)(CO)$_3$(2-PTZ)]** complex (1,68*10^{-4}M) in CH_3CN was prepared. 2 mL of the stock solution was transferred to a quartz cuvette and the emission spectrum of the solution was measured after successive additions (10 μL aliquots for 28 additions with $Zn(ClO_4)_2$ in CH_3CN, 5,37*10^{-4}M; 10 μL aliquots for 60 additions with $Cd(ClO_4)_2$ in CH_3CN, 2,38*10^{-4}M; 100 μL aliquots for 5 additions with $Cu(ClO_4)_2$ in CH_3CN, 2,69*10^{-4}M) of the ion solution at 2 min intervals;

A 10 mL stock solution ***fac*-[Re (bipy)(CO)$_3$(2-PTZ)]** complex (1,75*10^{-4}M) in CH_3CN was prepared. 2 mL of the stock solution was transferred to a quartz cuvette and the emission spectrum of the solution was measured after successive additions (10 μL aliquots for 23 additions with $Zn(ClO_4)_2$ in CH_3CN, 5,37*10^{-4}M; 10 μL aliquots for 50 additions with $Cd(ClO_4)_2$ in CH_3CN, 2,38*10^{-4}M; 100 μL aliquots for 6 additions with $Cu(ClO_4)_2$ in CH_3CN, 2,69*10^{-4}M) of the ion solution at 2 min intervals;

A 10 mL stock solution ***fac*-[Re(phen)(CO)$_3$]$_2$(1,3 BTB)** complex (8,97*10^{-5}M) in CH_2Cl_2 was prepared. 2 mL of the stock solution was transferred to a quartz cuvette and the emission spectrum of the solution was measured after successive additions (20 μL aliquots for 19 additions with $Zn(ClO_4)_2$ in CH_3CN, 5,37*10^{-4}M; 10 μL aliquots for 20 additions with $Cd(ClO_4)_2$ in CH_3CN, 2,38*10^{-4}M) of the ion solution at 2 min intervals.

A 10 mL stock solution ***fac*-[Re(bipy)(CO)$_3$]$_2$(1,3 BTB)** (9,37*10^{-5}M) in CH_3CN was prepared. 2 mL of the stock solution was transferred to a quartz cuvette and the emission spectrum of the solution was measured after successive additions (10 μL aliquots for 22 additions with $Zn(ClO_4)_2$ in CH_3CN, 5,37*10^{-4}M; 10 μL aliquots for 15 additions with $Cd(ClO_4)_2$ in CH_3CN, 2,38*10^{-4}M) of the ion solution at 2 min intervals;

A 10 mL stock solution ***fac*-[Re(phen)(CO)$_3$]$_2$(2,6 BTP)** complex (8,97*10^{-5}M) in CH_2Cl_2 was prepared. 2 mL of the stock solution was transferred to a quartz

cuvette and the emission spectrum of the solution was measured after successive additions (5 μL aliquots for 30 additions with $Zn(ClO_4)_2$ in CH_3CN, 5,37*10^{-4}M; 10 μL aliquots for 20 additions with $Cd(ClO_4)_2$ in CH_3CN, 2,38*10^{-4}M) of the ion solution at 2 min intervals;

A 10 mL stock solution ***fac*-[Re(bipy)(CO)$_3$]$_2$(2,6 BTP)** (9,37*10^{-5}M) in CH_2Cl_2 was prepared. 2 mL of the stock solution was transferred to a quartz cuvette and the emission spectrum of the solution was measured after successive additions (5 μL aliquots for 30 additions with $Zn(ClO_4)_2$ in CH_3CN, 5,37*10^{-4}M; 10 μL aliquots for 20 additions with $Cd(ClO_4)_2$ in CH_3CN, 2,38*10^{-4}M) of the ion solution at 2 min intervals;

X-ray crystallography

Crystal data and collection details for ***fac*-[Re(bipy)(CO)$_3$(2-PTZ)]**, ***fac*-[Re(phen)(CO)$_3$(2-PTZ)]·CH$_2$Cl$_2$**, ***fac*-[Re(phen)(CO)$_3$(2-QTZ)]·0.5CH$_2$Cl$_2$**, ***fac*-[Re(bipy)(CO)$_3$(2-PTZ)(CuPOP)][BF$_4$]·2Et$_2$O** and ***fac*-[Re(bipy)(CO)$_3$(2-QTZ)(CuPOP)][BF$_4$]·1.67CH$_2$Cl$_2$** are reported in Table S7. The diffraction experiments were carried out on a Bruker APEX II diffractometer equipped with a CCD detector and using Mo-Ka radiation. Data were corrected for Lorentz polarization and absorption effects (empirical absorption correction SADABS.[53] Structures were solved by direct methods and refined by full-matrix least-squares based on all data using F^2.[54] H-atoms were placed in calculated positions, and refined isotropically using a riding model. All non-hydrogen atoms were refined with anisotropic displacement parameters.

The asymmetric unit of the unit cell of ***fac*-[Re(phen)(CO)$_3$(2-QTZ)]·0.5CH$_2$Cl$_2$** contains two independent ***fac*-[Re(phen)(CO)$_3$(2-QTZ)]** molecules and one CH_2Cl_2 molecule.

One of the two Et_2O molecules of ***fac*-[Re(bipy)(CO)$_3$(2-PTZ)(CuPOP)][BF$_4$]·2Et$_2$O** is disordered. Thus, it has been split into two positions and refined using one occupancy parameter per disordered group. The geometries of the Et_2O molecules have been restrained to be similar (SAME line in SHELXL; s.u. 0.02) and their C-C and C-O distances restrained to 1.53 and 1.43 Å, respectively (DFIX line in SHELXL; s.u. 0.01). Similar *U* restraints (SIMU line in SHELXL; s.u. 0.01) were applied to all the C, O, F and N atoms.

The asymmetric unit of the unit cell of ***fac*-[Re(bipy)(CO)$_3$(2-QTZ)(CuPOP)][BF$_4$]·1.67CH$_2$Cl$_2$** contains three independent ***fac*-[Re(bipy)(CO)$_3$(2-QTZ)(CuPOP)]$^+$** cations, three $[BF_4]^-$ anions and five CH_2Cl_2 molecules. Some high residual electron densities remain close to the Re atoms due to absorption effects.

CCDC-1422231 (for ***fac*-[Re(bipy)(CO)$_3$2-PTZ)]**), -1422232 (for ***fac*-[Re(phen)(CO)$_3$(2-PTZ)]**), - 1422233 for (for ***fac*-[Re(phen)(CO)$_3$2-QTZ)]**), -1422234 (for **[Re-(2-PTZ)-Cu]$^+$**) -1422235 (for **[Re-(2-QTZ)-Cu]$^+$**) contain the supplementary crystallographic data for this chapter.

Table S7: Crystal data and collection details for ***fac*-[Re(bipy)(CO)$_3$(2-PTZ)]**, ***fac*-[Re(phen)(CO)$_3$(2-PTZ)]·CH$_2$Cl$_2$**, ***fac*-[Re(phen)(CO)$_3$(2-QTZ)]·0.5CH$_2$Cl$_2$**, ***fac*-[Re(bipy)(CO)$_3$(2-PTZ)(CuPOP)][BF$_4$]·2Et$_2$O** and ***fac*-[Re(bipy)(CO)$_3$(2-QTZ)(CuPOP)][BF$_4$]·1.67CH$_2$Cl$_2$**.

	***fac*-[Re(bipy)(CO)$_3$(2-PTZ)]**	***fac*-[Re(phen)(CO)$_3$(2-PTZ)]·CH$_2$Cl$_2$**	***fac*-[Re(phen)(CO)$_3$(2-QTZ)]·0.5CH$_2$Cl$_2$**
Formula	$C_{30}H_{32}N_7O_3Re$	$C_{22}H_{16}Cl_2N_7O_3Re$	$C_{25.5}H_{15}ClN_7O_3Re$
Fw	572.56	681.50	689.10
T, K	100(2)	100(2)	100(2)
λ, Å	0.71073	0.71073	0.71073
Crystal system	Triclinic	Orthorhombic	Orthorhombic
Space Group	$P\bar{1}$	*Pbca*	$P2_12_12_1$
a, Å	7.1047(9)	21.5431(8)	9.9769(7)
b, Å	8.6047(11)	9.3550(4)	21.4246(15)
c, Å	15.5783(19)	23.2990(9)	22.3643(14)
α, °	84.8870(10)	90	90
β, °	79.2250(10)	90	90
g, °	89.4700(10)	90	90
Cell Volume, Å^3	931.8(2)	4695.6(3)	4780.4(6)
Z	2	8	8
D_c, g cm^{-3}	2.041	1.928	1.915
μ, mm^{-1}	6.559	5.444	5.241
F(000)	548	2624	2664
Crystal size, mm	0.15×0.12×0.11	0.23×0.19×0.14	0.19×0.13×0.12
θ limits, °	2.38–27.00	1.75–27.10	1.32–27.00
Index ranges	-9≤ h ≤ 9 -10≤ k ≤ 10 -19≤ l ≤19	-27≤ h ≤27 -11≤ k ≤ 11 -29≤ l ≤ 29	-12≤ h ≤12 -27≤ k ≤ 27 -28≤ l ≤ 28

Reflections collected	10194	41766	61366
Independent reflections	4014 [R_{int} = 0.0339]	5146 [R_{int} = 0.0485]	10436 [R_{int} = 0.0735]
Completeness to θ max	99.0%	100.0%	100.0%
Data / restraints / parameters	4014 / 1 / 271	5146 / 0 / 316	10436 / 12 / 676
Goodness on fit on F^2	1.101	1.080	1.024
R_1 ($I > 2\sigma(I)$)	0.0314	0.0239	0.0301
wR_2 (all data)	0.0765	0.0558	0.0574
Largest diff. peak and hole, e Å^{-3}	1.936 / –0.989	1.695 / –0.945	1.404 / –1.266

	***fac*-[Re(bipy)(CO)$_3$(2-PTZ)(CuPOP)][BF$_4$]·2Et$_2$O**	***fac*-[Re(bipy)(CO)$_3$(2-QTZ)(CuPOP)][BF$_4$]·1.67CH$_2$Cl$_2$**
Formula	$C_{63}H_{60}BCuF_4N_7O_6P_2Re$	$C_{60.67}H_{45.33}BCl_{3.33}CuF_4N_7O_4P_2Re$
Fw	1409.67	1453.03
T, K	100(2)	100(2)
λ, Å	0.71073	0.71073
Crystal system	Triclinic	Triclinic
Space Group	$P\bar{1}$	$P\bar{1}$
a, Å	13.358(3)	19.7532(12)
b, Å	13.894(3)	21.2407(13)
c, Å	17.428(4)	21.6526(13)
a, °	73.596(3)	73.361(3)
β, °	89.985(3)	89.462(4)
g, °	79.009(3)	86.973(4)
Cell Volume, Å^3	3041.0(12)	8692.1(9)
Z	2	6
D_c, g cm^{-3}	1.539	1.666
μ, mm^{-1}	2.460	2.731
F(000)	1420	4332
Crystal size, mm	0.18×0.15×0.12	0.19×0.15×0.12
θ limits, °	1.56–25.03	0.98–25.03
Index ranges	-15≤ h ≤15 -16≤ k ≤ 16 -20≤ l ≤ 20	-23≤ h ≤23 -25≤ k ≤ 25 -25≤ l ≤ 25
Reflections collected	23738	125847
Independent reflections	10638 [R_{int} = 0.0564]	30668 [R_{int} = 0.1031]
Completeness to θ max	99.9%	99.8%
Data / restraints /	10638 / 434 / 762	30668 / 78 / 2053

parameters		
Goodness on fit on F^2	1.083	1.082
R_1 ($I > 2\sigma(I)$)	0.0637	0.0743
wR_2 (all data)	0.1692	0.2212
Largest diff. peak and hole, e $Å^{-3}$	3.199 / –1.572	5.318 / –2.836

Chapter 8

Heterobimetallic Ir(III) – Re(I) tetrazolate complexes

Abstract

Taking advantage of the peculiar reactivity through electrophiles displayed by Ir(III) and Re(I) tetrazolate complexes, a series of variously decorated covalently linked Ir(III)-Re(I) heterobimetallic dyads, with general formula fac-[Re(CO)$_3$(N^N)(L)(C^N)$_2$Ir]$^+$(N^N = bpy - 2,2′ bipyridine; phen - 1,10 phenantroline; C^N = ppy – phenylpyrdine; F$_2$ppy - 2,4-difuorophenylpyridine) have been synthesized and fully characterized. The resulting Ir(III)-Re(I) dyads differ in the nature of the tetrazolate bridging ligand used (L), namely [TPYZ]$^-$ (2-(1H-tetrazol-5-yl)pyridine) and [QTZ]$^-$ (2-(1H-tetrazol-5-yl)quinolone. All the reported Ir(III)-Re(I) heterobimetallic complexes displays higher PLQY (Φ) and longer decay times (τ) if compared to Ir(III) and exemplar Re(I) reference compounds, a behaviour that can be traced back to the ensuing electronic/photophysical variations introduced by the electrophilic addition reaction. Investigations concerning the eventual Ir→Re PEnT (photo induced energy transfer) are currently underway.

Introduction: Exploiting the potentialities of electrophilic addition

The chance of performing electrophilic addition on 5-aryl tetrazolate ([R-CN$_4$]$^-$) ligands has been exploited since when organometallic [CpFe$^{(II)}$(CO)(L)(N$_4$C-C$_6$H$_4$-CN)]-type complexes were at first synthesized (Cp = cyclopentadienyl anion).[22] The introduction of electrophiles such as –H$^+$ or –CH$_3^+$ at the coordinated tetrazolate ring resulted in both structural and electronic variations of Fe(II) complexes.[23] On these basis relies the development of the corresponding Ru(II) polypyridyl-tetrazolate complexes [Ru(bpy)$_2$(N^N)/(L)]$^+$ or [Ru(tpy)(bpy)(L)]$^+$,[24] (bpy = 2,2′-bypyridyl, tpy = 2,2′:6′,2″ terpyrdine, N^N or L = tetrazolate anions) which can undergo electrophilic substitution as their Fe(II) progenitor. In favour of their less thermal accessible ^{3}MC excited states, Ru(II) tetrazolate complexes were also capable of displaying weak ^{3}MLCT-based emissions. Variations upon the photoluminescent output of these Ru(II) polypyridyl has been detected as a consequence of electrophilic addition, in particular in regards of their emission maxima, which were found to be blue shifted of *c.a* 56 nm in respect of its precursors.[24] In this framework, third row transition metal compounds capable of displaying phosphorescence, *i.e* Ir(III) and Re(I) complexes, were subsequently investigated. In the first case, cyclometalated Ir(III) tetrazole –based complexes [Ir(C^N)$_2$(N^N)] (C^N = phenylpyrdine -ppy or 2,4-difuorophenylpyridine – F$_2$ppy, N^N = tetrazolate anion) were studied in respect of emission colour tuning, that has been achieved by the systematic variation of the tetrazolate moiety employed.[27, 28] In the same manner, the reactivity through electrophiles

was found to affect the photophysical output of the newly obtained cationic Ir(III) tetrazolate complexes, whose emission maxima appeared to be red shifted if compared to their neutral precursors of *c.a* 58 nm.[27, 28, 34] In its entirety, these results confirmed the essential role played by the tetrazolate ligands in determining the photoluminescent output of the corresponding Ir(III) metal complexes. On the other side, the coordination of tetrazolate anions to *fac*-[Re(CO)$_3$(N^N)(solv)]$^+$-type complexes, (where N^N = bpy, phen), produced a new class of phosphorescent neutral compounds which displayed a photoluminescent output congruent with previously reported Re(I) triscabonyl complexes.[45b] The emission properties of such neutral derivatives appeared to be strongly influenced by the nature of the tetrazolate anion coordinated to the metal centre. As previously discussed for Fe(II), Ru(II) ad Ir(III) tetrazolate systems,[24,27,28,34] also neutral *fac*-[Re(N^N)(CO)$_3$(L)] tetrazolate complexes may undergo electrophilic substitutions both in reversible or irreversible modalities. The ensuing structural and electronic modifications clearly affected the photoluminescent output of the resulting cationic Re(I) tetrazolate complexes, whose emission maxima appeared to be blue shifted if compared to those recorded from their neutral precursors.[30, 45b] In all the cases, a concomitant elongation of decay times, together with higher quantum yield values were detected in switching from neutral to cationic Re(I) tetrazolate complexes.

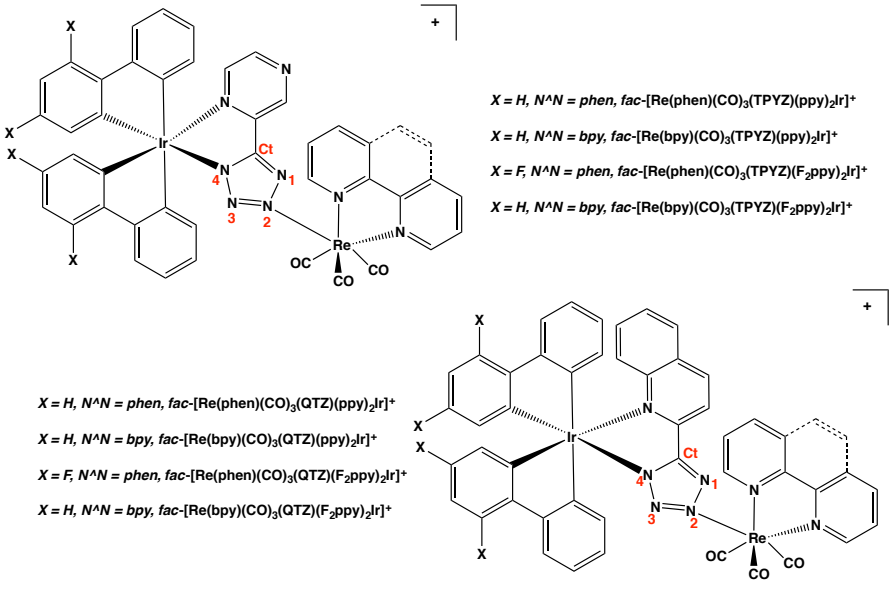

Figure 1.8: Structure, acronyms and [R-CN$_n$] numeration used for Ir(III)-Re(I) dyads

Recently, we have extended the scenario of luminescent ion pairs with the very first examples of "Fully Ir(III) tetrazolate soft salts",[34] a class of saline compounds in which two oppositively charged Ir(III) tetrazolate complexes

coexist as photophysical independent entities, returning an emission behaviour that corresponds to the rough sum of both anionic and cationic counterparts.

In the light of the above, the chance of performing electrophilic addition has been exploited to set up a series of Ir(III)-Re(I) heterobimetallic dyads (Figure 1.8) in which two different metal fragments are now covalently linked through various tetrazolate ligands, namely the deprotonated form of [H-TPYZ] (2-(1H-tetrazol-5-yl)pyrazine) and [H-QTZ] (2-(1*H*-tetrazol-5-yl)quinoline). The newly obtained Ir(III)-Re(I) cationic dyads, with general formulae *fac*-$[Re(CO)_3(N^N)(L)(C^N)_2Ir]^+$ (N^N = bpy, phen, C^N = ppy, F_2ppy, L = tetrazolate ligands), were studied in respect of their photoluminescent output, looking towards the effects produced by the addition of a cationic luminescent metal Re(I) fragment (*i.e*, the electrophile) to an neutral Ir(III) tetrazolate complex.

Results and discussion

Synthesis and spectroscopic characterization

By following the Koguro method[21], which involved the 1,3 dipolar cyclization reaction of the azide anion (N_3^-) with the corresponding nitrile precursors, the tetrazole ligands [H-QTZ] and [H-TPYZ] have been obtained in almost quantitative yields. The cationic Ir(III)-Re(I) dyads have been prepared by following a two step procedure which involve (i) the halide extraction of *fac*-[Re(*diim*)(CO)$_3$Br] (diim = bpy, phen) and the subsequent (ii) reaction of the resulting cationic [Re(*diim*)(CO)$_3$-(CH$_3$)$_2$CO]$^+$ with the appropriate neutral [Ir(C^N)(N^N)] tetrazolate complex (C^N = ppy, F$_2$ppy), in refluxing acetone for 24h. The cationic Ir(III)-Re(I) complexes were obtained as orange-yellowish precipitates as hexafluorophosphate salts, requiring no further purifications. (Figure 2.8).

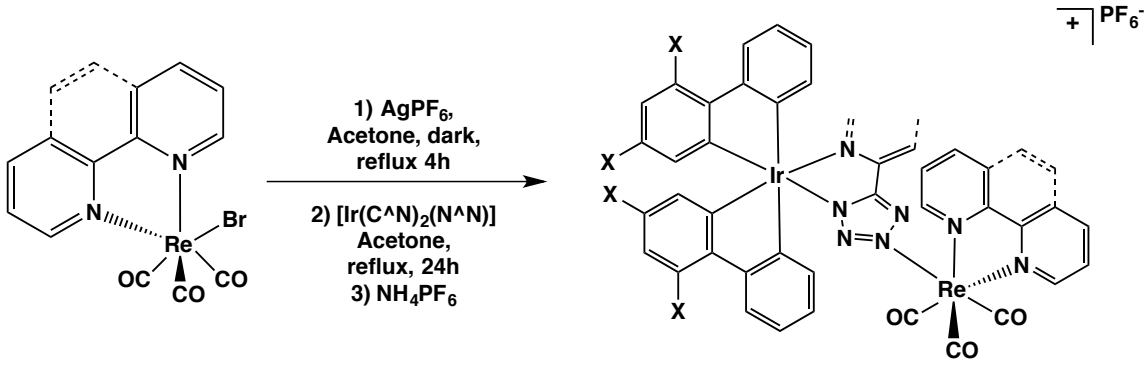

Figure 2.8: Synthetic procedure used for Ir(III)-Re(I) tetrazolate dyads

The neutral [Re(N^N)(CO)$_3$QTZ] and [Re(N^N)(CO)$_3$TPYZ], were synthesized according to a previously reported procedure[45a] and used as reference compounds in both spectroscopic and photophysical measurements.

Infrared (IR) spectroscopy from dichloromethane solutions provided results congruent with the formation of cationic species, with totally symmetric in-phase stretchings A′(1), (2034-2036 cm^{-1}) and broader bands at ca. 1931 cm^{-1}, which results from the superimposition of the totally symmetric out-of-phase stretching A′(2) and the asymmetric stretching A″. To confirm, these values were found at higher wavenumber in respect of those recorded from neutral Re(I) reference compounds (A′(1) = 2028-2030, A′(2) - A″ = 1923 cm^{-1}, Table 22).

Table 22: CO stretching values for Ir(III)-Re(I) complexes and Re(I) neutral complexes CH_2Cl_2 as the solvent

Complex	CO A'(1)	CO A'(2)/A''
fac-[Re(phen)(CO)$_3$(QTZ)]	2030	1923
fac-[Re(bpy)(CO)$_3$(QTZ)]	2028	1923
fac-[Re(phen)(CO)$_3$(TPYZ)]	2029	1923
fac-[Re(bpy)(CO)$_3$(TPYZ)]	2029	1923
fac-[Re(phen)(CO)$_3$(QTZ)(ppy)$_2$Ir]$^+$	2035	1931
fac-[Re(bpy)(CO)$_3$(QTZ)(ppy)$_2$Ir]$^+$	2034	1931
fac-[Re(phen)(CO)$_3$(QTZ)(F$_2$ppy)$_2$Ir]$^+$	2036	1932
fac-[Re(bpy)(CO)$_3$(QTZ)(F$_2$ppy)$_2$Ir]$^+$	2035	1932
fac-[Re(phen)(CO)$_3$(TPYZ)(ppy)$_2$Ir]$^+$	2035	1931
fac-[Re(bpy)(CO)$_3$(TPYZ)(ppy)$_2$Ir]$^+$	2034	1931
fac-[Re(phen)(CO)$_3$(TPYZ)(F$_2$ppy)$_2$Ir]$^+$	2036	1932
fac-[Re(bpy)(CO)$_3$(TPYZ)(F$_2$ppy)$_2$Ir]$^+$	2035	1932

The formation of the cationic Ir(III)-Re(I) complexes has been confirmed also by ESI-MS spectrometry, which provided the expected $[M]^+$ signals in the positive region ions (Figure 3.8 for *fac*-[Re(phen)(CO)$_3$(TPYZ)(ppy)$_2$Ir]$^+$), with isotopic patterns congruent with the presence of both Ir(III) and Re(I) metal centres. The signal of $[PF_6]^-$ counterion was found in the negative region ions at m/z = 145.

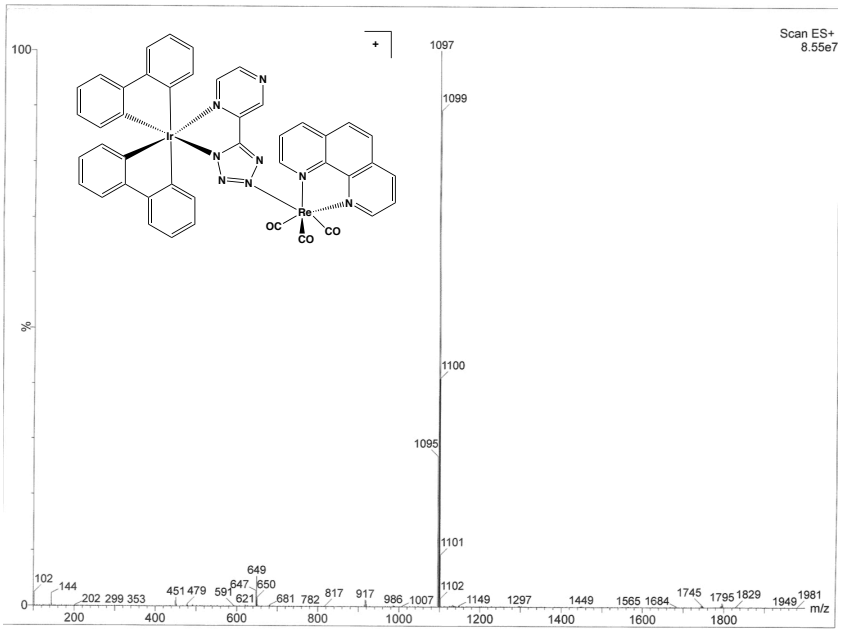

Figure 3.8: ESI-MS spectra of fac-[Re(phen)(CO)$_3$(TPYZ)(ppy)$_2$Ir]$^+$, $[M]^+$ = 1097 m/z, CH_3CN as the solvent

Useful informations regarding both symmetry and coordination modes adopted by the Ir(III) and Re(I) metal fragments in Ir(III)-Re(I) dyads has been discerned by NMR experiments.

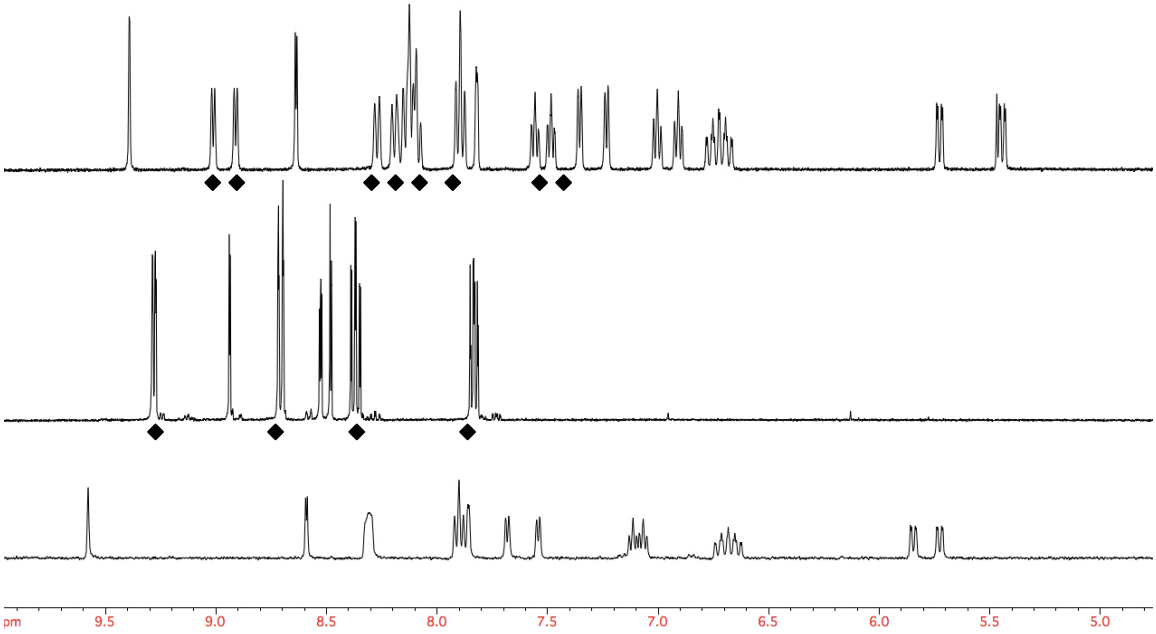

Figure 4.8: ^{1}H-NMR Stacking plot of (top): fac-[Re(bpy)(CO)$_3$(TPYZ)(F$_2$ppy)Ir]$^+$; (middle) fac-[Re(bpy)(CO)$_3$(TPYZ)]; (bottom) [Ir(F$_2$ppy)$_2$(TPYZ)], CD$_3$CN, 400 MHz, 298K

All the protonic resonances from the dinculear tetrazolate dyads were found in the aromatic region (10-5 ppm), as was observed for both neutral Re(I) reference compounds and mononuclear Ir(III) tetrazolate complexes in the same experimental conditions. It's worth noting the lack of symmetry of the diiminic ligand in passing from mononuclear Re(I) complex to the heterobimetallic dyad (◆ in Figure 4.8), resulting in a number of resonances equal to the total protons displayed by the molecule.

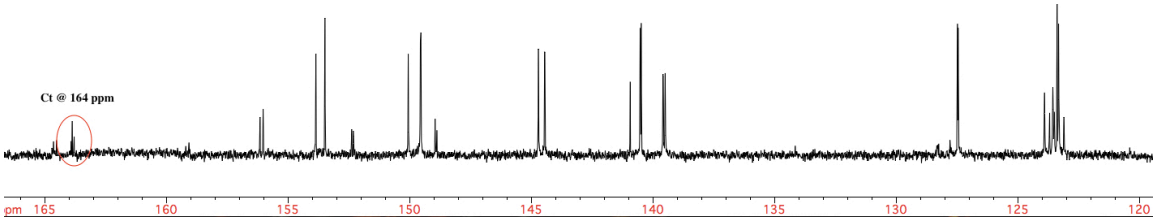

Figure 5.8: ^{13}C-NMR of fac-[Re(bpy)(CO)$_3$(TPYZ)(F$_2$ppy)$_2$Ir]$^+$, 100 MHz, CD$_3$CN

By the means of ^{13}C-NMR experiments was possible to claim that in all the cases, the Re(I) metal fragment is covalently linked to the Ir(III) unit through the N2 atom of the [R-CN$_4$]$^-$ group, as witnessed by the Ct chemical shift, that has been found at ca. 164 ppm (Figure 5.8, Figure 1.8 for labelling).

Crystal Structures

The structures of *fac*-[Re(bipy)(CO)$_3$(TPYZ)] and *fac*-[Re(phen)(CO)$_3$(QTZ)] reference compounds have been determined by single crystal X-ray diffraction studies (Figure 6.8). Their structures and bonding parameters coincide with previously reported *fac*-[Re(diim)(CO)$_3$(L)] complexes (diim = bipy, phen; L = tetrazolate ligands).

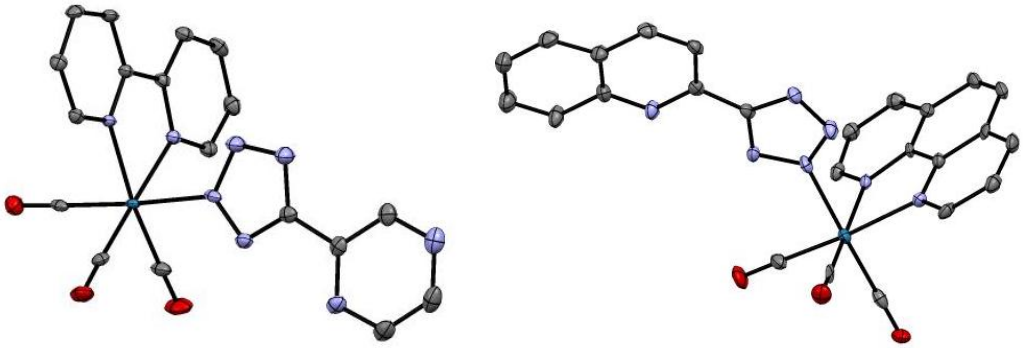

Figure 6.8: (left) Molecular structure of fac-[Re(bipy)(CO)$_3$(TPYZ)] and (right) fac-[Re(phen)(CO)$_3$(QTZ)]

Thus, the Re centres display an octahedral geometry being coordinated to three CO ligands in a *facial* arrangement, a *cis*-chelating diimine ligand (bipy or phen) and a substituted tetrazolate ring bonded to the metal through its N2 atom.
In the same manner, single crystals suitable for X-ray diffraction have been obtained from [Ir(ppy)$_2$QTZ] and [Ir(ppy)$_2$(TPYZ)] DCM/Et$_2$O solutions (Figure 7.8). In all the cases, the Ir(III) centre adopts a distorted octahedral coordination geometry with *cis*-metalated carbons and *trans*-phenylpyridine nitrogen atoms.

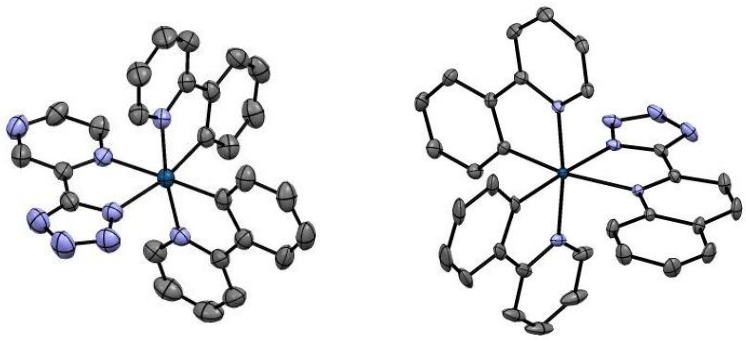

Figure 7.8: (left) Molecular structure of [Ir(ppy)$_2$(TPYZ)] and (right) [Ir(ppy)$_2$(QTZ)]

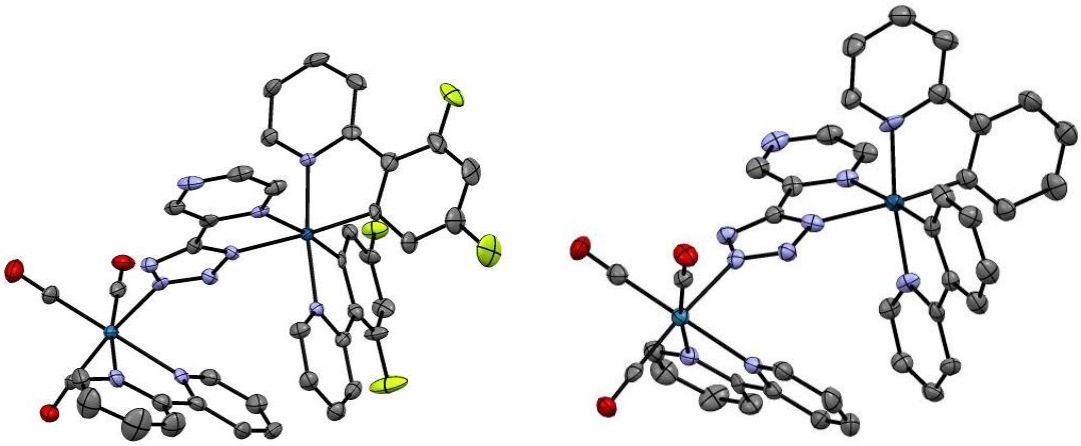

Figure 9.8: (left) Molecular structure of fac-[Re(bpy)(CO)$_3$(TPYZ)(F$_2$ppy)$_2$Ir]$^+$ and (right) fac-[Re(bpy)(CO)$_3$(TPYZ)(ppy)$_2$Ir]$^+$

The molecular structures of *fac*-[Re(bpy)(CO)$_3$(TPYZ)(F$_2$ppy)$_2$Ir]$^+$ and *fac*-[Re(bpy)(CO)$_3$(TPYZ)(ppy)$_2$Ir]$^+$ were obtained by slow diffusion of diethyl ether into a solution of the complex in dichloromethane. As witnessed by IR measurements and NMR experiments, the *facial* disposition of CO ligands, the expected N2 linkage of the Re(I) metal fragment, the usual mutual *trans* disposition of the phenylpyridinic nitrogens as well as the *cis* arrangement of the metalated carbon have been observed in Ir(III)-Re(I) tetrazolate dyads (Figure 9.8).

Photophysical properties

UV/Vis absorption and photophysical properties of the mononuclear complexes

The UV/Vis absorption spectrum of both [Ir(ppy)$_2$(TPYZ)] and [Ir(ppy)$_2$(QTZ)] and their associated steady-state luminescence spectrum, are shown in figure 10.8 (see also Table 23); these are representative of all mononuclear Ir(III) complexes from this family.

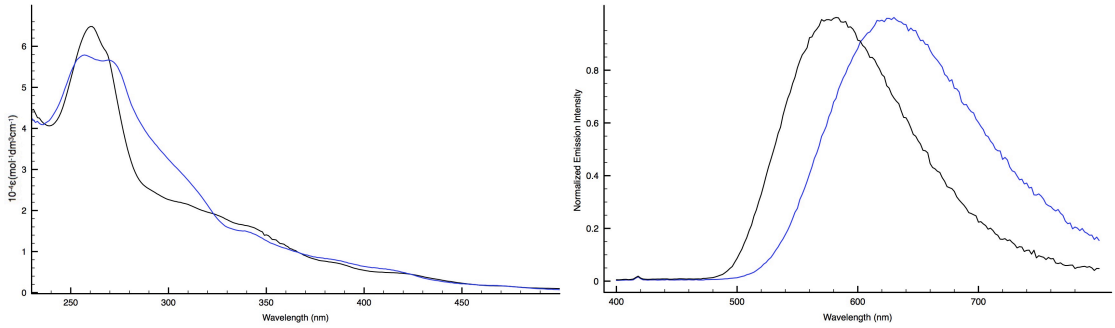

Figure 10.8: (Left) Absorption profiles of [Ir(ppy)$_2$(TPYZ)] (blue line) and [Ir(ppy)$_2$(QTZ)] (black line), 10^{-5}M, CH$_2$Cl$_2$; (right) Normalized Emission profiles of [Ir(ppy)$_2$(TPYZ)] (blue line) and [Ir(ppy)$_2$(QTZ)] (black line), 10^{-5}M, CH$_2$Cl$_2$, 298K

In detail, the UV region (250 – 350 nm) displays intense ligand centred spin allowed (^{1}LC) absorptions followed, at lower energy (350 – 500 nm), by weaker charge transfer (CT) bands consisting of spin allowed metal to ligand charge transfer (^{1}MLCT) type transitions responsible for the luminescence. The luminescence spectrum (Figure 10.8) is likewise typical, and shows the characteristic emission in the red region of the spectrum, with emission peak at 628 nm for [Ir(ppy)$_2$(TPYZ)] and 584 nm for [Ir(ppy)$_2$(QTZ)]; the broad, unstructured emission profiles are characteristic of an excited state with substantial ^{3}MLCT character based on Ir(III)→TPYZ/QTZ charge transfer. In degassed CH_2Cl_2 at room temperature these show lifetimes of around 0.15 and 0.85 μs, respectively (Table 23), which is reduced in air-equilibrated solution.

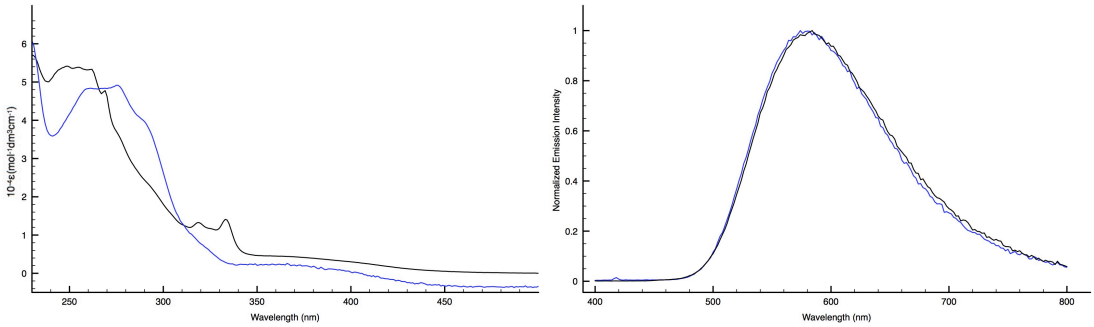

Figure 11.8: (Left) Absorption profile of fac-[Re(phen)(CO)$_3$(TPYZ)] (blue line) and fac-[Re(phen)(CO)$_3$(QTZ)] (black line), 10^{-5}M, CH_2Cl_2; (right) Normalized emission profile of fac-[Re(phen)(CO)$_3$(TPYZ)] (blue line) and fac-[Re(phen)(CO)$_3$(QTZ)] (black line), 10^{-5}M, CH_2Cl_2, 298K

For the *fac*-[Re(N^N)(CO)$_3$(TPYZ)] and *fac*-[Re(N^N)(CO)$_3$(QTZ)] reference compounds the ^{3}MLCT absorption occurs at 350 nm. The resulting luminescence – a characteristically broad, featureless signal – is comparable in energy with the mononuclear Ir(III) complexes, with emission maxima at 580 nm and a lifetime in degassed CH_2Cl_2 of 0.34 – 0.37 μs (Figure 11.8, Table 23).

Like all the Ir(III) tetrazolate complexes, this luminescence is strongly rigidochromic – a characteristic of the predominantly charge-transfer nature of the excited state – undergoing blue shifting to ca. 520 nm in a frozen solution at 77 K (Table 23).

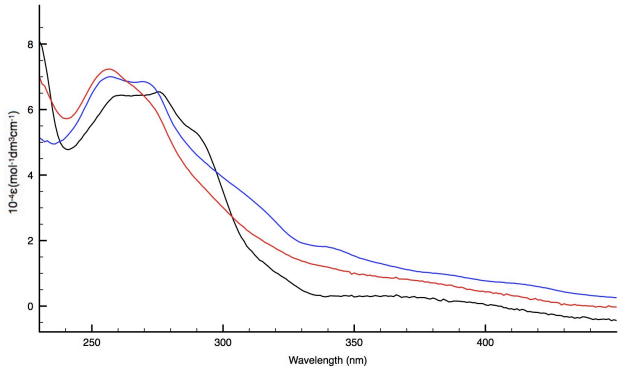

Figure 12.8: Absorption profiles of fac-[Re(phen)(CO)$_3$(TPYZ)(ppy)$_2$Ir]$^+$ (red line), fac-[Re(phen)(CO)$_3$(TPYZ)] (black line) and [Ir (ppy)$_2$(TPYZ)] (blue line), 10^{-5}M, CH$_2$Cl$_2$

As depicted in figure 12.8 for the exemplar dinuclear *fac*-[Re(phen)(CO)$_3$(TPYZ)(ppy)$_2$Ir]$^+$ and its mononuclear Ir(III) and Re(I) metal fragments, all the complexes displays closely related absorption profiles. In detail, the UV region (250 – 350 nm) displays intense ligand centred spin allowed (^{1}LC) absorptions followed, at lower energy (350 – 500 nm), by weaker charge transfer (CT) bands consisting of spin allowed metal to ligand charge transfer (^{1}MLCT) type transitions. It will be clear that overlap of the absorption spectra of the Ir(III) and Re(I) units means that selective excitation of one chromophore is not possible. All the Ir(III)-Re(I) dyads display typically broad and structureless emission profiles centred in the 580–600 nm region at room temperature (Figure 13.8 for the exemplar *fac*-[Re(phen)(CO)$_3$(TPYZ)(F$_2$ppy)$_2$Ir]$^+$). In all cases, the excited state lifetime (τ) and quantum yield (Φ) are both sensitive to the presence of dissolved O_2. Also, at 77 K, the emission profiles appear blue-shifted as a consequence of rigidochromism. Taken together, these data suggest that emission can be here ascribed mainly to phosphorescence from charge transfer states of triplet multiplicity, ^{3}CT (Table 23).

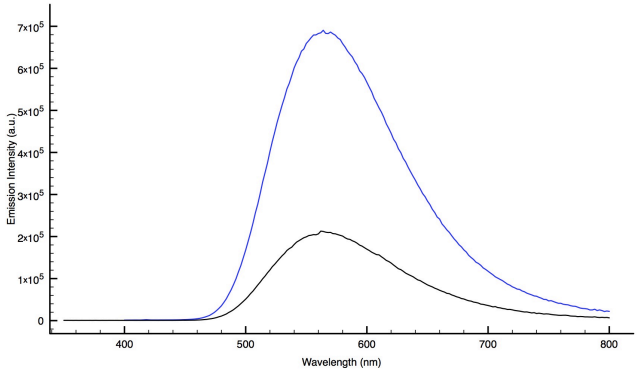

Figure 13.8: Emission profile of fac-[Re(phen)(CO)$_3$(TPYZ)(F$_2$ppy)$_2$Ir]$^+$, air equilibrated (black line) and deoxygenated solution, 10^{-5}M, CH$_2$Cl$_2$, 298K

Table 23: Photophysical data of Ir(III)-Re(I) dyads and Ir(III) and Re(I) mononuclear compounds

Complex	**Abs**	**Emission 298 K**					**Emission 77K**	
CH_2Cl_2 as the solvent	**λ(nm) ε($mol^{-1}dm^3cm^{-1}$)**	**λ_{max} (nm)**	**τ_{ox} (μs)**	**τ_{deox} (μs)**	**ϕ_{ox} (%)**	**ϕ_{deox} (%)**	**λ_{max} (nm)**	**τ (μs)**
fac-[Re(phen)(CO)$_3$(QTZ)(ppy)$_2$Ir]$^+$	251 (0.81) 341 (0.14) 379 (0.08)	600	0.48	1.32	6.8	36.95	556	3.90
fac-[Re(bpy)(CO)$_3$(QTZ)(ppy)$_2$Ir]$^+$	253 (0.43) 314 (0.15) 365 (0.04)	598	0.29	0.99	5.28	24.12	548	3.42
fac-[Re(phen)(CO)$_3$(QTZ)(F$_2$ppy)$_2$Ir]$^+$	256(5.29) 319 (1.49) 357 (1.02)	520 548	1	5.24	5.23	54.40	500 538 582 630	21
fac-[Re(bpy)(CO)$_3$(QTZ)(F$_2$ppy)$_2$Ir]$^+$	252 (5.84) 319 (1.73) 357 (1.07)	518 550 606	1.01	3.40	6.88	36.61	504 542 586 636	17.16
fac-[Re(phen)(CO)$_3$(TPYZ)(ppy)$_2$Ir]$^+$	256 (7.23) 274 (6.02) 300 (3.00) 366 (0.87)	646	0.15	0.26	7.66	10.88	584	3.13
fac-[Re(bpy)(CO)$_3$(TPYZ)(ppy)$_2$Ir]$^+$	247 (5.04) 292 (3.53) 319 (1.98) 364 (0.88)	646	0.16	0.25	3.62	6.84	574	5.83
fac-[Re(phen)(CO)$_3$(TPYZ)(F$_2$ppy)$_2$Ir]$^+$	273 (9.57) 351 (0.61)	568	0.53	1.39	25.3	82.3	540	7.4
fac-[Re(bpy)(CO)$_3$(TPYZ)(F$_2$ppy)$_2$Ir]$^+$	269 (5.86) 320 (1.38) 361 (0.56)	566	0.41	1.11	17.6	51.1	522	5.05
[Ir(ppy)$_2$(QTZ)]	260 (6.48) 340 (1.62) 385 (0.72)	584	0.19	0.85	5.70	26.74	556	3.29
[Ir(F$_2$ppy)$_2$(QTZ)]	258 (6.49) 316 (2.40) 352 (1.55)	542	0.44	1	2.48	11.67	502 538 578	8.18
[Ir(ppy)$_2$(TPYZ)]	258 (5.81) 340 (1.53) 410 (0.58)	628	0.15	0.16	3.59	5.54	560	5.89
[Ir(F$_2$ppy)$_2$(TPYZ)]	247 (5.75) 308 (2.60) 366 (0.97)	556	0.29	0.95	19.9	81.3	502	5.69
fac-[Re(bpy)(CO)$_3$(QTZ)]	280 (9.62) 338 (0.78) 422 (0.21)	596	0.10	0.12	1.2	7.9	528	2.7 (48) 5.6 (52)
fac-[Re(phen)(CO)$_3$(QTZ)]	255 (9.54) 319 (2.30) 370 (0.76)	580	0.34	0.94	6.15	18.8	520	6.81
fac-[Re(phen)(CO)$_3$(TPYZ)]	258 (4.79) 276 (4.91) 292 (3.80) 370 (0.21)	580	0.37	0.91	2.49	8.23	518	7.29
fac-[Re(bpy)(CO)$_3$(TPYZ)]	293 (3.16) 316 (2.25) 370 (0.39)	592	0.12	0.15	4.51	7.51	528	3.44

fac-[Re(N^N)(CO)$_3$(L)(ppy)$_2$Ir]$^+$-type dyads

The electrophilic substitution reaction performed on [Ir(ppy)$_2$(L)]-type complexes (L = TPYZ, QTZ) with a cationic [Re(N^N)(CO)$_3$-(CH$_3$)$_2$CO]$^+$ fragment (N^N = phen, bpy) resulted in a series of cationic *fac*-[Re(N^N)(CO)$_3$(L)(ppy)$_2$Ir]$^+$ dyads, whose photophysical details are listed in Table 24.

Table 24: Photophysical data of fac-[Re(N^N)(CO)$_3$(L)(ppy)$_2$Ir]$^+$-type dyads

Complex	**Abs**	**Emission 298 K**					**Emission 77K**	
CH_2Cl_2 as the solvent	**λ(nm) ε(mol^{-1}dm^{3}cm^{-1})**	**λ_{max} (nm)**	**τ_{ox} (μs)**	**τ_{deox} (μs)**	**ϕ_{ox} (%)**	**ϕ_{deox} (%)**	**λ_{max} (nm)**	**τ (μs)**
fac-[Re(phen)(CO)$_3$(QTZ)(ppy)$_2$Ir]$^+$	251 (0.81) 341 (0.14) 379 (0.08)	600	0.48	1.32	6.8	36.95	556	3.90
fac-[Re(bpy)(CO)$_3$(QTZ)(ppy)$_2$Ir]$^+$	253 (0.43) 314 (0.15) 365 (0.04)	598	0.29	0.99	5.28	24.12	548	3.42
fac-[Re(phen)(CO)$_3$(TPYZ)(ppy)$_2$Ir]$^+$	256 (7.23) 274 (6.02) 300 (3.00) 366 (0.87)	646	0.15	0.26	7.66	10.88	584	3.13
fac-[Re(bpy)(CO)$_3$(TPYZ)(ppy)$_2$Ir]$^+$	247 (5.04) 292 (3.53) 319 (1.98) 364 (0.88)	646	0.16	0.25	3.62	6.84	574	5.83

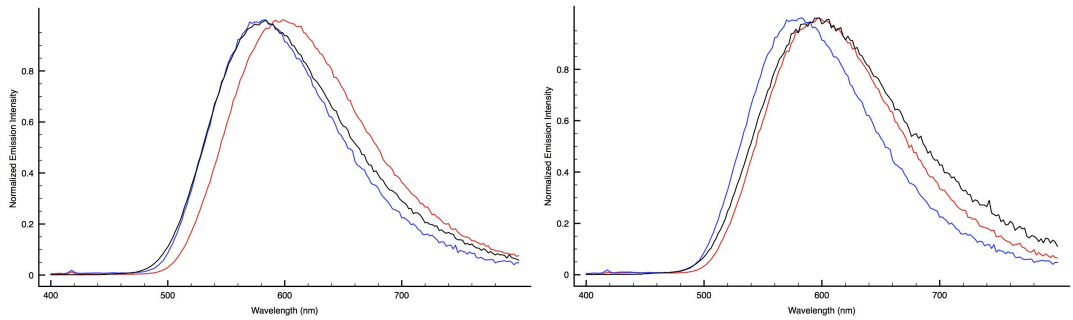

Figure 14.8: (left) Normalized Emission profiles of fac-[Re(phen)(CO)$_3$(QTZ)(ppy)$_2$Ir]$^+$ (red line), Ir(III) mononuclear complex (blue line) and Re(I) reference compound (black line); (left): Normalized Emission profiles of fac-[Re(bpy)(CO)$_3$(QTZ)(ppy)$_2$Ir]$^+$ (red line), Ir(III) mononuclear complex (blue line) and Re(I) reference compound (black line)

In all the cases, the addition of a [Re(N^N)(CO)$_3$- (CH$_3$)$_2$CO]$^+$-type electrophile to the neutral [Ir(ppy)$_2$(QTZ)] and [Ir(ppy)$_2$(TPYZ)] complexes produced a red shift of the emission maxima of the resulting *fac*-[Re(N^N)(CO)$_3$(L)(ppy)$_2$Ir]$^+$ dyads in respect of the observed λ_{emi} of the Ir(III) precursors (Figures 14.8 and 15.8). This behaviour can be traced back to the addition of a methyl group to neutral Ir(III)

tetrazolate complexes, even if its effects in terms of displacement of the emission maxima are now less pronounced.

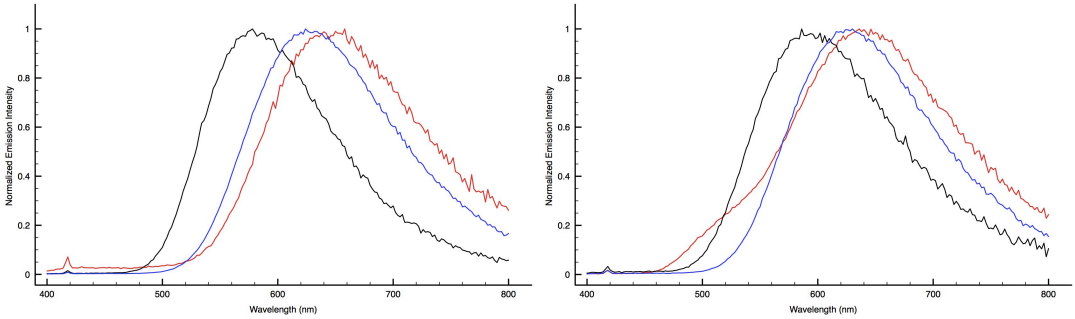

Figure 15.8: (left) Normalized Emission profiles of fac-[Re(phen)(CO)$_3$(TPYZ)(ppy)$_2$Ir]$^+$ (red line), Ir(III) mononuclear complex (blue line) and Re(I) reference compound (black line); (left): Normalized Emission profiles of fac-[Re(bpy)(CO)$_3$(TPYZ)(ppy)$_2$Ir]$^+$ (red line), Ir(III) mononuclear complex (blue line) and Re(I) reference compound (black line)

Its worth noting that quantum yield values and emission lifetimes of the *fac*-[Re(N^N)(CO)$_3$(L)(ppy)$_2$Ir]$^+$ dyads are higher than both Ir(III) mononuclear compounds and Re(I) reference compounds (Table 23 and 24), suggesting an enhancement of the emission performances in passing from mononuclear to dinuclear Ir(III)-Re(I) species, a behaviour which might suggest a Ir→Re energy transfer process.

fac-[Re(N^N)(CO)$_3$(L)(F$_2$ppy)$_2$Ir]$^+$-type dyads

Table 25: Photophysical data of fac-[Re(N^N)(CO)$_3$(L)(F$_2$ppy)$_2$Ir]$^+$-type dyads

Complex	**Abs**	**Emission 298 K**					**Emission 77K**	
CH_2Cl_2 as the solvent	**λ(nm) ε(mol^{-1}dm^{3}cm^{-1}**	**λ_{max} (nm)**	**τ_{ox} (μs)**	**τ_{deox} (μs)**	**ϕ_{ox} (%)**	**ϕ_{deox} (%)**	**λ_{max} (nm)**	**τ (μs)**
fac-[Re(phen)(CO)$_3$(QTZ)(F$_2$ppy)$_2$Ir]$^+$	256 (5.29) 319 (1.49) 357 (1.02)	520 548	1	5.24	5.23	54.40	500 538 582 630	21
fac-[Re(bpy)(CO)$_3$(QTZ)(F$_2$ppy)$_2$Ir]$^+$	252 (5.84) 319 (1.73) 357 (1.07)	518 550 606	1.01	3.40	6.88	36.61	504 542 586 636	17.16
fac-[Re(phen)(CO)$_3$(TPYZ)(F$_2$ppy)$_2$Ir]$^+$	273 (9.57) 351 (0.61)	568	0.53	1.39	25.3	82.3	540	7.4
fac-[Re(bpy)(CO)$_3$(TPYZ)(F$_2$ppy)$_2$Ir]$^+$	269 (5.86) 320 (1.38) 361 (0.56)	566	0.41	1.11	17.6	51.1	522	5.05

The introduction of the more energetic [Ir(F$_2$ppy)$_2$(QTZ)] or [Ir(F$_2$ppy)$_2$(TPYZ)] complexes in the construction of Ir(III)-Re(I) tetrazolate dyads actually resulted

in an hybrid photoluminescent behaviour of *fac*-[Re(N^N)(CO)$_3$(L)(F$_2$ppy)$_2$Ir]$^+$ -type dyads than those previously observed from *fac*-[Re(N^N)(CO)$_3$(L)(ppy)$_2$Ir]$^+$ (Figures 17.8 and 18.8).

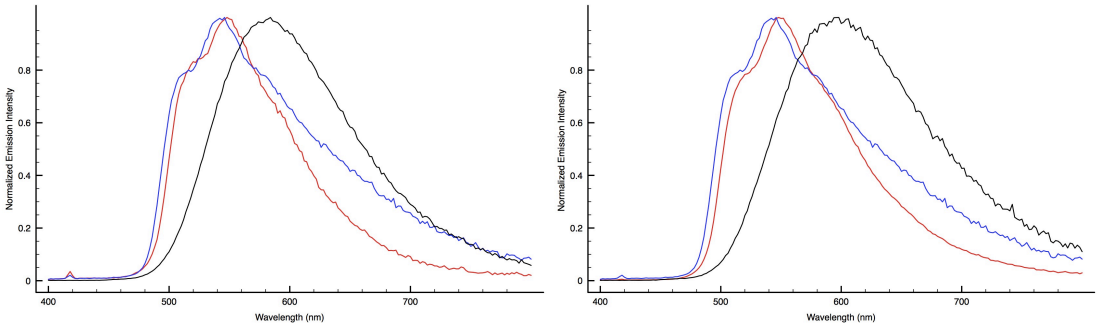

Figure 17.8: (left) Normalized Emission profiles of fac-[Re(phen)(CO)$_3$(QTZ)(F$_2$ppy)$_2$Ir]$^+$ (red line), Ir(III) mononuclear complex (blue line) and Re(I) reference compound (black line); (left): Normalized Emission profiles of fac-[Re(bpy)(CO)$_3$(QTZ)(F$_2$ppy)$_2$Ir]$^+$ (red line), Ir(III) mononuclear complex (blue line) and Re(I) reference compound (black line)

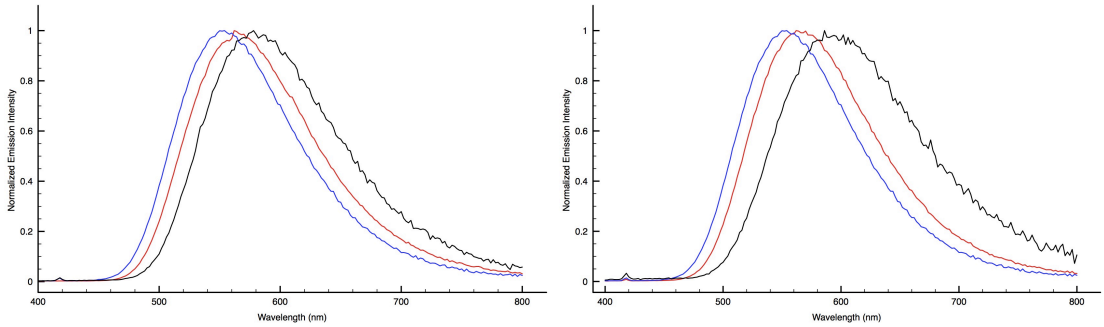

Figure 18.8: (left) Normalized Emission profiles of fac-[Re(phen)(CO)$_3$(TPYZ)(F$_2$ppy)$_2$Ir]$^+$ (red line), Ir(III) mononuclear complex (blue line) and Re(I) reference compound (black line); (left): Normalized Emission profiles of fac-[Re(bpy)(CO)$_3$(TPYZ)(F$_2$ppy)$_2$Ir]$^+$ (red line), Ir(III) mononuclear complex (blue line) and Re(I) reference compound (black line)

In all the cases, the emission maximum of *fac*-[Re(N^N)(CO)$_3$(L)(F$_2$ppy)$_2$Ir]$^+$ have been found red shifted if compared to mononuclear [Ir(F$_2$ppy)$_2$(L)] compounds and blue shifted if related to Re(I) reference compounds. This behaviour is consistent with the effects produced by electrophilic addition on both Ir(III) and Re(I) previously reported tetrazolate complexes.[26, 34, 45a] Anew, quantum yield values as well as decay time observed from *fac*-[Re(N^N)(CO)$_3$(L)(F$_2$ppy)$_2$Ir]$^+$-type dyads are superior than Ir(III) and Re(I) mononuclear compounds, an attitude that might entail energy transfer process (Table 23 and 25).

Conclusions

The study of the photophysical properties of mononuclear Ir(III) and Re(I) tetrazolate complexes and the investigation of the reactivity toward electrophiles of these derivatives offer a powerful and reliable tool for the preparation of multinuclear assemblies (dyads) based on 5 aryl tetrazolates. In particular, it was observed how the combination of two different tetrazolate complexes led to dinuclear species whose emission properties (PLQY, emission lifetimes) are superior in respect of the sum of the parent mononuclear complexes. This behaviour cane be rationalized on the basis of our background studies, in which we demonstrated how these parameters in mononuclear Ir(III) and Re(I) tetrazolate complexes can be enhanced by adding electrophiles. When the type of the electrophile changes from H^+ (or an alkyl group) to a whole metal fragment, the effect of the electrophilic addition on the luminescent output of tetrazolate complexes is always the same (enhancement of PLQY, elongation of emission lifetimes), while the position of the emission maxima (*i.e.* the emission colour) vary in consideration of the "photoemissive" nature (metal ion, ancillary ligands) of the tetrazolate complexes employed. However, the intervention of Ir-Re energy transfer though the tetrazolate ligand cannot be ruled out and intense effort for determining their influence are currently being undertaken.

Experimental section

General considerations. All the reagents and solvents were obtained commercially (e.g. Aldrich) and used as received without any further purification, unless otherwise specified. All the reactions were carried out under an argon atmosphere following Schlenk protocols. Where required, the purification of the Ir(III) complexes was performed via column chromatography with the use of neutral alumina as the stationary phase. ESI-mass spectra were recorded using a Waters ZQ-4000 instrument (ESI-MS, acetonitrile as the solvent). Nuclear magnetic resonance spectra (consisting of ^{1}H and ^{13}C) were always recorded using a Varian Mercury Plus 400 instrument (^{1}H, 400.1; ^{13}C, 101.0 MHz.) at room temperature. ^{1}H and ^{13}C chemical shifts were referenced to residual solvent resonances.

Photophysics. Absorption spectra were recorded at room temperature using a Perkin Elmer Lambda 35 UV/vis spectrometer. Uncorrected steady-state emission and excitation spectra were recorded on an Edinburgh FLSP920 spectrometer equipped with a 450 W xenon arc lamp, double excitation and single emission monochromators, and a Peltier-cooled Hamamatsu R928P photomultiplier tube (185–850 nm). Emission and excitation spectra were acquired with a cut-off filter (395 nm) and corrected for source intensity (lamp and grating) and emission spectral response (detector and grating) by a calibration curve supplied with the instrument. The wavelengths for the emission and excitation spectra were determined using the absorption maxima of the MLCT transition bands (emission spectra) and at the maxima of the emission bands (excitation spectra). Quantum yields (Φ) were determined using the optically dilute method by Crosby and Demas[41] at excitation wavelength obtained from absorption spectra on a wavelength scale [nm] and compared to the reference emitter by the following equation:[42]

$$\phi_s = \phi_r \left[\frac{A_r(\lambda_r)}{A_s(\lambda_s)}\right]\left[\frac{I_r(\lambda_r)}{I_s(\lambda_s)}\right]\left[\frac{n_s^2}{n_r^2}\right]\left[\frac{D_s}{D_r}\right]$$

where A is the absorbance at the excitation wavelength (λ), I is the intensity of the excitation light at the excitation wavelength (λ), n is the refractive index of the solvent, D is the integrated intensity of the luminescence, and Φ is the quantum yield. The subscripts r and s refer to the reference and the sample, respectively. A stock solution with an absorbance > 0.1 was prepared, then two

dilutions were obtained with dilution factors of 20 and 10, resulting in absorbances of about 0.02 and 0.08 respectively. The Lambert-Beer law was assumed to remain linear at the concentrations of the solutions. The degassed measurements were obtained after the solutions were bubbled for 10 minutes under Ar atmosphere, using a septa-sealed quartz cell. Air-equilibrated $[Ru(bpy)_3]Cl_2/H_2O$ solution (Φ = 0.028)[43] was used as reference. The quantum yield determinations were performed at identical excitation wavelengths for the sample and the reference, therefore deleting the $I(\lambda r)/I(\lambda s)$ term in the equation. Emission lifetimes (τ) were determined with the single photon counting technique (TCSPC) with the same Edinburgh FLSP920 spectrometer using pulsed picosecond LED (EPLED 360, fhwm < 800 ps) as the excitation source, with repetition rates between 1 kHz and 1 MHz, and the above-mentioned R928P PMT as detector. The goodness of fit was assessed by minimizing the reduced $\chi 2$ function and by visual inspection of the weighted residuals. To record the 77 K luminescence spectra, the samples were put in quartz tubes (2 mm diameter) and inserted in a special quartz dewar filled with liquid nitrogen. The solvent used in the preparation of the solutions for the photophysical investigations was of spectrometric grade. Experimental uncertainties are estimated to be ±8% for lifetime determinations, ±20% for quantum yields, and ±2 nm and ±5 nm for absorption and emission peaks, respectively.

Ligand synthesis

Following the general method reported by Koguro and co-workers,[21] tetrazole ligands [H-**QTZ**] 2-(1*H*-tetrazol-5-yl)quinoline and [H-**TPYZ**] 2-(1*H*-tetrazol-5-yl)pyrazine, were obtained in quantitative yield.

[H-**QTZ**] ^{1}H-NMR (DMSO d^6, 400 MHz) δ (ppm) = 8,65 (d, 1H, $J_{H\text{-}H}$ = 8,79 Hz), 8,31 (d, 1H, $J_{H\text{-}H}$ = 8,40 Hz), 8,17 (d, 1H, $J_{H\text{-}H}$ = 8,40 Hz), 8,12 (d, 1H, $J_{H\text{-}H}$ = 7,99 Hz), 7,90 (t, 1H), 7.74 (t, 1H). [H-**TPYZ**] ^{1}H-NMR, 400 MHz, DMSO-d^6 δ (ppm) = 9.39 (m, 1H); 8.87 (m, 2H).

General Procedure for the Preparation of the Neutral [Ir(C^N)$_2$(L)]- type complexes

In a two neck round bottom flask, 0.100 g of Ir-dichrlorobridged dimer (0.093 mmol for C^N = ppy and 0.082 mmol for C^N = F_2ppy) and 2.5 molar equiv of the desired tetrazole ligand L(either H-QTZ or H-TPYZ) were dissolved in a 3:1 mixture of DCM and EtOH, stirred at r.t. for 4-6 h. The crude was evaporated to

dryness and purificated by column chromatography over Al_2O_3 eluted with a mixture of DCM/Acetone 9:1.

[Ir(ppy)$_2$(TPYZ)] ^{1}**H-NMR** ($CDCl_3$, 400 MHz) δ (ppm) = 9.78 (s, 1H), 8.52 (d, 1H, J_{H-H} = 2.79 Hz), 7.89 – 7.84 (m, 2H), 7.76 (m, 1H), 7.73 – 7.68 (m, 2H), 7.66 – 7.60 (m, 4H), 7.39 – 7.37 (m, 1H), 7.03 – 6.99 (m, 1H), 6.97 – 6.91 (m, 3H), 6.89 – 6.82 (m, 2H), 6.37 – 6.35 (m, 1H), 6.28 – 6.26 (m, 1H). ^{13}**C-NMR** (CD_3CN, 100 MHz) δ (ppm) = 167.48, 150.18, 149.78, 149.42, 147.59, 147.22, 144.76, 144.22, 144.08, 144.026, 143.8, 138.32, 138.11, 131.82, 131.64, 130.16, 130.00, 129.53, 124.69, 124.32, 123.58, 123.13, 122.51, 122.12, 121.87, 119.56, 119.39; **ESI-MS** (*m*/*z*): [M+Na$^+$]= 743; [M+K$^+$] = 759.

[Ir(F$_2$ppy)$_2$(TPYZ)] ^{1}**H-NMR**, 400 MHz, CD_3CN, δ (ppm) = 9.58 (s, 1H), 8.59 (d, 1H J_{H-H} =2.8), 8.32(d, 2H, J_{H-H} = 2.80 Hz), 7.92-7.86 (m, 2H), 7,69 (d, 1H, J_{H-H} = 6 Hz), 7.55 (d, 1H, J_{H-H} =6Hz), 7.13-7.05 (m, 2H), 6.74-6.63 (m, 2H), 5.85 (d, 1H, J_{H-H} = 8.39 Hz), 5.73 (d, 1H, J_{H-H} = 2 Hz) ^{13}**C-NMR**, 100 MHz, CD_3CN, δ (ppm) = 163.74 (Ct),151.14, 150.04, 149.82, 147.95, 144.24, 144.16, 143.62, 139.34, 139.20, 124.06, 123.61, 123.57, 123.35, 123.15; **ESI-MS** (*m*/*z*): [M+Na$^+$]= 743; [M+K$^+$] = 759.

[Ir(ppy)$_2$QTZ] ^{1}**H-NMR** (CD_3CN, 400 MHz) δ (ppm): 8.61 – 8.53 (m, 2H), 8.06 – 8.00 (m, 2H), 7.97 – 7.92 (m, 2H), 7.89 – 7.87 (m, 1H), 7.81 – 7.68 (m, 4H), 7.53 – 7.49 (m, 1H), 7.33 – 7.32 (m, 1H), 7.19 – 7.15 (m, 1H), 7.06 – 7.02 (m, 1H), 6.99 – 6.93 (m, 3H), 6.90 – 6.87 (m, 1H), 6.83 – 6.79 (m, 1H), 6.49 – 6.48 (m, 1H), 6.15 – 6.13 (m, 1H). ^{13}**C-NMR** (CD_3CN, 100 MHz) δ (ppm) = 169.45, 168.55, 166.76 (Ct), 157.09, 155.48, 152.50, 151.96, 150.26, 149.05, 146.01, 145.18, 145.07, 142.16, 139.34, 139.27, 133.48, 132.33, 131.45, 130.82, 130.75, 130.26, 129.12, 129.11, 126.29, 126.17, 125.51, 124.59, 124.34, 123.25, 123.23, 121.20, 120.76. **ESI-MS** (*m*/*z*): [M+Na]$^+$ = 720.

General Procedure for the Preparation of the Neutral fac-[Re(N^N)(CO)$_3$L]-Type Complexes

A 0.100 g amount of *fac*-[Re(N^N)(CO)$_3$Br] (0.22 mmol for N^N = bpy; 0.13 mmol if N^N = phen) was dissolved in 20 mL of an ethanol/water mixture (3:1 v/v) under an argon atmosphere. A 5.0 mL portion of an ethanol/water (3:1 v/v) solution containing 1.5 molar equivalents of the appropriate tetrazolate salt was added drop wise. Once the addition was completed, the resulting suspension

was stirred at the reflux temperature for 24 h. After this time, the mixture was cooled to r.t. and filtered through a glass frit, affording the desired complexes as a yellow microcrystalline powder. The product complexes did not require any further purification process.

[Re(CO)$_3$(phen)(QTZ)] ^{1}**H-NMR** 400 MHz, Acetone-d^6 δ (ppm) = 9,74 (d, 2H, J_{H-H} = 6,40 Hz), 9,01 (d, 2H, J_{H-H} = 9,60 Hz), 8,34 (s, 2H), 8,23 (m, 3H), 7,99 (d, 1H, J_{H-H} = 8,79 Hz), 7,87 (m, 2H), 7,72 (m, 1H), 7,55 (m, 1H). ^{13}**C-NMR** 100 MHz, Acetone-d^6 δ (ppm) = 197, 31 (CO), 195,40 (CO), 189,9 (CO), 163,55 (Ct), 154,87 (C_{ipso}), 148,93, 147,76, 146,90, 140,29, 137,22, 130,79, 130,35, 129,41, 128,29, 128,23, 127,74, 127,24, 127,15, 120,15. **ESI-MS** [M] = 646 *m*/*z* (CH_3CN)

[Re(CO)$_3$(bpy)(QTZ)] ^{1}**H-NMR** 400 MHz, Acetone-d^6 δ (ppm) = 9,29 (m, 2H), 8,70 (d, 2H, J_{H-H} = 7,99 Hz), 8,37 (m, 2H), 8,24 (d, 1H, J_{H-H} = 8,79 Hz), 7,98 (m, 2H), 7,88 (d, 1H, J_{H-H} = 8,39 Hz), 7,85 (m, 2H), 7,13 (m, 1H), 7,53 (m, 1H). ^{13}**C-NMR** 100 MHz, DMSO-d^6 δ (ppm) = 164,18 (Ct), 156,77, 154,59, 149,54, 148,32, 141,69, 137,74, 130,85, 129,95, 129,07, 128,80, 128,27, 127,64, 125,08, 120,76. **ESI-MS** [M] = 623 *m*/*z* (CH_3CN).

[Re(CO)$_3$(phen)(TYPZ)] ^{1}**H-NMR** 400 MHz, Acetone-d^6 δ (ppm) = 9.69-8.68 (m, 2H), 8.98-8.96 (m, 2H), 8.77 (d, 1H, J_{H-H} = 1.6 Hz), 8.47-8.46(m, 1H), 8.43 (d, 1H, J_{H-H} = 2.8 Hz), 8.30 (s, 2H), 8.21-8.17 (m, 2H). ^{13}**C-NMR**, 100 MHz, CD_3CN, δ (ppm) = 162.26 (Ct), 155.33, 148.22, 146.33, 145.13, 144.72, 143.97, 140.53, 131.82, 128.80, 127.54. **IR** (cm^{-1}, DCM): 2029.85 (CO-A'(1)), 1923.34 (CO-A'(2)/A").

[Re(CO)$_3$(bpy)(TYPZ)] ^{1}**H-NMR** 400 MHz, Acetone-d^6 δ (ppm) = 9.29-9.27 (m, 2H), 8.94 (d, 1H, J_{H-H} = 1.6 Hz), 8.72-8.69(m, 2H), 8.53-8.52 (m, 1H), 8.48 (d, 1H, J_{H-H} = 2.8 Hz), 8.39-8.34 (m, 2H), 7.85-7.81 (m, 2H). ^{13}**C-NMR**, 100 MHz, CD_3CN, δ (ppm) = 162.37 (Ct), 157.47, 154.81, 146.47, 145.21, 144.79, 144.10, 141.41, 128.86, 124.85; **IR** (cm^{-1}, DCM): 2029.62 (CO-A'(1)), 1923.41 (CO-A'(2)/A").

General Procedure for the Preparation of the Cationic fac-[Re(N^N)(CO)$_3$(L)(C^N)$_2$Ir][PF$_6$]- type complexes

In a two neck round bottom flask protected from light, 0.068 g of [Re(CO)$_3$(N^N)Br] (0.128 mmol) and 0.036 g (0.141 mmol) of $AgPF_6$ were

dissolved in 20 mL of acetone and refluxed for 4h. The mixture was then allowed to cool to r.t. and filterd over a celite pad to remove AgBr. The crude was used without further purification for the next step. $[Re(CO)_3(N^N)(acetone)]^+$ and $[Ir(ppy)_2(L)]$ (0.083 g, 0.128 mmol) were dissolved in 20 mL of acetone and refluxed, overnight. The mixture was then allowed to cool to r.t. and a small amount of Et_2O (5mL) was added to the crude, inducing the precipitation of an orange-yellowish solid, which was collected by filtration and washed with Et_2O (2x5mL).

***fac*-[Re(phen)(CO)$_3$(QTZ)(ppy)$_2$Ir]$^+$** ^{1}**H-NMR**, 400 MHz, CD_3CN, δ (ppm) = 9.34 (m, 1H), 9.25 (m, 1H), 8.17 (m, 1H), 8.61 (m, 2H), 8.22 (m, 1H), 8.10 (m, 2H), 7.94 (m, 2H), 7.84 (m, 2H), 7.76 (m, 4H), 7.68 (m, 3H), 7.49 (m, 2H), 7.37 (m, 1H), 7.11 (m, 1H), 6.99 (m, 2H), 6.87 (m, 2H), 6.75 (m, 1H), 6.66 (m, 2H), 6.21 (m, 1H), 5.57 (m, 1H). ^{13}**C-NMR**, 100 MHz, CD_3CN, δ (ppm) = 168.55, 167.94 (Ct), 167.20, 154.99, 154.65, 153.00, 150.94, 149.80, 149.24, 148.58, 147.81, 147.73, 145.23, 143.89, 143.32, 142.03, 140.65, 140.61, 139.21, 139.02, 132.79, 132.43, 131.48, 131.39, 131.14, 130.79, 130.46, 129.96, 129.50, 128.77, 128.73, 128.70, 127.05, 126.89, 125.85, 125.12, 123.86, 123.81, 123.15, 123.11, 120.52, 120.31, 120.19. **ESI-MS**: *(m/z)* $[M^+]$ = 1146; $[M^-]$ = 145. MW: 1291 g/mol Y = 0.095g, 0.074 mmol, 74%.

***fac*-[Re(bpy)(CO)$_3$(QTZ)(ppy)$_2$Ir]$^+$** ^{1}**H-NMR**, 400 MHz, CD_3CN, δ (ppm) = 8.98 (d, 1H, $J_{H\text{-}H}$ = 3.99 Hz), 8.44 (d, 1H, $J_{H\text{-}H}$ = 3.99 Hz), 8.65 (d, 1H, $J_{H\text{-}H}$ = 7.99 Hz), 8.35 (d, 1H, $J_{H\text{-}H}$ = 7.99 Hz), 8.12 – 7.97 (m, 5H), 7.92 – 7.86 (m, 3H), 7.80 – 7.70 (m, 4H), 7.65 (d, 1H, $J_{H\text{-}H}$ = 7.99 Hz), 7.57 – 7.50 (m, 3H), 7.42 – 7.38 (m, 1H), 7.19 – 7.15 (m, 1H), 7.12 – 7.08 (m, 1H), 7.04 – 6.91 (m, 4H), 6.84 – 6.76 (m, 3H), 6.34 (d, 1H, $J_{H\text{-}H}$ = 7.99 Hz), 5.78 (d, 1H, $J_{H\text{-}H}$ = 7.99 Hz). ^{13}**C-NMR**, 100 MHz, CD_3CN, δ (ppm) = 167.66, 167.11, 166.40 (Ct), 156.23, 153.52, 153.15, 152.16, 150.30, 148.87, 148.27, 147.69, 144.34, 143.10, 141.42, 140.55, 140.51, 138.27, 138.20, 131.91, 131.52, 130.55, 130.21, 129.87, 129.58, 129.00, 128.58, 127.81, 127.37, 127.20, 124.92, 124.24, 123.75, 123.67, 123.17, 122.93, 122.33, 122.18, 119.60, 119.38, 119.36. **ESI-MS**: *(m/z)* $[M^+]$ = 1123; $[M^-]$ = 145. MW: 1268 g/mol Y = 0.009g, 0.008 mmol, 16.5%.

***fac*-[Re(phen)(CO)$_3$(QTZ)(F$_2$ppy)$_2$Ir]$^+$** ^{1}**H-NMR**, 400 MHz, CD_3CN, δ (ppm) = 9.39 (d, 1H, $J_{H\text{-}H}$ = 4.39 Hz), 9.26 (d, 1H, $J_{H\text{-}H}$ = 5.19 Hz), 8.74 (d, 1H, $J_{H\text{-}H}$ = 7.99 Hz), 8.67 (d, 2H, $J_{H\text{-}H}$ = 8.39 Hz), 8.34 (d, 1H, $J_{H\text{-}H}$ = 8.39 Hz), 8.11 (m, 2H), 8.01 (m, 2H), 7.91 (m,

2H), 7.79 (m, 3H), 7.64 (m, 2H), 7.56 (m, 1H), 7.34 (m, 1H), 6.90 (m, 1H), 6.82 (m, 1H), 6.73 (m, 3H), 5.71 (m, 1H), 5.03 (m, 1H). ^{19}**F-NMR**, 376 MHz, CD_3CN, δ (ppm) = -108.11, -108.14, -110.10, -110.32.

***fac*-[Re(phen)(CO)$_3$(TPYZ)(ppy)$_2$Ir]$^+$** ^{1}**H-NMR**, 400 MHz, CD_3CN, δ (ppm) = 9.36 (m, 1H), 9.31 (m, 1H), 9.23 (m, 1H), 8.69-8.63 (m, 2H), 8.52 (m, 1H), 8.08 (m, 1H), 7.97 (d, 1H, J_{H-H} = 7.99 Hz), 7.86 -7.74 (m, 5H), 7.72 (d, 1H, J_{H-H} = 7.99 Hz), 7.64 (m, 1H), 7.59 (d, 1H, J_{H-H} = 3.99 Hz), 7.14 (d, 1H, J_{H-H} = 5.59 Hz), 7.07-6.97 (m, 4H), 6.89-6.83 (m, 2H), 6.81-6.76 (m, 1H), 6.73-6.69 (m, 1H), 6.12 (d, 1H, J_{H-H} = 7.6 Hz), 5.84 (d, 1H, J_{H-H} = 7.99 Hz). ^{13}**C-NMR**, 100 MHz, CD_3CN, δ (ppm) = 166.99, 166.61, 163.86 (Ct), 154.09, 153.79, 149.70, 149.11, 148.80, 148.15, 146.87, 146.76, 144.79, 144.31, 144.14, 143.41, 141.46, 139.63, 139.61, 138.55, 138.33, 131.64, 131.60, 131.09, 130.48, 130.44, 130.16, 130.13, 129.49, 127.72, 127.68, 126.00, 125.97, 124.72, 124.30, 123.38, 122.76, 122.73, 122.18, 119.68, 119.24. **ESI-MS** (*m*/*z*): $[M]^+$ = 109; $[M]^-$ = 145 (PF_6); **IR (cm^{-1}, DCM):** 2035.24 (CO-A′(1)), 1931.93 (CO-A′(2)/A″).

***fac*-[Re(bpy)(CO)$_3$(TPYZ)(ppy)$_2$Ir]$^+$** ^{1}**H-NMR**, 400 MHz, CD_3CN, δ (ppm) = 9.32 (m, 1H), 8.98 (m, 1H), 8.93 (m, 1H), 8.57 (d, 1H, J_{H-H} =2.79), 8.21-8.01 (m, 4H), 7.96 (m, 1H), 7.86 – 7.80 (m, 5H), 7.53 – 7.45 (m, 2H), 7.34 – 7.32 (m, 1H), 7.20 – 7.18 (m, 1H), 7.09 – 7.01 (m, 3H), 6.95 – 6.84 (m, 4H), 6.24 (d, 1H J_{H-H} = 7.59), 6.01 (d, 1H, J_{H-H} = 8.39). ^{13}**C-NMR**, 100 MHz, CD_3CN, δ (ppm) = 167.15, 166.93, 164.02 (Ct), 156.15, 156.13, 153.65, 153.38, 149.78, 149.23, 149.16, 148.29, 145.12, 144.40, 144.31, 144.23, 143.76, 141.51, 140.60, 138.58, 138.47, 131.71, 131.38, 130.19, 129.59, 127.38, 127.36, 124.79, 124.35, 124.30, 123.59, 123.57, 123.46, 123.04, 122.79, 122.29, 119.74, 119.41. **ESI-MS** (*m*/*z*): $[M]^+$ = 1074; $[M]^-$ = 145 (PF_6); **IR** (cm^{-1}, DCM): 2034.64 (CO-A′(1)), 1931.15 (CO-A′(2)/A″).

***fac*-[Re(phen)(CO)$_3$(TPYZ)(F$_2$ppy)$_2$Ir]$^+$** ^{1}**H-NMR**, 400 MHz, CD_3CN, δ (ppm) = 9.39 (d, 1H, J_{H-H} = 5.19 Hz), 9.36 (s, 1H), 9.26 (d, 1H, J_{H-H} = 3.99 Hz), 8.72 (d, 1H, J_{H-H} = 7.19 Hz), 8.66 (d, 1H, J_{H-H} = 7.19 Hz), 8.59 (m, 1H), 8.22 – 8.20 (m, 1H), 8.08 (m, 3H), 7.91 – 7.78 (m, 4H), 7.73 (m, 1H), 7.19 (d, 1H, J_{H-H} = 5.19 Hz), 7.01 (d, 1H, J_{H-H} = 5.19 Hz), 6.94 – 6.91 (m, 1H), 6.80 – 6.76 (m, 1H), 6.73 – 6.62 (m, 2H), 5.61 (m, 1H), 5.23 (m, 1H). ^{13}**C-NMR**, 100 MHz, CD_3CN, δ (ppm) = 154.32, 153.84, 149.90, 149.47, 149.28, 144.63, 144.42, 139.52, 139.44, 139.34, 127.58, 126.05, 125.96, 123.82, 123.65, 123.30,

119.42, 117.31. **ESI-MS** (*m*/*z*): $[M]^+$ = 1170; $[M]^-$ = 145 (PF_6); **IR** (cm^{-1}, DCM): 2036.05 (CO-A'(1)), 1932.77 (CO-A'(2)/A").

***fac*-[Re(bpy)(CO)$_3$(TPYZ)(F$_2$ppy)$_2$Ir]$^+$ ^{1}H-NMR**, 400 MHz, CD_3CN, δ (ppm) = 9.39 (s,1H), 9.01 (d, J_{H-H} = 5.6 Hz, 1H) 8.91 (d, J_{H-H} = 5.6 Hz, 1H), 8.64 (d, J_{H-H} = 3.2 Hz, 1H), 8.27 (d, J_{H-H} = 8.4 Hz, 1H), 8.20-8.07 (m, 5H), 7.89 (t, J_{H-H} = 8.4 Hz, 1H), 7.82 (d, J_{H-H} = 1.6 Hz, 1H), 7.56(t, J_{H-H} = 6.8 Hz, 1H), 7.48 (t, J_{H-H} = 5.2 Hz, 1H), 7.36 (d, J_{H-H} = 6 Hz, 1H), 7.23 (d, J_{H-H} = 5.6 Hz, 1H), 7.00 (t, J_{H-H} = 8.4 Hz, 1H), 6.92-6.89 (m,1H), 6.76-6.70 (m, 2H), 5.73 (d, J_{H-H} = 10.8 Hz, 1H), 5.45 (d, J_{H-H} = 1.6 Hz, 1H), ^{13}**C-NMR** (CD_3CN, 100MHz) δ (ppm) = 163.91(Ct), 156.18, 156.05, 153.88, 153.51, 152.41, 152.35, 150.09, 149.59, 149.57, 148.98, 148.90, 144.74, 144.48, 140.96, 140.55, 140.50, 139.61, 139.53, 127.50, 127.47, 123.93, 123.71, 123.58, 123.52, 123.41, 123.35, 123.13. **ESI-MS** (*m*/*z*): $[M]^+$ =1146; $[M]^-$ = 145 (PF_6); **IR** (cm^{-1}, DCM): 2035.72 (CO-A'(1)), 1932.71 (CO-A'(2)/A").

Chapter 9

Ru(II) bis-tetrazolate complexes as thiocyanate-free sensitizers for DSSCs

Abstract

A series of polypyridyl Ru(II) tetrazolate complexes D1-4, which differs both for the nature and for the coordinating mode adopted by the tetrazolate ligands are presented. All the new complexes have been tested as photosensitizers into Dye-Sensitized Solar Cells (DSSCs), and the obtained performances have been analysed in comparison to those of the reference compound N719 dye that was measured under identical conditions by using the I/I_3^- couple as the electrolyte. Among the series of the Ru(II) complexes reported herein, the ones containing the anionic ligands deriving from 2(1,H tetrazol-5-yl) pyrazine (complex D2) and 4(1,H tetrazol-yl) bromobenzene,(complex D4) displays better photovoltaic performances, with J_{sc} values spanning from 2.15 mA/cm^2 to 2.55 mA/cm^2, respectively.

Introduction

Over the past decade, intense research efforts have been devoted to the study of the coordination chemistry of tetrazole and tetrazolate based compounds, which have found application as building blocks for Metal Organic Frameworks (MOFs),[83] as well as nitrogen rich molecules for energetic materials,[84] and polytopic ligands for the construction of luminescent metal- and lanthanide based complexes.[85] In very recent times, the applicative scenario of these synthetically versatile nitrogen rich heterocycles has been extended to the photovoltaic technologies with the incorporation of tetrazolate based chelates, such as the 2-pyridyl tetrazolate anion,[86] within the structure of Ru(II) photosensitizers for Dye Sensitized Solar Cells (DSSCs). In particular, it has been demonstrated how tetrazolate ligands can be regarded as a viable and robust alternative to the coordinated thiocyanates [NCS^-], the presence of which has been considered as one the limiting factor of the stability of the corresponding Ru(II) dyes.

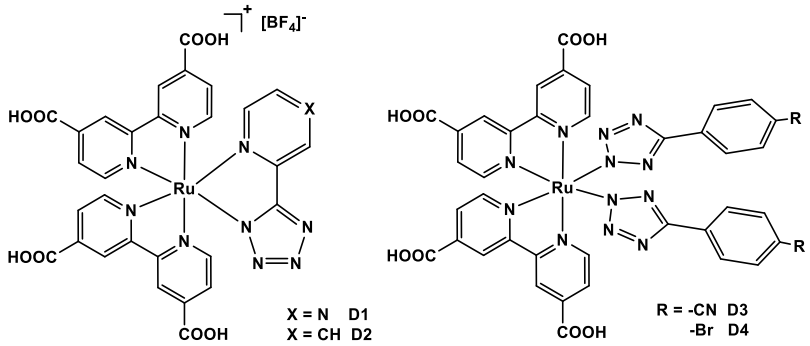

Figure 9.1: Ru(II) complexes and relative acronyms described in this chapter

Aiming at extending our past studies dealing with the preparation of photo and electrochemiluminescent Ru(II)-tetrazolate complexes to the design of new examples of tetrazolate-based DSSCs dyes, we now report the preparation, the characterization and of a set of two different classes of Ru(II) complexes, that differ both for the nature and for the coordinating mode adopted by the tetrazolate ligands (Figure 1.9). In the first instance, we have slightly modified the structure of the Ru(II) tetrazolate-based dyes reported by Dragonetti et al with the replacement of the 2-pyridyl substituent with the more electron withdrawing pyrazine ring (Class I complexes, Figure 1.9). Then, the preparation of a further and unprecedented class of tetrazolate-based Ru(II) dyes has been accomplished by decorating the traditional fragment cis-(bpy-4,4′-dicarboxylate)ruthenium(II) with two 5-aryl tetrazolate (class II complexes, Figure 1.9), leading therefore to new examples of thiocyanate free dyes in which two 5-aryl tetrazolate are introduced in place of the thiocyanate ligands. All the new complexes have been tested in DSSC devices, and the obtained performances have been analysed in comparison to those of reference compounds such as the recently reported cis-(bpy-4,4′-dicarboxylate)ruthenium(II)(2-pyridyltetrazolate) complex and the N719 dye that were measured under identical conditions by using the I^-/I_3^- couple as the electrolyte.

Results and Discussion

Synthesis, ESI-MS and NMR spectroscopy

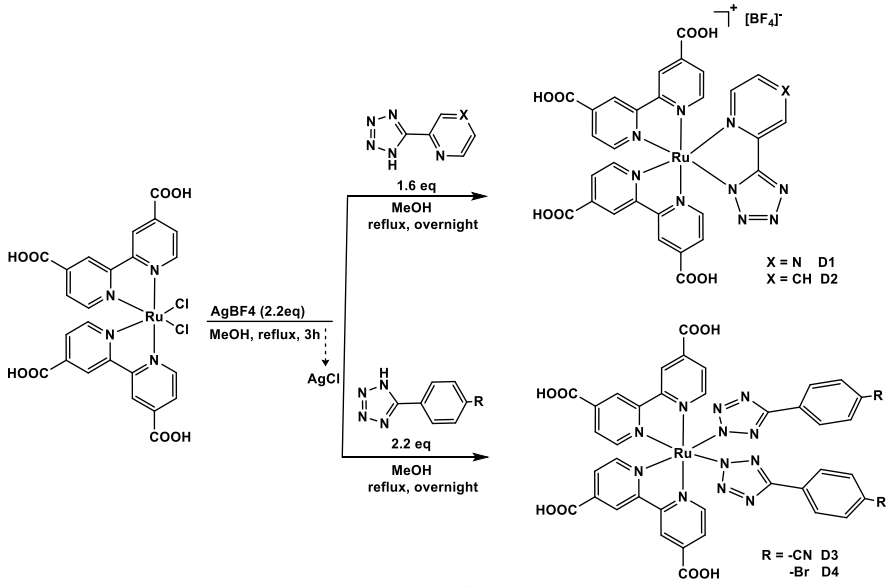

Figure 9.2: Synthetic procedures for complexes D1-4

By following two slightly different methods, the tetrazole ligands reported in this work has been prepared. Both of them involved the 1,3 dipolar cyclization of the azide anion (N_3^-) onto the appropriate nitrile precursor, more specifically 2 (1,H tetrazol-5yl)pyridine, 2(1,H tetrazol-5-yl) pyrazine and 4(1,H tetrazol-yl) benzonitrile were obtained in almost quantitative yield by adopting the procedure reported by Finnegan and coworkers;[20] the preparation of 4(1,H tetrazol-yl) bromobenzene (65% yield) was accomplished through the method described by Koguro and coworkers.[21] As depicted in Figure 2.9, the preparation of the ruthenium (II) complexes D1-4 was accomplished by a two step procedure that involved the preliminary reaction of the precursor *cis*-[Ru(dcbipy)$_2$Cl$_2$] (dcbipy = [2,2'-bipyridine]-4,4'-dicarboxylic acid) with a molar excess (2.2 equiv) of $AgBF_4$ in refluxing methanol. The removal of the precipitated silver salt afforded a red filtrate that was subsequently combined with a methanolic solution of the desired tetrazolate anion (1.6 equiv in the case of the cationic complexes D1 and D2, while 2.2 equiv were required for D3 and D4. The resulting reaction mixtures were refluxed overnight, and the desired crude complexes were precipitated from the reaction mixtures upon the addition of a copious amount of diethyl ether. The subsequent filtration through a glass frit led to the isolation of the complexes as red to brown microcrystalline solids that did not require purification by column chromatographies. The formation of all the Ru(II) complexes was at first deduced by ESI-MS mass spectroscopy, which provided *m*/*z* signals congruent with the expected neutral D3 and D4 [M+H] or [M+Na^+/K^+] or cationic complexes (D1 and D2) in the region of the positive ions.

The ^{1}H-NMR characterization of D3 and D4 revealed a number of resonances equal to the total number of protons in the complexes due to their C_s symmetry, while the spectrum from D1 and D2, according to their C_{2v} punctual group, displayed a number of resonances equal to the half of total protons of the molecules.

Redox Properties

The redox properties of all the reported Ru(II)-based dyes has been investigated by performing cyclic voltammetry (CV) experiments onto the corresponding methanol-acetonitrile solutions, and the relevant data are collected in Table 25. As previously reported,[26] the oxidation of the polypirydinic Ru(II) tetrazolate

complex D1 occurs at more positive potentials (1.31 V) than that of D2 (1.02 V), according to the remarkable electron withdrawing character of the pyrazinyl-tetrazolate ligand in respect of the pyridyl tetrazolate moiety (D1). Following a similar trend, the differences observed in dyes D3 and D4 can be attributed to the pronounced electron withdrawing character of the cyanide group of the tetrazole ligand (1.30 V) in respect of the bromine group in D4, which resulted in an oxidation peak found at 1.07 V.

Electronic Spectroscopy

The absorption spectra of D1-4 were recorded in methanol solutions and are depicted in Figure 1. For all the ruthenium species, the absorption profile displays the peculiarity of this class of complexes, with intense bands in the UV range (200-350 nm) which are assigned to LC (*ligand centred*) dcbipy-based π-π* transitions. Weaker absorption are found from 450 to 510 nm (visible region, Figure 3.9) and are mainly due to MLCT-type (*metal to ligand charge transfer*) transitions, which arise from Ru(II) metal centre to both dcbipy ancillary ligands and the different tetrazolate moieties employed for the reported complexes. According to their chemical structure (Figure 1.9 and 2.9), D1-4 dyes were compared with the well-known N719 dye, that in our hands exhibit an absorption profile with λ_{max} = 525 nm (ε = 1,26 × $10^{4}M^{-1}$ cm^{-1}). At first glance, the comparison between commercial N719 and D1-D4 results in the *ipsochromic* shift of the absorption maxima (reported in Table 25) which reaches its peak of *c.a* 70 nm for D1, while the average for D2-4 being $\Delta\lambda$ = 20-30 nm. The differences in absorption maximum between D1 and D2 can be attributed to the more electron withdrawing character of the pyrazine nitrogen located on the tetrazolate ligand of D1. Otherwise no substantial differences were found upon the series D3 and D4, which displays both an absorption maxima centred at 506 nm, as a further proof that the cyanide (for D3) and bromine (for D4) substituent on the 5-aryl-tetrazolate moieties does not influence consistently the absorption behaviour of these complexes.

Table 25. Optical and electrochemical properties of the reported dyes D1-D4

Sample	Abs	E_{ox} (V) vs SCE[a]	E_{red} (V) vs SCE[a]	E_{HOMO} (eV)[b]	E_{LUMO} (eV)[b]
D1	454	1.31	-1.01	-5.71	-3.39
D2	496	1.02	-1.01	-5.42	-3.39
D3	506	1.30	-1.36	-5.70	-3.04
D4	506	1.07	-1.59	-5.47	-2.81

[a] *Potential referred to SCE electrode.* [b] *: calculated with the general formula* $E_{HOMO} = -(E_{ox}+4.4)eV$; $E_{LUMO} = -(E_{red}+4.4)eV$;

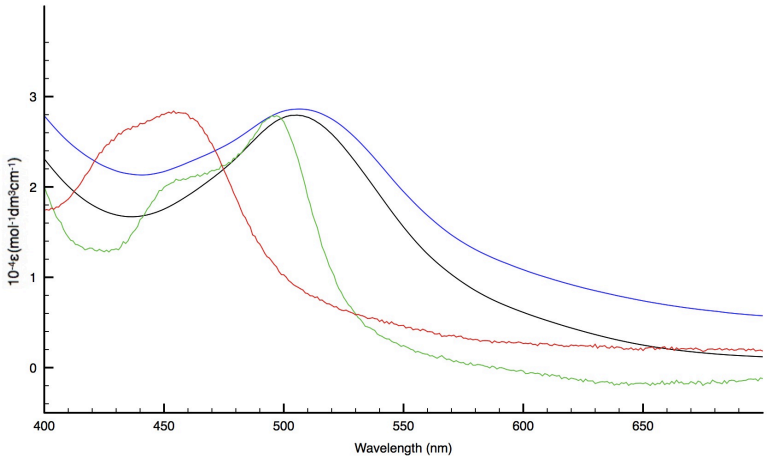

Figure 3.9: Absorption spectra of Ru(II) tetrazolate dyes (D1 – red line, D2 – green line, D3 – black line, D4 – blue line)

DSSC characterization

The electron injection ability of the Ru(II) –based dyes into the conduction band of TiO_2 (*c.a* -0.5 V vs NHE, -4 eV) was first evaluated by HOMO-LUMO energy levels, calculated according to the redox potentials acquired from CV analyses.[87] All values were found to be more negative than the TiO_2 conduction band edge, suggesting a fast electron injection all along the illumination inside the DSSC. As discussed before, the oxidation potentials of D1 and D3 were found to be more positive in respect of those stemming from D1 and D4 as a consequence of the pronounced electron withdrawing character of the 5-aryl substituents of the tetrazolate ligands used. According to the calculated energies of the LUMO levels, all of the reported Ru(II) species possess more positive E_{ox} potentials in respect of both recorded from the redox couple I^-/I_3^- used as supporting electrolyte (*c.a.* 0.4 V vs NHE, -4.9 eV) and the hypothetical I^-/I_3^- couple (*c.a* 0.79-

0.93 V vs NHE, -5.29 and -5.43 eV, respectively). These values suggest how Ru(II) tetrazolate dyes may be subjected to a fast regeneration within the solar cells.[88]

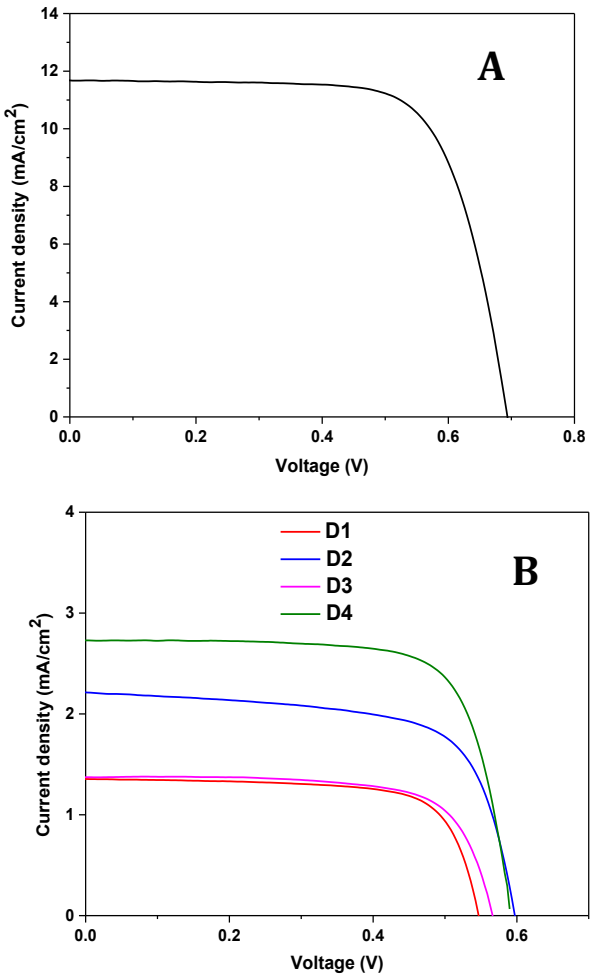

Figure 4.9. J-V curves measured for reference N719 (A) and dyes D1-4 (B)

The J-V curves obtained under illumination conditions from the Ru(II) dyes D1-4 (Figure 4.9 b), as well as the IPCE values (Figure 5.9 a, 5.9 b), has been referred for comparison to a N719 -sensitized DSSC fabricated in the same conditions (Figure 4.9 a). The whole list of the photovoltaic parameters is reported in Table 2.

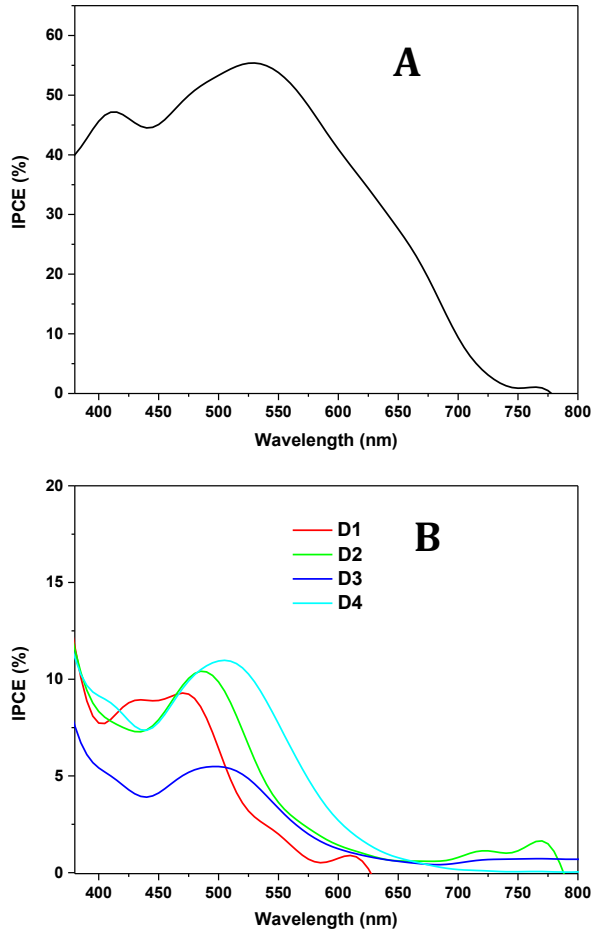

Figure 5.9. IPCE spectra for reference N719 (A) and dyes D1-4 (B)

Table 26. Photovoltaic parameters of DSCs and max IPCE value at the corresponding wavelength

Sample	Jsc (mA/cm²)	Voc (mV)	FF%	η%	IPCE% (λ nm)
D1	1.30±0.08	548±1	72±1	0.50±0.03	10 (470)
D2	2.15±0.07	564±11	70 ±4	0.87±0.02	11 (485)
D3	1.35±0.02	546±3	68±4	0.52±0.05	6 (500)
D4	2.55±0.24	592±2	73±1	1.10±0.11	12 (500)
N719	11.70±0.10	693±5	71±1	5.80±0.10	55 (525)

As regard of current density and Voc parameters, the performances of dyes D1-4 were found to be lower than N719 dye. These results are consistent with the *bathochromic shift* of their absorption maxima in respect of λ_{max} = 525 nm value recorded for N719.

In light of their photovoltaic parameters, dyes D2 and D4 were found to be the more efficient sensitizers in the D1-4 series (Jsc = 2.55 mA/cm², Voc = 592 mV, FF = 73 % and η = 1.10% for D4 and Jsc = 2.15 mA/cm², Voc = 564 mV, FF = 70 % and η = 0.7 % for D2).

These results suggest how Ru(II) dyes D2 and D4 can be considered as promising DSSC sensitizers. In particular, the performance variation found between the solar cells can be related to the highest photocurrent produced by D2 and D4 (2,15 and 2,55 mA/cm^2), as a consequence of their pronounced absorption capability (Table 26) enhancing finally the DSSC Voc value. Upon the series, D4 was found to be the more efficient Ru(II) –based dye, as a direct consequence of the influence produced from the bromine substituent on the Ru(II) → Ru(III) oxidation process.

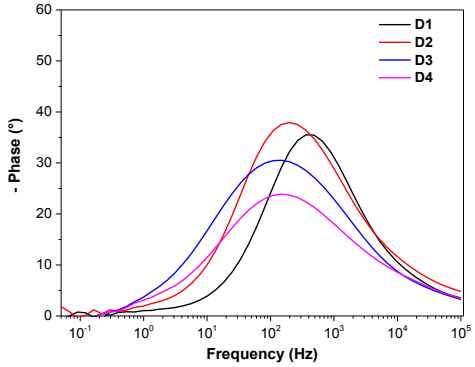

Figure 6.9. Bode phase plot of EIS analyses

By the means of electrochemical impedance analysis (EIS), charge transfer processes within DSSCs have been evaluated (Figure 6.9). The electronic properties of the sensitized photoanode, electrolyte and counter-electrode as well as the electronic properties of the interfaces created between them were investigated. The frequency zone spanning from 10^2 to 10^3 Hz in the Bode diagram (Figure 6.9), describe the electron recombination that occurs between TiO_2 film and electrolyte as function of electron lifetime (τ). The electron lifetime of each cells were determined by this following equation:

$$\tau = \frac{1}{2\pi f_{max}}$$

where f_{max} is the peak frequency extrapolated form the Bode phase plot acquired at open circuit voltage in dark conditions.

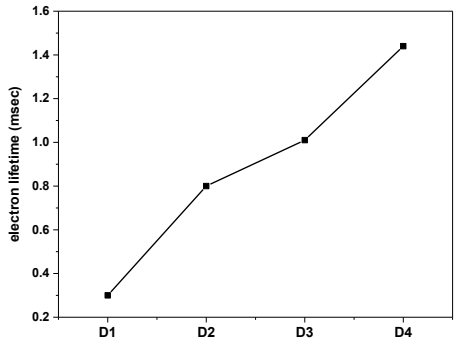

Figure 7.9. Electron lifetime calculated from Figure 4.9

In agreement with the results obtained from the photovoltaic characterization, the calculated electron lifetime values (Figure 7.9) suggest how dyes D2 and D4 are the more suitable Ru(II) complexes for DSSC fabrication. Indeed, the solar cell based on D2 posses an higher τ than that calculated for D1 as a direct consequence of the interaction that might occur between the pyrazinic nitrogen of the tetrazolate ligand and the I^-/I_3^- redox couple used as electrolyte, leading thus to a rapid charge recombination at the TiO_2/electrolyte interface, resulting in a low Voc value.[89] Similarly, D4 electron lifetime was found to be higher than that from D3, as outcome of the presence of the more electronegative –CN substituent.

Conclusions

In conclusion, we have synthesized and characterized a new series of Ru(II) polypyridyl tetrazolate complexes which were used as thiocyanate-free sensitizers in DSSCs. The new ruthenium(II) complexes featuring both chelated (D1, D2) or monocoordinated (D3, D4) tetrazole ligands possess photophysical and electrochemical properties suitable for DSSC application. A comparison between the presented ruthenium(II) complexes enlighten that D2 and D4 compounds exhibit promising photovoltaic DSSC performances if compared to commercial N719 dye, as a consequence of the pronounced electron-withdrawing character of the substituents chosen for the design of the tetrazolate ligands used. Prospectively, the Ru(II) polypyridyl tetrazolate sensitizer scaffold offers the potential to extended DSSC light-harvesting capability by introducing different chromophore at the tetrazole moiety.

Experimental Section

General considerations. All the reagents and solvents were obtained commercially (e.g. Alfa-Aesar) and used as received without any further purification, unless otherwise specified. All the reactions were carried out under an argon atmosphere following Schlenk protocols. ESI-mass spectra were recorded using a Waters ZQ-4000 instrument (ESI-MS, acetonitrile as the solvent). Nuclear magnetic resonance spectra (consisting of ^{1}H, and ^{13}C experiments) were always recorded using a Varian Mercury Plus 400 instrument (^{1}H, 400.1) at room temperature. ^{1}H chemical shifts were referenced to residual solvent resonances. Absorption spectra were recorded at room temperature using a Perkin Elmer Lambda 35 UV/vis spectrometer. Uncorrected steady-state emission and excitation spectra were recorded on an Edinburgh FLSP920 spectrometer equipped with a 450 W xenon arc lamp, double excitation and single emission monochromators, and a Peltier-cooled Hamamatsu R928P photomultiplier tube (185–850 nm). Emission and excitation spectra were corrected for source intensity (lamp and grating) and emission spectral response (detector and grating) by a calibration curve supplied with the instrument. The wavelengths for the emission and excitation spectra were determined using the absorption maxima of the MLCT transition bands (emission spectra) and at the maxima of the emission bands (excitation spectra). Cyclic voltammetry measurements were performed on a Autolab PGSTAT302N potentiostat using a glassy carbon 492/GC/3 or a platinum solid 492/PT/2 as working electrode and a SCE 303/SCG/6 reference electrode (Amel electochemistry instruments); scan rates 100 mV·s^{-1} were applied. The experiments were carried out in degassed solvents (spectroscopy grade) containing 0.1 M Bu_4NPF_6.

Ligand synthesis

Following the general method reported by Finnegan and co-workers,[20] 5-(4-bromophenyl)-1*H*-tetrazole) **TphBr**, 4-(1*H*-tetrazol-5-yl)benzonitrile **TphCN**, 2-(1*H*-tetrazol-5-yl)pyrazine **Tpyz**, 2-(1*H*-tetrazol-5-yl)pyridine **Tpyr**, 2,6-di(1*H*-tetrazol-5-yl)pyridine **TphBr** (Y = 84%), ^{1}**H-NMR**, 300 MHz, DMSO-d^6 δ (ppm) = 7.98 (d, 2H, $J_{H\text{-}H}$ = 5.99 Hz), 7.81 (d, 2H, $J_{H\text{-}H}$ = 5.99 Hz); **TphCN** (Y = 66%) ^{1}**H-NMR**, 400 MHz, DMSO-d^6 δ (ppm) = 8.06 (d, 2H, $J_{H\text{-}H}$ = 3.99 Hz), 8.31 (d, 2H, $J_{H\text{-}H}$ = 7.99 Hz); **Tpyz** (Y = 64%), ^{1}**H-NMR**, 400 MHz, DMSO-d^6 δ (ppm) = 9.37 (d, 1H, $J_{H\text{-}H}$ =

4.6 Hz), 8.85 (m, 2H); **Tpyr** (Y = 62%), ^{1}**H-NMR**, 400 MHz, DMSO-d^{6} δ (ppm) = 8.76 (d, 2H, $J_{H\text{-}H}$ = 3.99 Hz), 8.19 (d, 1H, $J_{H\text{-}H}$ = 4.6 Hz) 8.04 (m, 1H), 7.59 (m, 1H);

General Procedure for the Preparation of the cationic cis-[Ru(N^N)$_2$(L)]·[BF$_4$]-Type Complexes

cis-[Ru(bipy-COOH)$_2$Cl$_2$] (0.066 g, 0.10 mmol) was dissolved in methanol (60 mL) in a 100 mL round-bottom flask protected from light. A slight excess (2.2 equiv) of $AgBF_4$ was added, and the mixture was stirred at reflux for 3 h. The reaction mixture was filtered through a Celite pad, and the filtrate was added drop wise to a methanol (5 mL) solution of the appropriate tetrazolate ligand (1.6 equiv). Once the addition was complete, the deep-red solution was stirred at reflux temperature overnight. The mixture was then cooled to r.t., concentrated to about half of the initial volume and a copious amount of diethyl ether was added, causing the precipitation of a crude product, which was collected by suction filtration. **D1** ^{1}**H-NMR** (CD_3OD, 400 MHz) δ (ppm) = 9.5 (s, 1H), 9.17 (m, 2H), 9.12 (m, 2H), 8.42 (d, 2H), 8.2 (d, 1H), 8.15 (d, 1H), 8.05 (m, 2H), 7.95 (m, 3H), 7.9 (m 1H), 7.43 (m, 1H,). **D2** ^{1}**H-NMR** (CD_3OD, 400 MHz) δ (ppm) = 9.17 (m, 2H), 9.12 (m, 2H), 8.42 (d, 2H), 8.1 (m, 3H), 8.05 (d, 1H), 7.99 (m, 3H), 7.89 (m, 2 H), 7.68 (m 1H), 7.43 (t, 1H).

General Procedure for the Preparation of the neutral cis-[Ru(N^N)$_2$(L)$_2$]-Type Complexes

cis-[Ru(bipy-COOH)$_2$Cl$_2$] (0.046 g, 0.07 mmol) was dissolved in methanol (80 mL) in a 250 mL round-bottom flask protected from light. A slight excess (2.2 equiv) of $AgBF_4$ was added, and the mixture was stirred at reflux for 3 h. The reaction mixture was filtered through a celite pad, and the filtrate was added drop wise to a methanol (5 mL) solution of the appropriate tetrazolate ligand (2.2 equiv). Once the addition was complete, the deep-red solution was stirred at reflux temperature overnight. The mixture was then cooled to r.t., concentrated to about half of the initial volume and a copious amount of diethyl ether was added, causing the precipitation of a crude product, which was collected by suction filtration. **D3** ^{1}**H-NMR** (CD_3OD, 400 MHz) δ (ppm) = 10.04 (d, 2H, $J_{H\text{-}H}$ = 3.9 Hz), 9.02 (s, 2H), 8.90 (s, 2H), 8.18 (m, 2H), 8.02 (m, 2H), 7.97 (d, 4H, $J_{H\text{-}H}$ = 7.9 Hz), 7.74 (m, 2H), 7.70 (d, 4H, $J_{H\text{-}H}$ = 7.9 Hz). **D4** ^{1}**H-NMR** (CD_3OD, 400 MHz) δ (ppm) = 10.03 (d, 2H, $J_{H\text{-}H}$ = 7.9 Hz), 8.98 (s, 2H), 8.85 (s, 2H), 8.12 (m, 2H), 7.78 (m, 2H), 7.70 (d, 4H, $J_{H\text{-}H}$ = 7.9 Hz), 7.53 (m, 2H), 7.48 (d, 4H, $J_{H\text{-}H}$ = 7.9 Hz).

DSSC assembly and characterization

The TiO_2 inks were deposited onto Fluorine-doped Tin Oxide (FTO) glass substrates (sheet resistance 7 Ω/sq, Sigma-Aldrich) using a semi-automatic screen-printer AUR'EL 900, AUR'EL Automation s.p.a., Italy), and treated at 450°C for 30 minutes. Before this deposition, the substrates were coated with TiO_2 blocking layer (BL), deposited according to a procedure reported in our previous work.[90] Briefly, an ethanolic solution of $TiCl_4$ (50 mM) was spin coated onto the FTO substrates to obtain a thin compact TiO_2 film, and then treated at 450°C for 30 minutes. The thickness of the TiO_2 film (photoanode) was adjusted at about 8 μm. After sintering, the films were immersed in a 50mM $TiCl_4$ aqueous solution at 70°C, and then fired at 450°C for 30 minutes. The as obtained photoanodes were then dipped for 16 hours in as 0.3 mM absolute ethanol solution of each different dye. As a reference, also DSSCs sensitized with di-Tetrabutylammonium *cis*-bis (isothiocyanato)bis(2,2'-bipyridyl-4,4'-dicarboxylato)ruthenium(II), named N719 dye (Sigma-Aldrich) were prepared. A pre-drilled FTO coated glass covered with a sputtered Pt layer was used as the counter electrode. After the photoanode sensitization the electrodes were assembled into a sandwich type cell and sealed with a hot melt gasket made of Meltonix (thickness 25 μm, Solaronix, Switzerland). Electrolyte (Iodolyte Z100, Solaronix, Switzerland) was introduced in the cell via vacuum back filling through the hole in the counter electrode. The active area of the solar cells was fixed at 0.25 cm^2. In order to evaluate the DSSCs performance, current-voltage curves, Electrochemical Impedance Spectroscopy (EIS) and Incident Photon-to-electrical-Conversion Efficiency (IPCE) analyses were done. The J-V tests of devices were conducted on a Keithley Model 2400 with an AM 1.5G solar simulator (SUN 2000, Abet Technologies). The system was calibrated against a certified silicon solar cell and the light intensity of 1000 W m^{-2}. IPCE is determined using PVE300 (Bentham Instrument Ltd, Reading, Berkshire, UK) with dual xenon/quartz halogen light source, measured in DC mode and no bias light is used. Electrochemical Impedance Spectroscopy measurements were recorded using AutoLab PGSTAT302N+FRA32 (Metrohm Autolab, The Nederlands) in the dark at open circuit voltage. An alternating sinusoidal signal of 10 mV and frequency range from 100 KHz to 0,1 Hz were used. The

experimental points of impedance spectra were fitted with Z-View software (Scribner Associates Inc.).

List of Publications

A. Baschieri; S. Muzzioli; V. Fiorini; E. Matteucci; M. Massi; L. Sambri; S. Stagni, *Introducing a New Family of Biotinylated Ir(III)-Pyridyltriazole Lumophores: Synthesis, Photophysics, and Preliminary Study of Avidin-Binding Properties*, *Organometallics*, **2014**, *33*, pp. 6154 – 6164.

M. V. Werrett; G. S. Huff; S. Muzzioli; V. Fiorini; S. Zacchini; B. W. Skelton; A. Maggiore; J. M. Malicka; M. Cocchi; K. C. Gordon; S. Stagni; M. Massi, *Methylated Re(I) tetrazolato complexes: photophysical properties and Light Emitting Devices*, *Dalton Trans.*, **2015**, *44*, pp. 8379 – 8393.

V. Fiorini; A. M. Ranieri; S. Muzzioli; K. D. M Magee; S. Zacchini; N. Akabar; A. Stefan; M. I. Ogden; *M. Massi; *S. Stagni; *Targeting divalent metal cations with Re(I) tetrazolato complexes*, *Dalton Trans.*, **2015**, *44*, pp. 20597 – 20608.

V. Fiorini; A. D'Ignazio; K. D. M. Magee; M. I. Ogden; M. Massi; S. Stagni; , *Fully Ir(III) tetrazolate soft salts: the road to white-emitting ion pairs*, *Dalton Trans.*, **2016**, *45*, pp. 3256 – 3259.

V. Fiorini, S. Zacchini, P. Raiteri, R. Mazzoni, V. Zanotti, M. Massi, S. Stagni; *Negatively Charged Ir(III) cyclometalated complexes containing a chelating bis-tetrazolato ligand: synthesis, photophysics and the study of reactivity with electrophiles, Dalton. Trans.*, **2016**, *45*, pp 12884-12896

R. Esposito, L. Calvanese, M. E. Cucciolito, G. D'Auria, L. Falcigno, V. Fiorini, P. Pezzella, G. Roviello, S. Stagni, G. Talarico, F. Ruffo; *Oxidative Coupling of Imino, Amide Platinum (II) Complexes Yields Highly Conjugated Blue Dimers, Organometallics*, **2017**, *36(2)*, pp 384-390.

A. Toscani, K. A. Jantan, J. B. Hena, J. A. Robson, E. J. Parmenter, V. Fiorini, A. J. P. White, S. Stagni, J. D. E. T. Wilton-Ely; *The stepwise generation of multimetallic complexes based on a vinylbipyridine linkage and their photophysical properties, Dalton. Trans.*, **2017**, Advance Article, DOI: 10.1039/C6DT03810G

References

1 F. A. Cotton, G. Wilkinson, P. L. Gauss; *Basic Inorganic Chemistry*. Wiley Interscience: USA, **1995**.

2 a) V. Balzani, V. Carassiti; *Photochemistry of Coordination Compounds*. Accademic Press: London, UK, **1970**. b) N. J. Turro, V. Ramamutrthy, J. C. Scaiano; *Principles of Molecular Photochemistry: An Introduction*. University Science Books, **2009**.

3 F. Puntoriero, F. Nastasi, M. Galletta, S. Campagna; *Photophysics and Photochemistry of Non-Carbonyl-Containing Coordination and Organometallic Compounds*, **2013** Elsevier Ltd.

4 V. W-W. Yam, K. M-C. Wong; *Chem. Commun*., **2011**, *47*, 11579–11592 and references cited herein.

5 a) F. Scandola; *Chem. Rev.*, **1986**, *86*, 1; b) T. J. Meyer, J. V. Caspar; *Chem. Rev.*, **1985**, *85*, 18; c) G. A. Crosby; *Acc. Chem. Res.*, **1975**, *8*, 231; d) R. J. J. Watts; *Chem. Educ.*, **1983**, *60*, 834; e) J. F. Endicott,; *Acc. Chem. Res.*, **1988**, *21*, 59; f) F. Scandola, M. T. Indelli, C. Chiorboli, C. A. Bignozzi; *Top. Curr. Chem.*, **1990**, *158*, 73; g) L. De Cola, P. Belser, A. Von Zelewsky, F. Vöglte; *Inorg. Chim. Acta*, **2007**, *360*, 775; h) A. Juris, V. Balzani, S. Campagna, P. Belser, A. Von Zelewsky; *Coord. Chem. Rev.*, **1988**, *84*, 85; i) S. Campagna, F. Puntoriero, F. Nastasi, G. Bergamini, V. Balzani, ; *Top. Curr. Chem.*, **2007**, *280*, 117; j) J. V. Caspar, T. J. Meyer; *Inorg. Chem.*, **1983**, *22*, 24444; k) R. T. F. Jukes, V. Adamo, F. Hartl, P. Belser, L. De Cola; *Coord. Chem. Rev.*, **2005**, *249*, 1327; l) S. Welter, N. Salluce, P. Belser, M. Groeneveld, L. De Cola; *Coord. Chem. Rev.*, **2005**, *249*, 1360; m) S. Bonnet, J. -P. Collin, J.-P. Sauvage; *Inorg. Chem.*, **2006**, *45*, 4024; n) S. Bonnet, J.-P. Collin, J. -P. Sauvage; *Inorg. Chem.*, **2007**, *46*, 10520.

6 A. E. Friedman, J. C. Chambron, J. C Sauvage, N. J. Turro, J. K. Barton; *J. Am. Chem. Soc.*, **1990**, *112*, 4960-4962.

7 a) M. K. Nazeeruddin, S. M. Zakeeruddin, R. Humprhry-Baker, M. Jirousek, P. Liska, N. Vlachopoulos, V. Shklover, C. H. Fischer, M. Grätzel; *Inorg. Chem.*, **1999**, 38, 6298-6305 b) M. Grätzel; *Acc. Chem. Res.*, **2009**, *42*, 1788.

8 a) K. A. King, P. J. Spellane, R. J. Watts; *J. Am. Chem. Soc.*, **1985**, *107*, 1431; b) I. M. Dixon, J.-P. Collin, J.-P. Sauvage, L. Flamigni, S. Encinas, F. Barigelletti; *Chem. Soc. Rev.*, **2000**, *29*, 385. c) K. K. W. Lo, W. K. Hui, C. K. Chung, K. H. K. Tsang, D. C. M Ng, N. Y. Zhu, K. K. Cheung; *Coord. Chem. Rev.*, **2005**, *29*, 1434; d) M. S. Lowry, S. Bernhard; *Chem.–Eur. J.*, **2006**, *12*, 7970; e) R. C. Evans, P. Douglas, C. J. Winscom; *Coord. Chem. Rev.*, **2006**, *250*, 2093; f) M. A. Baldo, D. F. O'Brien, Y. You, A. Shoustikov, S. Sibley, M. E.Thompson, S. R. Forrest; *Nature*, **1998**, *395*, 151; g) S. Lamansky, P. Djurovich, D. Murphy, F. Abdel-Razzaq, R. Kwong, Z. Tsyba, M. Bortz, B. Mui, R. Bau, M. E. Thompson; *Inorg Chem.*, **2001**, *40*, 1704; h)

X. Yang, D. C. Müller, D. Neher, K. Meerholz; *Adv. Mater.,* **2006**, *18*, 948; i) Y. Chi, P-T. Chou; *Chem. Soc. Rev*., **2010**, *39*, 638.

9 L. Flamigni, A. Barbieri, C. Sabatini, B. Ventura, F. Barigelletti; *Top. Curr. Chem.* **2007**, *281*, 143.

10 A. Kumar, S-S. Sun, A. J. Lees; *Top. Organomet. Chem.*, **2010**, *29* Springer-Verlag Berlin Heidelberg .

11 M. Wrighton, D. L. Morse; *J. Am. Chem. Soc*., **1974**, *96*.

12 a) H. Takeda, K. Koike, H. Inoue, O. Ishitani; *J. Am. Chem. Soc*., **2008**, *130*, 2023; b) A. A. Abdel-Shafi, J. L. Bourdelande, S. S. Ali; *Dalton Trans*., **2007**, 2510 2516; c) W. Belliston-Bittner, A. R. Dunn, Y. H. L. Nguyen, D. J. Stuehr, J. R. Winkler, H. B. Gray; *J. Am. Chem. Soc.,* **2005,** *51*, 5169-5173; d) Y. Hayashi, S. Kita, B. S. Brunschwig, E. Fujita; *J. Am. Chem. Soc.,* **2003**, *39*, 11976 – 11987.

13 a) A. Kumar, S. S. Sun, A. J. Lees; *Coord. Chem. Rev.,* **2008**, *252*, 922; b) S. S. Sun, A. J. Less; *Coord. Chem. Rev.,* **2002**, *230*, 171; c) S. S. Sun, A. J. Lees; *Chem. Commun.*, **2000**, 1687; d) T. Mizuno, T. Fukumatsu, M. Takeuchi, S. Shinkai; *J. Chem. Soc. Perkin Trans.,* **2000**, *1*, 407; e) M. H. Keefe, R. V. Sloan, J. T. Hupp, K. F. Czaplewski, R. Q. Snurr, C. L. Stern; *Langmuir*, **2000**, *16*, 3964; f) M. Bakir, J. A. M. McKenzie; *J. Chem. Soc. Dalton Trans.,* **1997**, 3571.

14 a) N. J. Lundin, A. G. Blackman, K. C. Gordon, D. L. Officer; *Angew. Chem. Int. Ed.,* **2006**, *45*, 2582; b) C. Liu, J. Li, B. Li, Z. Hong, F. Zhao, S. Liu, W. Li; *Appl. Phys. Lett.,* **2006**, *89*, 243511; c) Z. Si, J. Li, B. Li, F. Zhao, S. Liu, W. Li; *Inorg. Chem*., **2007**, *46*, 6155; d) S. Ranjan, S. Y. Lin, K. C. Hwang, Y. Chi, W. L. Ching, C. S. Liu; *Inorg Chem.*, **2003**, *42*, 1248; e) Y. Zhang, Z. Huang, W. Zeng, Y. Cao; Polymer, **2008**, *49*, 1211; f) P. I. Lee, S. L. C. Hsu, C. T. Chung; *Synth. Metals,* **2007**, *156*, 907.

15 a) R. F. Victor, I. Correia, M. Videira, F. Marques, A. Paulo, J. C. Pessoa, G. Viola, G. G. Martins, I. Santos; *Chem. Bio. Chem*., **2008**, *9*, 131; b) D-L. Ma, C-M. Che, F-M. Siu, M. Yang, K-Y. Wong; *Inorg. Chem*., **2007**, *46*, 740; c) G. T. Ruiz, M. P. Juliarena, R. O. Lezna, E. Wolcan, M. R. Feliz, G. Ferraudi; *J. Chem. Soc. Dalton Trans*., **2007**, 2020; d) S. Y. Reece, D. G. Nocera; *J. Am. Chem. Soc*., **2005**, *127*, 9448; e) H. D. Stoeffler, N. B. Thornton, S. L. Temkin, K.S. Schanze; *J. Am. Chem. Soc*., **2005**, *117*, 7119.

16 (a) L. Fuks, E. Gniazdowska, J. Meiczkowski, N. Sadlej-Sosnowska; *Polyhedron*, **2008**, *27*, 1353; b) S. Tzanopoulou, I. C. Pirmettis, G. Patsis, M. Paaravatou-Petsotas, E. Livaniou, M. Papadopoulos, M. Pelecanou; *J. Med. Chem*., **2006**, *49*, 5408; c) A. R. Dunn, W. Belliston-Bittner, J. R. Winkler, E. D. Getzoff, D. J. Stuehr, H. B. Gray; *J. Am. Chem. Soc.,* **2005**, *127*, 5169; d) J. Zhang, J.

J. Vittal, W. Henderson, J. R. Wheaton, I. H. Hall, T. S. A. Hor, Y. K. Yan; *J. Organomet. Chem.*, **2002**, *650*, 123; e) H-J. Pietzsch, A. Gupta, M. Reisgys, A. Drews, S. Seifert, R. Syhre, H. Spies, R. Alberto, U. Abram, P. A. Schubiger, B. Johannsen; *Bioconjugate Chem.*, **2000**, *11*, 414.

17 a) S. L. Wittenberger; *Org. Prep. Proceed. Int'l.* **1994**, *26*, 499; S. J. Wittenberger; *Chem. Abstr.* **1995**, *122*, 31359. b) R. J. Herr, *Bioorg. Med. Chem.* **2002**, *10*, 3379. c) K. Vávrová, A. Hrabálek, *Eur. J. Org. Chem.* **2012**, 6101.

18 a)R. N. Butler; *Adv. Heterocycl. Chem.* **1977**, *21*, 323; b) R. N. Butler; *Comprehensive Heterocyclic Chemistry* (Eds.: A. R. Katritzky, C. W. Rees, E. F. V. Scriven), Pergamon, Oxford, U. K., **1996**, Vol. *4*, 2nd ed., 621; c) N. Gaponik, S. V. Voitekhovich, O. A. Ivashkevich; *Russ. Chem. Rev.* **2006**, *75*, 507; d) H. Singh, A. S. Chawla, V. K. Kapoor, D. Paul, R. K. Malhotra; *Prog. Med. Chem.* **1980**, *17*, 151; e) P. F. Juby, T. W. Hudyma, M. Brown; *J. Med. Chem.* **1968**, *11*, 111. f) J. V. Duncia, M. E. Pierce, J. B. Santella III; *J. Org. Chem.* **1991**, *56*, 2395; g) T. Hirata, J. Nomiyama, N. Sakae, K. Nishimura, M. Yokomoto, S. Inoue, K. Tamura, M. Okuhira, H. Amano; *Bioorg. Med. Chem. Lett.* **1996**, *6*, 1469; h) C. W. Thornber; *Chem. Soc. Rev.* **1979**, *8*, 563; i) C: A. Lipinski; *Annu. Rep. Med. Chem.* **1986**, *27*, 283; l) A. Burger; *Prog. Drug Res.* **1991**, *37*, 287.

19 a) D. E. Chavez, M. A. Hiskey, R. Gilardi; *Angew. Chem.* **2000**, *112*, 1861; b) D. E. Chavez, M. A. Hiskey, R. Gilardi; *Angew. Chem. Int. Ed.* **2000**, *39*, 1791; c) Y. Miyata, H. Kanou, S. Date, K. Hasue; *Sci. Technol. Energ. Mater.* **2005**, *66*, 233.

20 W. G. Finnegan, R. A. Henry, R. Lofquist; *J. Am. Chem. Soc.* **1958**, *80*, 3908-3911.

21 K. Koguro, T. Oga, S. Mitsui, R. Orita; *Synthesis* **1998**, 910–914.

22 Z. P. Demko, K. B. Sharpless; *Org. Lett.* **2001**, *3*, 4091–4094.

23 A. Palazzi, S. Stagni, S. Bordoni, M. Monari, S. Selva; *Organometallics*, **2002**, *21*, 3774-3781.

24 S. Stagni, A. Palazzi, S. Zacchini, B. Ballarin, C. Bruno, M. Marcaccio, F. Paolucci, M. Carano, M. Monari, A. J, Bard; *Inorg. Chem.*, **2006**, *45*, 695-709.

25 S. Zanarini, A. J. Bard, M. Marcaccio, A. Palazzi, F. Paolucci, S. Stagni; *J. Phys. Chem. B*, **2006**, *45*, 22551-22556.

26 S. Stagni, E. Orselli, A. Palazzi, L. De Cola, S. Zacchini, C. Femoni, M. Marcaccio, F. Paolucci, S. Zanarini; *Inorg. Chem.*, **2007**, *46*, 9126-9138.

27 S. Stagni, S. Colella, A. Palazzi, G. Valenti, S. Zacchini, F. Paolucci, M. Marcaccio, R. Q. Albuquerque, L. De Cola; *Inorg. Chem.*, **2008**, *47*, 10509-10521.

28 M V. Werrett, S. Muzzioli, P. J. Wright, A. Palazzi, P. Raiteri, S. Zacchini, M. Massi, S. Stagni; *Inorg. Chem.*, **2014**, *53*, 229-243.

29 M. Cocchi, J. Kalinowski, S. Stagni, S. Muzzioli; *Appl. Phys. Lett.*, **2009**, *84*, 08336.

30 R. A. Kirgan, B. P. Sullivan, D. P. Rillema; *Top. Curr. Chem.*, **2007**, *281*, 45–100.

31 M. V. Werrett, D. Chartrand, J. D. Gale, G. S. Hanan, J. G. MacLellan, M. Massi, S. Muzzioli, P. Raiteri, B. W. Skelton, M. Silberstein, S. Stagni; *Inorg. Chem.*, **2011**, *50*, 1229-1241.

32 C. A. Bader, E. A. Carter, A. Safitri, P. V. Simpson, P. J. Wright, S. Stagni, M. Massi, P. A. Lay, D. A. Brooks, S. E. Plush; *Molecular BioSystems*, **2016**, *12*, 2064-2068.

33 C. A. Bader, T. Shandala, E. A. Carter, A. Ivask, T. Guinan, S. M. Hickey, M.V: Werrett, P. J. Wright, P. V. Simpson, S. Stagni, N. H. Voelcker, P. A. Lay, M. Massi, S. E. Plush, D. A. Brooks; *PLoS ONE 11*(8): e0161557. doi:10.1371/journal.pone.0161557

34 V. Fiorini, A. D'ignazio, K. D. M. Magee, M. I. Ogden, M. Massi, S. Stagni; *Dalton. Trans,* **2016**, *45,* 3256.

35 F. Monti, M. G. La Placa, N. Armaroli, R. Scopelliti, M. Graẗzel, M. K. Nazeeruddin, K. Kessler; *Inorg. Chem*. **2015**, *54*, 3031−3042.

36 D. Di Censo, S. Fantacci, F. De Angelis, C. Klein, N. Evans, K. Kalayanasundaram, H. K. Bolink, M. Graẗzel**,** M. K. Nazeeruddin; *Inorg. Chem.* **2008**, *47*, 980-989.

37 H. –S. Chen, C. Wu, M.-C. Kuo, M. E. Thompson, K. –T. Wong; *J. Mater. Chem*., **2012**, 22, 9556.

38 a) C. Wu, H. –F. Chen, K. –T. Wong, M. E. Thompson; *J. Am. Chem. Soc.*, **2010**, *132*, 3133–3139; b) A. Ionescu, E. Ildyko Szerb, Y. J. Yadav, A. M. Talarico, M. Ghedini, N. Godbert; *Dalton Trans*., **2014**, *43*, 784; c) M. Mauro, K. C.

Schuermann, R. Prtt, A. Hafner, P. Mercandelli, A. Sironi, L. De Cola; *Angew. Chem. Int. Ed.* **2010**, *49*, 1222 –1226.

39 M. K. Nazeeruddin, R. Humphry-Baker, D. Berner, S. Rivier, L. Zuppiroli, M. Graẗzel; *J. Am. Chem. Soc.*, **2003**, *125*, 8790-8797.

40 N. Mohd Ali, V. L. MacLeod, P. Jennison, I. V. Sazanovich, C. A. Hunter, J. A. Weinstein, M. D. Ward; *Dalton Trans*., **2012**, *41*, 2408.

41 G. A. Crosby, J. N. Demas; *J. Phys. Chem.* 1971, **75**, 991-1024.

42 D. F. Eaton; *Pure Appl. Chem*. 1988, **60**, 1107-1114.

43 K. Nakamura, *Bull. Chem. Soc. Jpn.* 1982, **55**, 2697–2705.

44 V. Fiorini, S. Zacchini, P. Raiteri, R. Mazzoni, V. Zanotti, M. Massi, S. Stagni; *Dalton. Trans,* **2016**, *45,* 12884-12896.

45 a) V. Fiorini, A. M. Ranieri, S. Muzzioli, K. D. M. Magee, S. Zacchini, N. Akabar, A. Stefan, M. I. Ogden, M. Massi, S. Stagni; *Dalton Trans.*, **2015**, *44*, 20597–20608; b) M. V. Werrett, G. S. Huff, S. Muzzioli, V. Fiorini, S. Zacchini, B. W. Skelton, A. Maggiore, J. M. Malicka, M. Cocchi, K. C. Gordon, S. Stagni, M. Massi; *Dalton Trans*., **2015**, *44*, 8379–8393; c) K. D. M. MaGee, P. J. Wright, S. Muzzioli, C. M. Siedlovskas, P. Raiteri, M. V. Baker, D. H. Brown, S. Stagni, M. Massi; *Dalton Trans*., **2013**, *42*, 4233–4236;

46 a) S. Bhandari, M. F. Mahon, K. C. Molloy, J. S. Palmer and S. F. Sayers, *Dalton Trans.,* **2000**, 1053; b) D.-Z. Wang; *Polyhedron*, **2012**, 35, 142; c) Cu X.-H. Huang, T.-L. Sheng, S.-C. Xiang, R.-B. Fu, S.-M. Hu, Y.-M. Li, X.-T. Wu, Chin; *J. Struct. Chem*., **2007**, *26*, 161.

47 A. R. Katritzky Novruz, G. Akhmedov, I. Ghiviriga, R. Maimait; *J. Chem. Soc*., *Perkin Trans*, **2002**, *2*, 1986–1993.

48 J. Tomasi, B. Mennucci, R. Cammi; *Chem. Rev*., **2005**, *105*, 2999–3094.

49 M. J. Frisch, G. W. Trucks, H. B. Schlegel, G. E. Scuseria, M. A. Robb, J. R. Cheeseman, G. Scalmani, V. Barone, B. Mennucci, G. A. Petersson, H. Nakatsuji, M. Caricato, X. Li, H. P. Hratchian, A. F. Izmaylov, J. Bloino, G. Zheng, J. L. Sonnenberg, M. Hada, M. Ehara, K. Toyota, R. Fukuda, J. Hasegawa, M. Ishida, T. Nakajima, Y. Honda, O. Kitao, H. Nakai, T. Vreven, J. A. Montgomery Jr., J. E. Peralta, F. Ogliaro, M. Bearpark, J. J. Heyd, E. Brothers, K. N. Kudin, V. N.

Staroverov, R. Kobayashi, J. Normand, K. Raghavachari, A. Rendell, J. C. Burant, S. S. Iyengar, J. Tomasi, M. Cossi, N. Rega, J. M. Millam, M. Klene, J. E. Knox, J. B. Cross, V. Bakken, C. Adamo, J. Jaramillo, R. Gomperts, R. E. Stratmann, O. Yazyev, A. J. Austin, R. Cammi, C. Pomelli, J. W. Ochterski, R. L. Martin, K. Morokuma, V. G. Zakrzewski, G. A. Voth, P. Salvador, J. J. Dannenberg, S. Dapprich, A. D. Daniels, Ö. Farkas, J. B. Foresman, J. V. Ortiz, J. Cioslowski, D. J. Fox; *Gaussian 09, Revision A.02*.

50 T. Yanai, D. P. Tew, N. C. Handy; *Chem. Phys. Lett.*, **2004**, *393*, 51–57.

51 D. Andrae, U. Haeussermann, M. Dolg, H. Stoll, H. Preuss; *Theor. Chim. Acta*, **1990**, *77*, 123–141.

52 G.M Sheldrick, SADABS, Program for Empirical Absorption Correction, University of Göttingen, Germany, 1996.

53 G. M. Sheldrick, SHELX97-Program for the refinement of Crystal Structure, University of Göttingen, Germany, 1997.

54 a) K. J. Waldron, N. J. Robinson; *Nature Rev. Microbiol.* **2009**, *7*, 25–35. b) C. Andreini, I. Bertini, A. A. Rosato; *Bioinformatics* **2004**, *20*, 1373–1380.

55 a) J. J. Harrison, H. Ceri, C. Stremick, R. J. Turner; *Environ. Microbiol.*, **2004**, *6*, 1220–1227; b) D. H. Nies; *Appl. Microbiol. Biotechnol.*, **1999**, *51*, 730–750.

56 J. A. Lemire, J. J. Harrison, R. J. Turner; *Nature Reviews Microbiology,* **2013**, *11,* 371–384 and references cited herein.

57 a) A. Braud, F. Hoegy, K. Jezequel, T. Lebeau, I. J. Schalk; *Environ. Microbiol.* **2009**, *11*, 1079–1091; b) J. A. Imlay, S. M. Chin, S. Linn; *Science*, **1988**, *240*, 640–642; c) L. Macomber, C. Rensing, J. A. Imlay; *J. Bacteriol.*, **2007**, *189*, 1616–1626; d) J. J. Harrison *et al; Environ. Microbiol.* **2009**, *11*, 2491–2509; e) J. M. Perez *et al.; PLoS ONE*, **2007**, *2*, e211; f) T. Nunoshiba *et al.; J. Biol. Chem.*, **1999**, **274**, 34832–34837; g) D. Touati, M. Jacques, B. Tardat, L. Bouchard, S. Despied; *J. Bacteriol.* **1995**, *177*, 2305–2314; h) S. L. Warnes, C. W. Keevil; *Appl. Environ. Microbiol.*, **2011**, *77*, 6049–6059; i) S. L. Warnes, V. Caves, C. W. Keevil; *Environ. Microbiol.*, **2012**, *14*, 1730–1743.

58 J. A. Imlay; *Annu. Rev. Microbiol.*, **2003**, *57*, 395–418.

59 a) M. Valko, H. Morris, M. T. D. Cronin; *Curr. Med. Chem.*, **2005**, *12*, 1161–1208; b) S. J. Stohs, D. Bagchi; *Free Radic. Biol. Med.*, **1995**, *18*, 321–336.

60 a) J. Middaugh *et al.; J. Biol. Chem.*, **2005**, *280*, 3159–3165; b) L. Macomber, S. P. Elsey, R. P. Hausinger; *Mol. Microbiol.,* **2011***, 82*, 1291–1300.

61 M. Valko, C. J. Rhodes, J. Moncol, M. Izakovic, M. Mazur; *Chem. Biol. Interact.,* **2006***, 160*, 1–40.

62 N. Falzone, L. Bohm, J. C. Swarts, C. E. Van Rensburg; *Anticancer Res.,* **2006** *26***,** 147–152. b) J. Rajput *et al.; J. Organomet. Chem.,* **2004**, 689**,** 1553–1568. c) P. V. Simpson, C. Schmidt, I. Ott, H. Bruhn, U. Schatzschneider; *Eur. J. Inorg. Chem.,* **2013**, 5547–5554.

63 F. Neve, M. La Deda, A. Crispini, A. Bellusei, F. Puntoriero, S. Campagna; *Organometallics,* **2004**, *23*, 5856.

64 Q. Zhao, S. Liu, M. Shi, C. Wang, M. Yu, L. Li, F. Li, T. Yi, C. Huang; *Inorg. Chem.,* **2006**, *45*, 6152.

65 A.U. Khan, M. Kasha; *J. Chem. Phys.,* **1963**, *39*, 2105.

66 *American Association of Textile Chemists and Colorists, RTP, NC, USA* **2015**.

67 A. Kirgan, B. P. Sullivan, D. P. Rillema; *Top. Curr. Chem.*, **2007**, *281*, 45–100; b) A. Kumar, S. Sun, A. Lees; *Top. Organomet. Chem.,* **2010**, *29*, 1–35.

68 a) K. Y. Zhang, K. K.-W. Lo; *Chemosensing and Diagnostics, in Coordination and Organometallic Chemistry of Comprehensive Inorganic Chemistry* II, b) K. K.-W. Lo, S. P.-Y. Li; *RSC Adv.*, **2014**, *4*, 10560– 10585; c) K. K. W. Lo, K. Y. Zhang, S. P.-Y. Li; *Eur. J. Inorg. Chem.,* **2011**, 3551–3568, and references cited therein.

69 a) V. Fernandez-Moreira, F. L. Thorp-Greenwood, M. P. Coogan; *Chem. Commun.*, **2010**, *46*, 186–202, and references cited therein; b) L. A. Mullice, S. J. A. Pope; *Dalton Trans.,* **2010**, *39*, 5908–5917; c) M.-W. Louie, H.-W. Liu, M. H.-C. Lam, T.-C. Lau, K. K.-W. Lo; *Organometallics*, **2009**, *28*, 4297–4307.

70 a) D. S. Silvester, S. Uprety, P. J. Wright, M. Massi, S. Stagni, S. Muzzioli; *J. Phys. Chem. C.*, **2012**, *116*, 7327–7333; c) P. J. Wright, S. Muzzioli, M. V. Werrett, P. Raiteri, B. W. Skelton, D. S. Silvester, S. Stagni, M. Massi; *Organometallics*, **2012**, *31*, 7566– 7578; d) P. J. Wright, S. Muzzioli, B. W. Skelton, P. Raiteri, J. Lee, G. Koutsantonis, D. S. Silvester, S. Stagni, M. Massi; *Dalton Trans.,* **2013**, *42*, 8188–

8191; e) P. J. Wright, M. G. Affleck, S. Muzzioli, B. V. Skelton, P. Raiteri, D. S. Silvester, S. Stagni, M. Massi; *Organometallics*, **2013**, *32*, 3728–3737.

71 C. A. Bader, R. D. Brooks, Y. S. Ng, A. Sorvina, M. V. Werrett, P. J. Wright, A. G. Anwer, D. A. Brooks, S. Stagni, S. Muzzioli, M. Silberstein, B. W. Skelton, E. M. Goldys, S. E. Plush, T. Shandala, M. Massi; *RSC Adv.*, **2014**, *4*, 16345–16351.

72 Z. Liu, W. He, Z. Guo; *Chem. Soc. Rev.*, **2013**, *42*, 1568– 1600, and references cited therein.

73 R. Butler, V. Garvin, *J. Chem. Soc., Perkin Trans*. **1981**, *1*, 390–393.

74 C. Femoni, S. Muzzioli, A. Palazzi, S. Stagni, S. Zacchini, F. Monti, G. Accorsi, M. Bolognesi, N. Armaroli, M. Massi, G. Valenti, M. Marcaccio; *Dalton Trans.*, **2013**, *42*, 997– 1010.

75 R. Czerwieniec, J. Yu, H. Yersin; *Inorg. Chem.*, **2011**, *50*, 8293–8301. (b) U. Monkowius, S. Ritter, B. König, M. Zabel, H. Yersin; *Eur. J. Inorg. Chem.*, **2007**, 4597– 4606; c) S.-H. Kuang, D. G. Cuttell, D. R. McMillin, P. E. Fanwick, R. A. Walton; *Inorg. Chem.*, **2002**, *41,* 3313–3322; d) D. G. Cuttell, S.-H. Kuang, P. E. Fanwick, D. R. McMillin, R. A. Walton; *J. Am. Chem. Soc.*, **2002**, *124*, 6–7.

76 a) Q. Zhang, Q. Zhou, Y. Cheng, L. Wang, D. Ma, X. Jing, F. Wang; *Adv. Funct. Mater.*, **2006**, *16*, 1203–1208; b) L. Yang, J.-K. Feng, A.-M. Ren, M. Zhang, Y.-G. Ma, X.-D. Liu; *Eur. J. Inorg. Chem.*, **2005**, 1867–1879.

77 a) P. W. N. M. van Leeuwen, P. C. J. Kamer, J. N. H. Reek, P. Dierkes, *Chem. Rev.*, **2000**, *100*, 2741–2770; b) L. A. van der Veen, P. K. Keeven, G. C. Schoemaker, J. N. H. Reek, P. C. J. Kamer, P. W. N. M. van Leeuwen, M. Lutz, A. L. Spek; *Organometallics*, **2000**, *19*, 872–883; c) P. C. J. Kamer, P. W. N. M. van Leeuwen, J. N. H. Reek; *Acc. Chem. Res.*, **2001**, *34*, 895–904; d) M. Kranenburg, Y. E. M. van der Burgt, P. C. J. Kamer, P. W. N. M. van Leeuwen, K. Goubitz, K. Fraanje; *Organometallics*, **1995**, *14*, 3081–3089.

78 K. K. Wing Lo, K. Y. Zhang, S. P.-Y. Li; *Eur. J. Inorg. Chem.*, **2011**, 3551–3568, and references cited therein.

79 M.-W. Louie, H.-W. Liu, M. H.-C. Lam, T.-C. Lau, K. K.-W. Lo;

Organometallics, **2009**, *28*, 4297–4307.

80 V. J. Caspar, T. J. Meyer; *J. Phys. Chem.*, **1983**, *87*, 952−957.

81 L. A. Mullice, S. J. A. Pope; *Dalton Trans.*, **2010**, *39*, 5908–5917, and references cited therein.

82 G. J. Kubas; *Inorg. Synth.*, **1979**, *19*, 90.

83 a) M. Dinca, A. Dailly, Y. Liu, C. M. Brown, D. A. Neumann, J. R. Long H.; *J. Am. Chem. Soc.* **2006**, *128*, 16876-16883; b) Zhao, Z.-R. Qu, H.-Y. Ye, R.-G. Xiong; *Chem. Soc. Rev.* 2008, *37*, 84-100 and references cited therein.

84 G. Steinhauser, T. M. Klapötke; *Angew. Chem. Int. Ed.* **2008**, *47*, 3330 –3347.

85 a) N. M. Shavaleev, S. V. Eliseeva, R. Scopelliti, J.-C. G. Bünzli; *Inorg. Chem.* **2014**, *53*, 5171−5178; b) D. D'Alessio, S. Muzzioli, B. W. Skelton, S. Stagni, M. Massi, M. I. Ogden; *Dalton Trans.*, **2012**, *41*, 4736–4739.

86 A. Colombo, C. Dragonetti, M. Magni, D. Meroni, R. Ugo, G. Marotta, M. G. Lobello, P. Salvatoric, F. De Angelis; *Dalton Trans.*, **2015**, *44*, 11788.

87 B. W. D. Andrade, S. Datta, S. R. Forrest, P. Djurovich, E. Polikarpov, M. E. Thompson; *Organic Electronics*, **2005**, *6*, 11-20.

88 G. Boschloo, E. A. Gibson, A. Hagfeldt; *J. Phys. Chem. Lett.*, **2011**, *2*, 3016-3020.

89 C. Yun, T. Bihai, C. Pi-Tai; *Coordination Chemistry Reviews*, **2014**, *281*, 1-25.

90 A. Sangiorgi, R. Bendoni, N. Sangiorgi, A. Sanson, B. Ballarin; *Ceramics International*, **2014,** 40, 10727-10735.